Hydraulic Fracturing Designs for Low Permeability Gas Condensate Reservoirs Having Different Compositions

Miss Karanthakarn Mekmok

A Thesis Submitted in Partial Fulfillment of the Requirements

for the Degree of Master of Engineering Program in Petroleum Engineering

Department of Mining and Petroleum Engineering

Faculty of Engineering

Chulalongkorn University

Academic Year 2016

การออกแบบไฮโดรลิคแฟรกเจอริงในแหล่งกักเก็บก๊าซธรรมชาติเหลวที่มีความสามารถในการซึมผ่านต่ำและองค์ประกอบแตกต่างกัน

นางสาวกรันฑการย์ เมฆหมอก

วิทยานิพนธ์นี้เป็นส่วนหนึ่งของการศึกษาตามหลักสูตรปริญญาวิศวกรรมศาสตรมหาบัณฑิต
สาขาวิชาวิศวกรรมปิโตรเลียม ภาควิชาวิศวกรรมเหมืองแร่และปิโตรเลียม
คณะวิศวกรรมศาสตร์ จุฬาลงกรณ์มหาวิทยาลัย
ปีการศึกษา 2559

Thesis Title	Hydraulic Fracturing Designs for Low Permeability Gas Condensate Reservoirs Having Different Compositions
By	Miss Karanthakarn Mekmok
Field of Study	Petroleum Engineering
Thesis Advisor	Assistant Professor Jirawat Chewaroungroaj, Ph.D.

Accepted by the Faculty of Engineering, Chulalongkorn University in Partial Fulfillment of the Requirements for the Master's Degree

.....Dean of the Faculty of Engineering

(Associate Professor Supot Teachavorasinskun, D.Eng.)

THESIS COMMITTEE

.....Chairman

(Assistant Professor Suwat Athichanagorn, Ph.D.)

.....Thesis Advisor

(Assistant Professor Jirawat Chewaroungroaj, Ph.D.)

.....Examiner

(Falan Srisuriyachai, Ph.D.)

.....External Examiner

(Piyarat Wattana, Ph.D.)

กรันฑการย์ เมฆหมอก : การออกแบบไฮโดรลิคแฟรกเจอริงในแหล่งกักเก็บก๊าซธรรมชาติเหลวที่มีความสามารถในการซึมผ่านต่ำและองค์ประกอบแตกต่างกัน (Hydraulic Fracturing Designs for Low Permeability Gas Condensate Reservoirs Having Different Compositions) อ.ที่ปรึกษาวิทยานิพนธ์หลัก: ผศ. ดร. จิรวัฒน์ ชีวรุ่งโรจน์, 140 หน้า.

แหล่งกักเก็บก๊าซธรรมชาติเหลวสร้างความท้าทายให้กับนักวิชาการในวงการปิโตรเลียมมามากกว่าสิบปี เพราะคุณสมบัติอันซับซ้อนของการไหลในแหล่งกักเก็บ เมื่อความดันในหลุมผลิตลดต่ำลงจนถึงจุดกลั่นตัว ก๊าซธรรมชาติเหล่านั้นจะควบแน่นของเหลวออกมาสะสมตัวรอบหลุมกีดขวางเส้นทางการไหลและลดประสิทธิภาพการผลิต ปรากฏการณ์นี้เรียกว่า การกีดขวางของก๊าซธรรมชาติเหลว จากผลการศึกษาของนักวิชาการอันหลากหลายชี้ให้เห็นว่าการกีดขวางของก๊าซธรรมชาติเหลวสร้างผลเสียให้กับแหล่งกักเก็บธรรมชาติเหลวหลายแห่ง และผลเสียนี้จะรุนแรงมากขึ้นในแหล่งกักเก็บที่มีความสามารถในการซึมผ่านต่ำ การทำไฮดรอลิคแฟรคเจอริงสำหรับหลุมในแนวนอนเป็นวิธีที่เชื่อว่าสามารถลดผลเสียของการกีดขวางของก๊าซธรรมชาติเหลว และเพิ่มผลการผลิตได้ด้วยการกระจายความดันรอบหลุมขุดเจาะ โปรแกรมจำลองแหล่งกักเก็บชนิดพิจารณาองค์ประกอบถูกนำมาใช้ศึกษาการออกแบบการทำไฮดอรลิคแฟรคเจอริงในแหล่งกักเก็บที่มีความสามารถในการซึมผ่านต่ำ จุดประสงค์หลักของผลงานชิ้นนี้ คือเพื่อศึกษาตัวแปรของค่าความไหลผ่านในรอยแตกในก๊าซธรรมชาติเหลวที่มีองค์ประกอบแตกต่างกัน และค่าความอิ่มตัวของก๊าซธรรมชาติเหลวใกล้หลุมขุดเจาะ

ผลจากการศึกษาพบว่าความกว้างของรอยแตกมีผลต่อการควบคุมการผลิตในระยะแรก เมื่อความกว้างของรอยแตกเพิ่มขึ้น ผลผลิตก๊าซธรรมชาติเหลวในแหล่งกักเก็บที่มีก๊าซธรรมชาติเหลวอยู่ในสัดส่วนที่น้อยและในสัดส่วนที่มากเพิ่มขึ้นถึง 18.45% และ 12.15% เปรียบเทียบกับกรณีที่ยังไม่ได้ทำไฮดรอลิคแฟรคเจอริง ทางด้านการเพิ่มจำนวนของรอยแตกพบว่าสามารถช่วยให้เพิ่มผลผลิตของก๊าซธรรมชาติเหลวในแหล่งกักเก็บที่มีก๊าซธรรมชาติเหลวอยู่ในสัดส่วนที่น้อยและในสัดส่วนที่มากได้มากถึง 18.45% และ 11.68% เพราะการเพิ่มจำนวนรอยแตกช่วยเพิ่มพื้นที่สัมผัสระหว่างแหล่งกักเก็บและรอยแตกได้มากขึ้น นอกจากนี้จำนวนของรอยแตกยังเป็นตัวแปรสำคัญในการศึกษาการออกแบบการกระตุ้นแหล่งกักเก็บในปริมาณที่ถูกกระตุ้นเท่ากันอีกด้วย ในขณะที่การศึกษาค่าความสามารถในการซึมผ่านในรอยแตกแสดงผลผลิตที่ไม่แตกต่างกันมากนักเมื่อเพิ่มค่าความซึมผ่านในรอยแตกจาก 50,000 มิลลิดาร์ซีถึง 150,000 มิลลิดาร์ซี เพราะค่าความซึมผ่านในรอยแตกที่ 50,000 มิลลิดาร์ซีนั้นสูงเพียงพอแล้วเมื่อเทียบกับค่าความซึมผ่านของแหล่งกักเก็บที่ 0.2 มิลลิดาร์ซี นอกเหนือจากนี้ผลจากการศึกษาค่าความอิ่มตัวของก๊าซธรรมชาติเหลวใกล้หลุมขุดเจาะพบว่าการทำไฮดรอลิคแฟรคเจอริงสามารถลดการกีดขวางของก๊าซธรรมชาติเหลวได้อย่างมีประสิทธิภาพ โดยเฉพาะในก๊าซธรรมชาติเหลวในแหล่งกักเก็บที่มีก๊าซธรรมชาติเหลวอยู่ในสัดส่วนที่มากที่เกิดปรากฏการณ์การระเหยของของเหลวที่ควบแน่นออกมา พบว่าผลควบคู่ของการทำไฮดรอลิคแฟรคเจอริง และการระเหยของของเหลวที่ควบแน่นออกมามีผลต่อการลดการกีดขวางของก๊าซธรรมชาติเหลวดีกว่าการพิจารณาผลจากการระเหยของของเหลวที่ควบแน่นออกมาเพียงอย่างเดียว

ภาควิชา วิศวกรรมเหมืองแร่และปิโตรเลียม ลายมือชื่อนิสิต .....

สาขาวิชา วิศวกรรมปิโตรเลียม ลายมือชื่อ อ.ที่ปรึกษาหลัก .....

ปีการศึกษา 2559

5771201521 : MAJOR PETROLEUM ENGINEERING
KEYWORDS: HYDRAULIC FRACTURING / CONDENSATE BLOCKAGE / CONDENSATE BANKING / GAS CONDENSATE RESERVOIR

KARANTHAKARN MEKMOK: Hydraulic Fracturing Designs for Low Permeability Gas Condensate Reservoirs Having Different Compositions. ADVISOR: ASST. PROF. JIRAWAT CHEWAROUNGROAJ, Ph.D., 140 pp.

Gas condensate reservoirs have been challenging all researchers in petroleum industry for decades because of their complexities in flow behavior. After dew point pressure is reached, gas condensate will drop liquid out and increase liquid saturation near wellbore vicinity creating production loss due to the phenomenon called condensate banking or condensate blockage. Many studies indicate the damage from condensate banking in many gas condensate fields all over the world and it can be more severe if the permeability of the reservoir is low. Hydraulic fracturing in horizontal well has been proved to be a reliable method to mitigate condensate banking and to increase productivity of condensate well by means of pressure redistribution in the near wellbore vicinity. In this work, compositional reservoir simulator had been implemented to study several designs of hydraulic fracturing in low permeability condensate reservoir. The objectives of this study are to study the effect of parameters of dimensionless fracture conductivity with different fluid compositions and saturation profile near wellbore vicinity had been observed.

The results indicate that fracture width has impact on controlling inertial effect. Increasing fracture width improves condensate productions in both lean and rich condensate compositions to 18.45% and 12.15% compared to non-fracture case. While, higher number of fractures allow larger contact area between fracture and reservoir and increasing condensate production to 18.45% and 11.68% in lean and rich condensate compositions respectively. Moreover, number of fractures also plays an important role in the condition of having the same Stimulated Reservoir Volume (SRV). The investigation of fracture permeability shows small benefit from increasing fracture permeability from 50,000 mD to 150,000 mD because fracture permeability at 50,000 mD is already high enough compared to reservoir permeability at 0.2 mD. In addition, from the study of condensate saturation near wellbore indicates that condensate banking can be reduced effectively with the introduction of hydraulic fracturing. Especially in rich condensate composition where revaporization occurred. The couple effect of revaporization and hydraulic fracturing has benefit on decreasing condensate banking more than considering the effect of revaporization alone.

Department:	Mining and Petroleum Engineering	Student's Signature	.....
Field of Study:	Petroleum Engineering	Advisor's Signature	.....
Academic Year:	2016		

ACKNOWLEDGEMENTS

I would like to express my deepest gratitude to my advisor, Asst. Prof. Jirawat Chewaroungroaj, for his support and invaluable guidance through this research. His continued support led me to the right path.

My sincere appreciation to all the professor and my committee – I could learn a lot from them when taking their classes and from many discussions. All classmates for their friendships and Chulalongkorn University for the education I have received and for being home that I could never forget. Many person have contributed either directly or indirectly to my thesis; I wish to express my thanks to them sincerely.

More importantly, my parents and my family who have been very supportive throughout the years. Their unconditional love and understanding cannot be forgotten.

CONTENTS

Page

Page

LIST OF TABLES

LIST OF FIGURES

LIST OF ABBREVIATIONS

bbl	barrel (bbl/d, bpd: barrel per day)
Bcf	billion standard cubic feet
CGR	condensate-gas ratio
CH_4 or C_1	Methane
C_2H_6 or C_2	Ethane
C_3H_8 or C_3	Propane
i-C_4H_{10}, i-C_4 or I-C_4	Iso-Butane
C_4H_{10}	n-Butane
C_5H_{11}, i-C_5 or I-C_5	Iso-Pentane
C_5H_{12} or C_5	Pentane
C_6H_{14} or C_6	Hexane
C_7H_{16} or C_7	Heptane
C_8H_{18} or C_8	Octane
C_9H_{20} or C_9	Nonane
$C_{10}H_{22}$ or C_{10}	Decane
$C_{11}H_{24}$ or C_{11}	Undecane
$C_{12}H_{26}$ or C_{12}	Dodecane
CO_2	Carbon dioxide
cP	centipoise
D	Darcy
ft	foot
ft^3	cubic feet
ft^3/lb-mole	cubic feet per pound mole
FVF	formation volume factor
GOR	gas-oil ratio
IFT	interfacial tension
in	inch

lb/ft^3	pound per cubic feet
LGR	local grid refinement
mD	millidarcy
Mscf/day	thousand standard cubic feet per day
Mstb	thousand stock tank barrels
psi	pounds per square inch
psia	pounds per square inch absolute
rb/stb	reservoir barrel per stock tank barrel
SRV	Stimulated reservoir volume
stb	stock tank barrels
THP	tubing head pressure
VFP	vertical flow performance

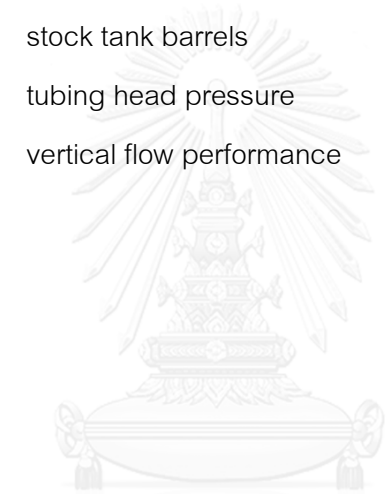

NOMENCLATURE

F_{CD}	dimensionless fracture conductivity
a	relative capacity
f	weighting function
k	reservoir permeability
k_f	fracture permeability
k_{rg}	relative permeability to gas
k_{ro}	relative permeability to oil
k_{rw}	relative permeability to water
$k_r\alpha_I$	relative permeability for capillary dominated (immiscible) flow
$k_r\alpha_M$	relative permeability for capillary dominated (miscible) flow
N_c	capillary number
N_{cbp}	base capillary number
N_{cnp}	normalized capillary number equation
p	pressure
p_d	dew point pressure
r	radius
r'_w	effective wellbore radius
r'_{wD}	dimensionless effective wellbore radius
s_f	skin in fracture
s_r	residual saturation
s_w	water saturation
v	velocity
v_g	gas velocity
w	fracture width

x_f	fracture half-length
$k^*_{r\alpha}$	end-point relative permeability

GREEK LETTER

α	phase indicator (gas, condensate)
β	non-Darcy flow coefficient
ε	Corey exponent that fixes the curvature of the relative permeability function
μ	viscosity of the fluid
μ_g	gas viscosity
σ_{og}	condensate-gas interfacial tension
ρ	density of the fluid
ϕ	porosity

CHAPTER 1
INTRODUCTION

The production of condensate reservoir exhibits a complex behavior because of the characteristic of fluids that are contained in the reservoir can change their compositions after reservoir pressure reaches dew point pressure. At this point, condensate will drop liquid out of gas and increases liquid saturation near wellbore vicinity creates production loss due to the phenomenon called condensate banking or condensate blockage that has been challenging many researchers in the petroleum industry.

Several techniques have been proposed and implemented to remediate the condensate banking and one of the most favorable technique is hydraulic fracturing. It can increase productivity index by two factors which are; giving high fracture conductivity and decreasing condensate banking by means of pressure redistribution in the near wellbore vicinity. However, this approach is not a prevention but only introduced to mitigate the effect of condensate banking and prolonging the production time for condensate reservoir.

The compositional model, ECLIPSE 300, is applied in this study to aid the understanding on the effect of parameters of dimensionless fracture conductivity in low permeability gas condensate reservoir with different fluid compositions, which are lean and rich condensate. In addition, condensate saturations near wellbore are investigated to see the effect of hydraulic fracturing on condensate banking and compared those results between non-fractured and fractured case.

1.1 Objectives

1. To study the effect of parameters of dimensionless fracture conductivity with different fluid compositions on well productivity and hydrocarbon recovery in low permeability gas condensate reservoir

2. To investigate condensate saturation profile in unfractured and hydraulically fractured wells

1.2 Outline of Methodology

1. Review and study related published papers to identify essential input parameters for reservoir simulation model.
2. Data collection prior the study
3. Generate compositional reservoir model by using ECLIPSE 300
4. Study effect of parameters of dimensionless fracture conductivity on different fluid compositions. The studied parameters are
    - Fracture width
    - Number of fractures
    - Fracture permeability
5. Study effect of stimulated reservoir volume (SRV) on different fluid compositions
6. Investigate condensate saturation profile in both unfractured and hydraulically fractured wells
7. Results and discussion
8. Conclusions and recommendations

1.3 Review of Chapters

This thesis is divided into six chapters. The outlines of each chapter are described below.

Chapter 2 presents a literature review on gas condensate reservoir, studies on mitigating condensate banking by using hydraulic fracturing, and impact of positive coupling and inertial effects.

Chapter 3 explains theory and concepts related to the study.

Chapter 4 describes reservoir model description, gridding and fluids in the study.

Chapter 5 exhibits results and discussion that obtained from the studying on the effect of parameters of dimensionless fracture conductivity and condensate saturation profile near wellbore.

Chapter 6 concludes results from this study, including recommendations for future works.

CHAPTER 2
LITERATURE REVIEW

2.1 Gas Condensate Reservoir

A gas condensate reservoir originally has single fluid, gas phase, in the reservoir when pressure is higher than dew point pressure and composed mainly methane, other light hydrocarbons dominate and small portion of heavy ends. As the production continues, pressure will eventually fall below the dew point pressure, then the composition that rich in heavy ends will drop the liquid out of the gas causing the change from single phase into two phase composed of gas phase and liquid phase as they are shown in Figure 2.1.

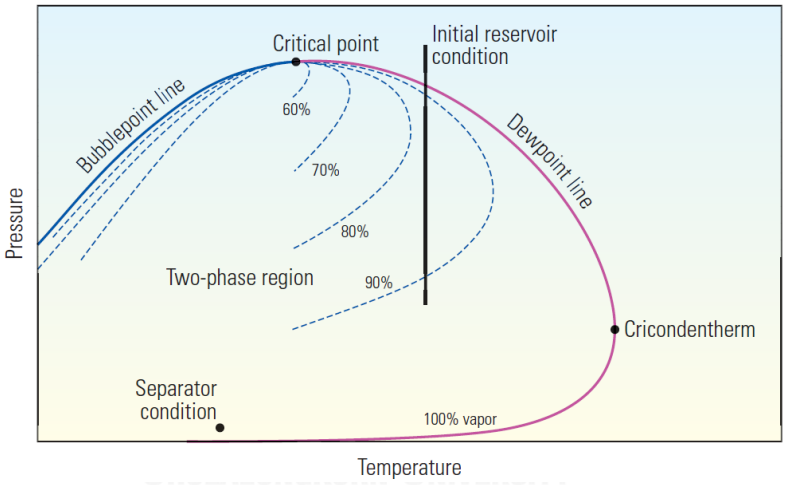

Figure 2.1: Phase diagram of a gas condensate reservoir [1]

Fan et al. [1] stated that at the early time of liquid form out of condensate, the liquid is trapped in the pore because capillary forces acts on the fluids, those liquid accumulations and normally mobility can be neglected when it is faraway except near wellbore this effect becomes significant. As it can be seen in Figure 2.2 that once liquid drops out and forms condensate banking around the wellbore, relative permeability of gas decreases when relative permeability of liquid increases. This is because two fluids, gas and liquid, try to compete each other for flow path. Consequently, there are two drawbacks from this effect. Firstly, gas and condensate production decrease because of

near wellbore condensate. Secondly, produced gas contains fewer valuable heavy ends because they have been lost while flowing toward the well during production.

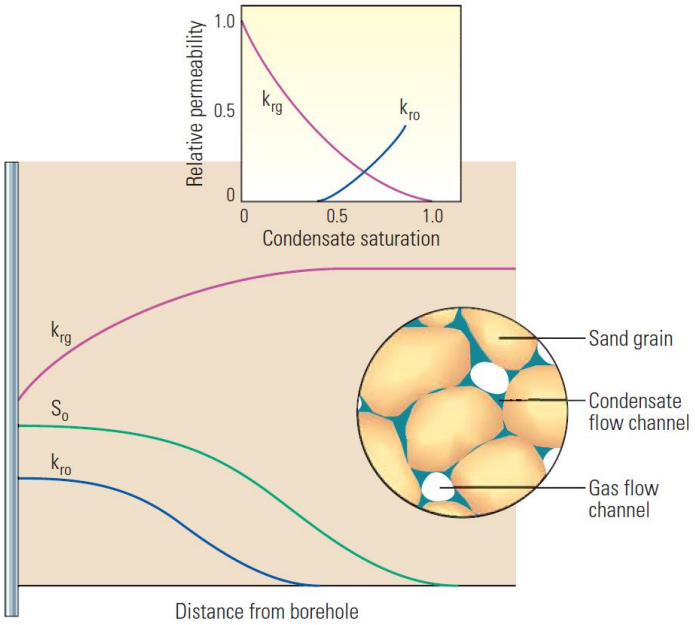

Figure 2.2: The effect of condensate banking on relative permeability to gas and liquid [1]

The amount of liquid that drop out of the gas is not only depending on pressure and temperature but also depending on compositions of the fluid itself. Akpabio et. al. [2] mentioned the classification of gas condensate fluid can be categorized based on the condensate gas ratio (CGR) into four types which are lean, medium, rich and very rich condensate as they are shown in Table 2.1.

Table 2.1 Classification of gas condensate fluids [2]

	Lean	Medium	Rich	Very rich
CGR (STB/MMSCF)	< 50	50-125	125-250	>250

The loss of production due to condensate banking accumulation near wellbore have been reported in many field. Afidick et al. [3] proved the effect of condensate banking by using the plot of productivity index with reservoir pressure and compositional simulation. The results indicated strong evidence of reduction in productivity index affected by condensate banking and in some wells the loss are higher than 50%.

Barnum et al. [4] also reported a loss of production that can be shown as gas recoveries below 50% and show clear evidence in low permeability reservoir, kh is lower than 1,000 md-ft. as a result some wells died in severe cases.

Fevang and Whitson [5] developed the study of Jones and Raghavan [6] and proposed the pseudo pressure integral model which separated a conceptual area around the wellbore into three regions that has been widely used in several literatures as they are shown in Figure 2.3 and 2.4 which are

Region 1 condensate and gas are mobile, and flowing composition is constant. This zone is the major cause of well productivity loss due to the competition between gas and liquid flow in porous media where liquid saturation in this region exceeds critical liquid saturation. The range of this region is depending on gas condensate type. For lean gas, it can be only tens feet away. While for rich condensate, the range can extent to hundreds of feet from the wellbore.

Region 2 two-phase region, where condensate is immobile and gas is mobile. In this zone, fluid saturation keeps increasing, hence, it reduces relative permeability to gas. The inner boundary of this region has saturation almost equal to critical liquid saturation where liquid starts to flow.

Region 3 single phase region with constant composition, equal to the original fluid reservoir. The inner boundary of this region is where the condensate banking starts to form because it has pressure equal to dew point pressure as it is shown in Figure 2.3 and this boundary will move outward as pressure is deplete throughout the reservoir and eventually disappear when pressure at the outer boundary falls below dew point pressure.

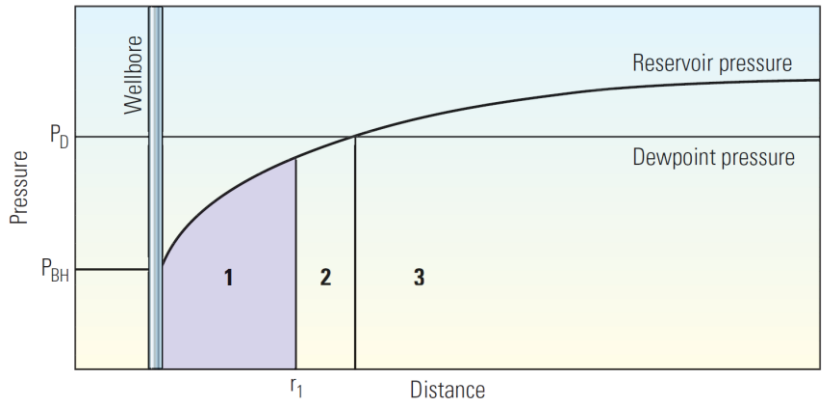

Figure 2.3: Condensate pressure profile in a gas condensate reservoir [1]

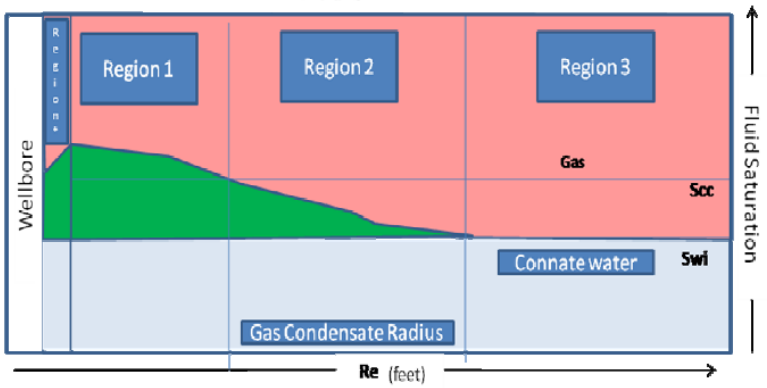

Figure 2.4: Condensate saturation profile in a gas condensate reservoir [5]

However, their approach of pseudo-pressure integral still has limitation on how to quantifying gas productivity because their model does not take condensate blockage as skin near wellbore but instead they take it as pressure expression. Hence, it cannot explain the reduction of gas when condensate banking occurs explicitly.

Another study of El-Banbi et al. [7] shows the unusual production data of moderately rich gas condensate reservoir that productivity of the well was initially decrease rapidly and then increase again when reservoir pressure was depleted. The reason of this behavior is that when pressure throughout the reservoir falls lower than dew point pressure gas that flowing into the wellbore become leaner. Hence, this leaner gas makes condensate saturation near wellbore decrease then relative permeability to gas increases and productivity of the well increase at the late time.

2.2 Mitigating Condensate Banking Effect by Hydraulic Fracturing

The loss of production in condensate reservoir leads to several techniques that have been used to reduce and prevent this problem such as

- Chemical and solvents in wettability alteration to reduce the impact of condensate banking
- Gas cycling and injecting dry gas such as nitrogen and carbon dioxide to maintain pressure inside the reservoir
- Drilling horizontal wells, acidizing and hydraulic fracturing to increase well productivity

Carlson and Myer [8] originally forecast production from condensate well for development and they found the productivity loss from condensate banking. Introducing hydraulic fracturing to the well was effective and was their recommendation to reduce pressure drawdown and thus reduce the effect from condensate banking.

Settari et al. [9] studied effects of condensate banking on productivity index of hydraulically fractured wells. They found that the proppant fracturing appears to be the effective approach to reduce condensate banking on productivity index. The multiphase flow can cause a significant loss on productivity index for unfractured well. While in case of fractured well can bring productivity index back to the similar or even higher value than the unfractured one. However, the effectiveness of hydraulic fracturing in returning productivity index is depending on reservoir heterogeneity and volume of condensate in the pore space.

Al-Hashim and Hashmi [10] investigated the effect of hydraulically fractured well comparing with unfractured well on multi-layered rich gas condensate reservoir by using compositional simulator. From their study, it shows that hydraulic fracturing can improve the productivity of condensate wells both above and below the dew point pressure. Moreover, it can prolong the time for pressure to reach the dew point pressure thus keep the plateau production longer than unfractured well. However, the main problem that may

occur in hydraulically fractured well is the fracture-face damage from the accumulation of liquid and cause impairment in the permeability normal to the fracture face.

Carvajal et al. [11] evaluated the impact of positive coupling and inertial effect on design of fracturing and well performance by using compositional parameter and found that the negative impact is mainly limited to the fracture region, while the positive coupling contribution comes from matrix region. They also suggested that fracture width is important for controlling the inertial effect in hydraulically fractured well for condensate.

Mahdiyar et. al. [12] studied productivity of hydraulic fracturing in horizontal well and compared those results between steady and pseudo steady states conditions. In their study, they found that at the same pressure drop, inertial effect shows higher effect on longer fracture and it is decreased if fracture width is increased.

CHAPTER 3

THEORY AND CONCEPT

3.1 Effect of Velocity Dependent Relative Permeability Near Wellbore

Ali et al. [13] studied the effect of high velocity flow near wellbore both experiment and simulation, and reported that at high velocity the relative permeability of gas tends to increase and also gas deliverability. This is because of high capillary number.

Narayanaswamy et al. [14] modeled a single wellbore of lean gas condensate and study the action of both velocity dependent relative permeability and non-Darcy flow. They indicated that high velocity tends to increase gas relative permeability of near wellbore vicinity but in same time, non-Darcy flow can be occurred and cause the disadvantage on well productivity.

Mott [15] and Belhaj et al. [16] suggested that in forecasting gas condensate well productivity, the effect of non-Darcy flow or inertial effect and capillary numbers that can affect the relative permeability should be included into the simulator. Otherwise, the simulator would show an inaccurate productivity. In addition, the net effect of the two high velocity phenomena has benefit on productivity more than considering the effect of non-Darcy alone.

Non-Darcy Flow Effect

It has been reported in several literatures that conventional Darcy's equation is not capable of explaining gas flow behavior accurately since gas normally flows at high velocity because of the its low viscosity. Especially, in the near wellbore vicinity, this problem would become more severe because of excessive pressure drop due to inertial effect. To solve this issue, non-Darcy flow in quadratic equation was introduced by Forchheimer [17] as it is shown in Equation 3.1.

$$\frac{dp}{dr} = \left(\frac{\mu}{k}\right) v + \beta \rho v^2 \qquad (3.1)$$

Where

$\frac{dp}{dr}$ = pressure gradient at radius r $\left(\frac{atm}{cm}\right)$

μ = viscosity of the fluid (cp)

β = non-Darcy flow coefficient (cm^{-1})

k = permeability (Darcy)

ρ = density of the fluid $\left(\frac{gm}{cc}\right)$

v = velocity $\left(\frac{cm}{sec}\right)$

Chaudhry [18] mentioned that in simulating the model, non-Darcy effect is mostly and should be taken as rate dependent skin, and the non-Darcy flow coefficient (β) can be identified multiple test of flow rate. However, in Forchheimer equation, the non-Darcy flow coefficient (β) considers only for single phase of gas but in the study of condensate reservoir that near wellbore vicinity contains two phase of gas and liquid which will cause higher condensate dropout because of the inertial effect between two phases. Therefore, choosing an appropriate correlation is required in the calculation of non-Darcy flow coefficient (β) which can be seen in the study of Geertsma [19] that takes permeability, gas relative permeability, porosity and water saturation as it is shown in Equation 3.2.

$$\beta = \frac{0.005}{(kk_{rg})^{0.5}[\emptyset(1-s_w)]^{5.5}} \quad (3.2)$$

Where

β = non-Darcy flow coefficient (cm^{-1})

k = reservoir permeability (cm^2)

k_{rg} = gas relative permeability (fraction)

$\emptyset$ = porosity (fraction)

s_w = water saturation (fraction)

Capillary Number Effect

When the flow velocity is high, especially gas flow, one might take consideration of including the capillary number effect into the calculation. Several studies such as Asar and Handy [20], Ali et. al. [13] and McDougall [21] reported the measurement of relative permeability of gas and condensate as the function of the interfacial tension (IFT). These studies show that when relative permeability of gas increase significantly, the IFT between gas and condensate decreases. Blom and Hagoort (1998) [22] explained the definition of capillary number as the ratio of viscous force on capillary force of the trapped phase (IFT).

$$N_c = \frac{v_g \mu_g}{\sigma_{og}} \tag{3.3}$$

Where

N_c = capillary number

v_g = gas velocity

μ_g = gas viscosity

σ_{og} = condensate-gas interfacial tension

There is a point where capillary number has no effect on the phase relative permeability, which is called “base capillary number” or N_{cbp}. It is included in “normalized capillary number equation” or $N_{cnp.}$

$$N_{cnp} = \frac{N_{cbp}}{N_{cp}} \tag{3.4}$$

Generally, N_{cbp} can be determined experimentally at near ambient conditions. Therefore, the reservoir gas and condensate are at different in compositions and gas-oil surface tension is likely to be at its maximum. While, the low-pressure gas viscosity is likely to be at its minimum. The use of capillary number can be applied into two classes which are Corey relative permeability function and the interpolation between immiscible and miscible relative permeability functions.

Capillary Number Dependent Corey Coefficient.

In this correlation, Corey coefficients depend on capillary number as it is shown in the Equation 3.5. Benefits from using Corey function is that it is based on important aspects of relative permeability such as tortuosity and non-conductivity saturation. Therefore, the effect of low interfacial tension and high velocity can be translated directly on this function. Secondly, it allows the relative permeability characteristic can be changed independently as a function of capillary number. And lastly, plausible relationship between relative permeability and capillary number can be generated without experimental data. However, this function is highly non-linear, so that fitting the function to a large data set may give convergence problem.

$$k_{r\alpha}(S_\alpha, N_c) = k^*_{r\alpha}(N_c)\left(\frac{S_\alpha - S_{r\alpha}(N_c)}{1 - S_{r\alpha}(N_c)}\right)^{\varepsilon_\alpha(N_c)} \quad (3.5)$$

Where

$k^*_{r\alpha}$ = end-point relative permeability

S_r = residual saturation

ε = Corey exponent that fixes the curvature of the relative permeability function

α = phase indicator (gas, condensate)

Interpolation Between Immiscible and Miscible Relative Permeability Functions

Relative permeability curves at near critical conditions have often been represented by a weighted linear function of immiscible (low capillary number) and miscible (high capillary number) relative permeability curve, where the weighting factor is a function of the capillary number as it is shown in Equation 3.6. This approach is particularly suitable for large sets of measured data on relative permeability at varying capillary numbers. The capillary number is more explicit than the previous approach, so that less problem on convergence issue. However, it has the problem on residual saturation and gives undesirable consequence when this correlation is used in the simulation.

$$k_{r\alpha}(S_\alpha, N_c) = f_\alpha(N_c) k_{r\alpha I}(S_\alpha) + \{1-f_\alpha(N_c)\} k_{r\alpha M}(S_\alpha) \quad (3.6)$$

Where

$k_{r\alpha I}$	=	relative permeability for capillary dominated (immiscible) flow
$k_{r\alpha M}$	=	relative permeability for capillary dominated (miscible) flow
f	=	weighting function
α	=	phase indicator (gas, condensate)

3.2 Fundamental of Hydraulic Fracturing

Based on rock mechanic theory, the procedure of increasing hydrocarbon production by using hydraulic fracturing can be performed by injecting fluid into the target formation at the sufficient pressure to create fractures at tensile failure on the minimum stress of the rock with higher conductivity extending from wellbore and allow fluid to flow into fractures and then wellbore easily. Hence, making that tight formation can be produced at economical rate.

However, as the depth increases, the overburden stress in the vertical direction also increases, then reservoir will be suppressed by confining pressure from the load of overlaying rock and fractures attempt to close themselves at the end of fracture tips. Therefore, proppants are required in the procedure to keep fractures remain open, and permit fluid to flow along their operational lives.

Moreover, when the costs associate with drilling, completion and condensate banking complication in condensate reservoir, hydraulic fracturing in horizontal direction has become more competitive because it positively gives higher hydrocarbon production due to the higher contact area of fracture and reservoir. Moradi et al. [23] investigated the comparison of well direction and mentioned that pressure drawdown and condensate banking is smaller for a horizontal well compared to the vertical well.

The orientation of fracture planes in horizontal well can be divided into two configurations which are longitudinal and traverse depending on wellbore orientation drilling through horizontal stress of the rock. Longitudinal fractures are occurred as the

function of wellbore orientation drill along the maximum horizontal stress, while transverse fractures are results of wellbore orientation drill along the minimum horizontal stress as it is represented in Figure 3.1. And typically, transverse fracture gives higher production.

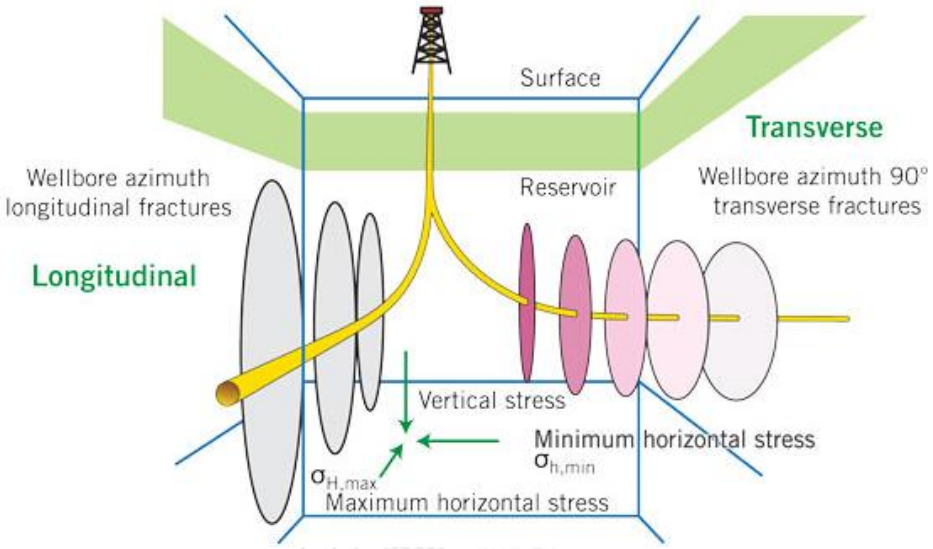

Figure 3.1: Fracture development as a function of wellbore orientation [24]

3.3 Effective Parameters on Hydraulic Fracturing

Economides *et al.* [25] showed fracture conductivity represents the ease of fluid to flow inside the fracture to wellbore. Relative capacity, “a”, from pressure profile in fractured reservoir is presented in Equation 3.7.

$$a = \frac{\pi k x_f}{2 k_f w} \tag{3.7}$$

Dimensionless fracture conductivity is the relative measurement between ability of produced fluid flow inside fracture compared to the ability of the formation to feed fluid into the fractures, and it can be defined from works of Argawal [26] by the following equation

$$F_{CD} = \frac{k_f w}{k x_f} \tag{3.8}$$

From Equation 3.7 and 3.8, they can be combined and presented as

$$F_{CD} = \frac{\pi}{2a} \tag{3.9}$$

Moreover, dimensionless effective wellbore radius in hydraulic fractured well was another concept that was introduced, the relative capacity and effective well radius have a relationship is shown in Figure 3.2

$$r'_{wD} = \frac{r'_w}{x_f} \tag{3.10}$$

$$r'_w = r_w e^{-s_f} \tag{3.11}$$

When

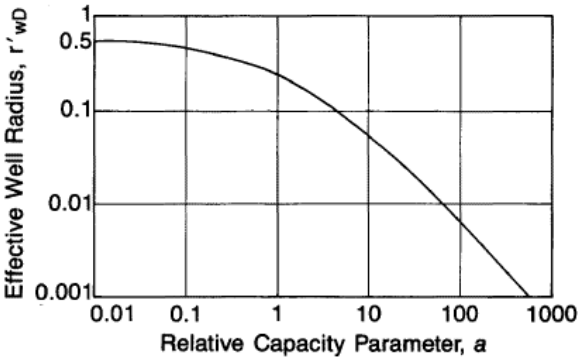

Figure 3.2: The concept of effective wellbore radius vs. relative capacity [25]

From Figure 3.2, at a small value of relative capacity or at high fracture conductivity gives the following equation

$$r'_w = \frac{x_f}{2} \tag{3.12}$$

Where

a	=	relative capacity
F_{CD}	=	dimensionless fracture conductivity
k_f	=	fracture permeability
w	=	fracture width
x_f	=	fracture half-length
r'_w	=	effective wellbore radius
r'_{wD}	=	dimensionless effective wellbore radius
s_f	=	skin in fracture

Economides [27] mentioned that typically fracture width of a hydraulic fracture is 0.25 in. (0.02083 ft.) or less, while effective fracture half-length can reach up to the length of 3,000 ft. from tip to tip. Moreover, he also concluded that in the reservoir with high fracture conductivity or small relative capacity which can be implied that it has low permeability reservoir, fracture half-length would be more effective than fracture permeability. And the effective wellbore radius will be equal to half of the fracture half-length. When relative capacity is very large or reaching to 1,000, effective wellbore radius will be decreased. Hence, when fracture is designed it should have relative capacity less than 1 ($a < 1$) or fracture conductivity higher than 1.6 ($F_{CD} > 1.6$)

Fracture spacing is one of the important parameter on hydraulic fracturing. From the study of Soliman et al. [28] they studied the effect of number of fracture in the constant wellbore length, which can be implicitly understand that when number of fracture increases then fracture spacing will decrease. However, at some point of increasing number of fractures, the cumulative production and rate of production might show gradual increment on the production. Hence, from their study indicated that optimum number of transverse fractures depends on reservoir and fluid properties, also including reservoir area and more than two fractures is recommended to drain the reservoir.

To keep created hydraulic fracture width opening and create highly conductive system of fracture, propping material such as sand, resin coated sand and ceramics are suggested to be used. Each type of the proppant has the ability to withstand closure pressure differently as they are shown in Figure 3.3. While, typical proppant and their characteristics are shown in Table 3.1.

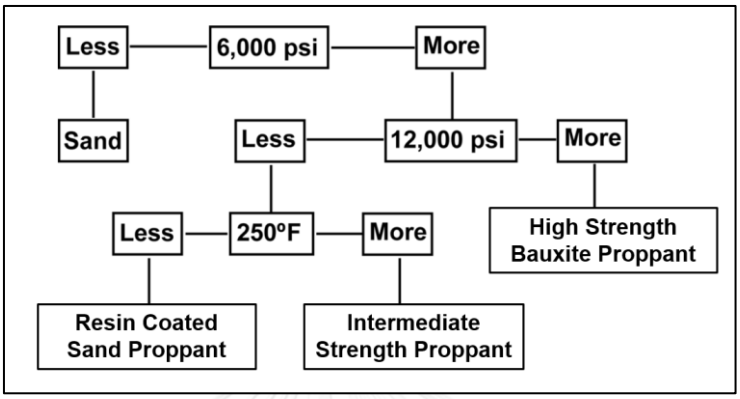

Figure 3.3 Proppant selection based on closure pressure [29]

Table 3.1 Typical proppants and their characteristics [25]

Type	Mesh Size	Particle Size (in.)	Density (lb/ft^3)
Northern White sand	12/20	0.0496	165
	16/30	0.0350	165
	20/40	0.0248	165
Texas Brown sand	12/20	0.0496	165
	16/30	0.0350	165
	20/40	0.0248	165
Curable resin-coated sand	12/20	0.0496	160
	16/30	0.0350	160
	20/40	0.0248	160
Precured resin-coated sand	12/20	0.0496	160
	16/30	0.0350	160
	20/40	0.0248	160
ISP	12/20	0.0496	198
	20/40	0.0248	202
ISP-lightweight sintered bauxite	20/40	0.0248	170
	16/20	0.0400	231
	20/40	0.0248	231
	40/70	0.0124	231
Zirconium oxide	20/40	0.0248	197

Larger proppant sizes give higher permeability. However, they are more liable to be crushed at higher closure pressure because strength of proppant decreases when proppant size increases. Also with the fact that larger grain sizes construct larger pore sizes where fragments of crushed proppants can migrate and occupy inside those pore spaces. Hence, their advantage might disappear at higher stress.

Therefore, several properties should be considered for proppant selection because they have long term effect on fracture conductivity such as grain size and its distribution, and permeability of proppant pack. These properties are all affected by the stress value at different stages in the life of the reservoir as they are shown in Figure 3.3 from the study of Butula et.al. [30]

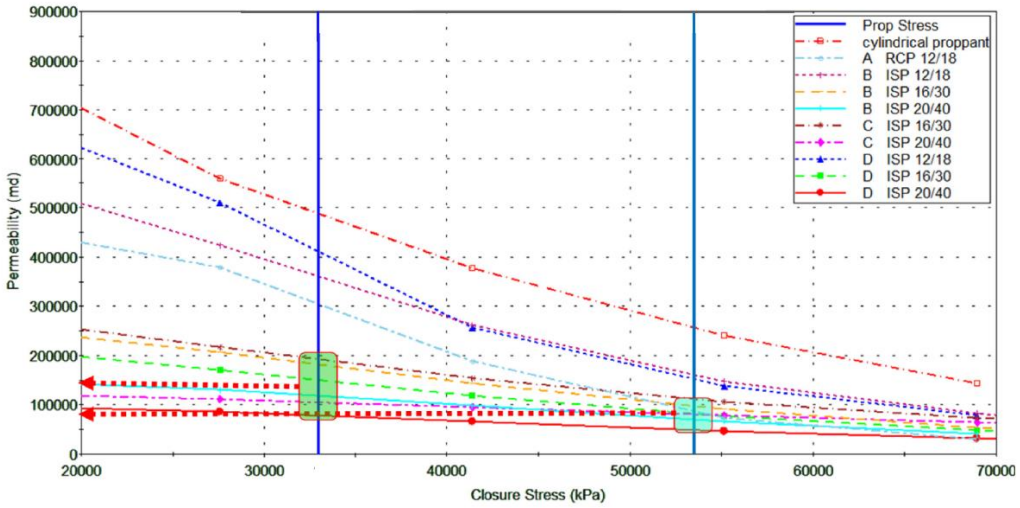

Figure 3.4 Proppant permeability for different effective stresses at different stages in the life of reservoir [30]

3.4 Condensate Blockage in Simulation

There are several models that can be implemented in condensate banking study which are the single well model and full field model.

In a single well model, the well is treated as the two dimensional of radial distance and height. Mostly, grid blocks near wellbore are designed to be a small size and increase logarithmically as it is farther away. By doing this, it will give a good result where the complexity of saturation comes becomes the main effect of well productivity reduction. The capillary number, viscous and inertial forces are also allowed to be included in this model appropriately, which increases benefit of accuracy to this model.

In full field model couples with the use of local grid refinement (LGR) is also pronounced to be one of the most accurate approach to study near wellbore behavior in gas condensate reservoir. However, using LGR may significantly increase computation time and cost.

Another alternative approach that has been used largely is the use of full field model with pseudo-pressure. The flow equation for gas in the reservoir is integrated over pressure. By using this approach, model in the reservoir will be characterized into three separate regions based on fluid behavior and saturation as it is mentioned in the study of Fevang and Whitson [5] and led to the further study of generalized pseudo-pressure approach which can be seen in many general commercial simulators.

However, according to the study of Barker [31] that performed comparative study between those three models that have been mentioned above. The result from his study shows that, the finely-gridded, compositional, single well models which could be radial or otherwise with the consideration of velocity dependent relative permeability and non-Darcy flow, is considered to be the most accurate model in his study yet uncertainty still remains on the input parameter. While generalized pseudo-pressure gives optimistic result when it is used in field scale study, even with fine scale resolution (LGR) also computationally prohibitive and creates problem of convergence when solving. Hence, there is no one hundred percent accuracy in any model, but the appropriate model can be chosen based on the aspect of certain study.

CHAPTER 4

RESERVOIR SIMULATION MODEL

In order to determine optimal production on each scenario, reservoir simulation is used as an instrument to predict and assist the understanding of reservoir and fluid behavior. Therefore, the result can be seen explicitly and the best strategy can be obtained. The reservoir simulator, Eclipse 300 is chosen in this study because its specialized function in compositional modelling and also provide accurate calculation by allowing the non-Darcy flow and capillary number effect to be included.

4.1 Reservoir Model Description

The simulation model is a single homogeneous layer in rectangular shape, low permeability condensate reservoir, top of the model is at 8,000 ft. and fracture fully penetrates the vertical extent of the formation with parameters that are shown in Table 4.1

Table 4.1: Key reservoir and model parameters

Parameter	Value	Unit
Reservoir porosity	15	%
Formation permeability	0.2	mD
Vertical permeability	0.02	mD
Water saturation	20	%
Initial reservoir pressure	3,500	psia
Reservoir temperature	228	Fahrenheit
Reservoir depth	8,000	ft.
Net pay	110	ft.
Horizontal well length	2,700	ft.
Tubing diameter	2-7/8	in. (OD)

4.2 Gridding

Cartesian grid model and block centered geometry are used for this model. The reservoir dimensions are 3,100 ft. × 1,550 ft. × 110 ft. with 31 × 31 × 11 cells in the x-, y- and z- direction respectively. Grid block sizes in each direction are shown in Table 4.2.

Table 4.2: Sizes of grid blocks

Dimension	x-direction	y-direction	z-direction
Grid block (No.)	31	31	11
Size (ft)	100	50	10
Total (ft)	3,100	1,550	110

4.3 Local Grid Refinement

To capture the change of saturation in both gas and condensate near wellbore and to enhance the accuracy of near wellbore region and fracture calculation, the local grid refinement (LGR) is applied in this study. LGR allows the user to refine parent grid blocks into smaller grid blocks with variable sizes and reservoir properties. Therefore, fracture properties such as porosity, permeability and width can be specified from this option. However, applying LGR to the entire model would be a tedious work. Hence, LGR in this study is applied only to some sections of the reservoir which are near wellbore section and fractured regions. The horizontal well is placed in the middle of the reservoir model at coordinate of I-16, J-16 and K-6 along x-direction with the length of 2,700 ft. The summary of local grid refinement on each coordinate and number of cells are shown in Table 4.3.

Table 4.3: Local grid refinement

LGR Name	LGR Coordinate			Number of refinement cells		
	I	J	K	X	Y	Z
WELL	3-29	1	1-11	243	9	1-11

Hegre [32] and Kroemer et. al. [33] suggested to specify small grid size near fractures and then increase those grid size away from the fracture would be the most applicable method in the study of hydraulic fracturing. In this study, 50 ft. wide grid blocks are refined into 9 smaller grids and logarithmically increased both sides of the fractures in x-direction. Three fracture widths and their sizes are shown in Table 4.4.

Table 4.4: Sizes of locally refined fracture grid blocks for fractures

Fracture width (ft)	Local grid size (ft)								
	L#1	L#2	L#3	L#4	L#5	L#6	L#7	L#8	L#9
0.00833	40.0	9	0.9	0.0958	0.00833	0.0958	0.9	9	40.0
0.01250	36.1	12.5	1.25	0.125	0.0125	0.125	1.25	12.5	36.1
0.02500	22.2	25	2.5	0.25	0.025	0.25	2.5	25	22.2

Figure 4.1 and Figure 4.2 show the aerial view of the simulation grid and LGR that has been defined near fracture plane and wellbore grid structure to capture the abrupt change of pressure near wellbore vicinity and Figure 4.3 exhibits the side view of the reservoir model that horizontal wellbore has been placed in the middle of the formation.

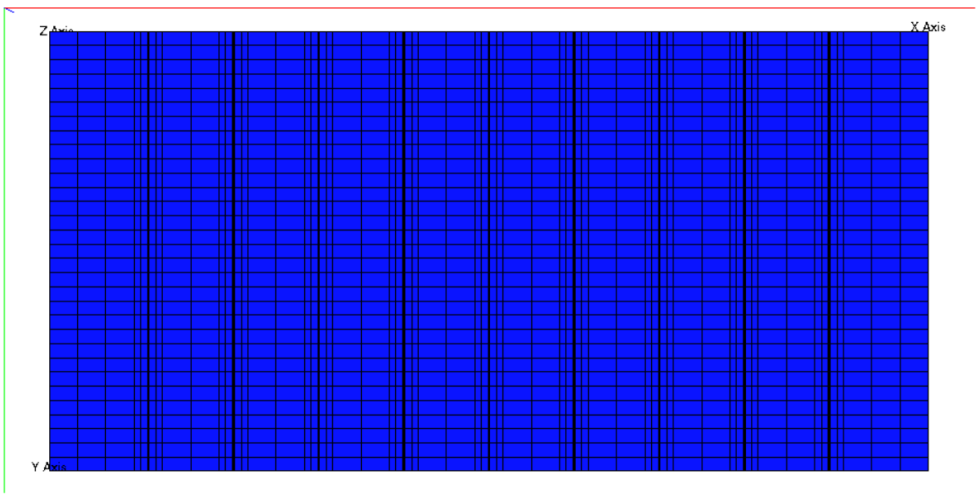

Figure 4.1: Aerial view of the reservoir model with 9 fractures

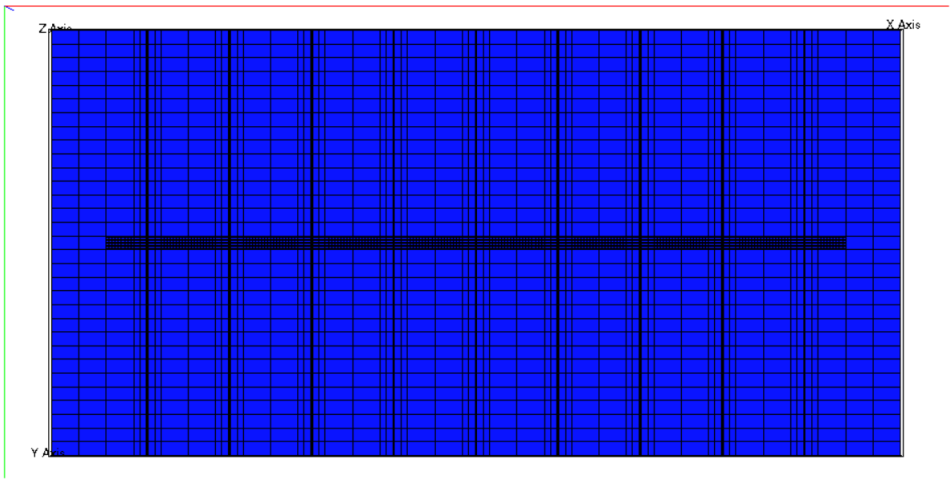

Figure 4.2: Aerial view of the reservoir model at the middle layer showing wellbore grid structure

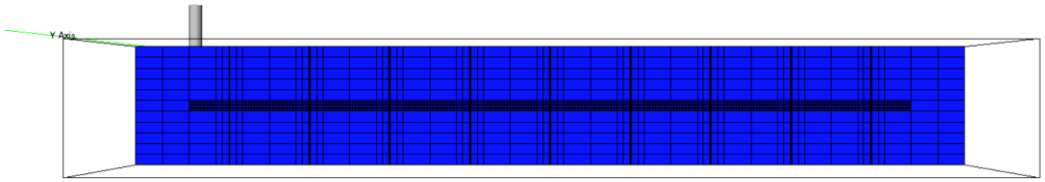

Figure 4.3: Side view of the reservoir model

4.4 Fluid Section

4.4.1 PVT Modeling

The reservoir temperatures are set at 228 °F for lean condensate and 330 °F for rich condensate. The initial fluid compositions, water PVT and fluid densities are shown in Table 4.5, Table 4.7 and Table 4.8 respectively. Lean condensate composition is from the study of Thitaram [34] and the actual field data of rich condensate was provided by Carigali-PTTEPI Operating Company.

Table 4.5: Initial fluid compositions

Component	Formula	Mole percent	
		Lean Condensate	Rich Condensate
Carbon dioxide	CO_2	1.06	0.17
Nitrogen	N_2	0.21	0.19
Methane	C_1	64.81	53.39
Ethane	C_2	5.27	11.14
Propane	C_3	6.23	5.97
Iso-Butane	i-C_4	1.67	2.83
n-Butane	C_4	3.09	2.45
Iso-Pentane	i-C_5	1.37	5.63
Pentane	C_5	1.31	4.88
Hexane	C_6	1.59	5.66
Heptane	C_7	13.39	-
Heptane-plus	C_{7+}	-	7.69

. A compositional PVT equation of state based program PVT*i* is used for characterizing a type of fluid samples. Phase behavior of lean and rich condensate compositions are shown in Figure 4.4 and Figure 4.5. Lean condensate has dew point pressure at 3,499 psia with the CGR at 18.09 STB/MMSCF. Rich condensate has dew point pressure at 3,423 psia and CGR is 125.67 STB/MMSCF. Type of fluid can be specified by using the classification in the study of Akpabio et. al. [2] that was mentioned before in Chapter 2.

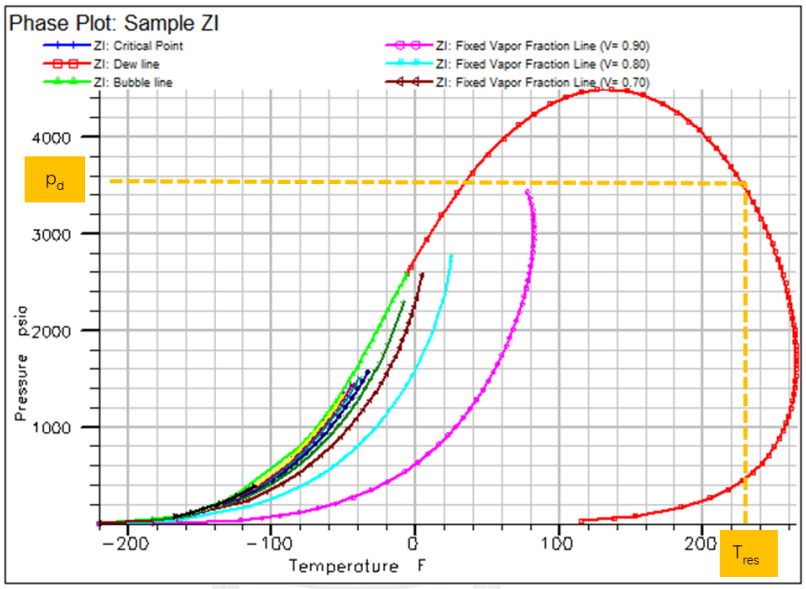

Figure 4.4: Phase behavior of lean condensate composition

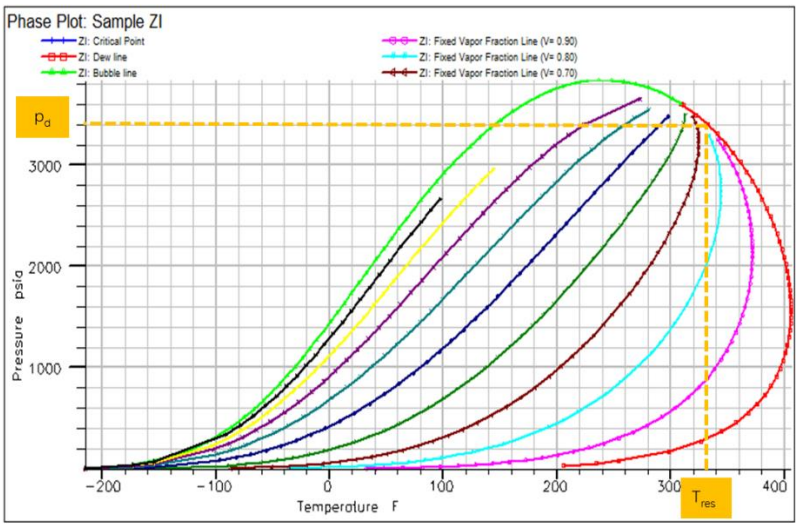

Figure 4.5 Phase behavior of rich condensate composition

The physical properties of each component are obtained from Engineering Data Book [35] as they are shown in Table 4.6.

Table 4.6: Physical properties of each component

Component	Formula	Boiling Point (°R)	Critical pressure (psia)	Critical temperature (°R)	Critical Volume (ft3/lb-mole)	Molecular Weight	Acentric factor
Methane	CH_4	201.28	667.0	343.34	0.0988	16.043	0.0108
Ethane	C_2H_6	332.54	707.8	550.07	0.0783	30.07	0.0972
Propane	C_3H_8	416.27	615.0	665.92	0.0727	44.097	0.1515
Iso-Butane	C_4H_{10}	470.78	527.9	734.41	0.0714	58.123	0.1852
n-Butane	C_4H_{10}	491.08	548.8	765.51	0.0703	58.123	0.1981
Iso-Pentane	C_5H_{11}	542.09	490.4	828.96	0.0684	72.15	0.2286
Pentane	C_5H_{12}	556.89	488.1	845.7	0.0695	72.15	0.251
Hexane	C_6H_{14}	615.7	439.5	911.8	0.0688	86.177	0.299
Heptane	C_7H_{16}	669.07	397.4	970.9	0.0682	100.204	0.3483
Carbon dioxide	CO_2	350.76	1069.5	547.73	0.0342	44.01	0.2667
Nirtrogen	N_2	139.56	492.8	227.51	0.051	28.013	0.037

Table 4.7: Water PVT properties

Properties	Value
Reference pressure, psi	3,500
Water FVF at the reference pressure, rb/stb	1.071
Water compressibility, psi^{-1}	4.06E-06
Water viscosity at the reference pressure, cP	0.18
Water viscosity, psi^{-1}	8.57E-06

Table 4.8: Fluid densities and rock properties

Parameter		Lean condensate	Rich Condensate
Fluid densities and rock properties	Oil density, lb/ft^3	56.23	52.42
	Water density, lb/ft^3	0.99	0.99
	Gas density, lb/ft^3	0.85	0.77
Rock properties	Reference pressure, psia	3,500	
	Rock compressibility, psi^{-1}	3.06E-06	

4.4.2 SCAL (Special Core Analysis) Section

The average SCAL values are obtained from gas field in Gulf of Thailand [34]. The relationship between of gas saturation, gas relative permeability and oil relative peremeability is tabulated in Table 4.9 and Figure 4.6. And water saturation, water relative permeability and oil relative peremeability is tabulated in Table 4.10 and shown in Figure 4.7.

Table 4.9: Gas saturation, gas relative permeability and oil relative permeability

S_g	k_{rg}	k_{ro}
0	0	0.80000001
0.15000001	0	0.33750001
0.20625	0.001171875	0.22609863
0.26249999	0.009375	0.14238282
0.31874999	0.031640626	0.082397461
0.375	0.075000003	0.042187501
0.43125001	0.14648438	0.017797852
0.48750001	0.25312501	0.005273438
0.54374999	0.40195313	0.00065918
0.60000002	0.60000002	0
0.80000001	1	0

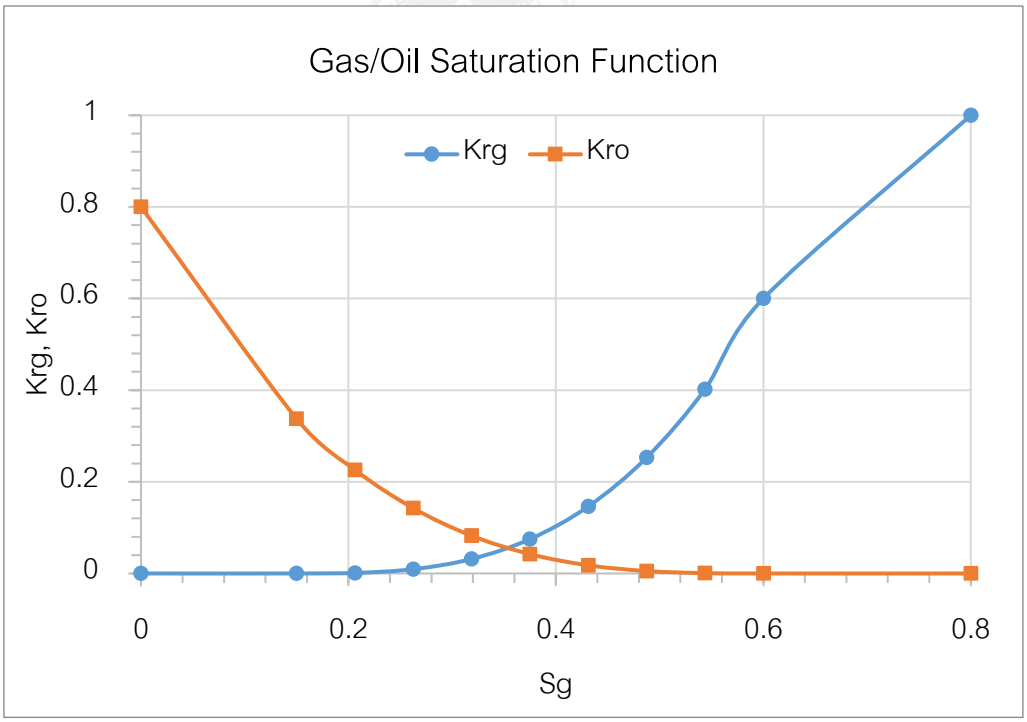

Figure 4.6: Gas/Oil Saturation Function

Table 4.10: Water saturation, water relative permeability and oil relative permeability

S_w	k_{rw}	k_{ro}
0.2	0	0.80000001
0.26666668	4.57E-05	0.56186557
0.33333334	0.000731596	0.37640604
0.40000001	0.003703704	0.23703703
0.46666667	0.011705533	0.1371742
0.53333336	0.028577961	0.070233196
0.60000002	0.059259258	0.029629629
0.66666669	0.10978509	0.00877915
0.73333335	0.18728852	0.001097394
0.80000001	0.30000001	0

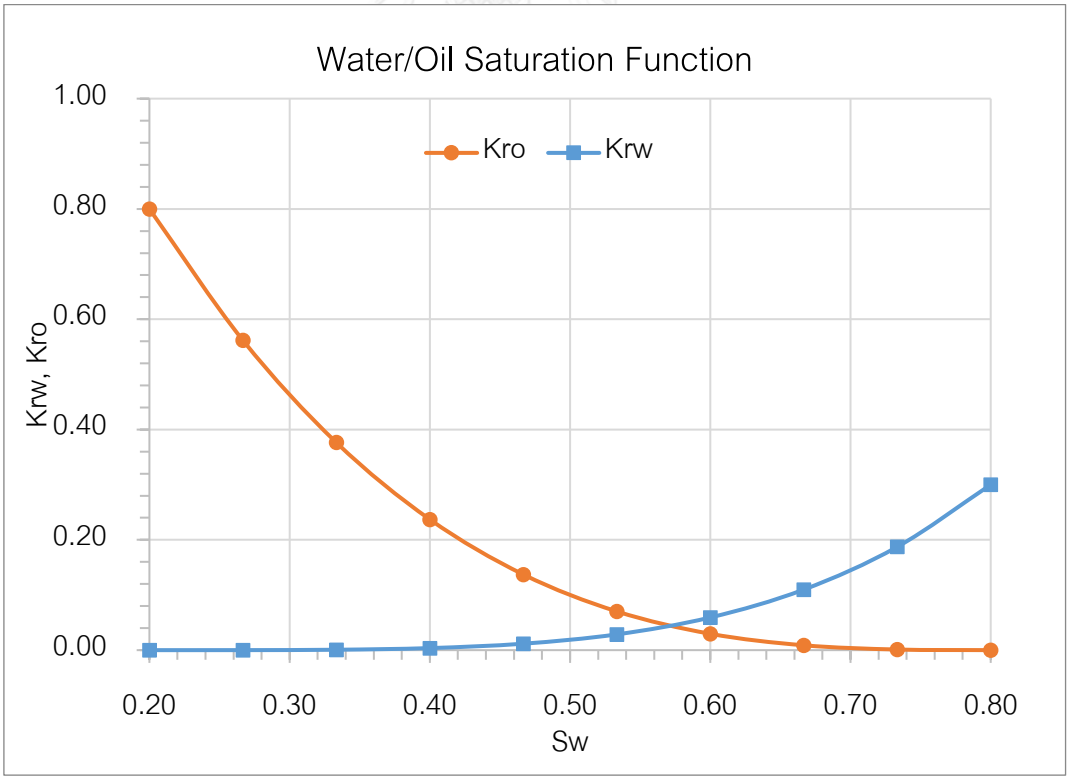

Figure 4.7: Water/Oil Saturation Function

4.5 Wellbore Section

The horizontal well is located at the depth of 8,055 ft. with wellbore diameter of 6 ½ in. and tubing diameter of 2 $^{7}/_{8}$ in. is placed along the production formation along x-direction for 2,700 ft. Well head is located in local grid HZ3 at the reference depth of 8,000 ft. and simulator is set to produce gas as the preferred phase as they are shown in Table 4.11 and Table 4.12.

Table 4.11 LGR Well Specification (WELSPECL)

Parameters	Well P1
Name of local refine grid	HZ3
I Location of well head in local grid	1
J Location of well head in local grid	5
Reference depth for bottom hole pressure (ft)	8,000
Preferred phase	Gas

Table 4.12 Completion data for wells in local grids (COMDATL)

Parameters	Well P1
K location connecting block in local grid	1-6
Local grid name	HZ3 to HZ29
Wellbore diameter	0.5417 ft

Pressure losses and detailed description of fluid flow in the wellbore along the horizontal section can be calculated by multisegment well, the extended option in ECLIPSE. This option allows user to define an appropriate wellbore friction option and to divide the wellbore into several one-dimensional segments. From Figure 4.6, each segment has its own set of independent variables to describe fluid conditions and with the combination of pressure drop that is precalculated from VFP tables, multisegment well can potentially offer greater accuracy in the calculation.

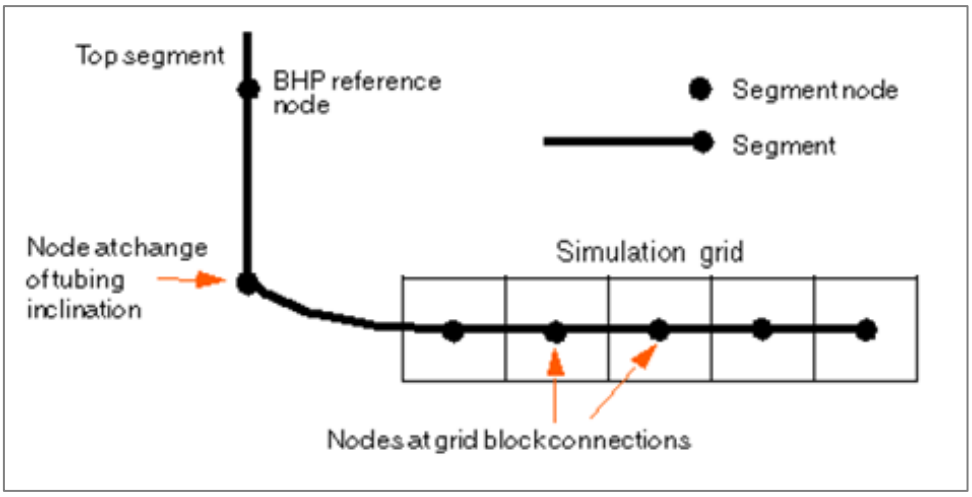

Figure 4.8: A multisegment well [36]

Table 4.13 and Table 4.14 exhibit the value of multisegment well that was applied along the horizontal well. Each multisegment has the length of 100 ft. and further divided into 9 LGR grid block with the length of 11.11 ft.

Table 4.13 Segment structure of multisegment well (WELSEGS)

Parameters	Well P1
Depth of the nodal point of the top segment (ft)	8,055
Segment number from start to end	3 to 29
The length of each segment (ft)	100

Table 4.14 Multisegment well completion in a local grid (COMPSEGL)

Parameters	Well P1
Multisegment blocks	HZ3 to HZ29
LGR-I for each block	9
Length (ft)	11.11
Direction	X

Tubing head pressure in this study is specified at 450 psia, and the gas target rate at 10,000 Mscf/day. Simulator was commanded to be executed if gas production rated fell below 500 Mscf/day. Well control and well economic limit in this study can be found in Table 4.15 and Table 4.16.

Table 4.15 Production Well Control (WCONPROD)

Parameters	Well P1
Open/shut flag	Open
Control mode	Gas rate target
Gas rate target (Mscf/day)	10,000
THP target (psia)	450

Table 4.16 Production Well Economic Limits (WECON)

Parameters	Well P1
Minimum gas production rate (Mscf/day)	500
End run flag	Yes

PROSPER software is used to generate VFP tables for the pressure loss calculation along the tubing string in the vertical section. Table 4.17 exhibits that vertical section of the well is drilling straight down to the depth of 8,055 ft. Where geothermal gradient of each condensate has surface temperature of 60 °F and 75 °F for lean and rich condensate respectively as they can be seen in Table 4.18. Default values of average heat capacities in prosper are applied for each fluid as they are shown in Table 4.19. Lastly, the vertical flow performance is varied based on different gas rate from 250 Mscf/day to 15,000 Mscf/day as they are shown in Table 4.20.

Table 4.17 Deviation Survey

Measured Depth (ft)	True Vertical Depth (ft)
0	0
8,055	8,055

Table 4.18 Geothermal Gradient

True vertical depth (ft)	Formation Temperature (°F)
0	60 and 75
8,055	229 and 332
Overall heat transfer coefficient: 3 BTU/h/ft^2/F	

Table 4.19 Average Heat Capacities

Input parameters	Value
Cp Oil	0.53 BTU/lb/F
Cp Gas	0.51 BTU/lb/F
Cp Water	1 BTU/lb/F

Table 4.20 Vertical Flow Performance (VFPPROD)

Parameter	Lean condensate			Rich Condensate	
Top Node Pressure (psia)	450				
Water Gas Ratio (STB/MMscf)	0				
Total GOR (Mscf/STB)	55.2731			7.9572	
Surface Equipment Correlation	Beggs and Brill				
Vertical Lift Correlation	Petroleum Experts 2				
Gas rate (Mscf/day)	250	500	1,000	1,500	2,500
	5,000	7,500	10,000	12,500	15,000

CHAPTER 5
RESULTS AND DISCUSSION

The natural reservoir model used the reservoir properties that are previously mentioned in the last chapter. Then the effects of the following parameters on gas and condensate productions are designed

- Fracture width
- Number of fractures and fracture spacing
- Fracture permeability

The constant gas production rate is 10,000 Mscf/day and the economic rate is 500 Mscf/day. Reservoir performance of each condition in this study is evaluated based on gas recovery factor, cumulative gas production, cumulative condensate production and saturation profile near wellbore. Table 5.1 exhibits the variable parameters in this study.

Table 5.1: Studied variable parameters

Parameter		Value		
Dimensionless Fracture Conductivity	Fracture width (ft)	0.0083	0.0125	0.025
	Fracture half length (ft)	775		
	Fracture permeability (mD)	50,000	100,000	150,000
	Reservoir permeability (mD)	0.2		
Number of fractures and fracture spacing (ft)		3 Fractures	6 Fractures	9 Fractures
		1,150	400	200
Stimulated reservoir volume (ft^3)		6,394		

5.1 Non-Fractured Well Simulation Results

It can be recognized from the results in the Table 5.2 and from Figure 5.1 to Figure 5.4 that fluid compositions have large effects on both gas and condensate production in non-fractured well.

Figure 5.1 shows that for lean condensate, the plateau rate can be maintained at 10,000 Mscf/day only for 19 days. Meanwhile, for rich condensate condition, the gas production rate can reach up to the target of 10,000 Mscf/day only a few second before drop drastically to the rate of 2,520 Mscf/day within 7 days and keeps decreasing steadily until it reaches the end of production of 4,261 days. While condensate production rate in Figure 5.2 depicts the effect of rich condensate composition gives high amount of condensate production rate up to 1,000 stb/d at the first day before drastically drops to about 200 stb/d within two months. While in lean condensate has low composition of heavy ends can produces only 115 stb/d at the beginning before decreasing continuously until the end of production at 8 years.

Gas recovery for lean condensate can be produced up to 53.45% with the cumulative gas production of 6.46 Bcf within 2,954 days or about 8 years but in rich condensate condition can give gas recovery only 48.55% with cumulative gas production of 5.28 Bcf as they are shown in Figure 5.3 and Table 5.2. However, Figure 5.4 and Table 5.2 indicates that rich condensate condition gives higher cumulative condensate production of 333.46 Mstb while in the lean condition only 55.53 Mstb can be obtained.

Figure 5.5 show reservoir pressure for lean condensate at the abandonment is 1,656 psia while in rich condensate stopped its production at 1,746 psia. The different in fluid composition gives the potential of the reservoir to produce through the abandonment pressure differently. Lean condensate has mainly methane for its composition. Therefore, the production from this reservoir contain mostly gas and has smaller portion of liquid drop out when phase behaviors change at different pressures, because of this reason, gas can be produced easily with less impediment of condensate near wellbore. Therefore, pressure in lean condensate reservoir can be drawn down to 1,656 psia, with condensate saturation of 0.022 left in the reservoir as it shown in Figure 5.6.

While in rich condensate composition that has higher portion of heavy ends in its composition gives higher chance for liquid to condense out of gas. Those condensed liquids occupy pore spaces in the reservoir are the obstruction for hydrocarbon to flow, especially, for condensate that flow harder than gas because of its high viscosity. Evidence is at the abandonment pressure at 1,746 psia of non-fractured well in rich condensate reservoir which has condensate saturation near wellbore of 0.21 which is above critical condensate saturation in the reservoir as it is shown in Figure 5.7.

Table 5.2: Comparison results between lean and rich condensate

Case	Gas recovery factor (%)	Cumulative gas production (Bcf)	Cumulative condensate production (Mstb)	Production time (Days)
Lean condensate	53.45	6.46	55.53	2,954
Rich condensate	48.55	5.28	333.46	4,261

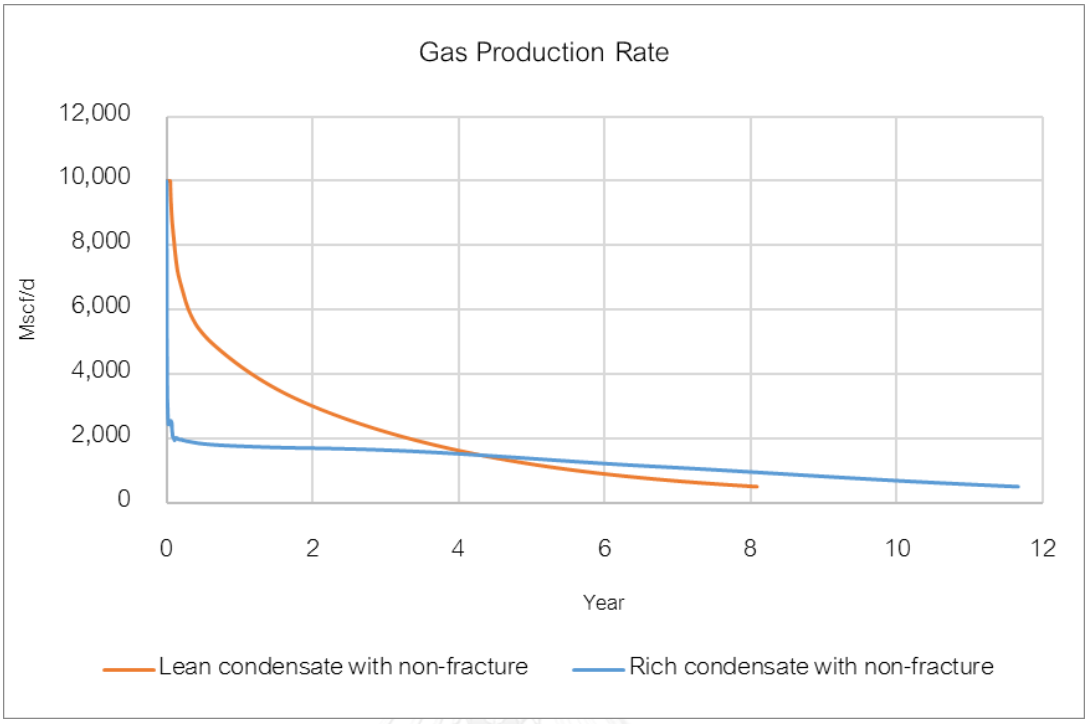

Figure 5.1: Gas production rate of non-fractured reservoir

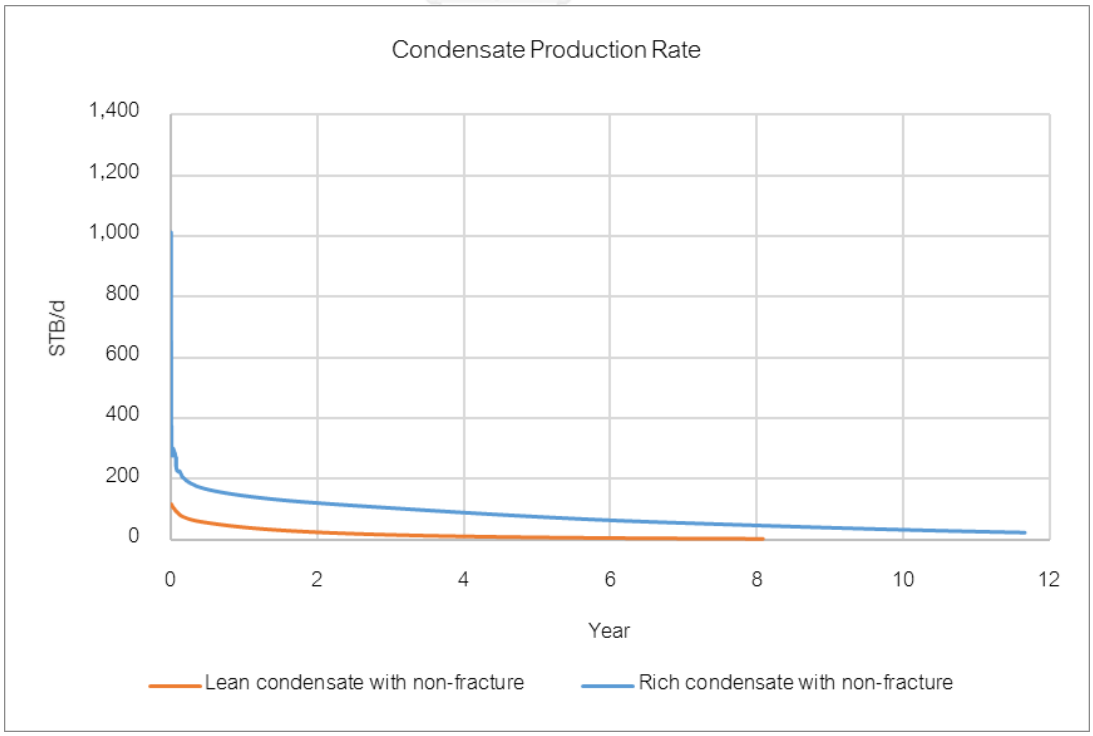

Figure 5.2: Condensate production rate of non-fractured reservoir

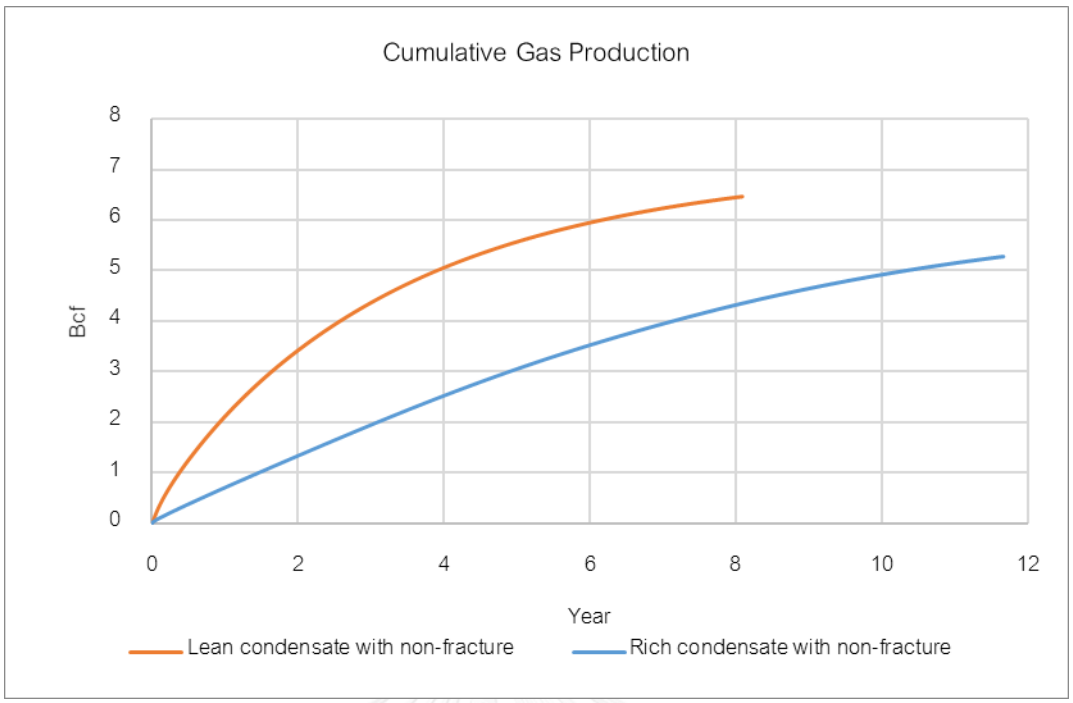

Figure 5.3: Cumulative gas production of non-fractured reservoir

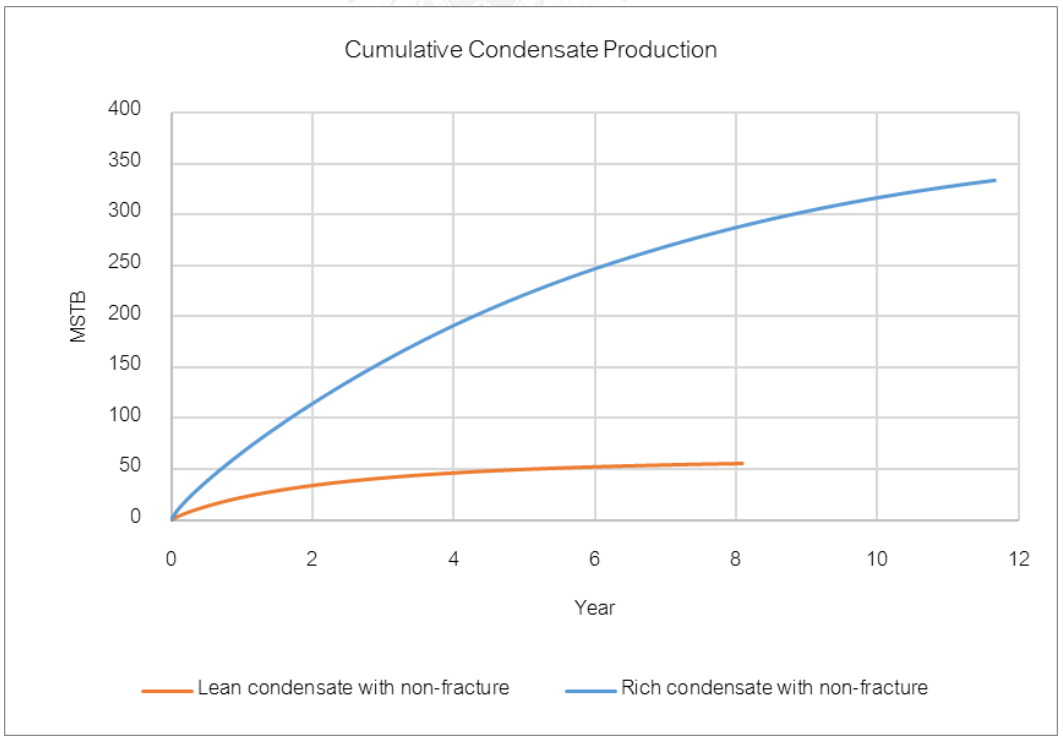

Figure 5.4: Cumulative condensate production of non-fractured reservoir

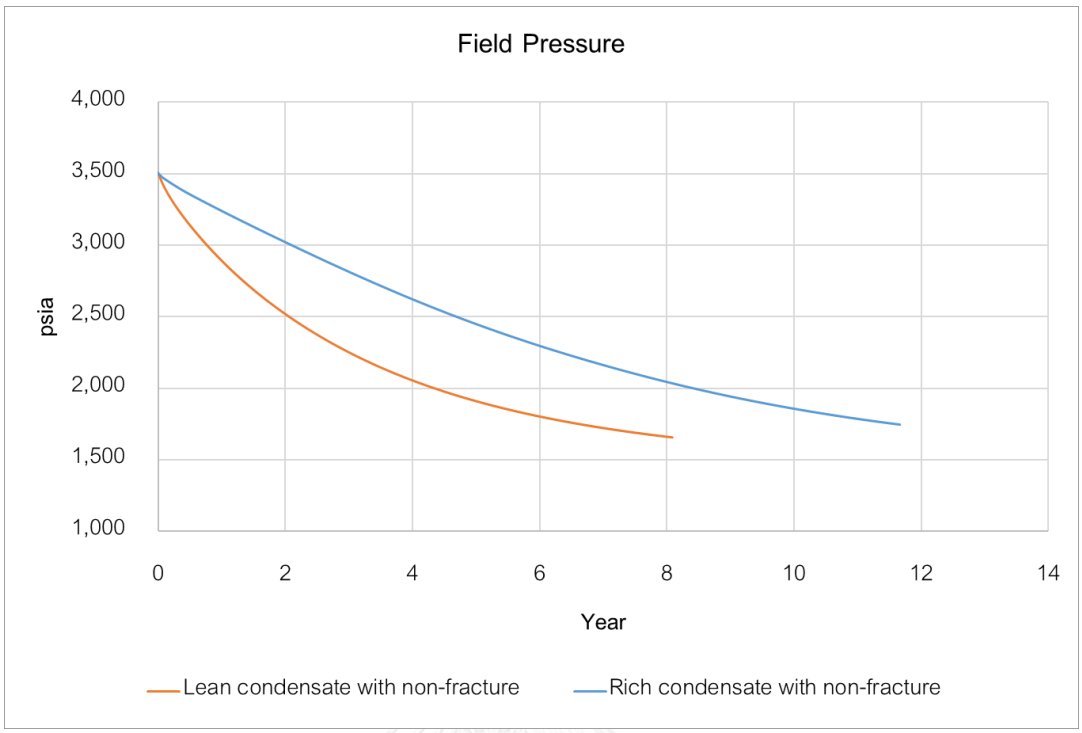

Figure 5.5: Reservoir pressure of non-fracture reservoir

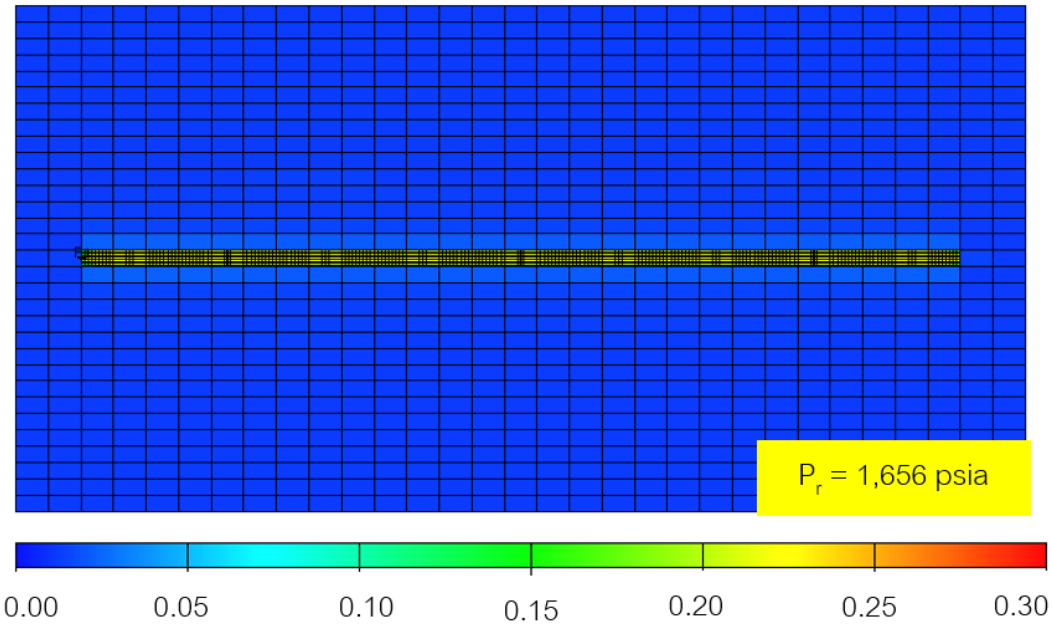

Figure 5.6 Condensate saturation at the end of production of non-fracture case in lean condensate reservoir

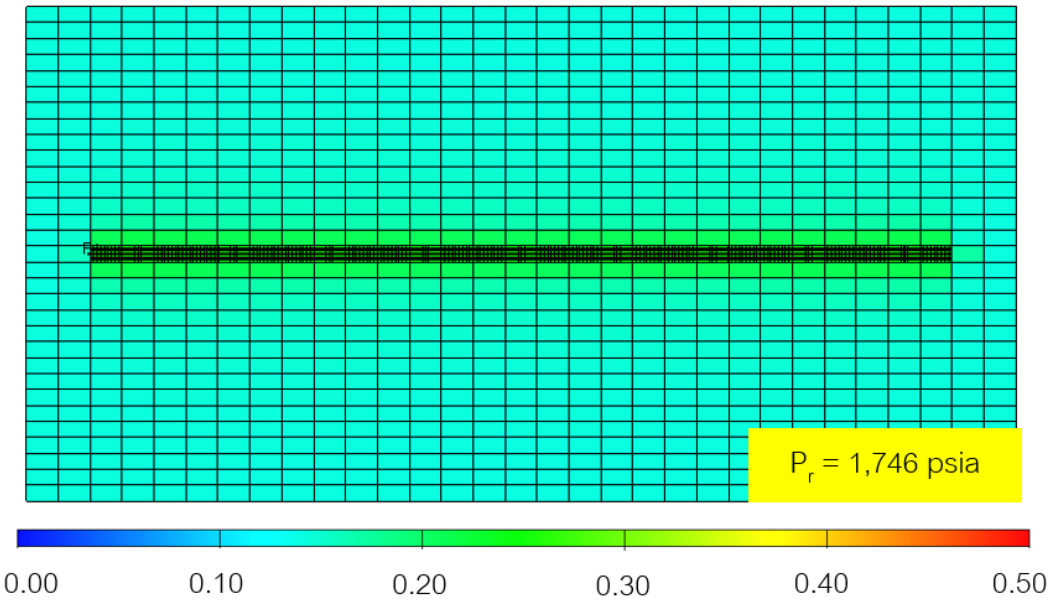

Figure 5.7 Condensate saturation at the end of production of non-fracture case in rich condensate reservoir

5.2 Fractured Well Simulation Results

5.2.1 Effect of Fracture Width

To obtain comparative results in the studying the effect of fracture width, fracture spacing of 200 ft. with 9 fractures and fracture permeability of 100,000 mD were kept constant. Fracture half-length and fracture height were defined to penetrate equally in both directions with the value of 775 ft. and 55 ft. respectively. The investigation of fracture width composed of 3 values; 0.0083 ft., 0.0125 ft. and 0.025 ft.

Lean Condensate

Figure 5.8 and Figure 5.9 exhibit the effect of fracture widths on cumulative gas and cumulative condensate production. And effect of fracture width has higher effect in cumulative condensate production than it has on cumulative gas production, as it is shown in Table 5.3 that the highest fracture width of 0.025 ft. gas only increased by 6.75% while condensate increased by 18.45% compared with non-fractured case.

The reason is because when fracture width increase, it consequently decreases the inertia effect or non-Darcy flow which means that gas relative permeability is decreased. Hence, when gas relative permeability is decreased then condensate relative permeability might increase and have higher chance to flow into the fracture planes better. Therefore, condensate can be obtained more than gas when fracture width is increased as they can be noticed in the percent increment in Table 5.3.

Figure 5.10 and 5.11 exhibit the gas and condensate production rate. The higher fracture width, the longer plateau rate can be maintained. The highest fracture width of 0.025 ft. gives plateau about 368 days while the non-fracture case can maintain plateau rate for 19 days. Noticing that when gas production rate can be maintained, the condensate production decreases linearly then exponentially until the end of its production in every case.

Figure 5.13, 5.14 and 5.15 exhibit condensate saturation profile at the end of production at different fracture width of 0.0083 ft., 0.0125 ft. and 0.025 ft. respectively. According to the reservoir pressure in Figure 5.12, it can be noticed that when fracture width is increased or higher fracture conductivity, the larger pressure drawdown can be obtained. Hence, it increases the potential of the reservoir to release hydrocarbon out of the reservoir. Especially for condensate production because fracture width has impact on controlling inertial effect Therefore, we can see smaller condensate saturation occupy in the reservoir when fracture width is increased.

Table 5.3: Effect of fracture width in lean condensate condition

Fracture width (ft)	Gas recovery factor (%)	Cumulative gas production (Bcf)	% increase of gas	Cumulative condensate production (Mstb)	% increase of condensate	Production time (Day)
Non-frac	53.45	6.46		55.53		2,954
0.0083	55.99	6.77	4.78	63.28	13.95	1,955
0.0125	56.39	6.82	5.52	64.24	15.67	1,768
0.025	57.03	6.90	6.75	65.78	18.45	1,476

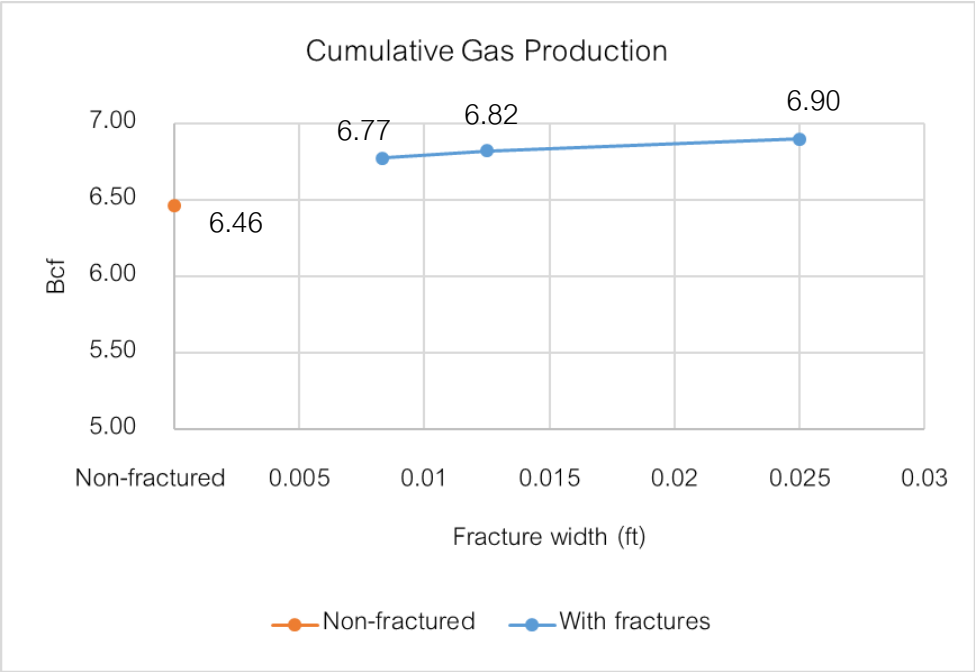

Figure 5.8: Comparison of cumulative gas production for different fracture widths in lean condensate

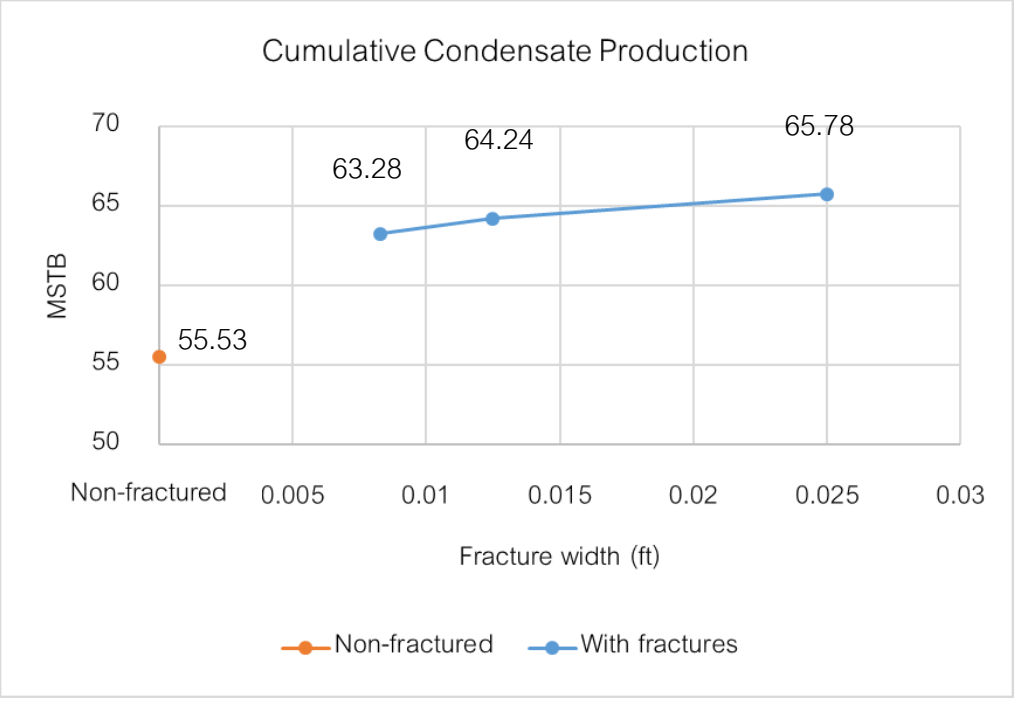

Figure 5.9: Comparison of cumulative condensate production for different fracture widths in lean condensate

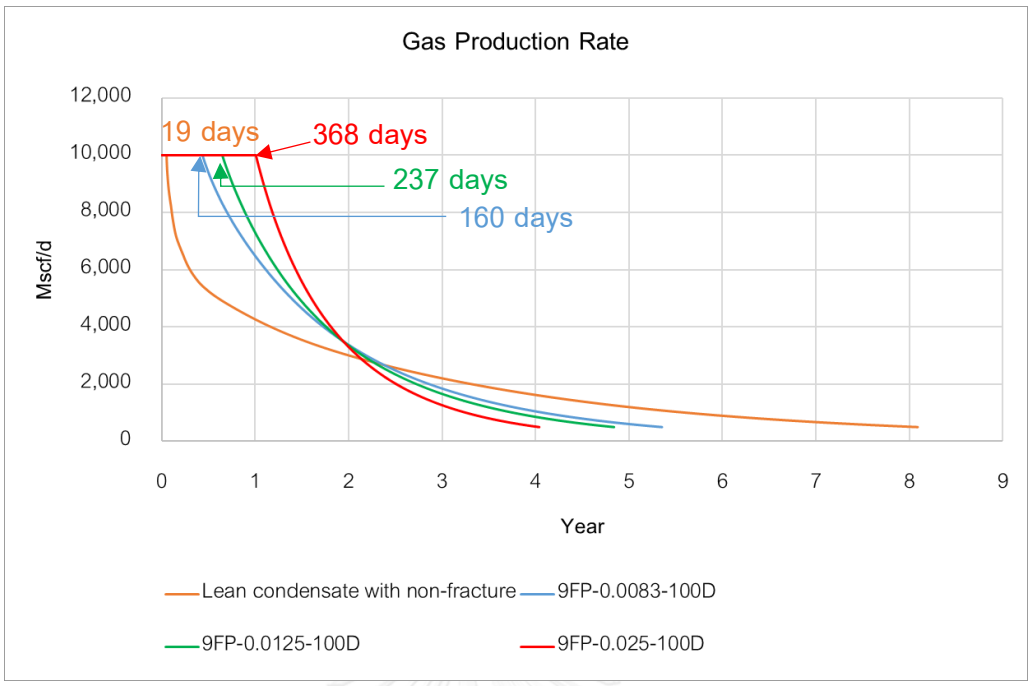

Figure 5.10: Gas production rate of different fracture widths in lean condensate

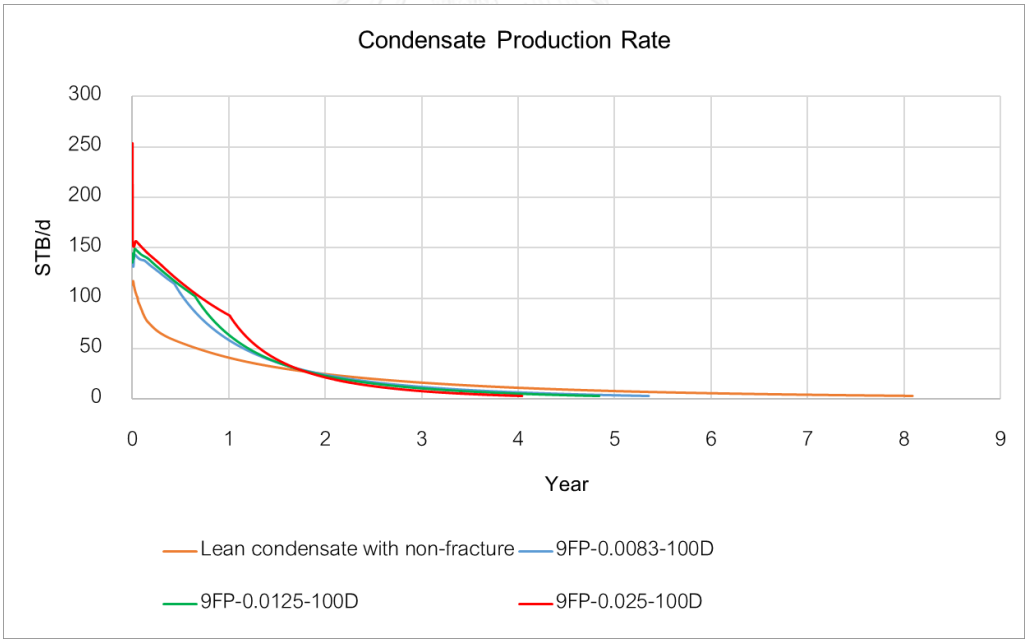

Figure 5.11: Condensate production rate of different fracture widths in lean condensate

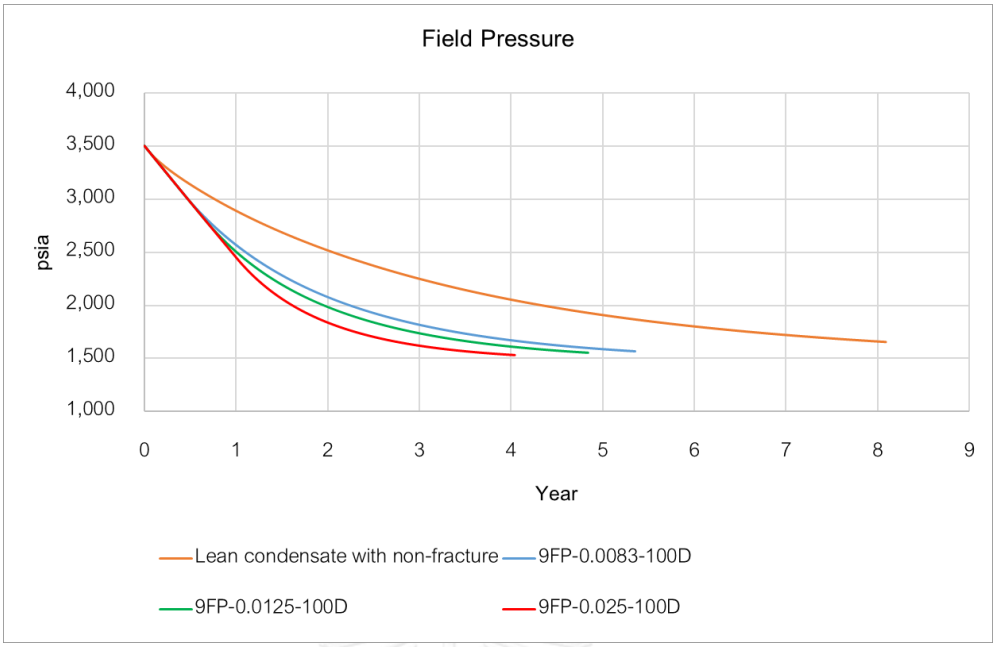

Figure 5.12: Effect of fracture widths on reservoir pressure in lean condensate

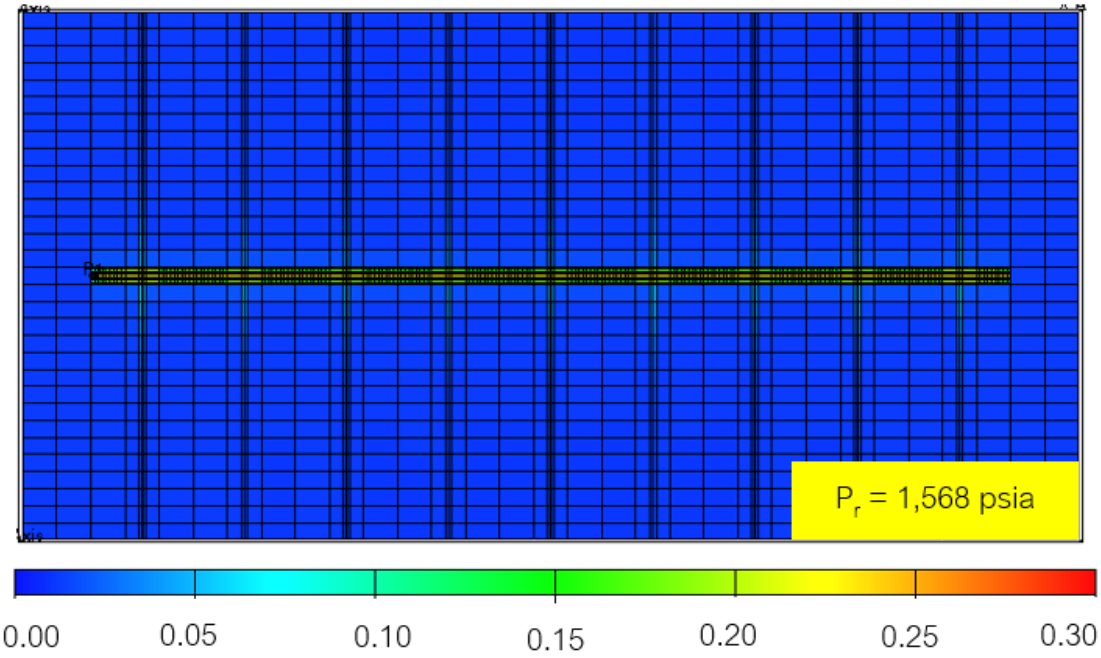

Figure 5.13 Effect of fracture width of 0.0083 ft. on condensate saturation profile at the end of production in lean condensate

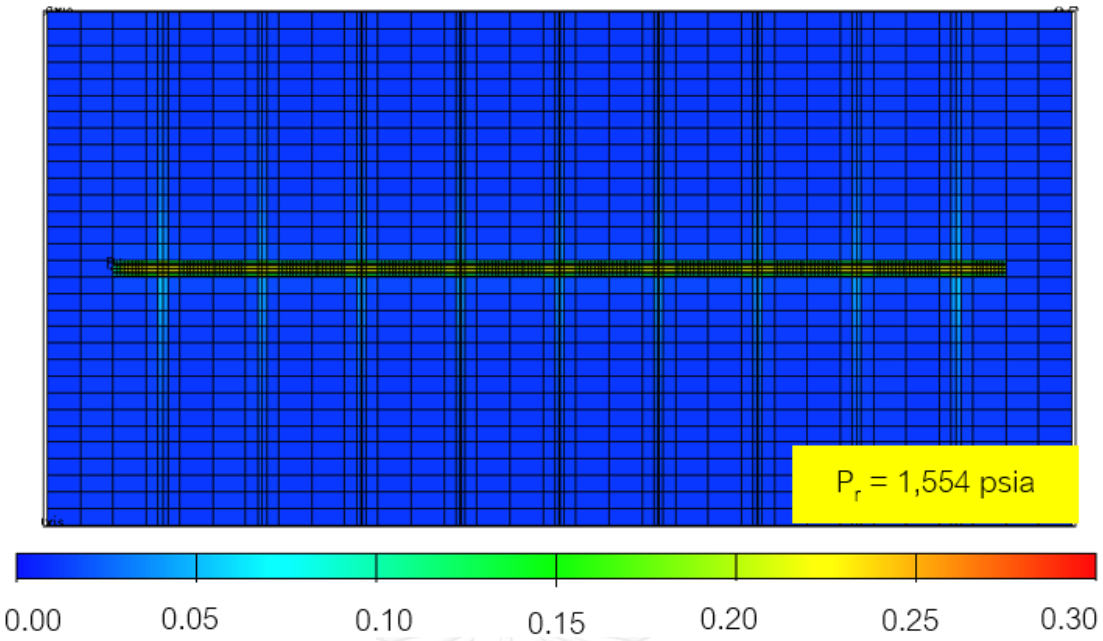

Figure 5.14 Effect of fracture width of 0.0125 ft. on condensate saturation profile at the end of production in lean condensate

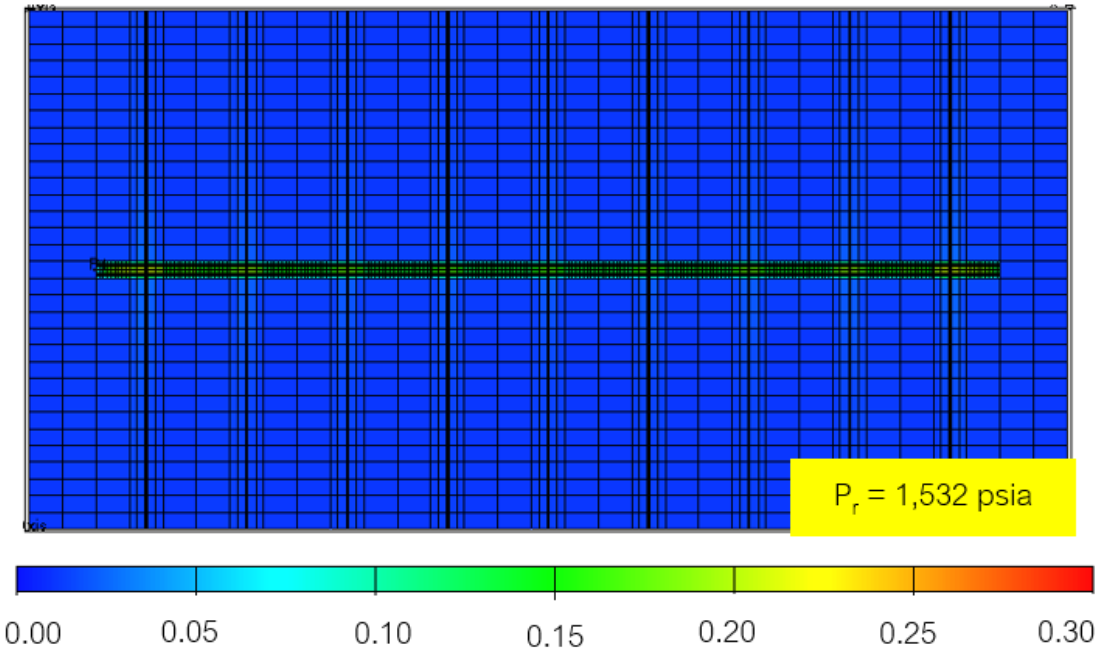

Figure 5.15 Effect of fracture width of 0.025 ft. on condensate saturation profile at the end of production in lean condensate

Rich Condensate

Results from Figure 5.16 and Figure 5.17 shows similar behavior of lean condensate that, the larger fracture, the higher gas and condensate production can be obtained. However, from Table 5.4 it can be observed that fracture width has higher impact on condensate recovery more than it has on gas recovery. The highest percent increase of gas is 10.63% compared to non-fracture when fracture width of 0.025 ft. was performed. While the highest percent increment of condensate is 12.15% compared to non-fracture case. This is because fracture width is important for controlling the inertial effect. Increasing fracture width consequently decreases non-Darcy flow, therefore, condensate relative permeability and condensate production also increased.

Gas and condensate production rates are shown in Figure 5.18 and Figure 5.19. The gas target rate at 10,000 Mscf/day can be reached only for 2 days before dropping drastically in every case of fracture width. While the condensate production of the largest fracture width can reach the rate of 1,200 stb/day only for several hours.

Condensate saturation profiles at the end of production for different fracture widths are shown in Figure 5.21, 5.22 and 5.23 for fracture width of 0.0083 ft., 0.0125 ft. and 0.025 ft. respectively. The relationship between reservoir pressure in Figure 5.20 and condensate saturation at the abandonment can be observed that the higher fracture width gives the potential of reservoir pressure to drawdown larger and higher chance of releasing hydrocarbon out of the reservoir. Therefore, highest fracture width 0.025 ft. exhibits an abandonment pressure at 1,554 psia with the condensate saturation of 0.15 compared to the smallest fracture width 0.0083 ft. that has an abandonment pressure at 1603 psia with condensate saturation of 0.16.

Table 5.4: Effect of fracture width in rich condensate condition

Fracture width (ft.)	Gas recovery factor (%)	Cumulative gas production (Bcf)	% increase of gas	Cumulative condensate production (Mstb)	% increase of condensate	Production time (Day)
Non-frac	48.55	5.28		333.46		4,261
0.0083	52.83	5.68	7.55	372.79	11.79	2,439
0.0125	53.42	5.74	8.76	373.98	12.15	2,141
0.025	54.32	5.84	10.63	372.41	11.68	1,675

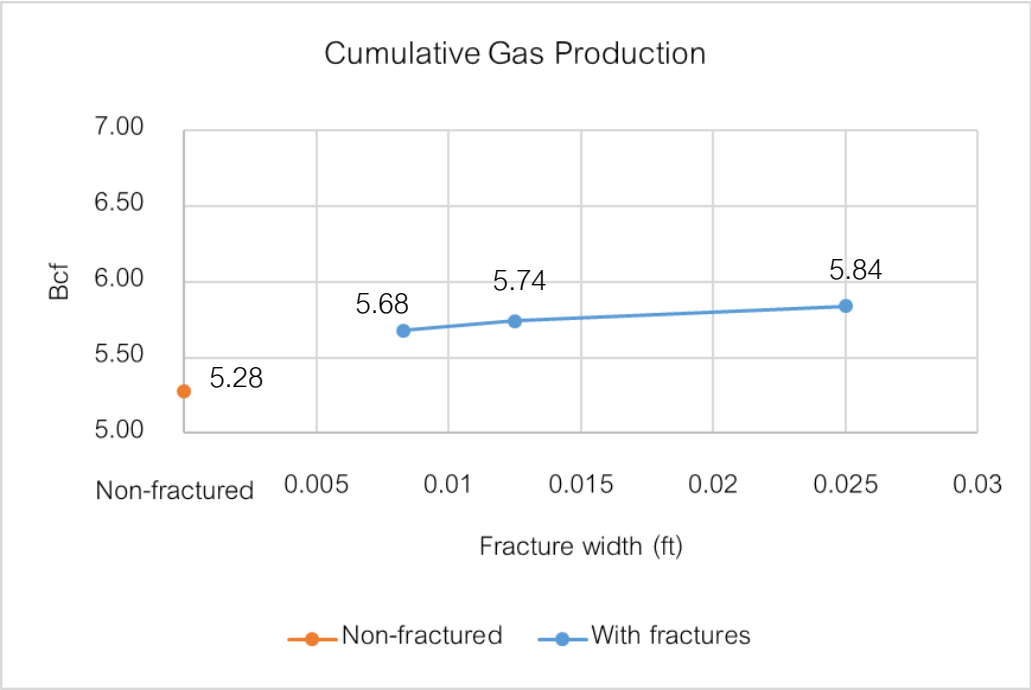

Figure 5.16: Comparison of cumulative gas production for different fracture widths in rich condensate

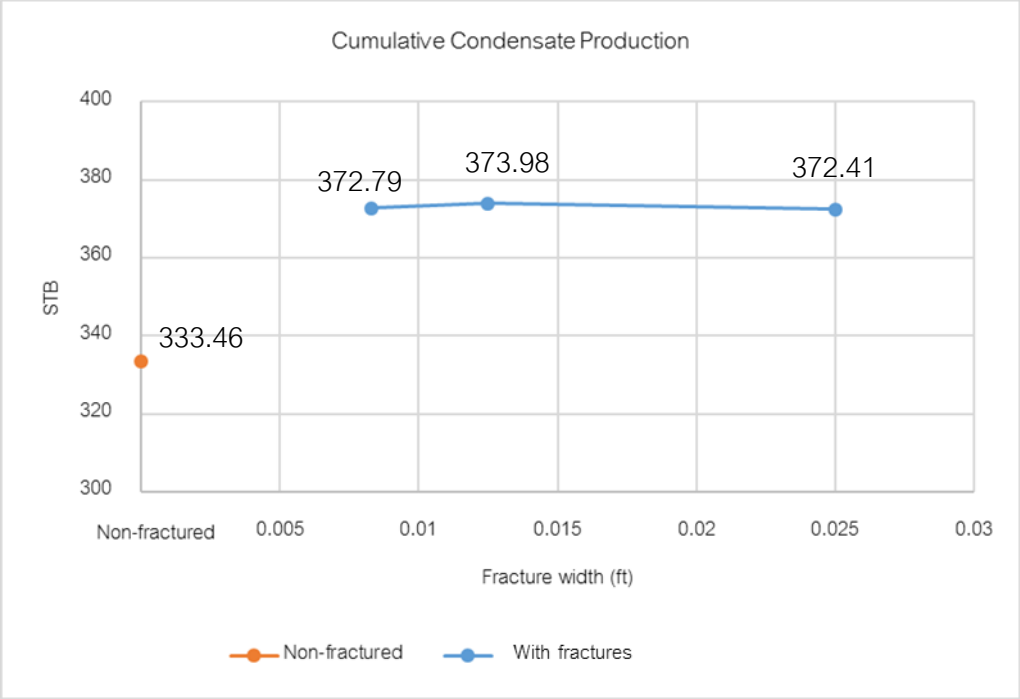

Figure 5.17: Comparison of cumulative condensate production with different fracture widths in rich condensate

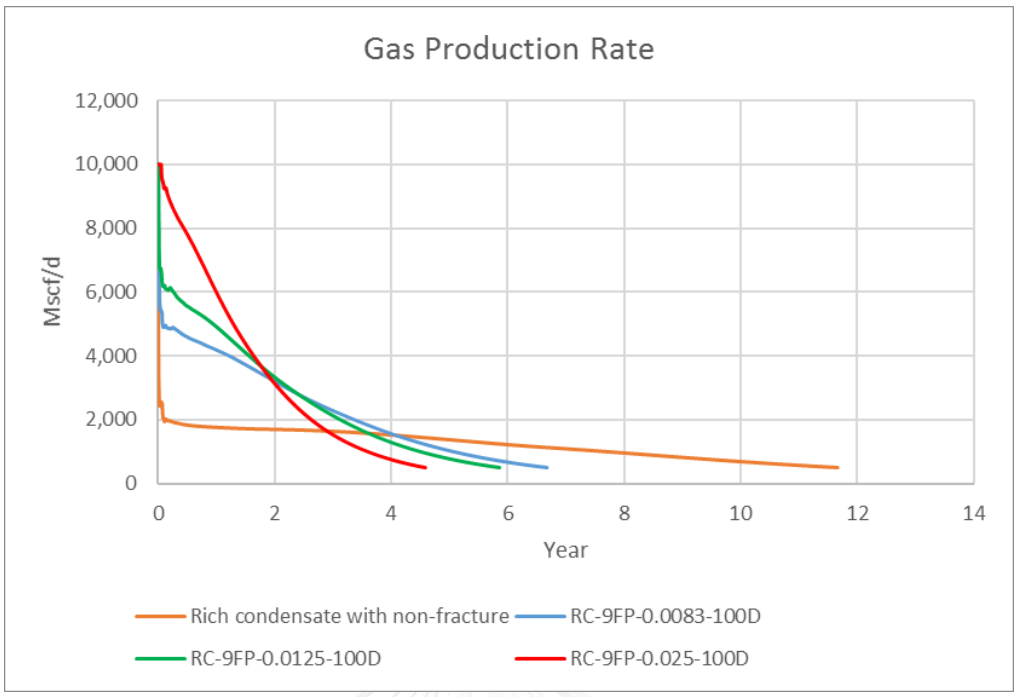

Figure 5.18: Gas production rate of different fracture widths in rich condensate

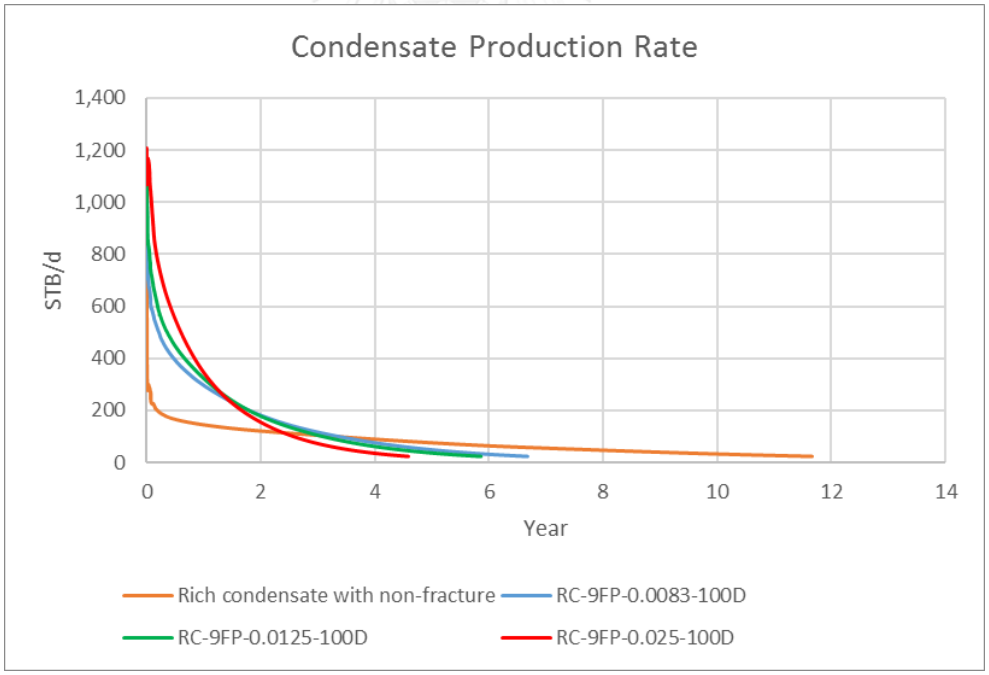

Figure 5.19: Condensate production rate of different fracture widths in rich condensate

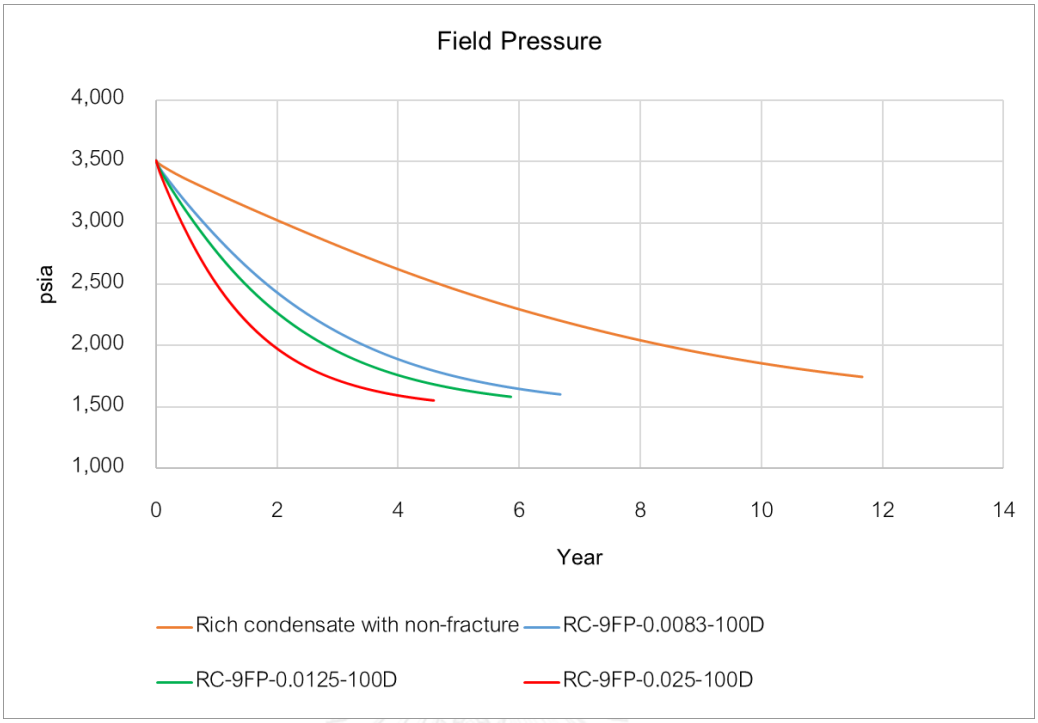

Figure 5.20: Effect of fracture widths on reservoir pressure in rich condensate

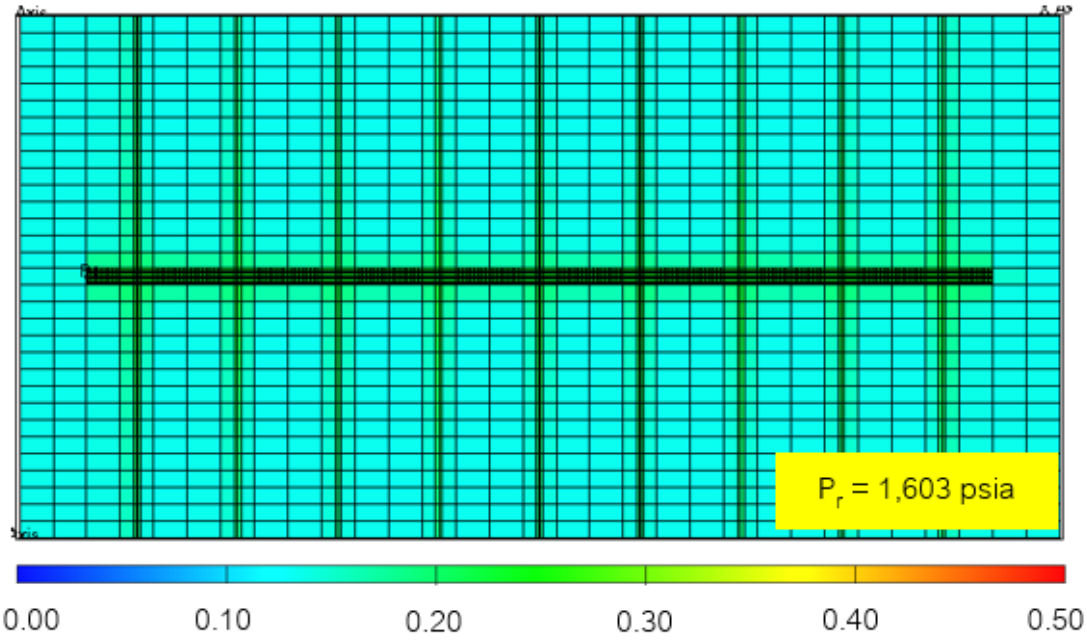

Figure 5.21 Effect of fracture width of 0.0083 ft. on condensate saturation profile at the end of production in rich condensate

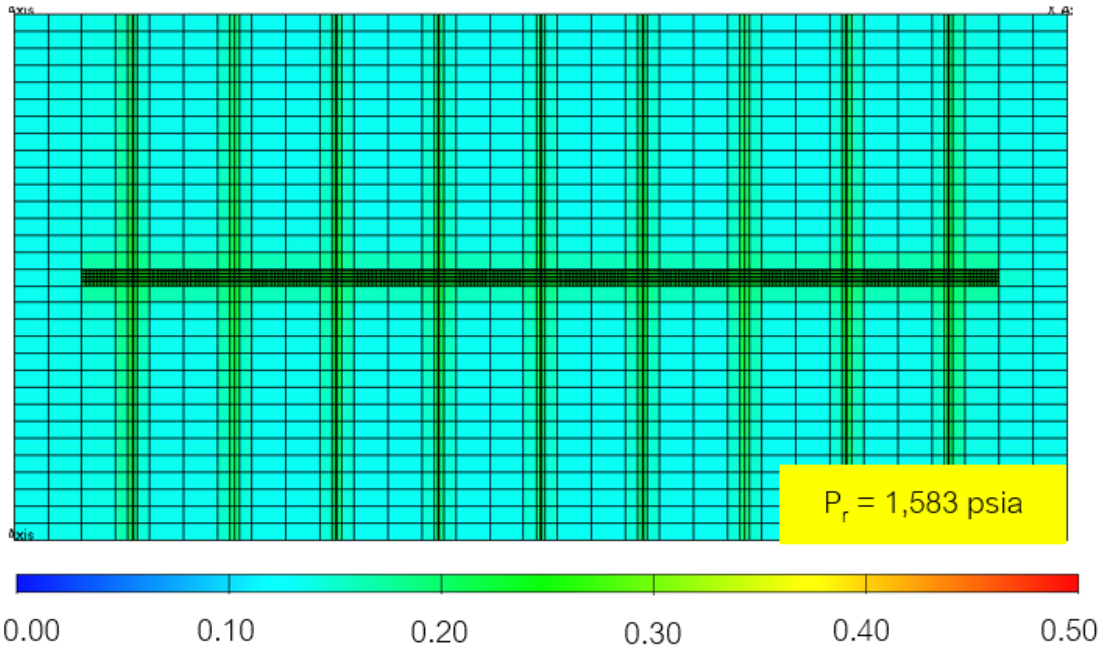

Figure 5.22 Effect of fracture width of 0.0125 ft. on condensate saturation profile at the end of production in rich condensate

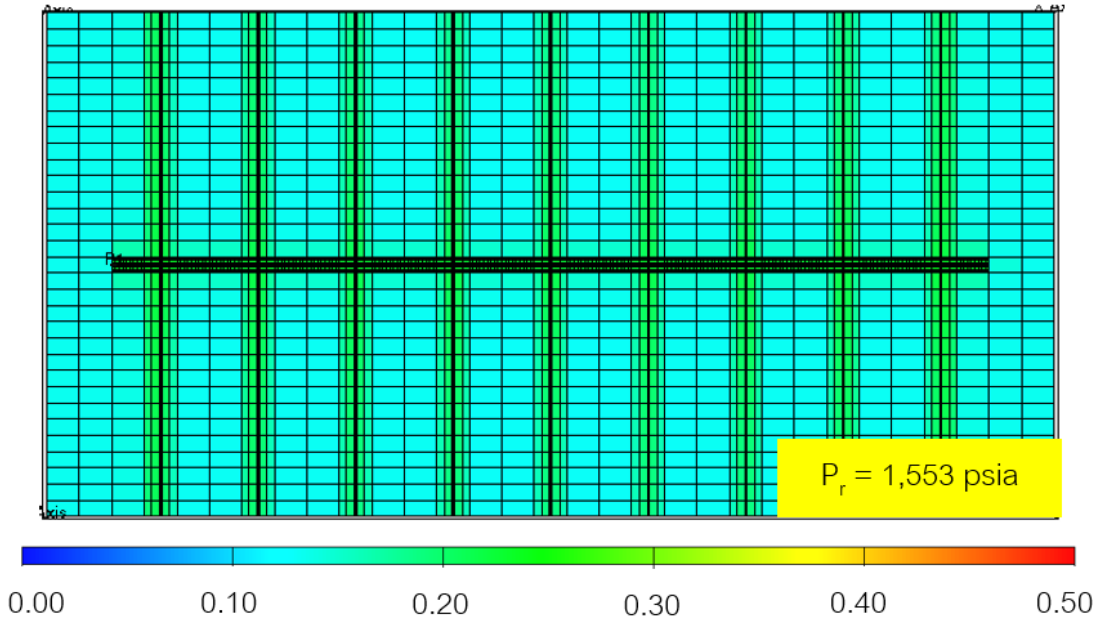

Figure 5.23 Effect of fracture width of 0.025 ft. on condensate saturation profile at the end of production in rich condensate

5.2.2 Effect of Number of Fractures and Fracture Spacing

Number of fracture has the effect on increasing contact area between reservoir and fractures. Fracture width, fracture permeability and fracture half-length were kept constant at 0.025 ft., 100,000 mD and 775 ft. in all cases. While three values of number of fracture are varied, which are; 3 fractures, 6 fractures and 9 fractures, fracture spacing of these case are 1,150 ft., 400 ft. and 200 ft. respectively. The performance of three number were compared with non-fractured case in each fluid composition.

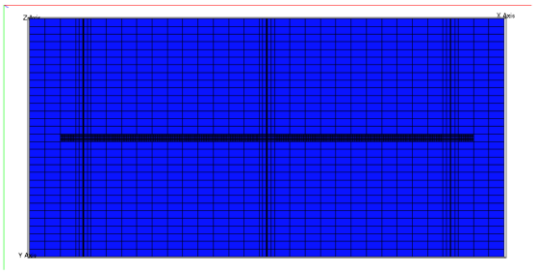

Figure 5.24: Aerial view of the 3 fractures model with fracture spacing of 1,150 ft.

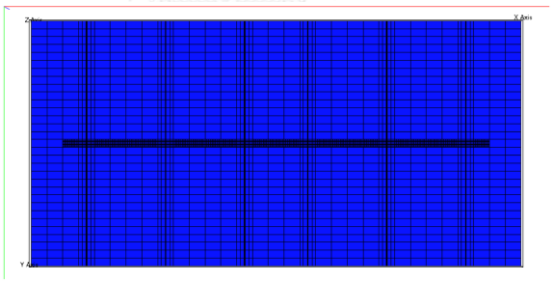

Figure 5.25: Aerial view of the 6 fractures model with fracture spacing of 400 ft.

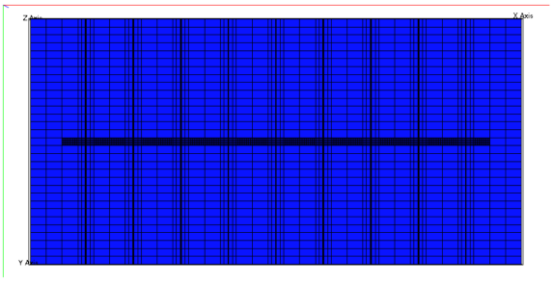

Figure 5.26: Aerial view of the 9 fractures simulation model with fracture spacing of 200 ft.

Lean Condensate

Figure 5.27 and Figure 5.28 present cumulative gas production and cumulative condensate production respectively. Note that the highest number of fracture of 9 gives the highest gas cumulative production of 6.90 Bcf or about 57.03% of gas recovery from Table 5.5 and cumulative condensate production of 65.78 Mstb. However, higher number of fractures has only small effect on percent increase of gas, but it shows larger differences on percent increase of condensate. Applying higher number of fracture possibly give higher condensate production. The reason is because higher number of fracture allows larger contact area between fractures and reservoir. Therefore, hydrocarbon can flow from low permeability reservoir to the fracture and wellbore easier.

The advantages of the higher number of fracture, the longer plateau rate of gas production rate and the higher gas and condensate recovery can be obtained. From Figure 5.29, it exhibits the results of 3 fractures, 6 fractures and 9 fractures that can maintain plateau rate for 132 days, 282 days and 368 days respectively compared to non-fractured case that can maintain plateau rate only for 19 days. While Figure 5.30 depicts the condensate production rate of each case. It can be noticed that when gas production rates are maintained at plateau rate, the condensate production rates are decreased linearly then exponentially at the same time when the gas plateau rates end. This is because when pressure decreases phase behavior of gas condensate is changed and drops liquid out. Those condensed liquids occupy pore spaces near wellbore and block the flow of gas to the well and overall energy output is decreased, consequently causing the reduction of gas and condensate production rates.

Figure 5.31 exhibits reservoir pressure for each number of fracture, and it can be observed that 9 fractures has the lowest reservoir at the abandonment about 1,532 psia compared to 3 fractures and 6 fractures which has only 1,576 psia and 1,547 psia. This, consequently, affects the potential of releasing hydrocarbon out of the reservoir that can be seen in the form of condensate saturation at the end of production from Figure 5.32, 5.33 and 5.34. and the lowest condensate saturation is 0.014 for 9 fractures case.

Table 5.5: Effect of number of fractures in lean condensate condition

No. of fracture	Gas recovery factor (%)	Cumulative gas production (Bcf)	% increase of gas	Cumulative condensate production (Mstb)	% increase of condensate	Production time (Day)
Non-frac	53.45	6.46		55.53		2,954
3	55.75	6.74	4.32	60.72	9.35	2,056
6	56.60	6.85	5.92	63.95	15.15	1,672
9	57.03	6.90	6.75	65.78	18.45	1,476

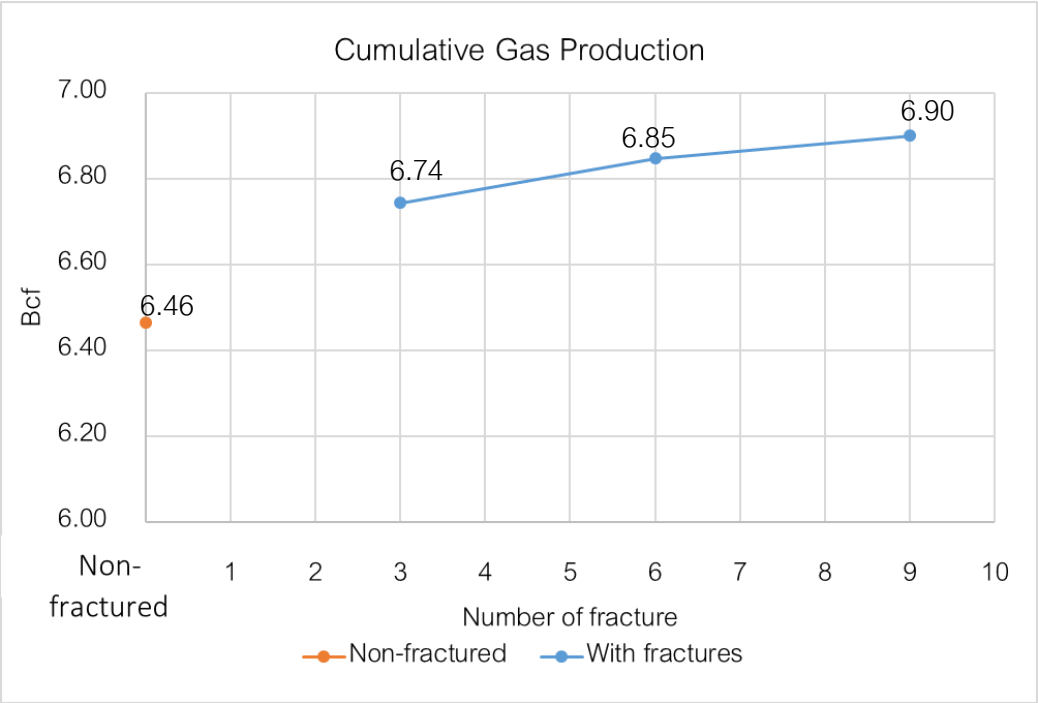

Figure 5.27: Comparison of cumulative gas production for different number of fractures in lean condensate

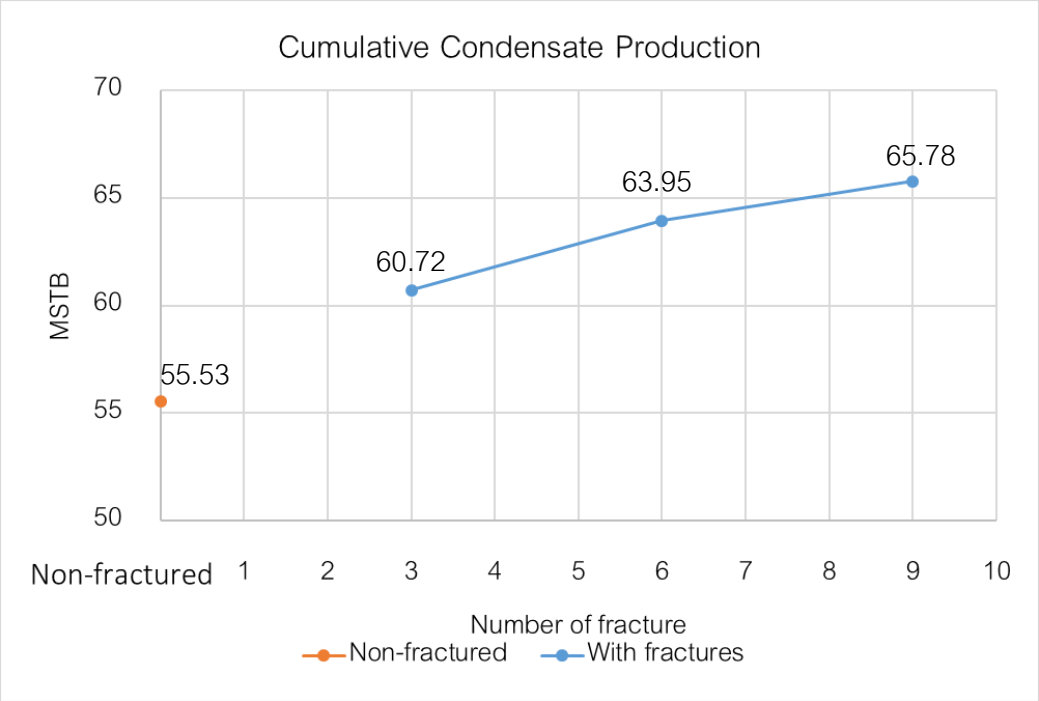

Figure 5.28: Comparison of cumulative condensate production for different number of fractures in lean condensate

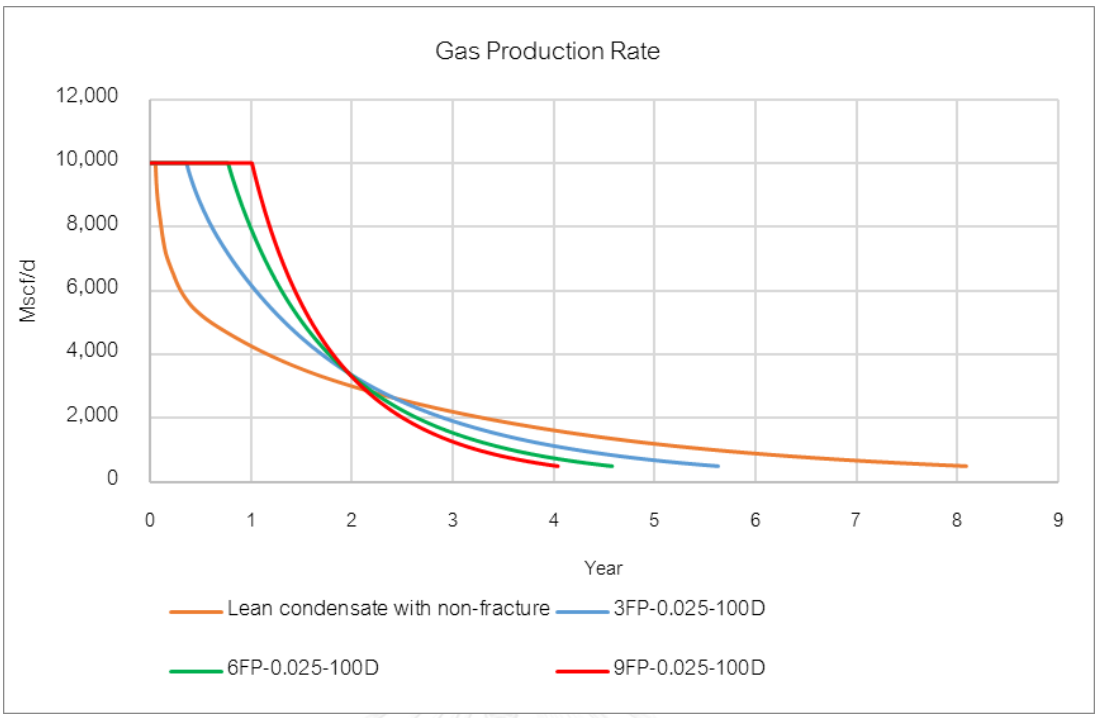

Figure 5.29: Gas production rate for different number of fractures in lean condensate

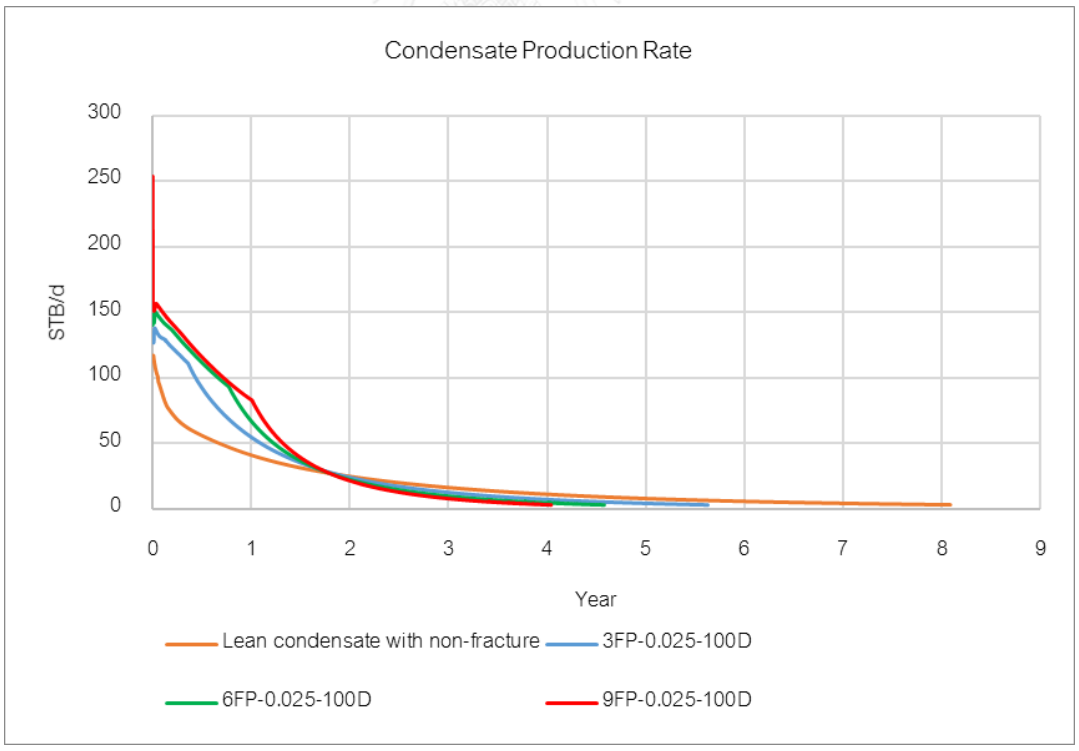

Figure 5.30: Condensate production rate for different number of fractures in lean condensate

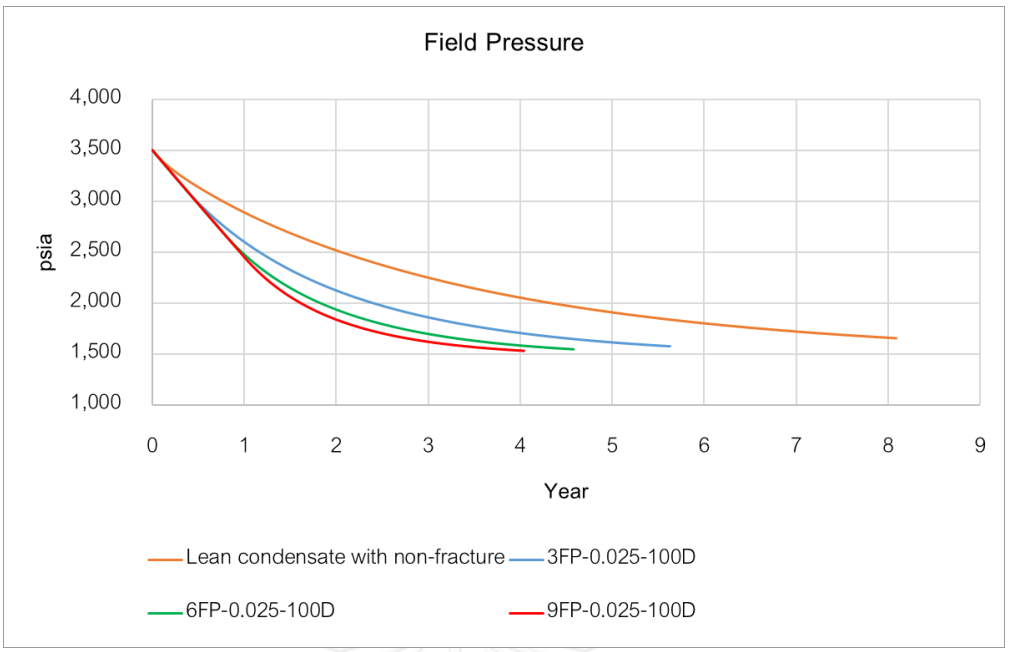

Figure 5.31: Effect of number of fractures on reservoir pressure in lean condensate

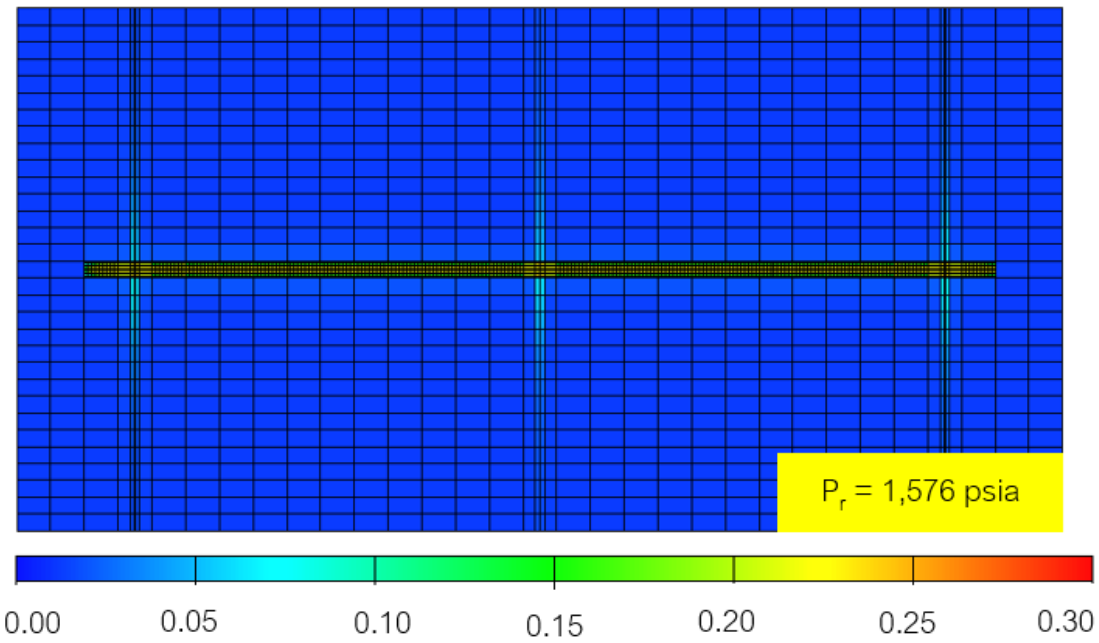

Figure 5.32 Effect of 3 fractures. on condensate saturation profile at the end of production in lean condensate

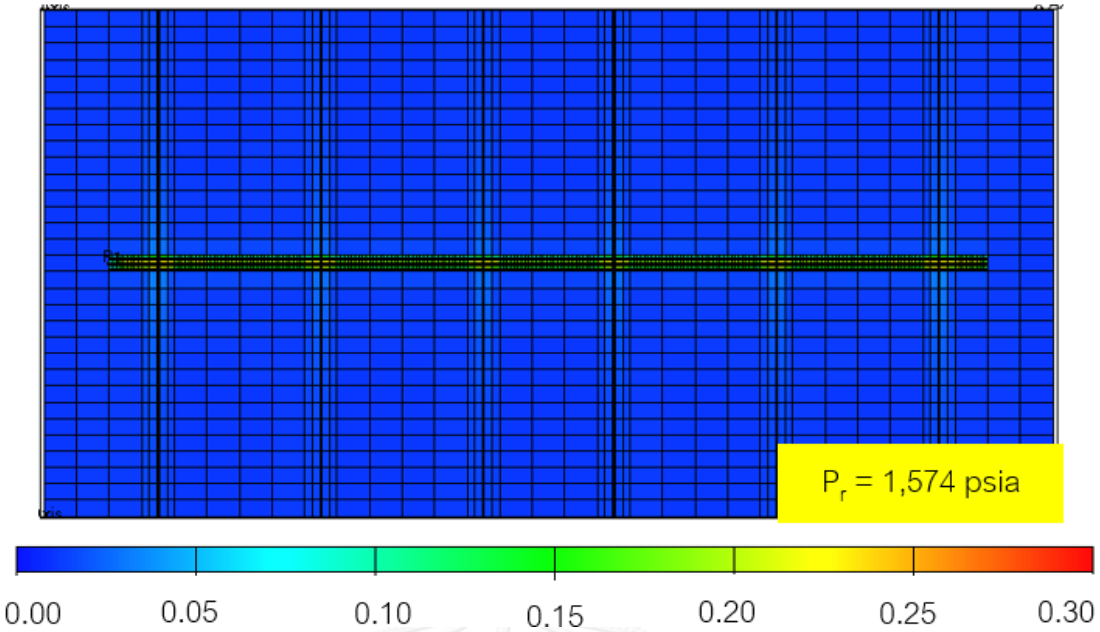

Figure 5.33 Effect of 6 fractures on condensate saturation profile at the end of production in lean condensate

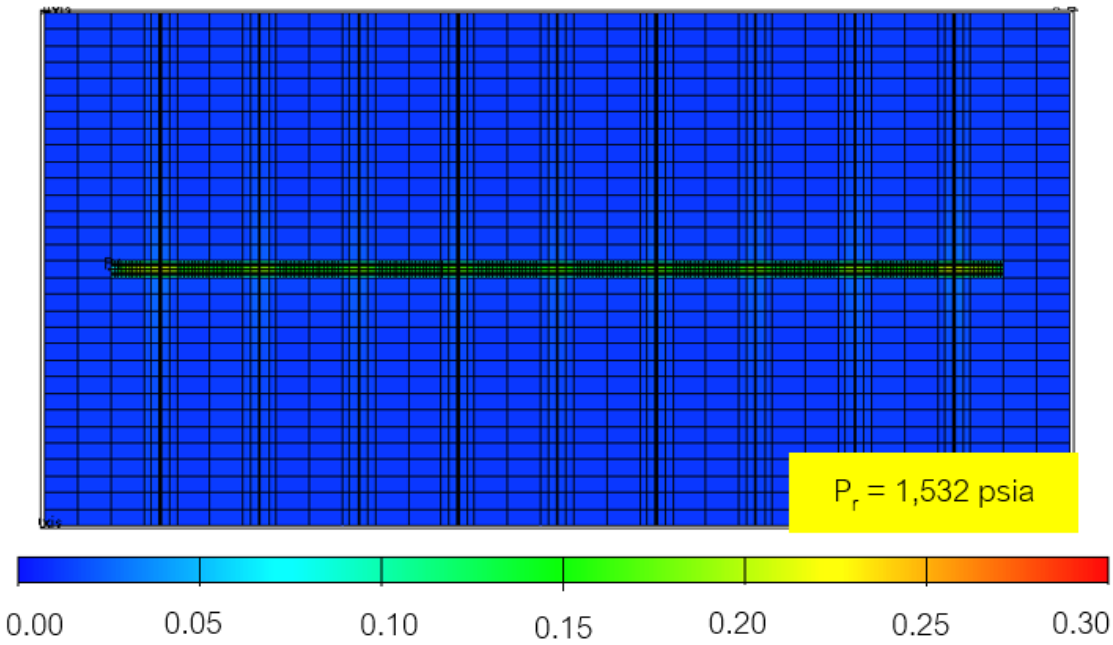

Figure 5.34 Effect of 9 fractures on condensate saturation profile at the end of production in lean condensate

Rich Condensate

Figure 5.35 and Figure 5.36 present result of cumulative gas production and cumulative condensate production which increase when higher number of fractures is applied. The highest production case is at 9 fractures shows cumulative production about 5.84 Bcf for gas and 372.41 Mstb for condensate or 10.63% increase of gas and 11.68% increase of condensate compared to non-fracture case in Table 5.6.

Effects of the number of fractures in rich condensate composition also exhibit similar results to lean condensate composition that when number of fractures increase (fracture spacing decreases), the longer plateau rate can be maintained but only for a short time of 2 days, 4 days and 20 days for 3, 6 and 9 fractures respectively before they decrease abruptly as they are shown in Figure 5.37. While the non-fracture case cannot even reach the gas production rate of 10,000 Mscf/d but only reaches up to about 5,000 Mscf/d. before declines slowly until the end of production of 11.67 years.

However, the comparison of cumulative condensate production with different number of fracture in Figure 5.36 shows an interesting result that the effect of number of fracture seems to be small after 6 fractures has been performed. This small benefit between 6 and 9 fractures can be noticed in the form of reservoir pressure in Figure 5.39 that 6 fractures has an abandonment pressure at 1,575 psia while 9 fractures has 1,553 psia. They are consistent with condensate saturations at the end of production in Figure 5.40, 5.41 and 5.42 where 6 and 9 fractures show a close result of condensate saturation at 0.15 and 0.155. This is because the heavy ends in rich condensate compositions that condense and occupy in the pore space decrease the effectiveness of number of fracture. Economic analysis based on practical situation is recommended to evaluate the performance of number of fractures based on operational cost and production.

Table 5.6: Effect of number of fractures in rich condensate condition

Number of fracture	Gas recovery factor (%)	Cumulative gas production (Bcf)	% increase of gas	Cumulative condensate production (Mstb)	% increase of condensate	Production time (Days)
Non-frac	48.55	5.28		333.46		4,261
3	52.28	5.62	6.43	357.38	7.17	2,669
6	53.66	5.77	9.26	369.07	10.68	2,027
9	54.32	5.84	10.63	372.41	11.68	1,675

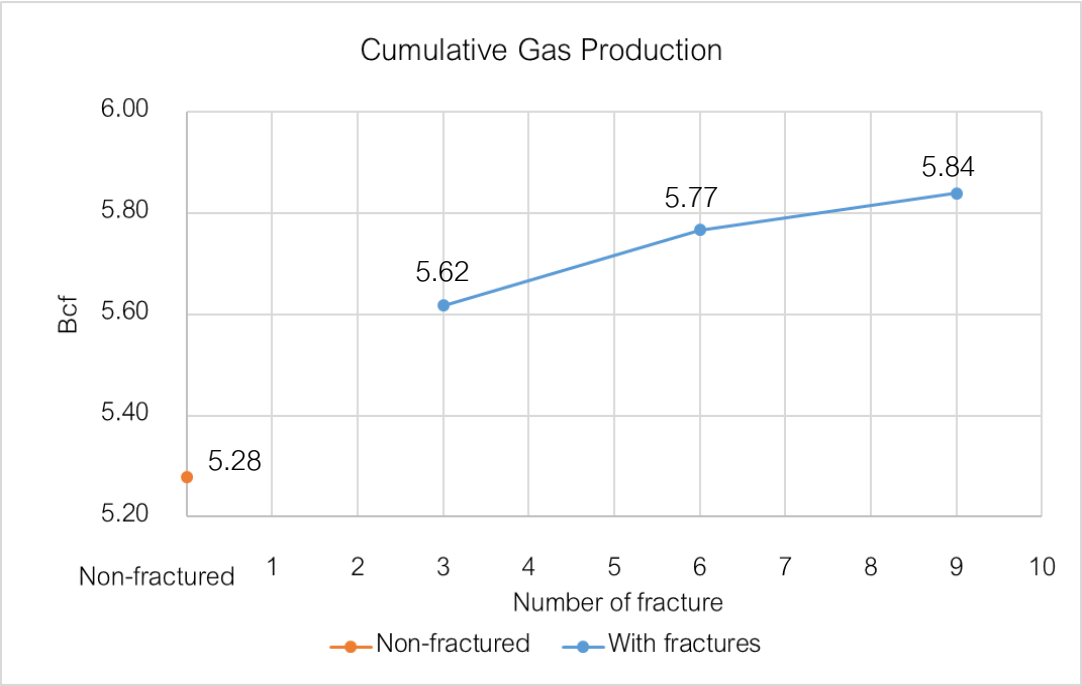

Figure 5.35: Comparison of cumulative gas production for different number of fractures in rich condensate

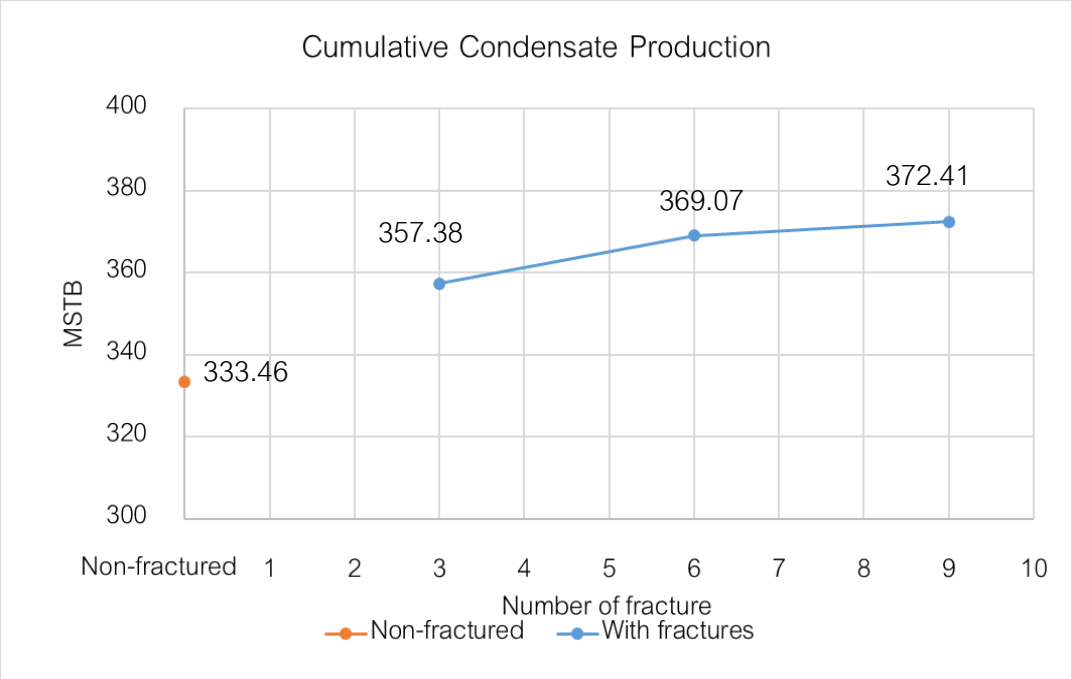

Figure 5.36: Comparison of cumulative condensate production for different number of fractures in rich condensate

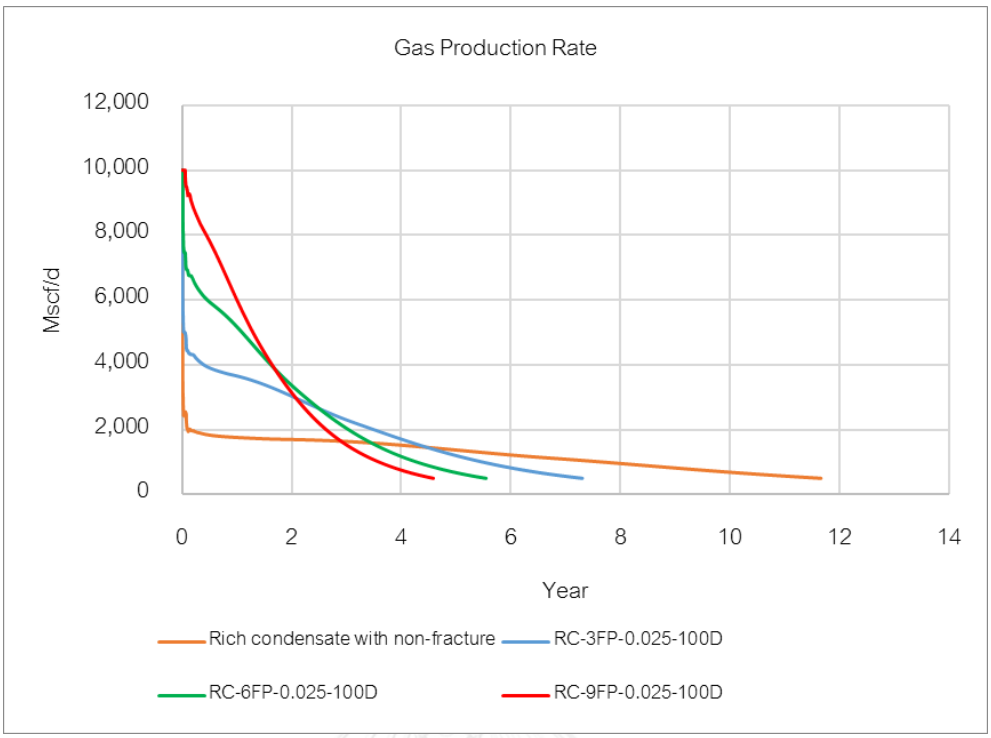

Figure 5.37: Gas production rate for different number of fractures in rich condensate

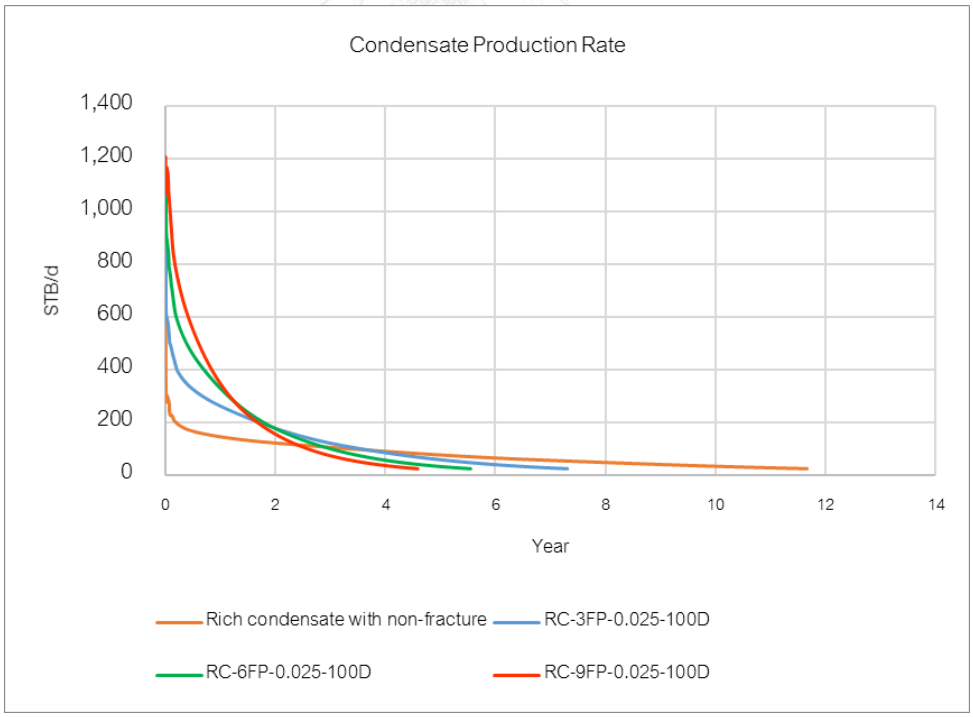

Figure 5.38: Condensate production rate for different number of fractures in rich condensate

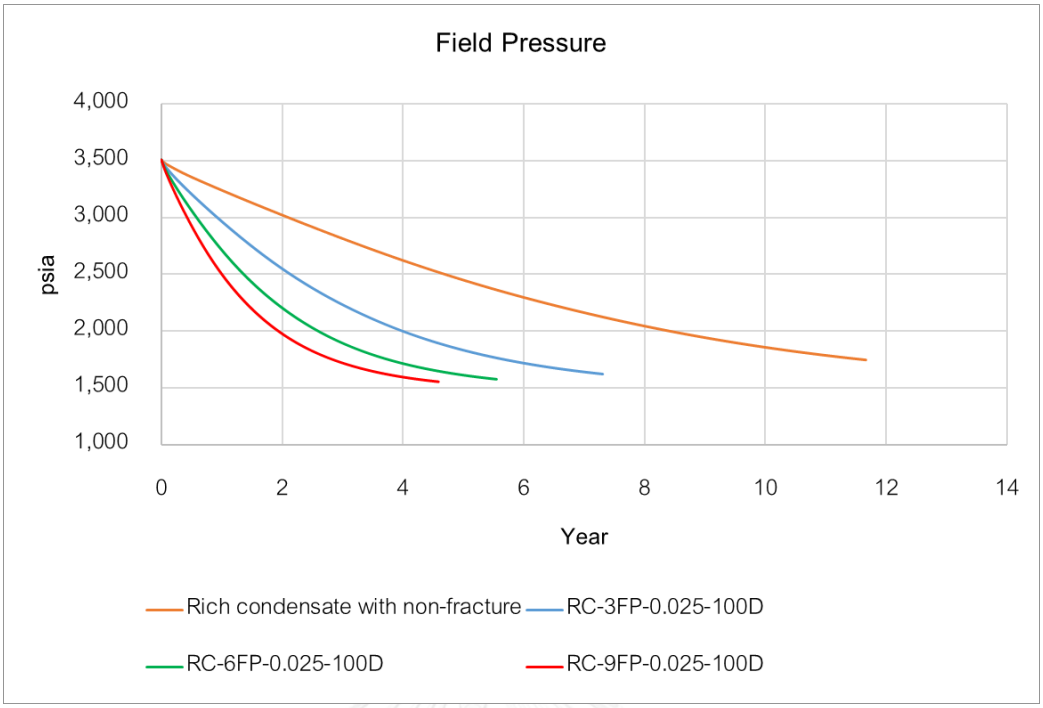

Figure 5.39: Effect of number of fractures on reservoir pressure in rich condensate

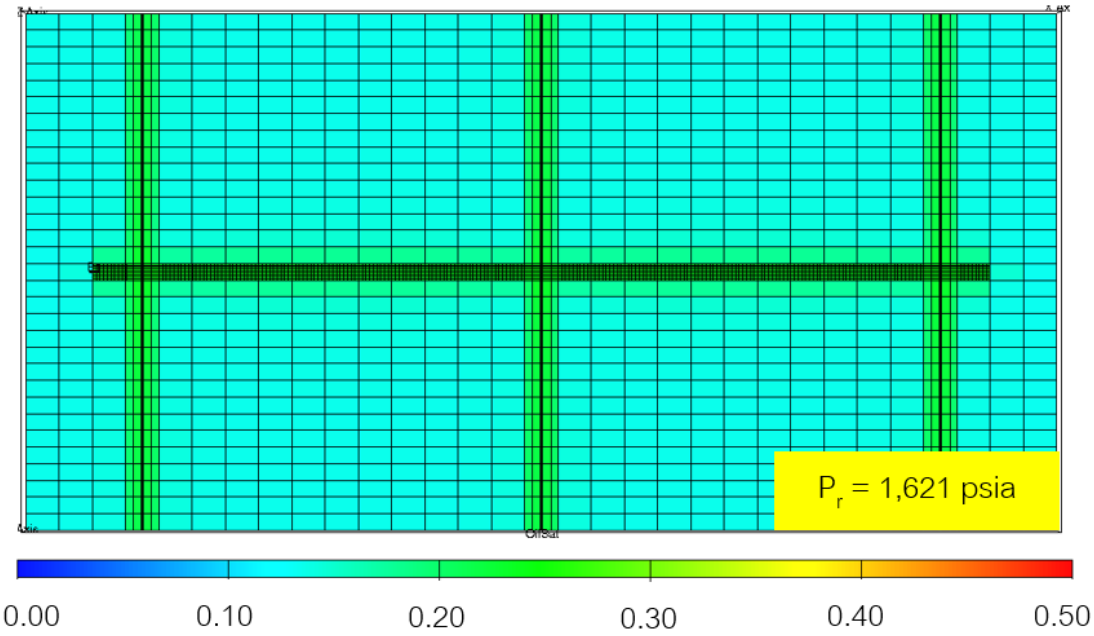

Figure 5.40 Effect of 3 fractures. on condensate saturation profile at the end of production in rich condensate

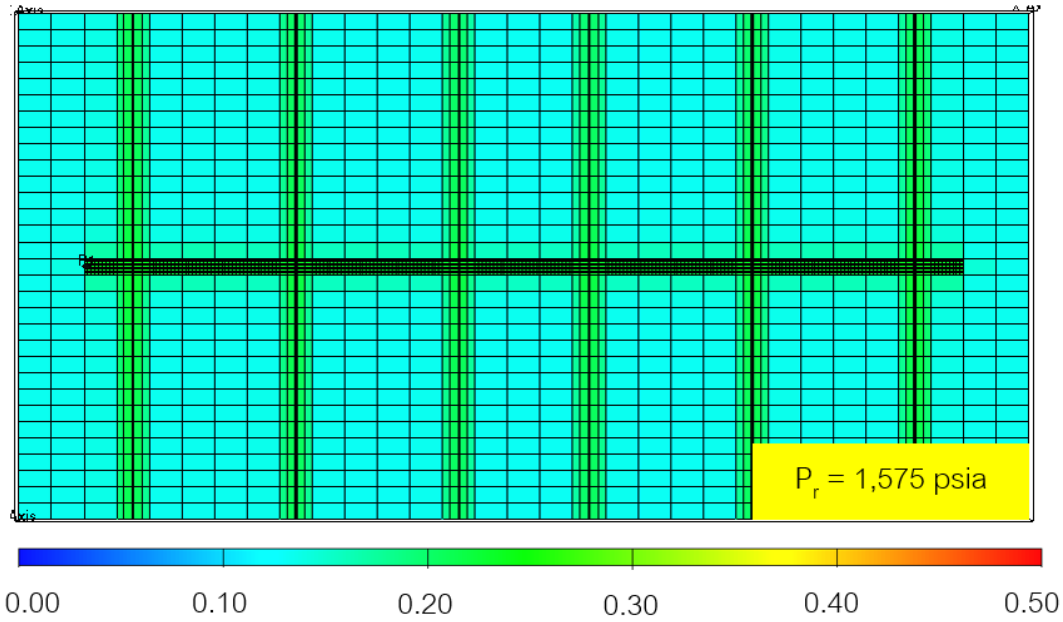

Figure 5.41 Effect of 6 fractures on condensate saturation profile at the end of production in rich condensate

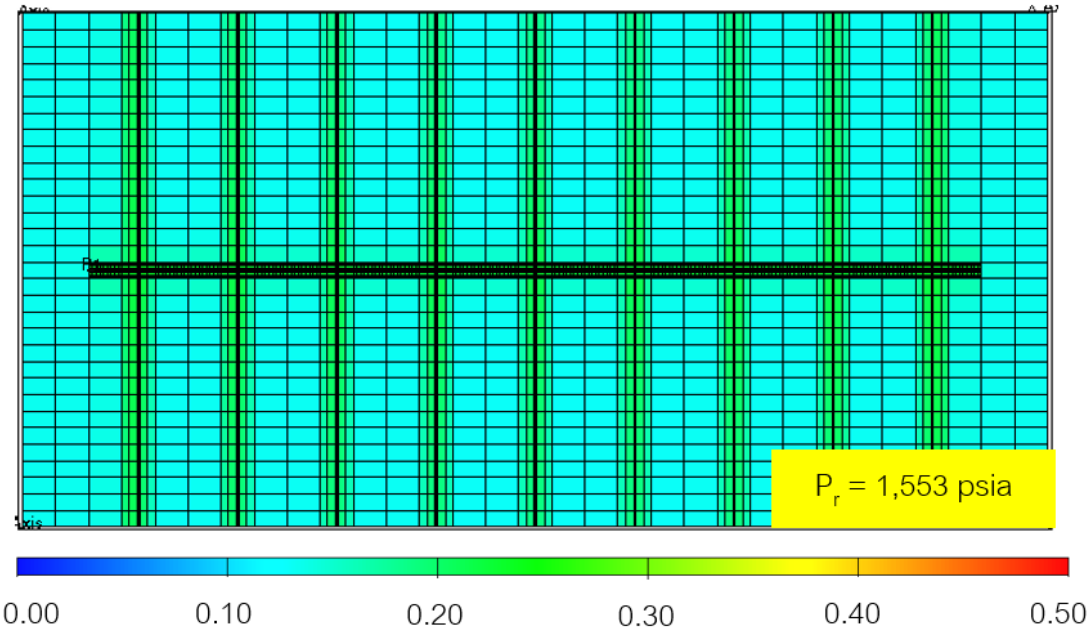

Figure 5.42 Effect of 9 fractures on condensate saturation profile at the end of production in rich condensate

5.2.3 Effect of Stimulated Reservoir Volume (SRV)

Fracture width, fracture half-length and fracture planes were designed to be able to have the same SRV as they are shown in Table 5.7. Fracture permeability was kept constant at 100,000 mD and gas production rate of 10,000 Mscf/day were set for all cases.

Table 5.7: Stimulated reservoir volume designs

Case	No. of fracture	Fracture width (ft)	Thickness (ft)	Fracture half-length (ft)	SRV (ft^3)
A	9	0.0083	110	775	6,394
B	6	0.0125	110	775	6,394
C	3	0.0250	110	775	6,394

Lean Condensate

Cumulative gas production in Figure 5.43 and cumulative condensate production in Figure 5.44 also show the close results between each case which cannot be seen clearly, therefore, Table 5.8 is useful for giving a closer look that the cumulative gas production is in the range between 6.74 Bcf to 6.77 Bcf or about 4.32% to 4.8 % increase of gas, and cumulative condensate production is in the range of 60.72 Mstb to 63.28 Mstb or 9.35% to 13.95% increment of condensate compared to non-fractured case.

Effects of SRV from case A, B and C show closed results in both cumulative gas production and cumulative condensate production which can be seen in Figure 5.45 and 5.46 respectively. The plateau rate of each case has small different duration which are 160 days, 152 days and 132 days for case A, B and C respectively before decline exponentially and end within about 5.5 years. While condensate production rates decline linearly about 5.5 years related to the plateau rate in gas production rate before decline exponentially until the end of production in every case.

From results in Table 5.8 it can be observed that case A gives the highest gas recovery, cumulative gas production, cumulative condensate production and fastest production time. This is because case A has higher contact area between reservoir and wellbore from 9 fractures. Therefore, this increases the chance for fluid to flow into the wellbore higher than case B and case C which have 6 fractures and 3 fractures.

Figure 5.47 exhibits less different results of abandonment pressures which are 1,568 psia, 1,571 psia and 1,576 psia with the condensate saturation of 0.0165, 0.017 and 0.018 for case A, B and C respectively as they are shown in Figure 5.48, 5.49 and 5.50. However, a closer look on draw down pressure behavior and production time indicate that case C, which has only 3 fractures in its design has lower potential to draw pressure out like other case. Therefore, it can be concluded that number of fractures has larger effect and is superior to fracture width in the study of the same SRV but different designs. Even though, fracture width can control inertial effect near fracture but higher number of fractures provides larger area for hydrocarbon to flow into the reservoir.

Table 5.8: Effect of stimulated reservoir volume in lean condensate

Case	Gas recovery factor (%)	Cumulative gas production (Bcf)	% increase of gas	Cumulative condensate production (Mstb)	% increase of condensate	Production time (Day)
Non-frac	53.45	6.46		55.53		2,954
A	55.99	6.77	4.78	63.28	13.95	1,955
B	55.92	6.76	4.63	62.57	12.67	1,981
C	55.75	6.74	4.32	60.72	9.35	2,056

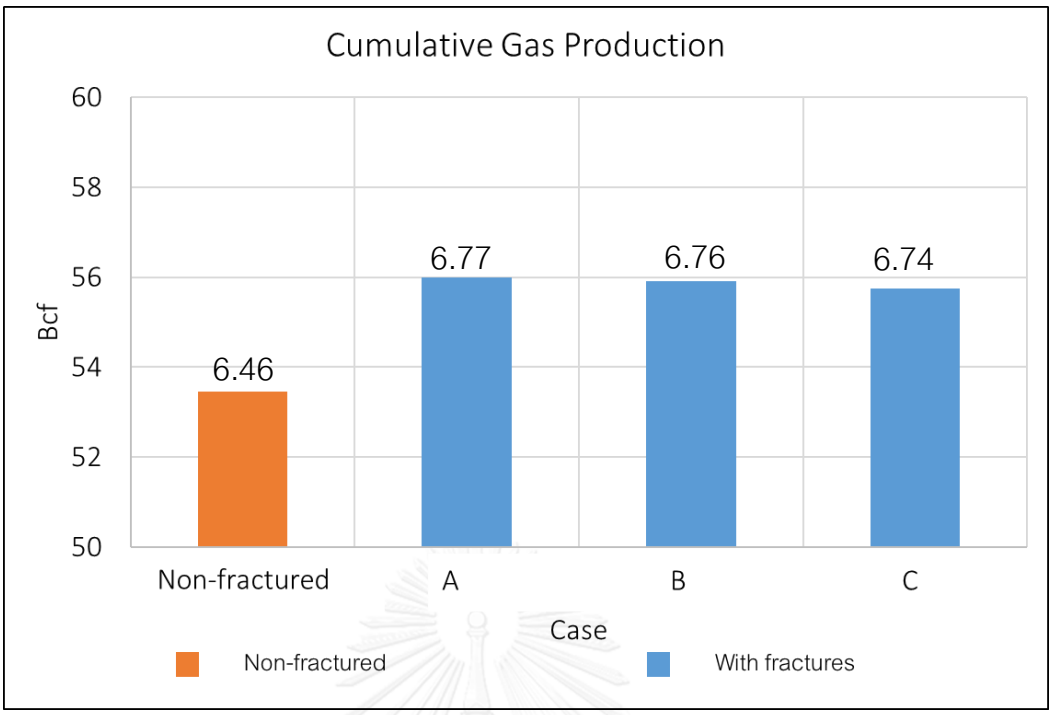

Figure 5.43: Comparison of cumulative gas production for the same SRV in lean condensate

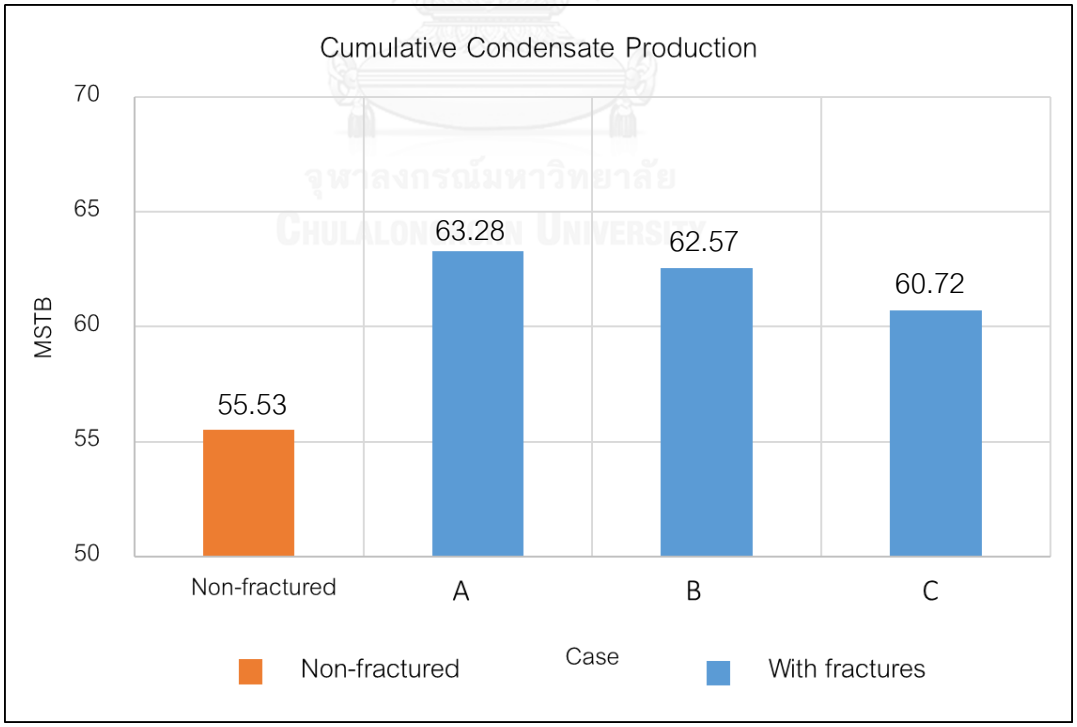

Figure 5.44: Comparison of cumulative gas production for the same SRV in lean condensate

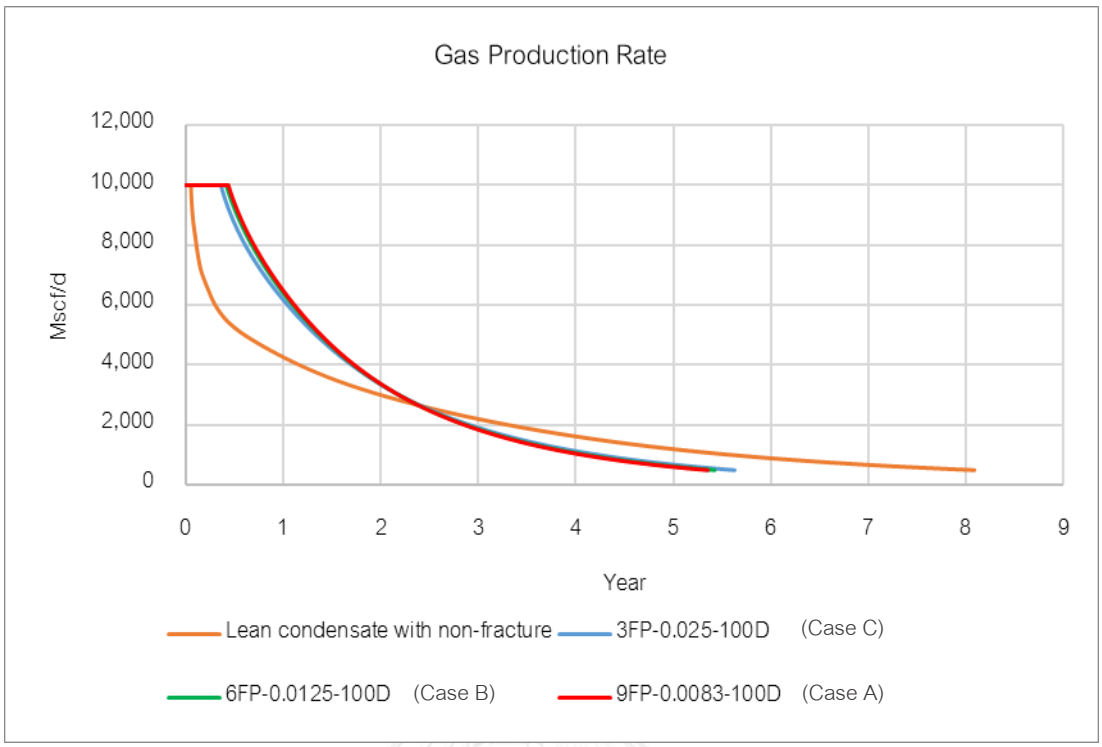

Figure 5.45: Gas production rate for the same SRV in lean condensate

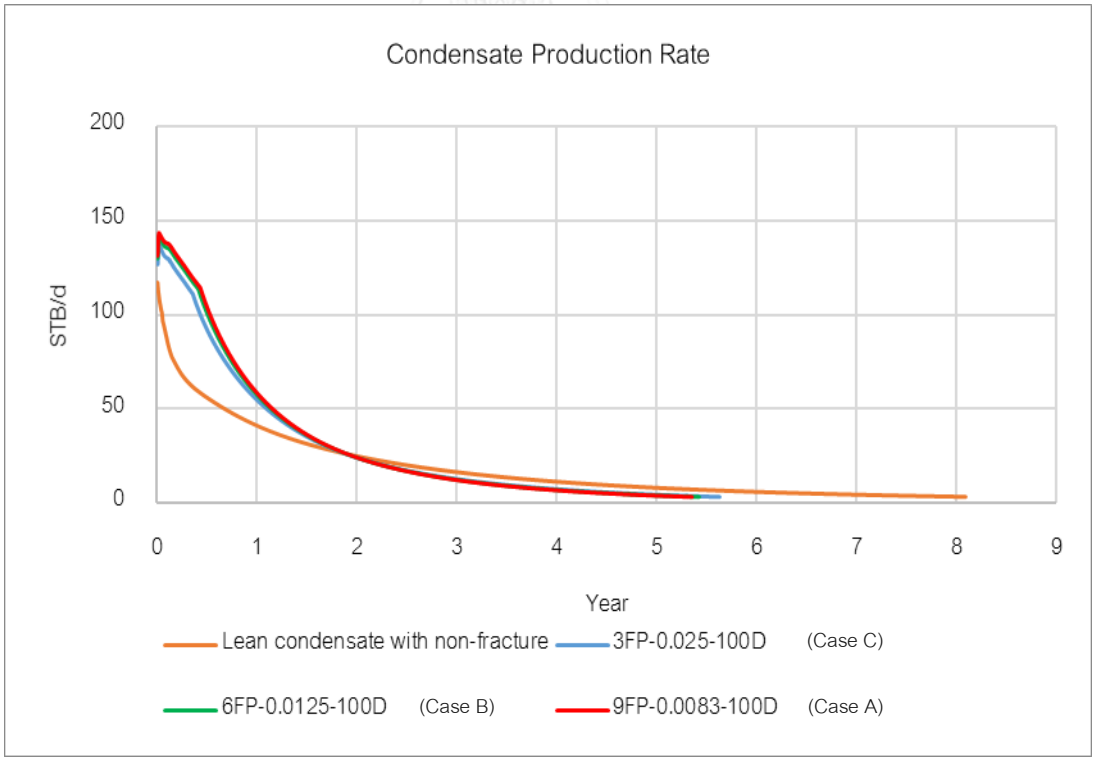

Figure 5.46: Condensate production rate for the same SRV in lean condensate

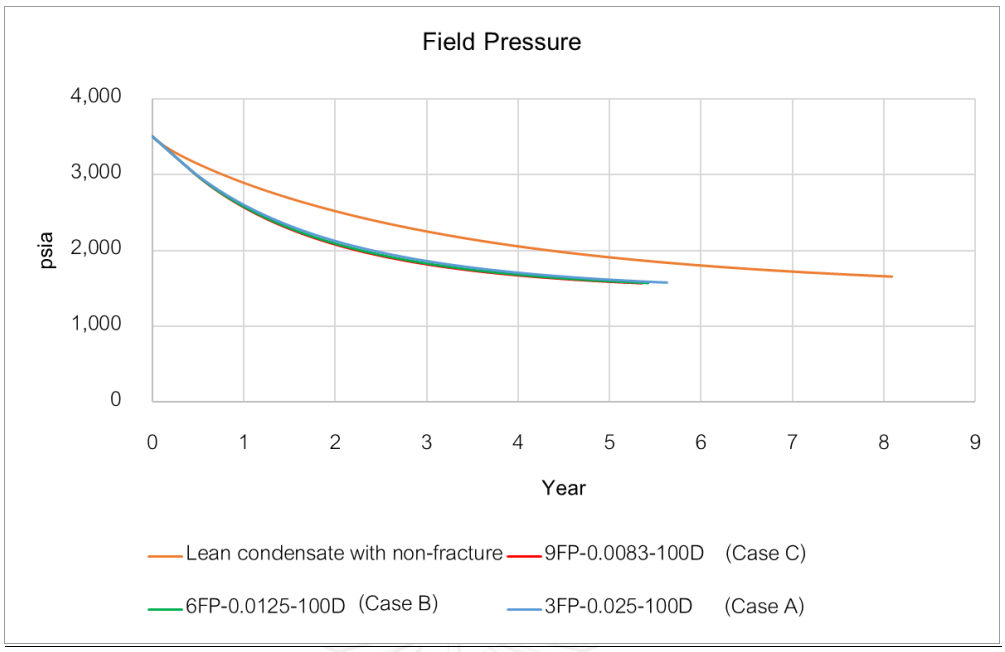

Figure 5.47: Effect of SRV at different designs on reservoir pressure in lean condensate

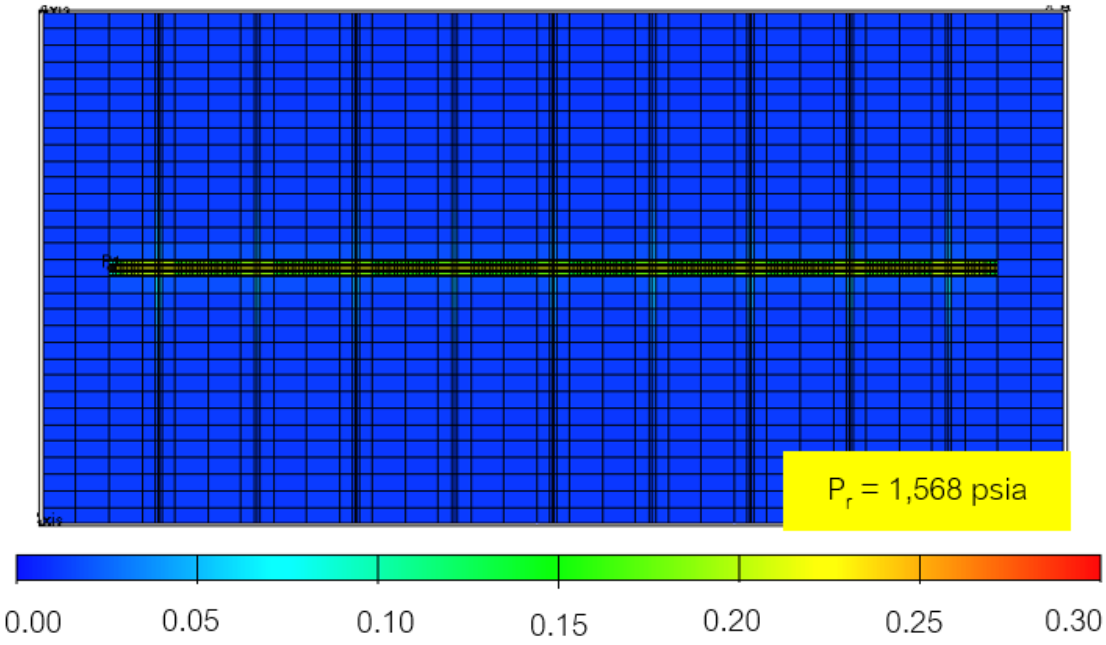

Figure 5.48 Effect of SRV (case A) on condensate saturation profile at the end of production in lean condensate

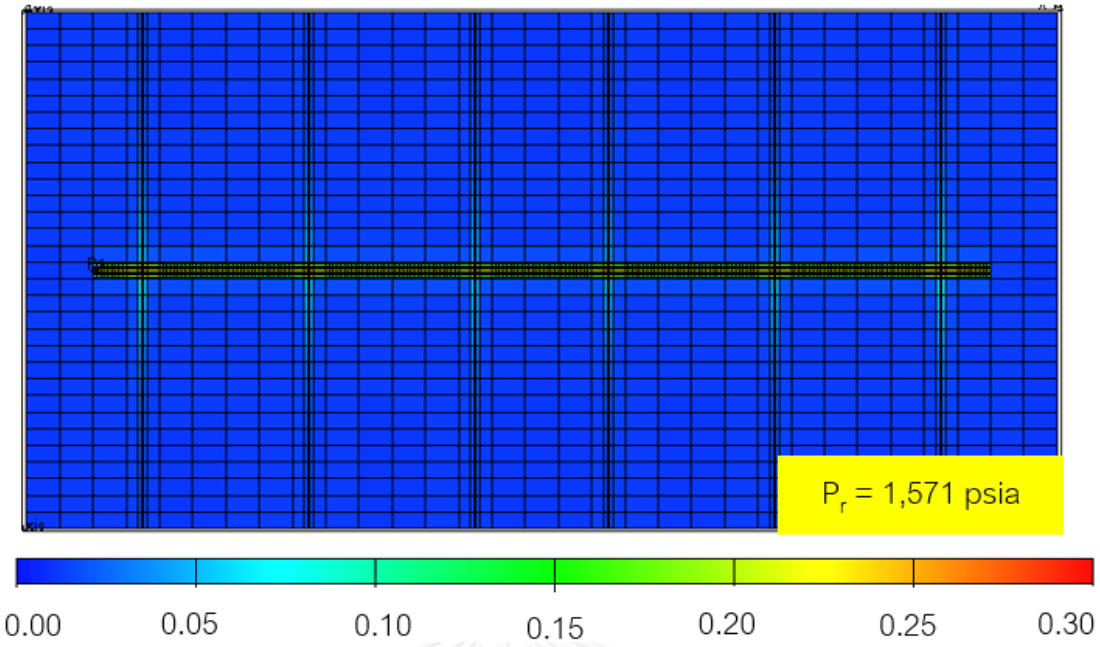

Figure 5.49 Effect of SRV design (case B) on condensate saturation profile at the end of production in lean condensate

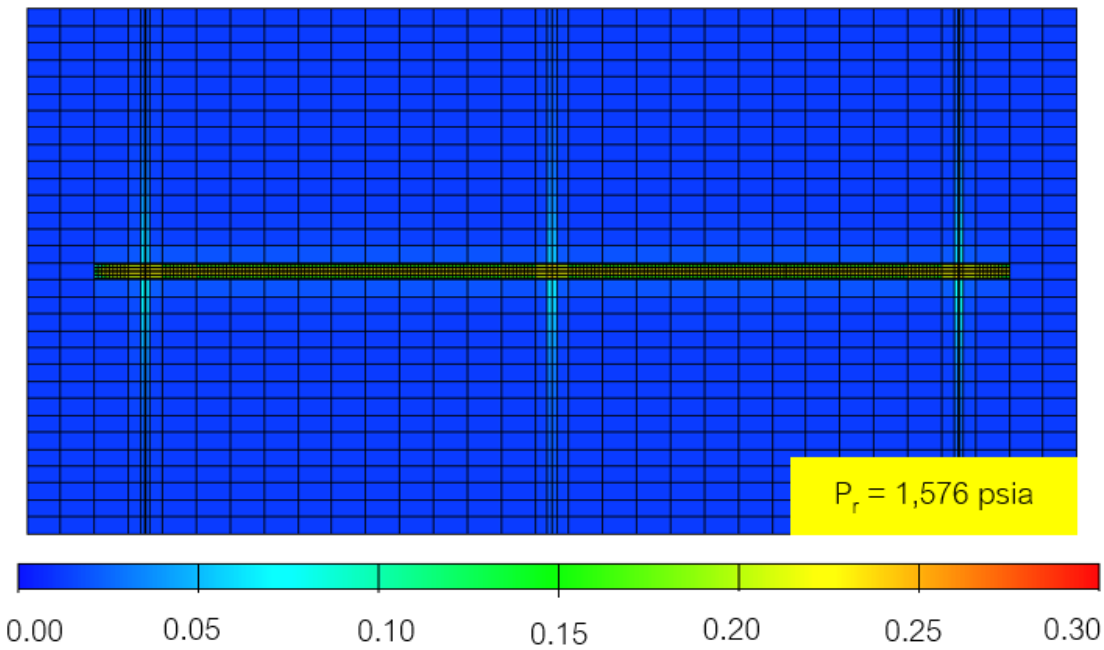

Figure 5.50 Effect of SRV design (case C) on condensate saturation profile at the end of production in lean condensate

Rich Condensate

Figure 5.51 and Figure 5.52 exhibit the comparison of cumulative gas production and cumulative condensate production at the same SRV but different design. Noticing that every case has close results in the range of 5.62 Bcf to 5.68 Bcf for cumulative gas production and in the range of 357.38 Mstb to 372.79 Mstb for cumulative condensate production.

Effect of SRV on rich condensate composition shows a similar trend to lean condensate composition which has close results in gas production rate as they are shown in Figure 5.53 and condensate production rate in Figure 5.54. Plateau rates can be maintained for 2 days in every case and condensate production rates decrease drastically until reach the end of production at about 7 years.

A closer look on Table 5.9 gives more details of percent increases compared to non-fractured case which are in the range of 6.43% to 7.55% for gas production and 7.17% to 11.79% for condensate production, and gas recovery is between 52.28%-52.83% compared to non-fractured which gives only 48.55 of gas recovery. It can be observed that case A gives the highest gas recovery, cumulative gas production, cumulative condensate production and fastest production time.

This is because case A gives higher chance for hydrocarbons to flow to the wellbore from 9 fractures more than 3 fractures of case C. Therefore, conclusion in this section is suggested that number of fractures has greater effect than fracture width in rich condensate composition.

Table 5.9: Effect of stimulated reservoir volume in rich condensate

Case	Gas recovery factor (%)	Cumulative gas production (Bcf)	% increase of gas	Cumulative condensate production (Mstb)	% increase of condensate	Production time (Day)
Non-frac	48.55	5.28		333.46		4,261
A	52.83	5.68	7.55	372.79	11.79	2,439
B	52.68	5.66	7.25	369.11	10.69	2,497
C	52.28	5.62	6.43	357.38	7.17	2,669

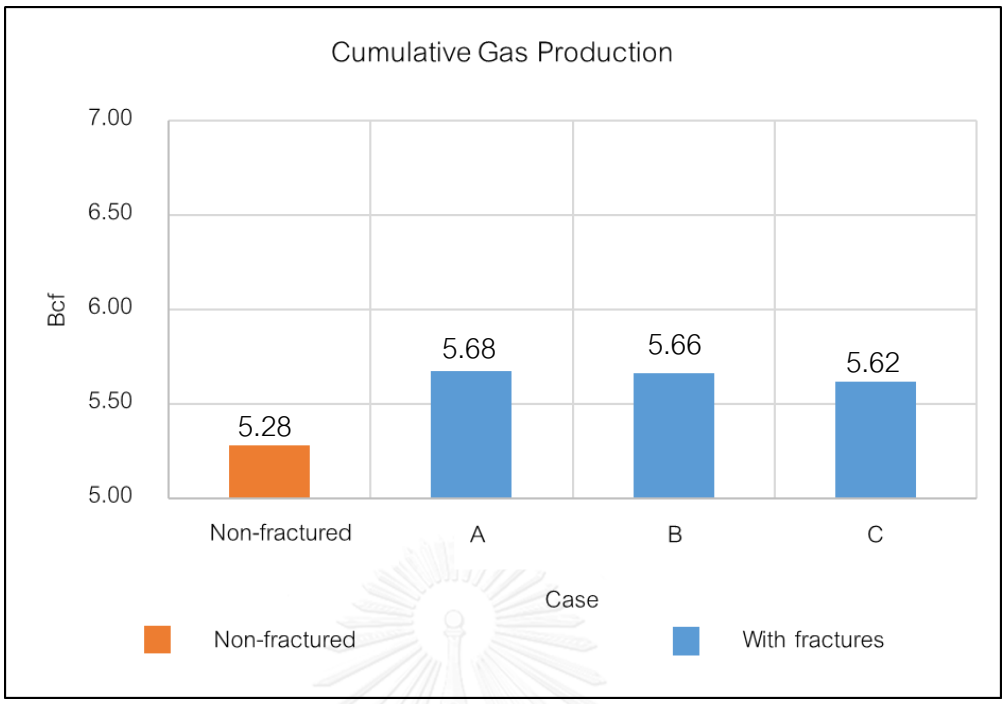

Figure 5.51: Cumulative gas production for the same SRV in rich condensate

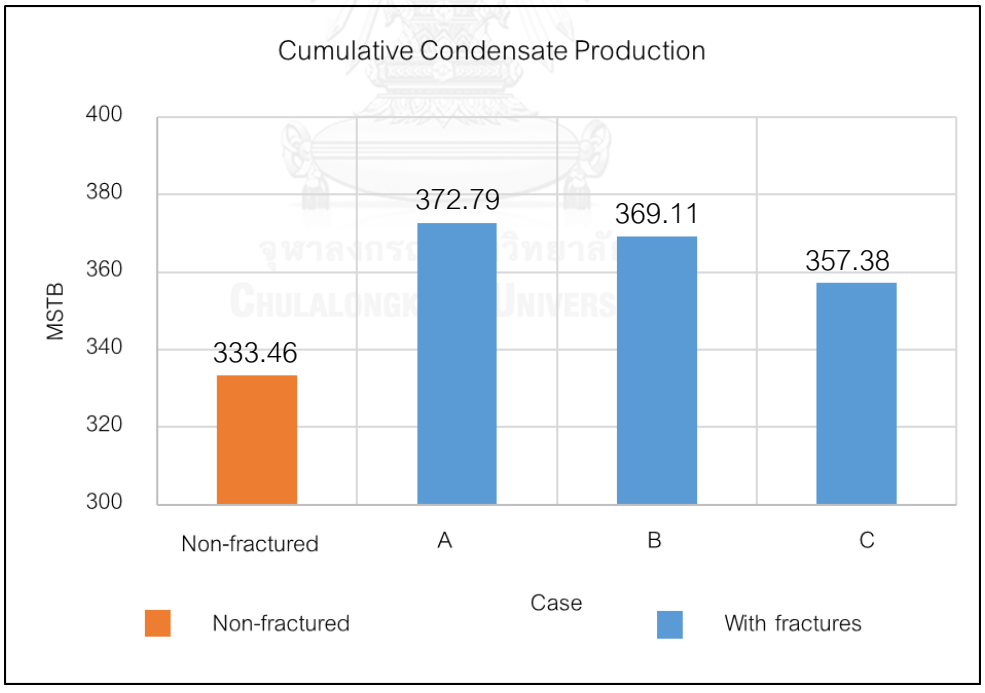

Figure 5.52: Cumulative condensate production for the same SRV in rich condensate

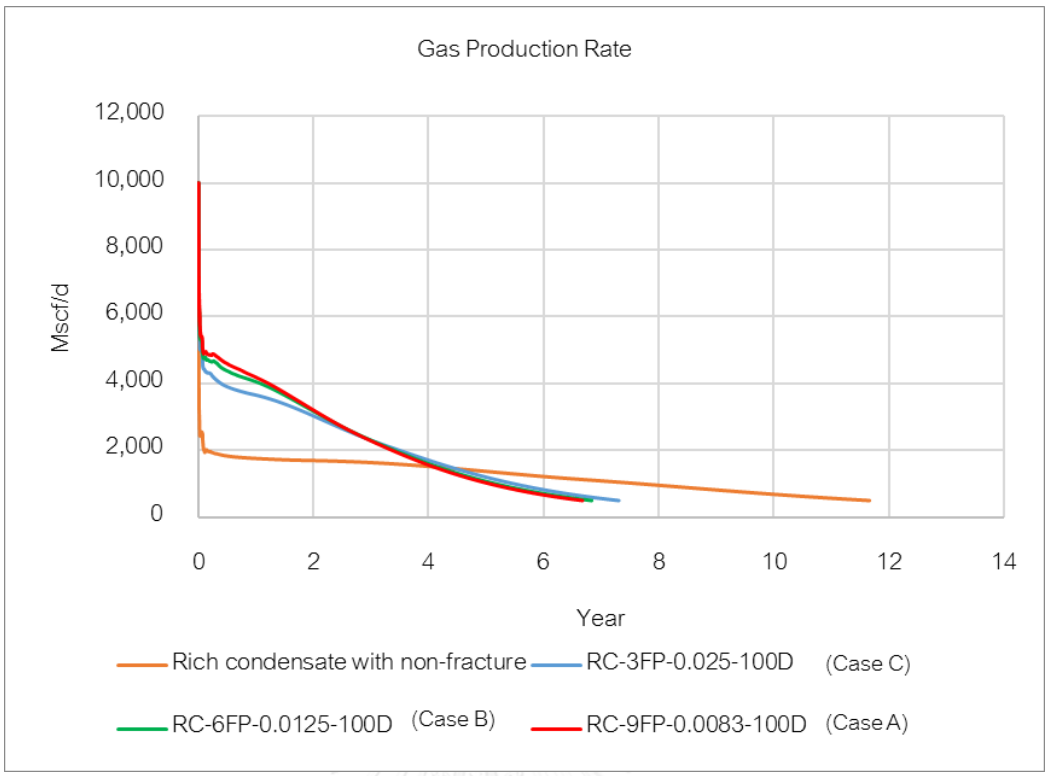

Figure 5.53: Gas production rate for the same SRV in rich condensate

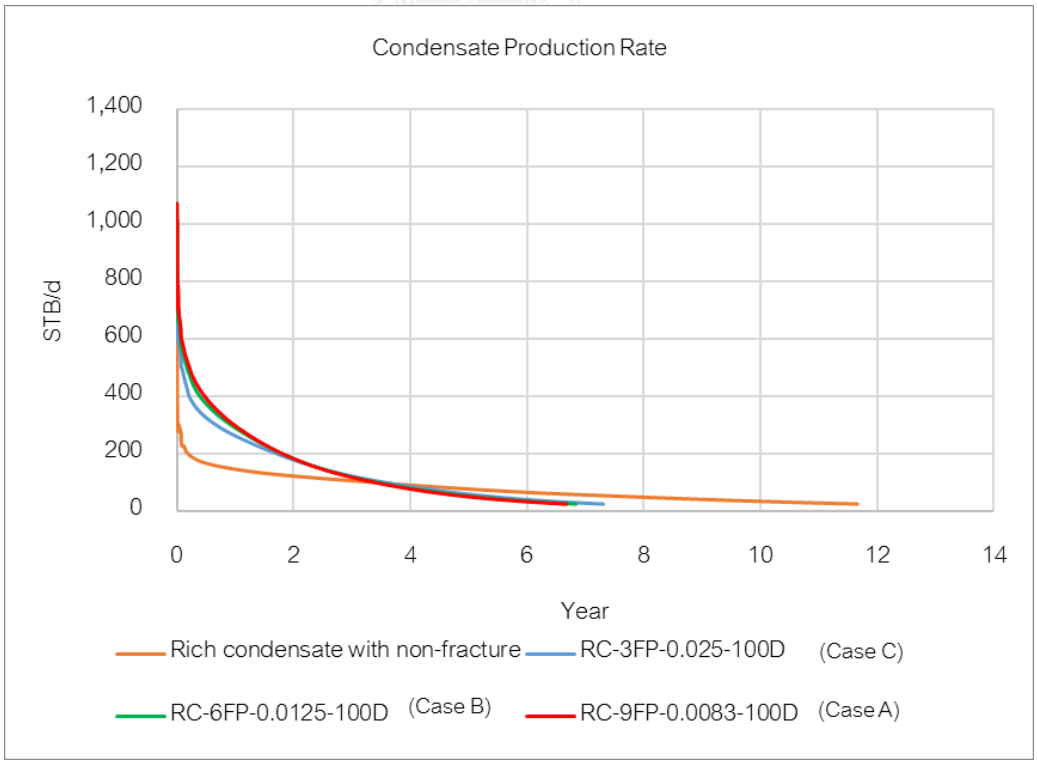

Figure 5.54: Condensate production rate for the same SRV in rich condensate

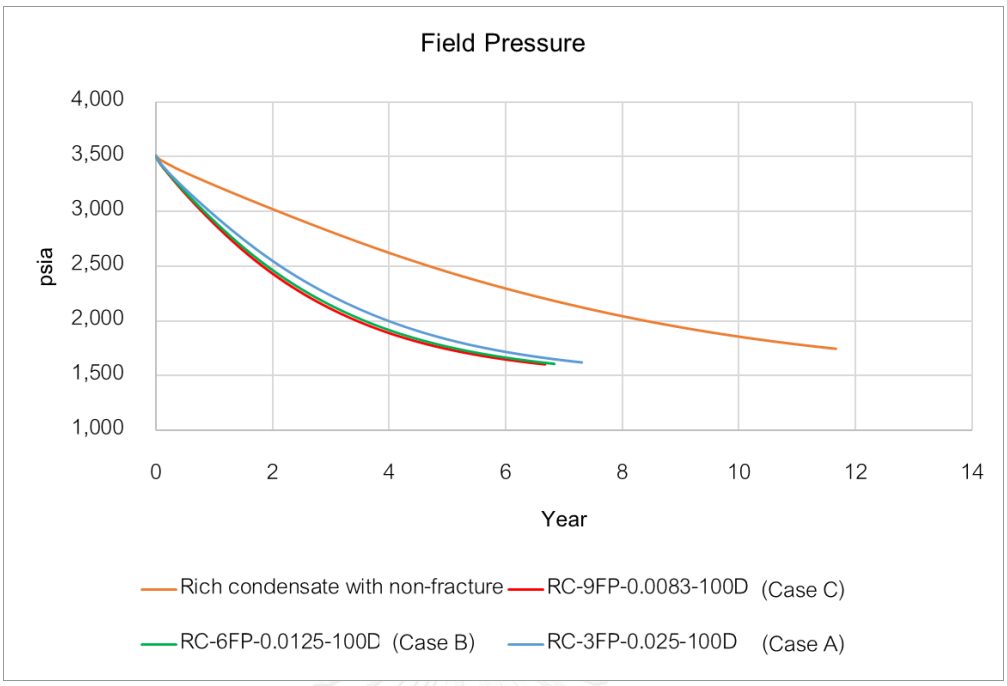

Figure 5.55: Effect of SRV at different designs on reservoir pressure in rich condensate

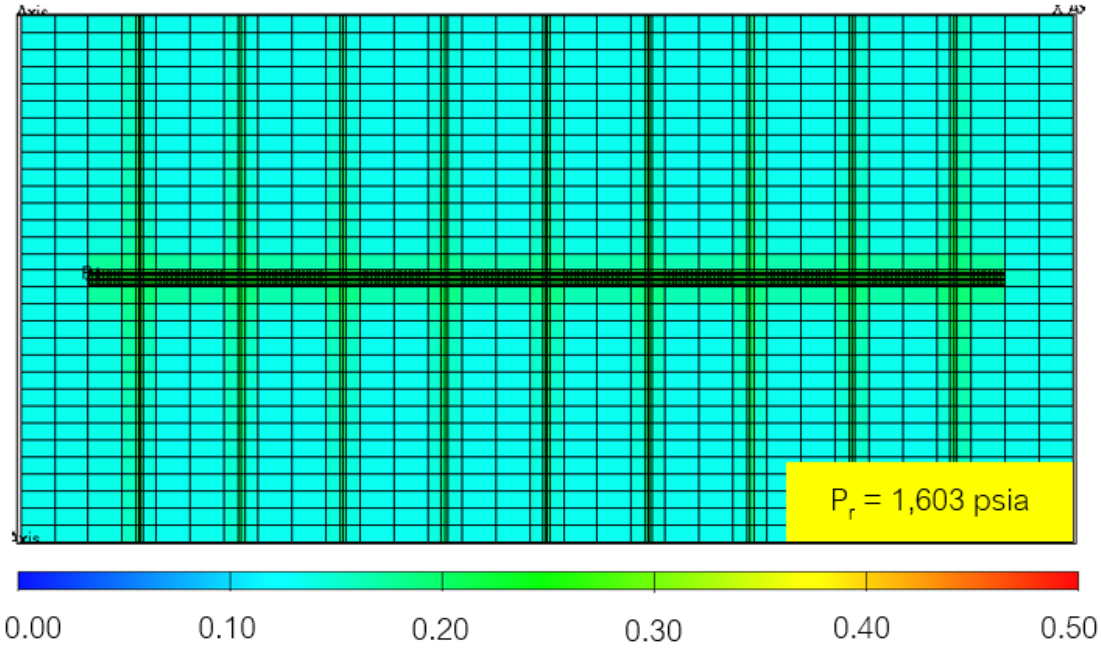

Figure 5.56 Effect of SRV (case A) on condensate saturation profile at the end of production in rich condensate

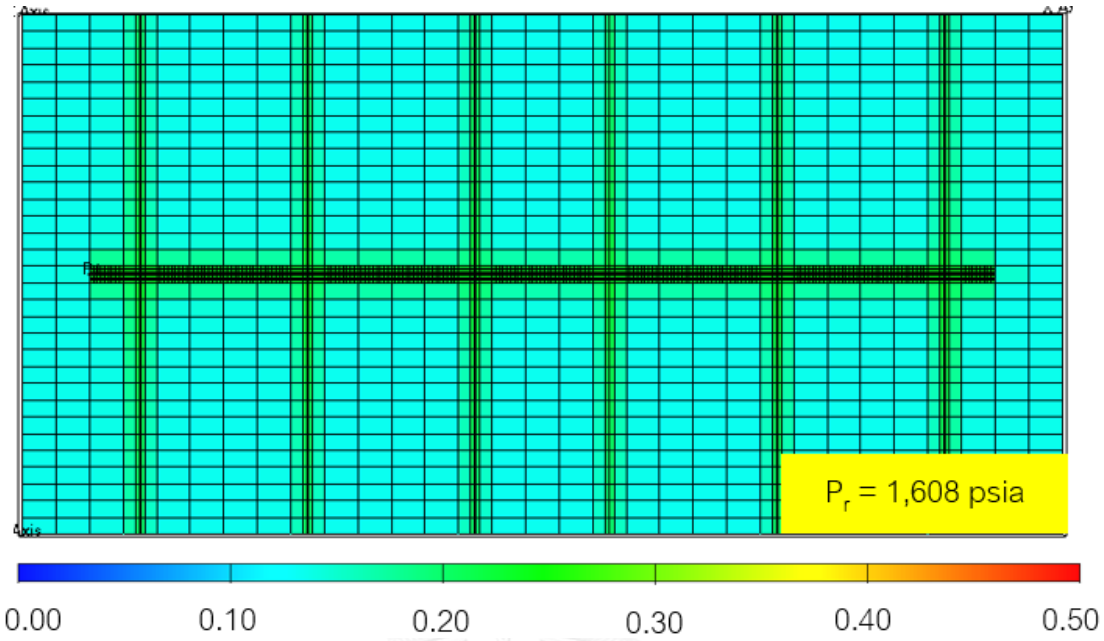

Figure 5.57 Effect of SRV design (case B) on condensate saturation profile at the end of production in rich condensate

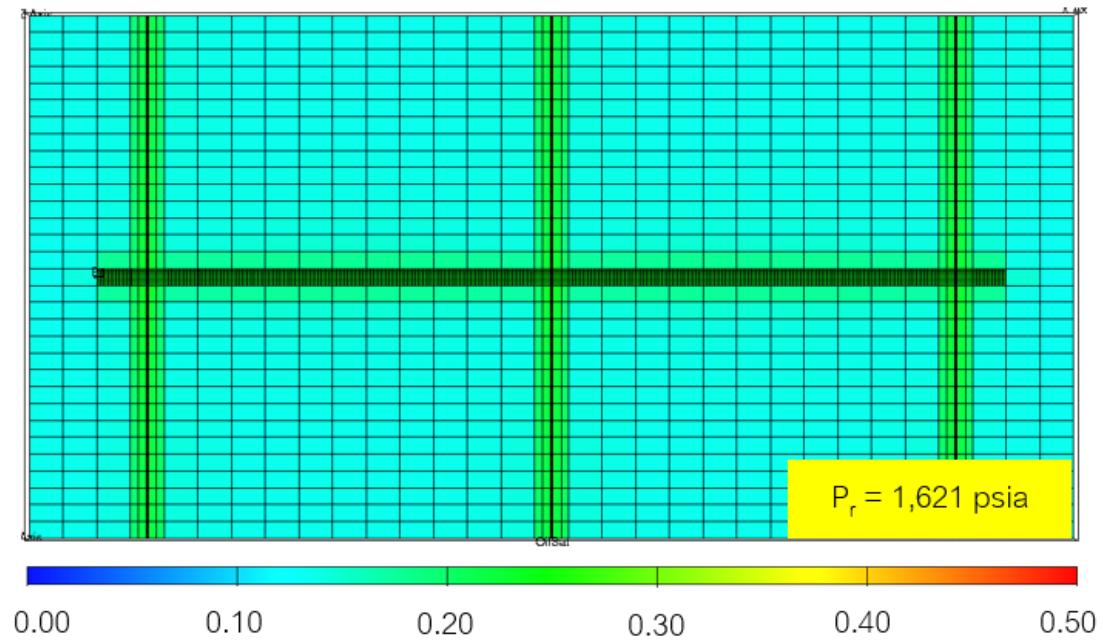

Figure 5.58 Effect of SRV design (case C) on condensate saturation profile at the end of production in rich condensate

5.2.4 Fracture Permeability

According to the last section, the best SRV is case A. Therefore, three values of fracture permeability will be varied which are 50,000 mD, 100,000 mD and 150,000 mD. The selection of fracture permeability in this study based on the stress value of the reservoir at the depth of 8,000 ft. and suitable size of proppant which related to grain size of the reservoir. Meanwhile we kept other parameters constant such as fracture width, number of fractures and fracture half-length at 0.0083 ft., 9 fractures and 775 ft. respectively corresponding case A design as they are shown in Table 5.7 in previous section.

Lean Condensate

Figure 5.59 shows small different cumulative gas productions which are in the range between 6.71 Bcf to 6.81 Bcf or 4.63% to 6.50% increment of gas production compared to non-fractured case as they are shown in Table 5.10. While cumulative condensate production is in the range of 61.87 Mstb to 64.02 or 1.90% to 2.55% increment of condensate production compared to non-fractured case. However, only small increment of gas and condensate production from 50,000 mD to 150,000 mD can be observed. The reason is because fracture permeability at 50,000 mD is already high enough compared to reservoir permeability at 0.2 mD.

The higher fracture permeability the longer plateau rate at 10,000 Mscf/d can be maintained as they are shown in Figure 5.61. Figure 5.62 depicts the condensate production rates that decline linearly when gas production shows plateau rate before drop exponentially until it reaches their end of production within 6 years.

Further investigation on the effect of fracture permeability can be observed in Figure 5.63 where reservoir pressure of each fracture permeability is shown. Even reservoir pressure at the abandonment has quite different, such as 1,586 psia for 50,000 mD, 1,568 psia for 100,000 mD and 1,558 psia for 150,000 mD, but the condensate at the end of the production of those cases has less different result which are 0.0174, 0.0163

and 0.0156 for 50,000 mD, 100,000 mD and 150,000 mD respectively as they are shown in Figure 5.64, Figure 5.65 and Figure 5.66. Therefore, it can be concluded in this section that increasing fracture permeability higher than 50,000 mD cannot give much more improvement on hydrocarbon production.

Table 5.10: Effect of fracture permeabilities in lean condensate

Fracture Permeability (mD)	Gas recovery factor (%)	Cumulative gas production (Bcf)	% increase of gas	Cumulative condensate production (Mstb)	% increase of condensate	Production time (Days)
Non-frac	53.45	6.46		55.53		2,954
50,000	55.46	6.71	4.63	61.87	1.90	2,188
100,000	55.99	6.77	5.85	63.28	2.32	1,955
150,000	56.28	6.81	6.50	64.02	2.55	1,822

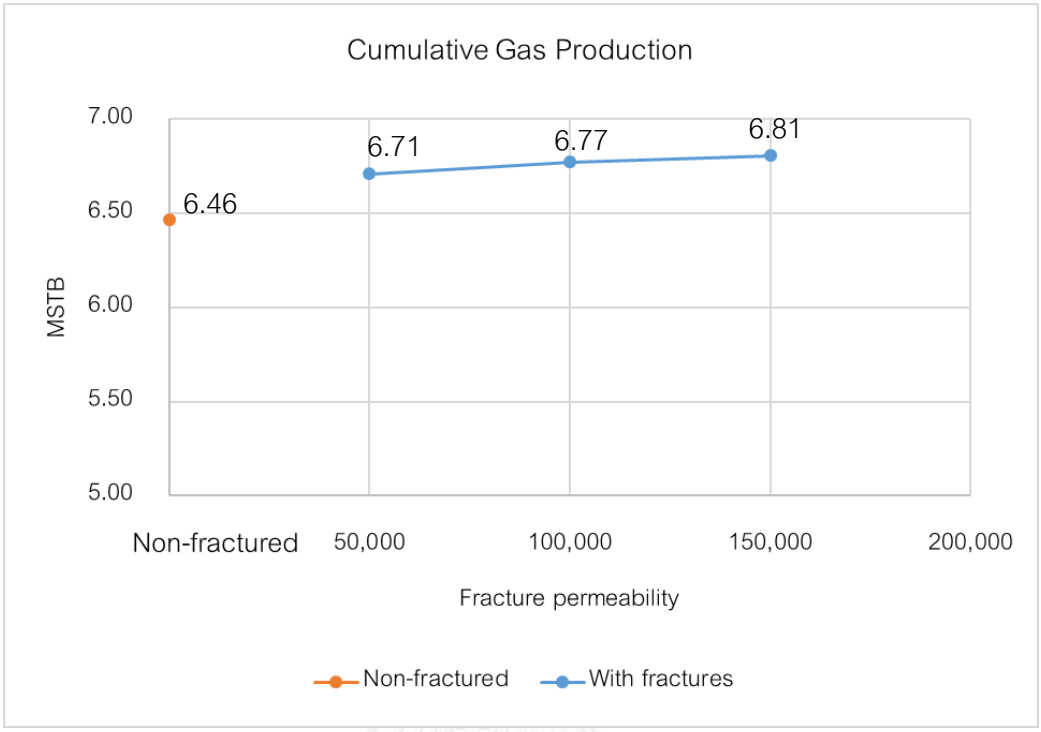

Figure 5.59: Cumulative gas production with different fracture permeabilities in lean condensate

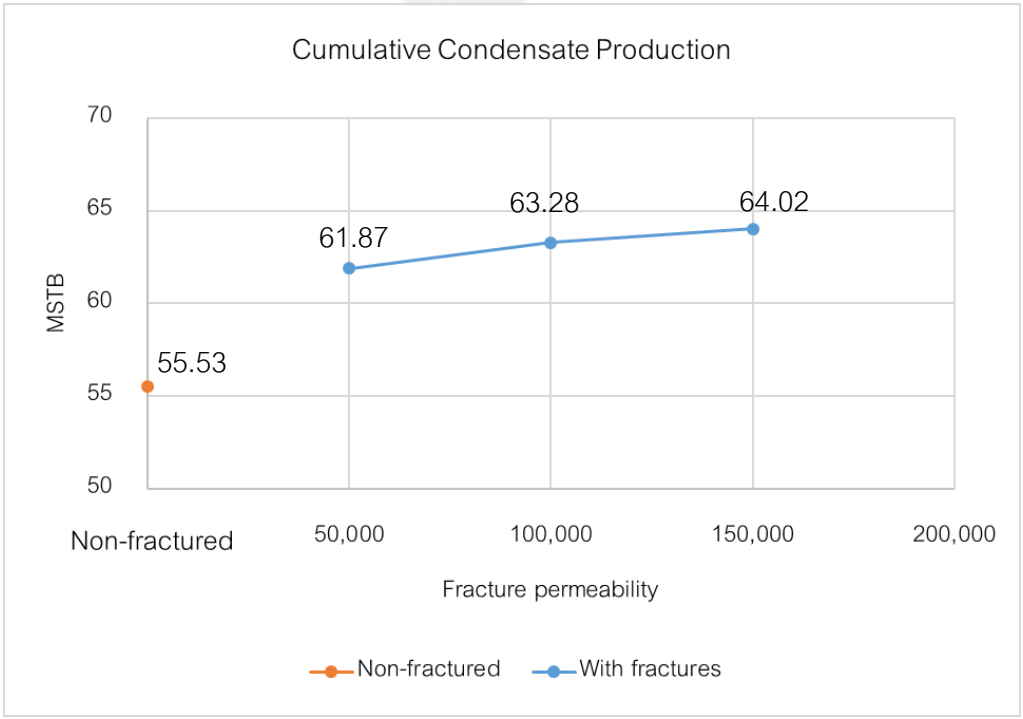

Figure 5.60: Cumulative condensate production with different fracture permeabilities in lean condensate

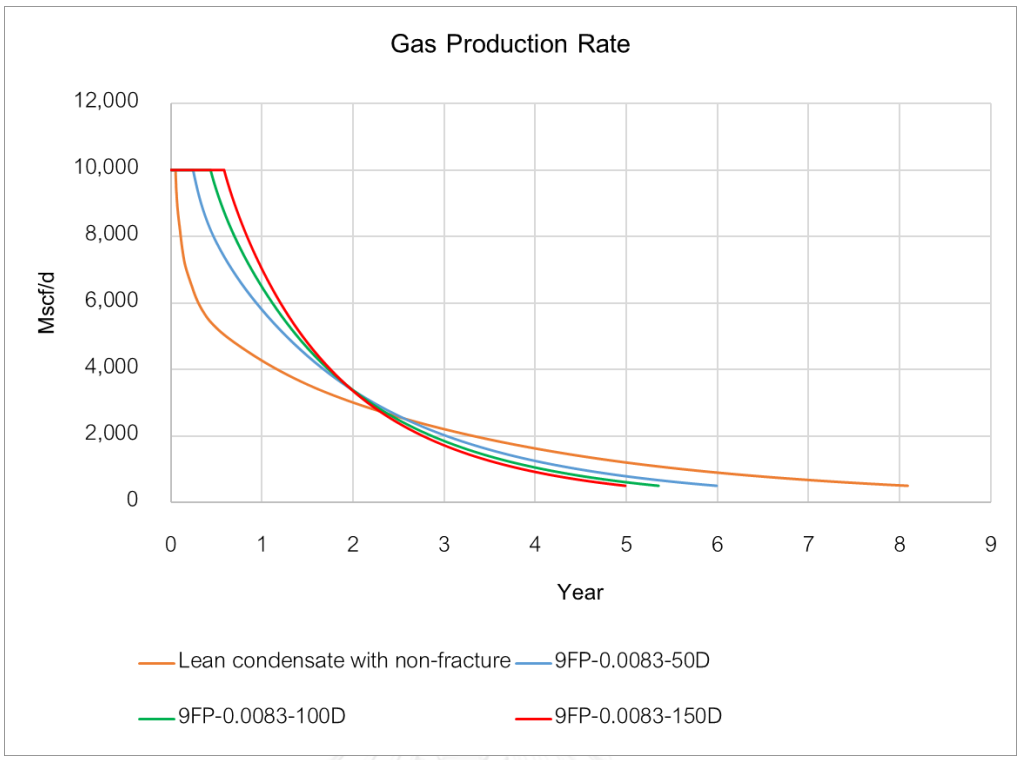

Figure 5.61: Gas production rate with different fracture permeabilities in lean condensate

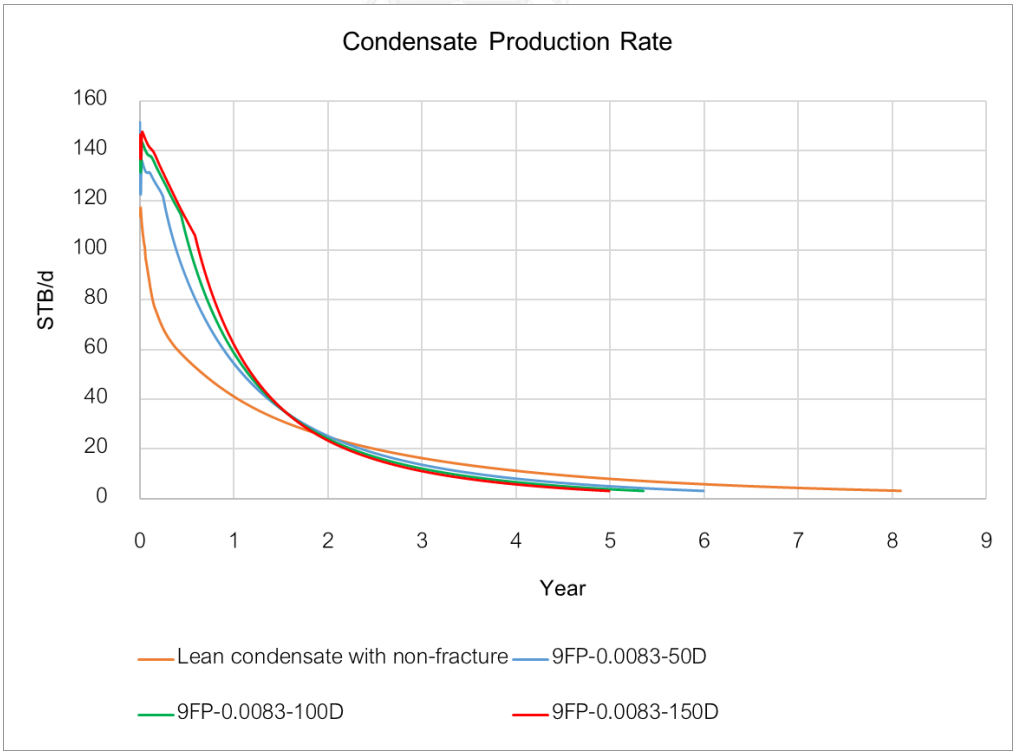

Figure 5.62: Condensate production rate with different fracture permeabilities in lean condensate

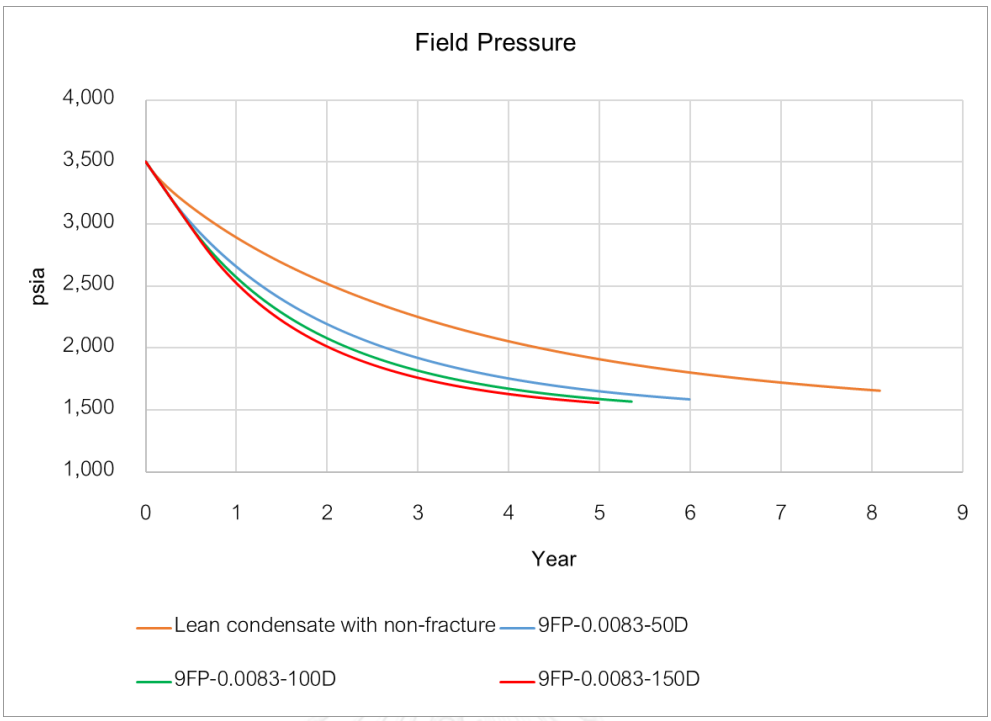

Figure 5.63: Effect of fracture permeabilities on reservoir pressure in lean condensate

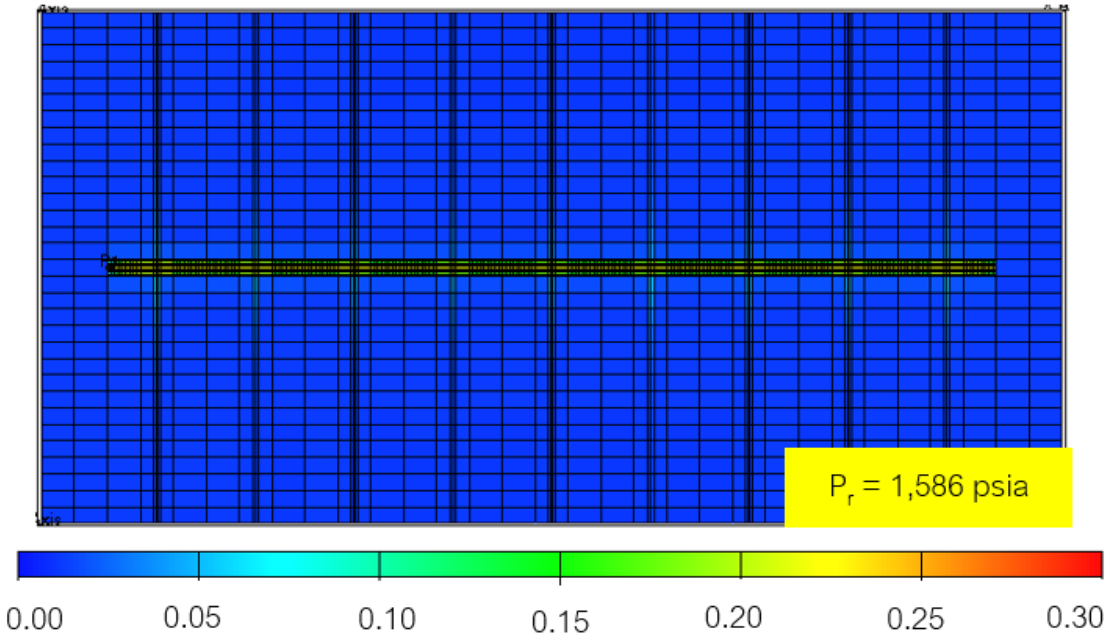

Figure 5.64 Effect of fracture permeability at 50,000 mD on condensate saturation profile at the end of production in lean condensate

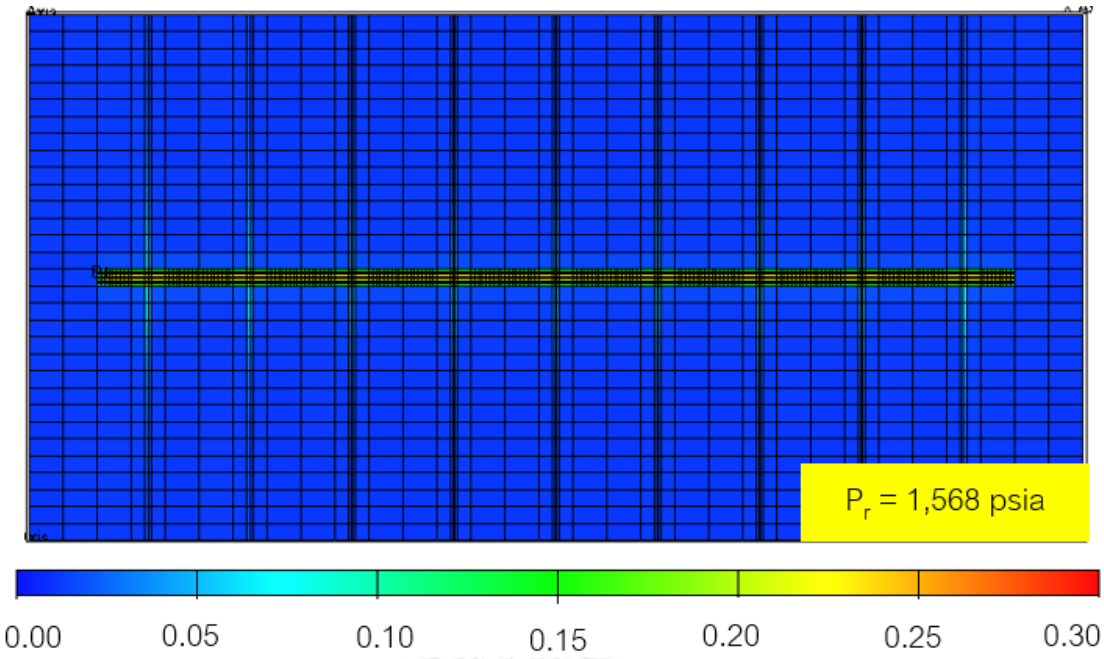

Figure 5.65 Effect of fracture permeability at 100,000 mD on condensate saturation profile at the end of production in lean condensate

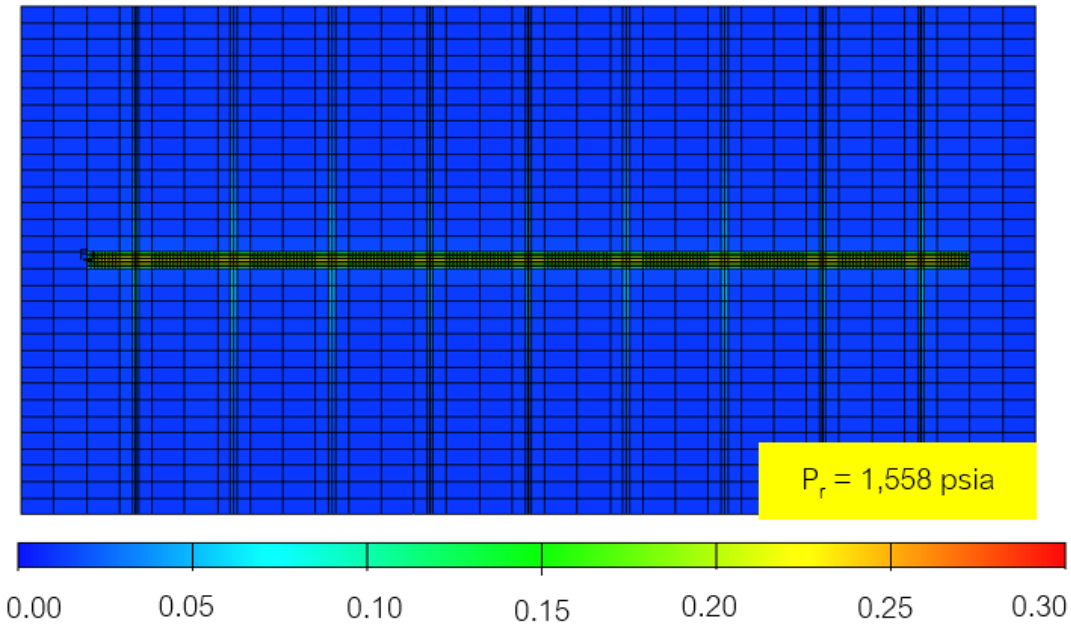

Figure 5.66 Effect of fracture permeability at 150,000 mD on condensate saturation profile at the end of production in lean condensate

Rich Condensate

Figure 5.67 exhibits comparison of cumulative gas production which in the range of 5.60 Bcf to 5.72 Bcf or 6.00% to 8.41% increment of gas production compared to non-fracture case as they are shown in Table 5.11. While Figure 5.68 depicts results of cumulative condensate production which in the range of 368.85 Mstb to 374.15 Mstb or 10.61% to 12.20% increment of condensate production compared to non-fracture case in Table 5.11. However, an interesting trend can be noticed in Figure 5.68 there are small improvements of cumulative condensate production after fracture 50,000 mD was performed. However, it still pronounces its benefit in the form of production time that is, the higher permeability, the faster production time can be obtained.

Gas production rates can be maintained shorter than lean condensate case in every case at the same design as they are depicted in Figure 5.69. Only the highest fracture permeability at 150,000 mD shows the potential of maintaining plateau rate for 3 days while other cases can maintain only for 2 days. Rich condensate cases also show theirs effects on condensate production rates in Figure 5.70 where rates decline drastically since the early time.

Effect of fracture permeability can be investigated further in Figure 5.71 where reservoir pressures are shown and from Figure 5.72, Figure 5.73 and Figure 5.74 that show condensate saturation profiles at the abandonment.

The highest fracture permeability of 150,000 mD gives the ability to draw faster and abandon at the lowest pressure at 1,558 psia. With this low pressure at abandonment, hydrocarbon can be produced and released more than other cases. However, the improvements between each case are quite small because fracture permeability at 50,000 mD is quite high compared to reservoir permeability at 0.2 mD. Therefore, increasing permeability up to 100,000 mD and 150,000 mD might be less important. However, economic analysis is recommended to evaluated the initial cost and production of each case before final conclusion could be made.

Table 5.11: Effect of fracture permeabilities in rich condensate

Fracture Permeability (mD)	Gas recovery factor (%)	Cumulative gas production (Bcf)	% increase of gas	Cumulative condensate production (Mstb)	% increase of condensate	Production time (Days)
Non-frac	48.55	5.28		333.46		4,261
50,000	52.07	5.60	6.00	368.85	10.61	2,814
100,000	52.83	5.68	7.55	372.79	11.79	2,439
150,000	53.25	5.72	8.41	374.15	12.20	2,223

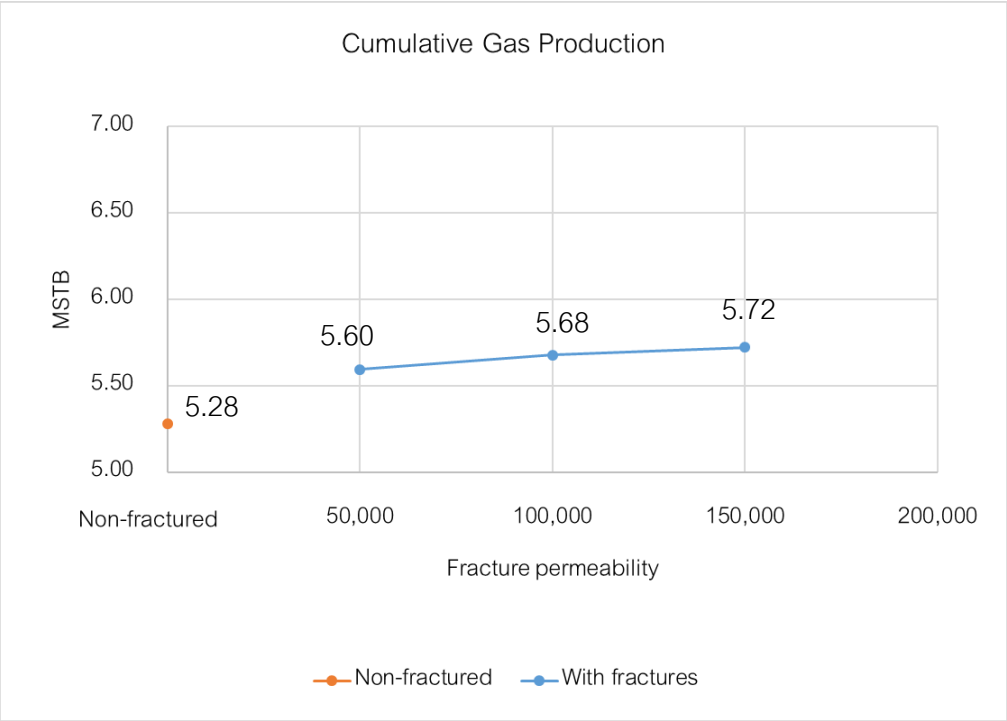

Figure 5.67: Comparison of cumulative gas production with different fracture permeabilities in rich condensate

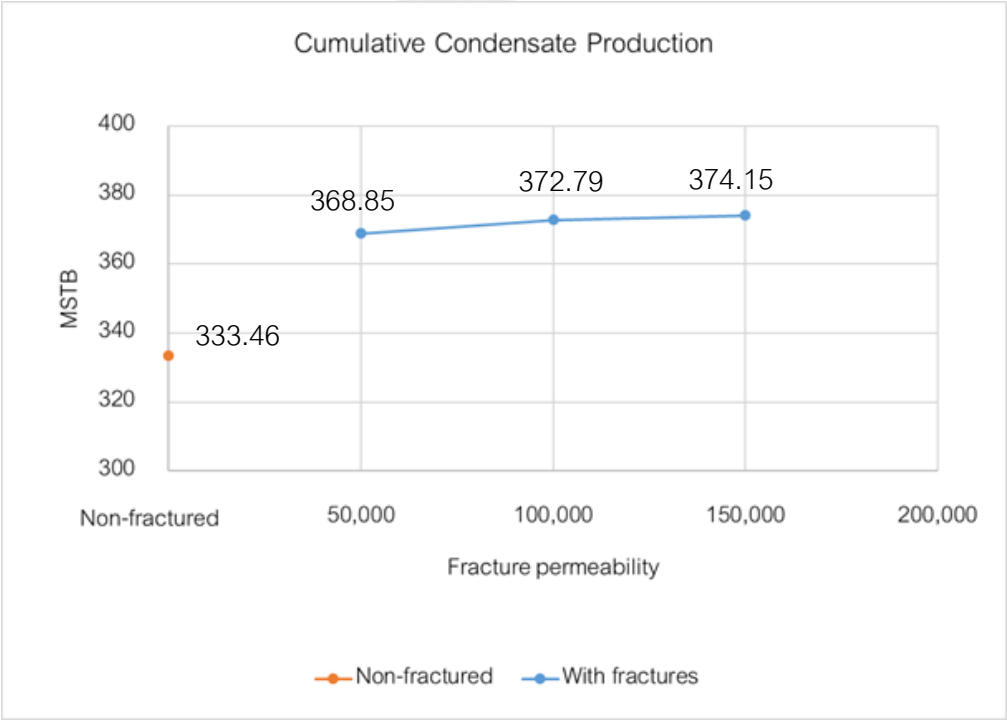

Figure 5.68: Comparison of cumulative condensate production with different fracture permeabilities in rich condensate

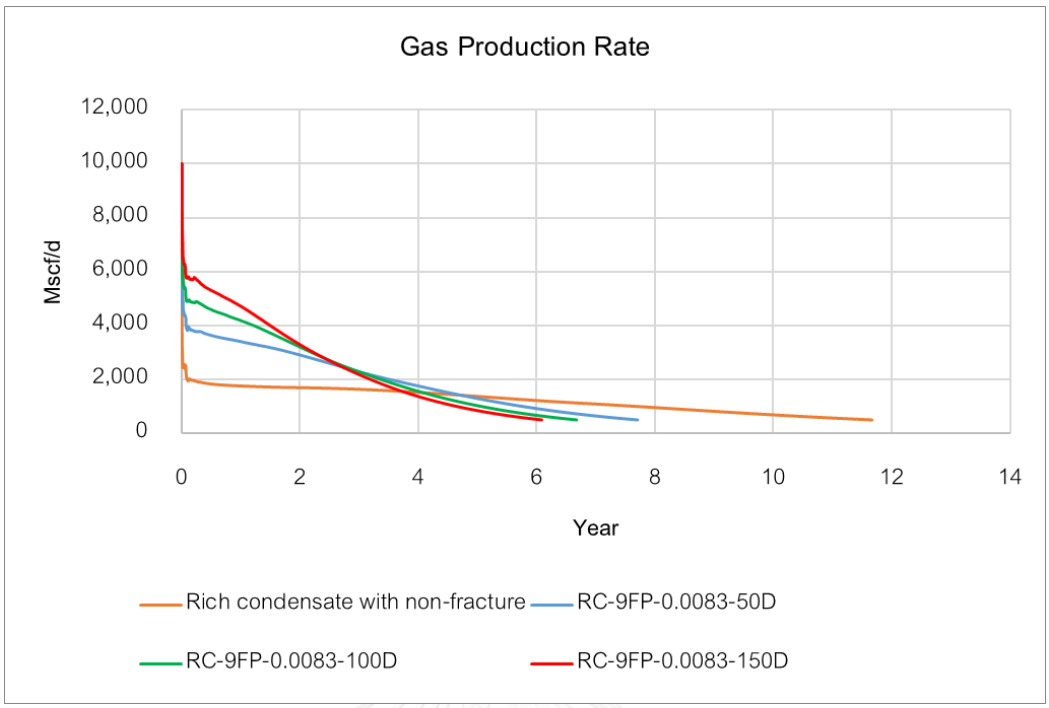

Figure 5.69: Gas production rate with different fracture permeabilities in rich condensate

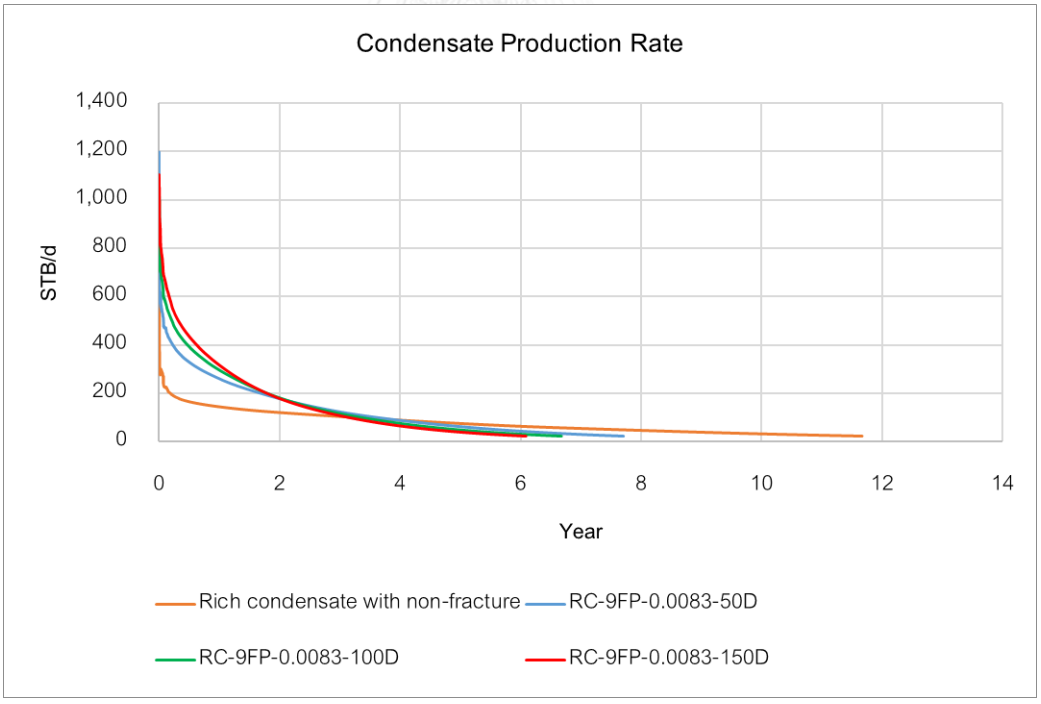

Figure 5.70: Condensate production rate with different fracture permeabilities in rich condensate

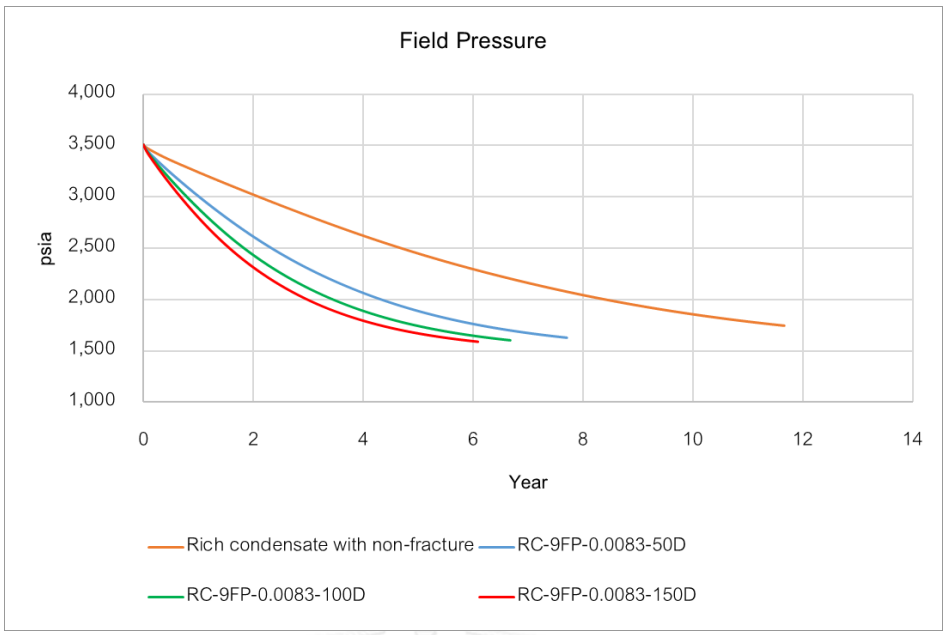

Figure 5.71: Effect of fracture permeabilities on reservoir pressure in rich condensate

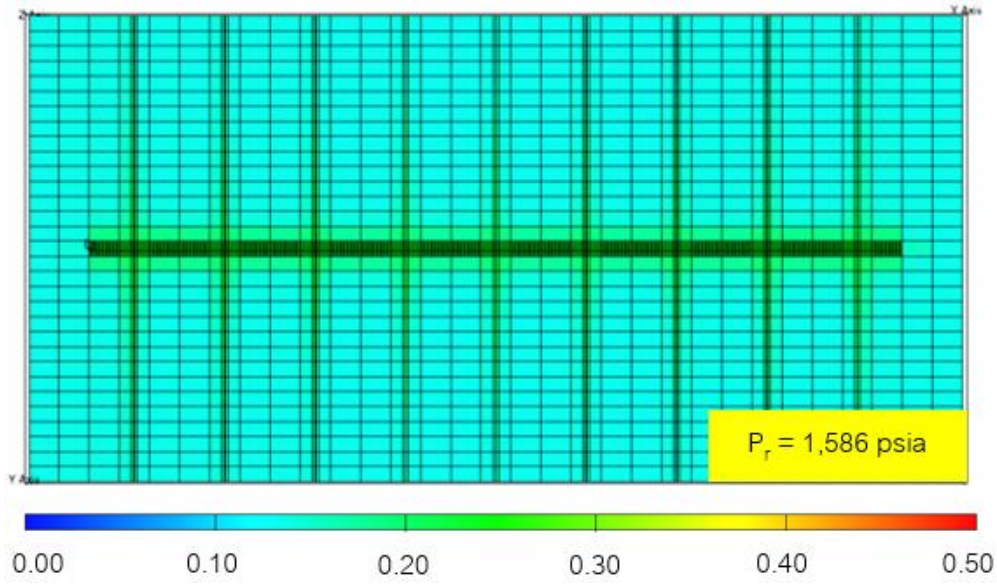

Figure 5.72 Effect of fracture permeability at 50,000 mD on condensate saturation profile at the end of production in rich condensate

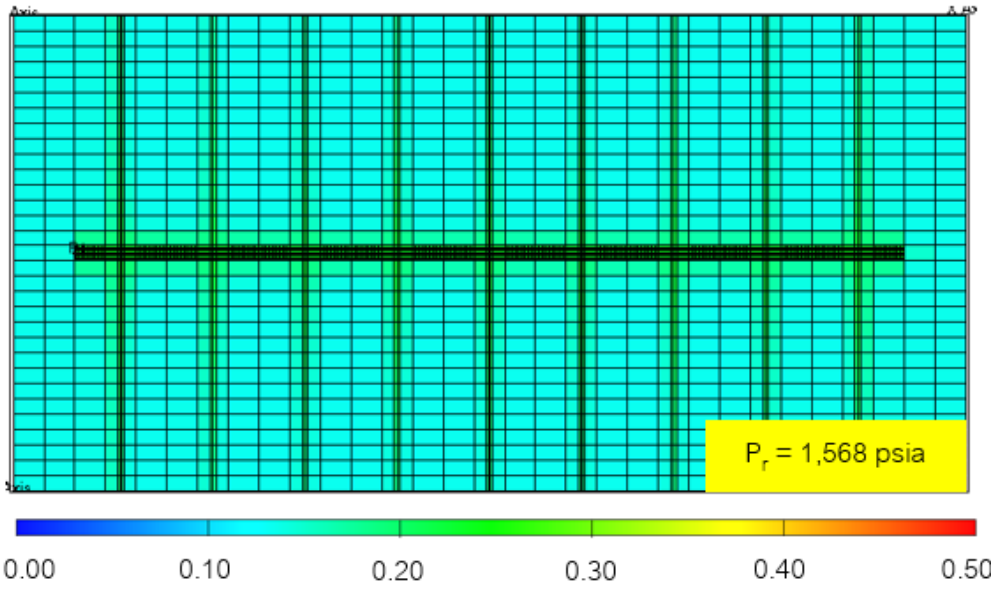

Figure 5.73 Effect of fracture permeability at 100,000 mD on condensate saturation profile at the end of production in rich condensate

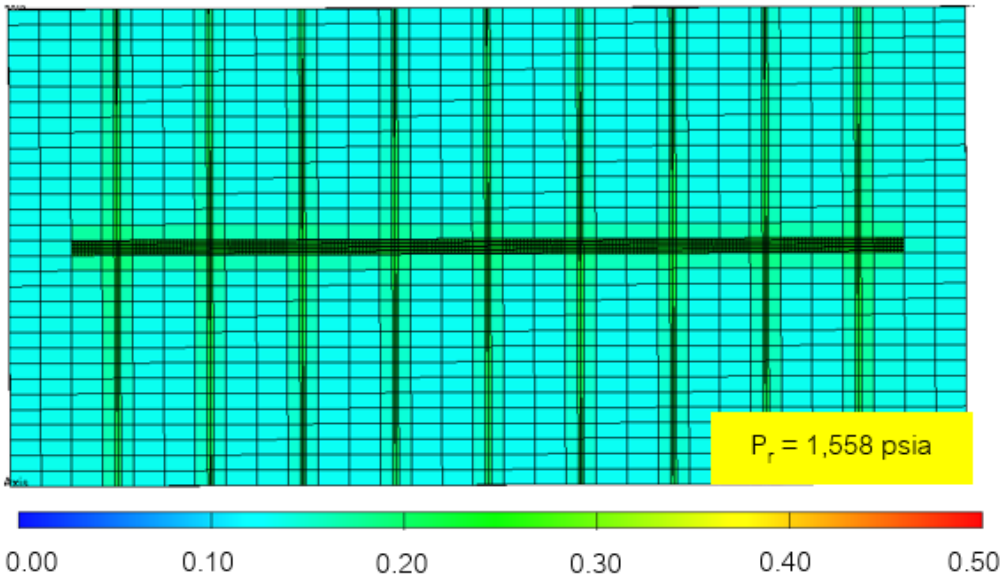

Figure 5.74 Effect of fracture permeability at 150,000 mD on condensate saturation profile at the end of production in rich condensate

5.3 Saturation Profiles Near Wellbore

The investigation of condensate saturation profile near wellbore versus time is defined by the nearest block beside the wellbore. Then region of condensate banking around wellbore at the highest condensate saturation will be studied, cross-section along y-direction was made to observe the change of region as it is shown in Figure 5.75. The result of fractured cases from each case in each studied parameter is evaluated compared to non-fracture case to see the effect of hydraulic fracturing near wellbore.

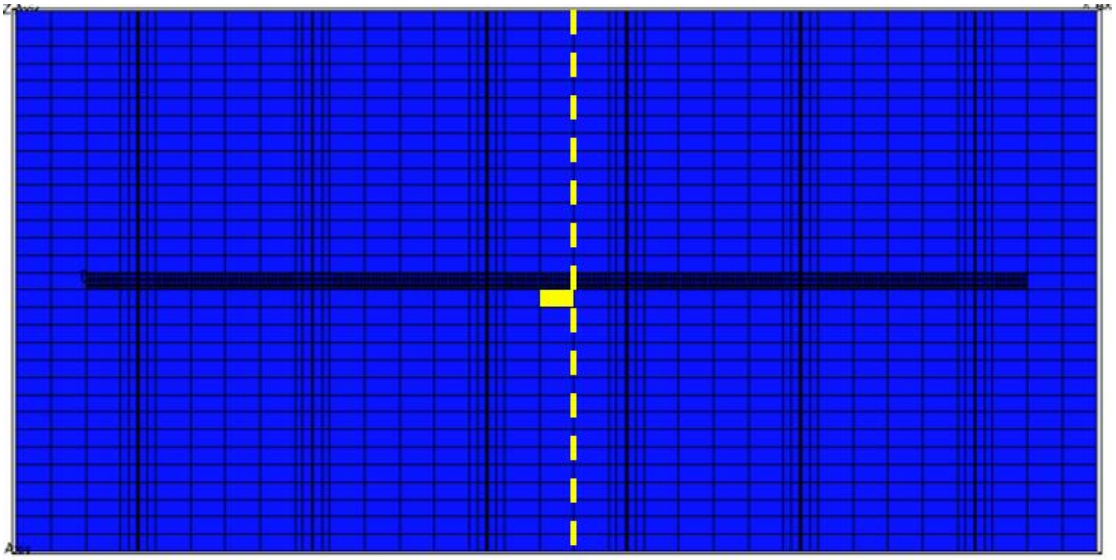

Figure 5.75 Near wellbore location and cross-section along y-direction

Lean Condensate

After the production started and pressure continued to deplete, the liquid started to form near wellbore. The 6 folds increasing or the fraction of 0.022 condensate saturation can be observed for the case of non-fractured well from the third year until the end of production of 8 years. Once the hydraulic fracturing was performed, it reduces condensate saturation near wellbore in every studied parameter.

From Figure 5.76, fracture width decreases condensate saturation near wellbore to 0.0165, 0.015 and 0.014 for 0.0083 ft, 0.0125 ft and 0.025 ft. fractures respectively.

In the study of number of fractures, in Figure 5.77, condensate saturations are reduced to 0.0185, 0.015 and 0.014 for 3, 6 and 9 fractures respectively, compared with non-fracture case at the fraction of 0.022.

While in case of the same stimulated reservoir volume, as they were mentioned before in the last section that there are only small differences between each case in gas production rate, condensate production rate, cumulative gas production and cumulative condensate production respectively. However, when the condensate saturation profile near wellbore is assessed in this study the clearer results can be observed that number of fractures have higher effect than the fracture width and show themselves in different condensate saturations with time. Table 5.12 is assisted to recall the SRV designs. Figure 5.78 exhibits that case A gives the lowest condensate saturation at 0.0165. While in case C, it can reduce to 0.0185.

The last investigated parameter is fracture permeability; three different values of fracture permeability gives only small differences on gas and condensate cumulative productions as they were mentioned previously. The behavior of condensate saturation near wellbore exhibits similar behavior, however, they have small gap between each value which are 0.017, 0.016 and 0.015 for 50,000 mD, 100,000 mD and 150,000 mD respectively as they are shown in Figure 5.79.

Table 5.12 Stimulated reservoir volume designs

Case	No. of fracture	Fracture width (ft)	Thickness (ft)	Fracture half-length (ft)	SRV (ft^3)
A	9	0.0083	110	775	6,394
B	6	0.0125	110	775	6,394
C	3	0.0250	110	775	6,394

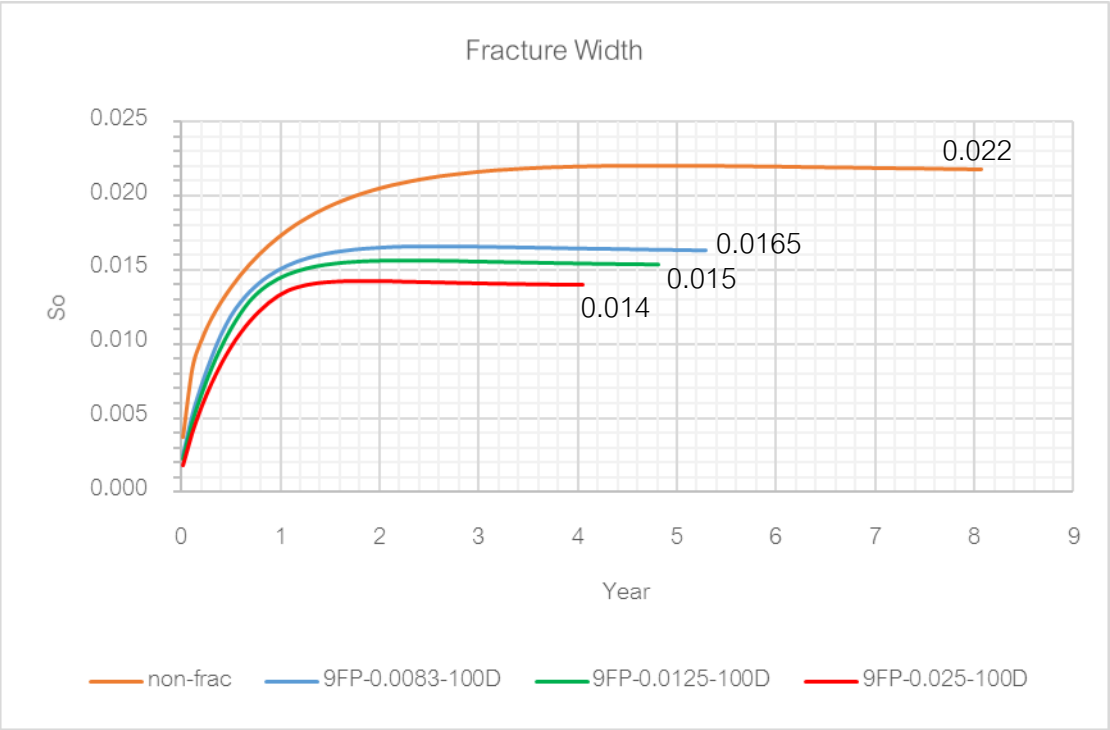

Figure 5.76: Condensate saturation near wellbore vs. time with different fracture widths in lean condensate

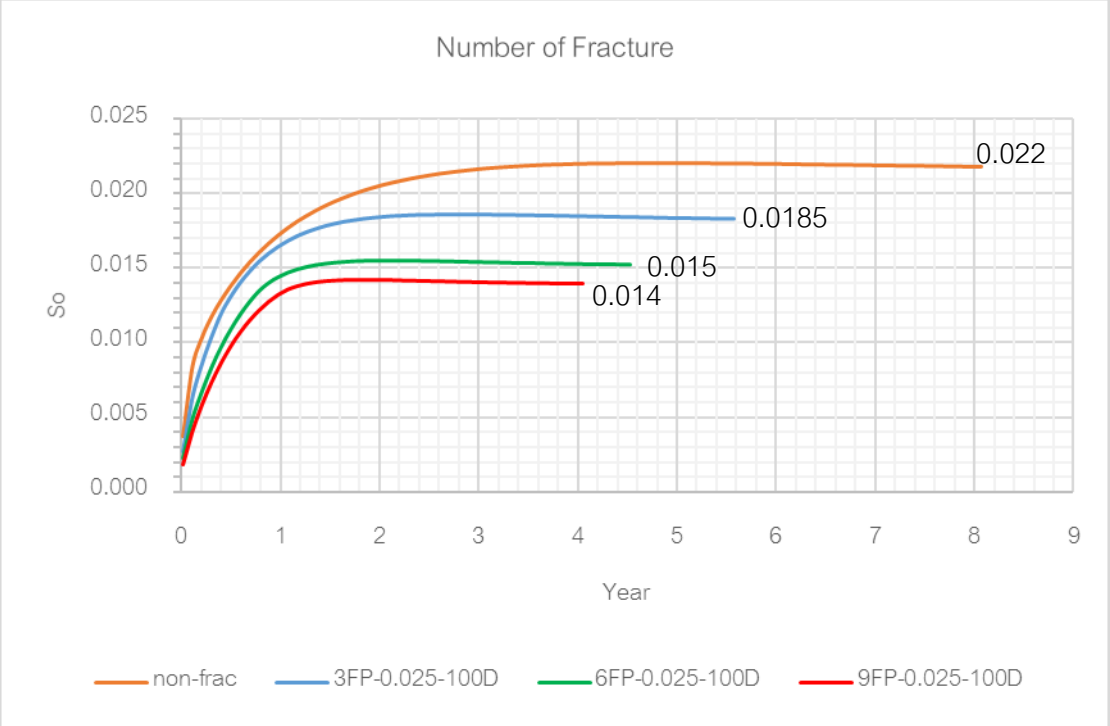

Figure 5.77: Condensate saturation near wellbore vs. time with different number of fractures in lean condensate

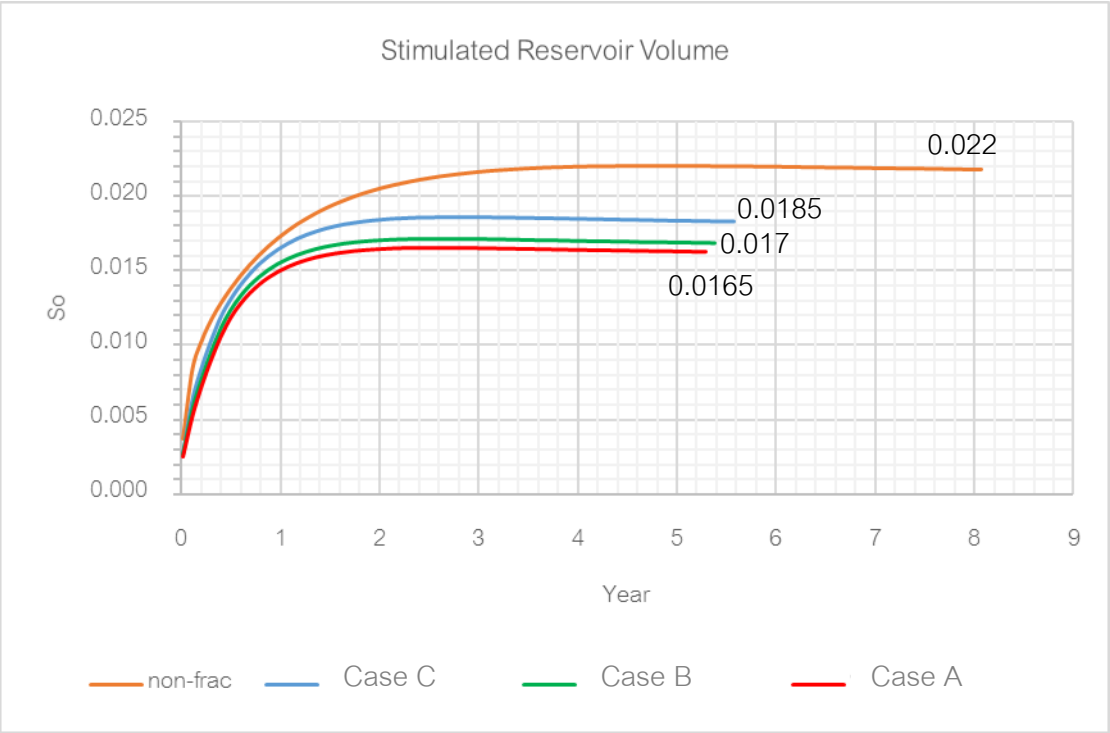

Figure 5.78: Condensate saturation near wellbore vs. time at the same stimulated reservoir volume but different designs in lean condensate

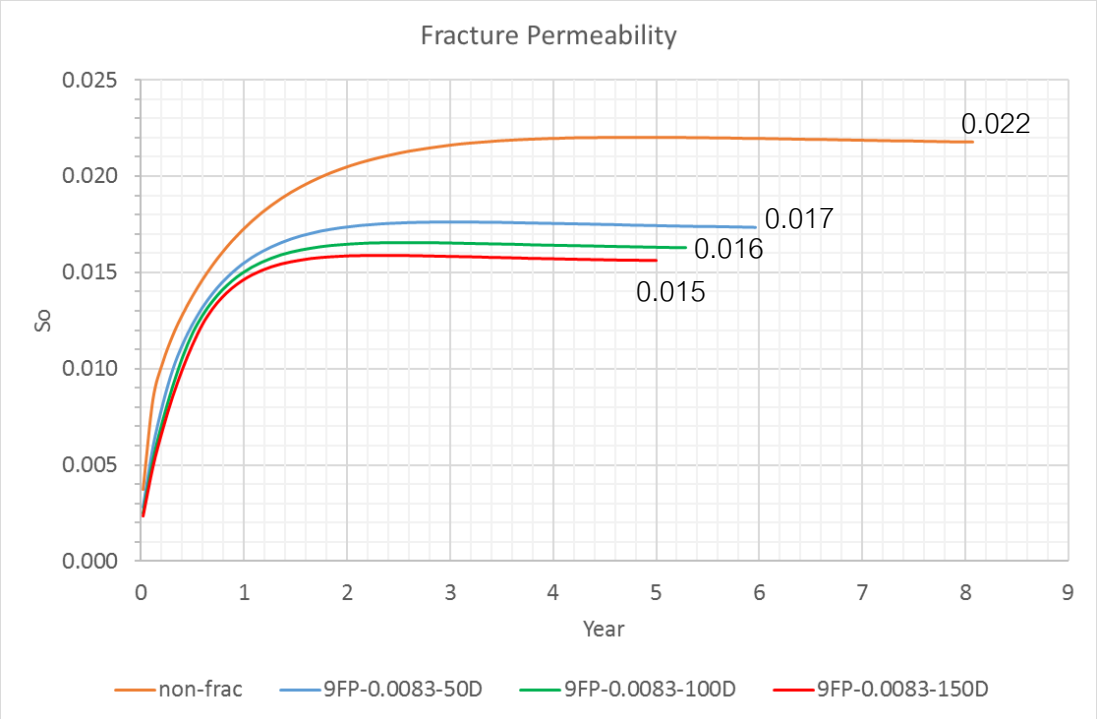

Figure 5.79: Condensate saturation near wellbore vs. time with different fracture permeabilities in lean condensate

To observed effects of each parameter on condensate banking clearly, the study of condensate banking region at the highest condensate saturation was performed. Figure 5.80 shows the region of condensate banking at the highest condensate saturation in non-fractured case. It can be observed that condensate saturations keep increasing but not reaching critical condensate saturation. This region is considered to be region 2 according to the study of Fevang and Whitson [5]

When hydraulic fracturing was applied to the reservoir, it helps decreasing pressure drawdown and decreasing condensate saturation near wellbore. For example, in the study of number of fractures, it decreases condensate saturation to 0.0185, 0.0155 and 0.014 for 3 fractures and 9 fractures as they are shown in Figure 5.81, Figure 5.82 and Figure 5.83 compared to non-fracture case at 0.022 in Figure 5.80.

In summary, hydraulic fracturing helps decreasing pressure drawdown of the reservoir and increasing pathway for hydrocarbon to flow out and to be produced. However, when pressure is changed, phase behavior of gas condensate also change as they are shown in Figure 5.84. Phase envelopes of lean condensate shift to the left-hand side and increasing dew point pressure when production with hydraulic fracturing continues compared to initial condition. Mole percent in Table 5.14 are used to update phase diagram, and it can be recognized that only N_2 and C_1 increase while other components from C_2 to C_7 decrease. This indicates the revaporized of lean condensate. More results of the study in fracture widths, number of fractures, SRV and fracture permeabilities are shown in Appendix A and B.

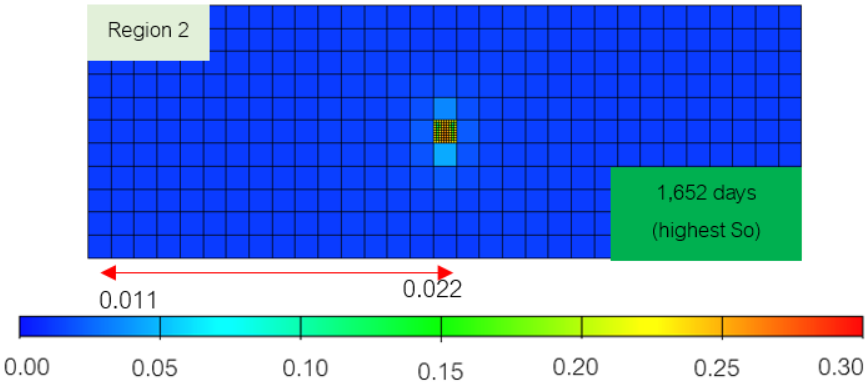

Figure 5.80 Cross-section of non-fractured case at the highest condensate saturation in lean condensate

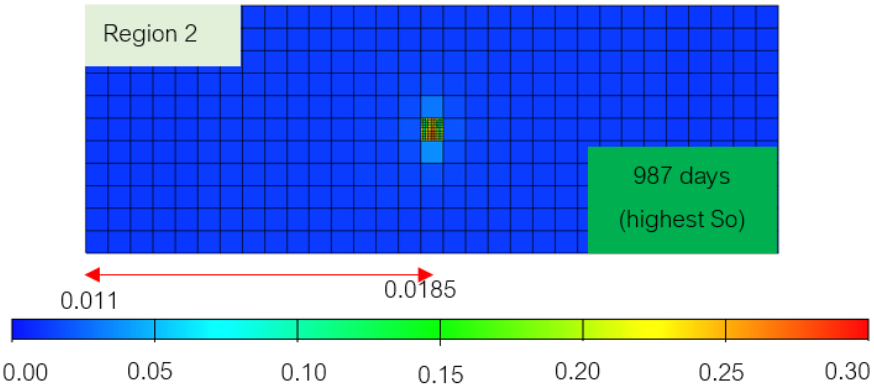

Figure 5.81 Cross-section of 3 fractures case (3FP-0.025-100D) at the highest condensate saturation in lean condensate

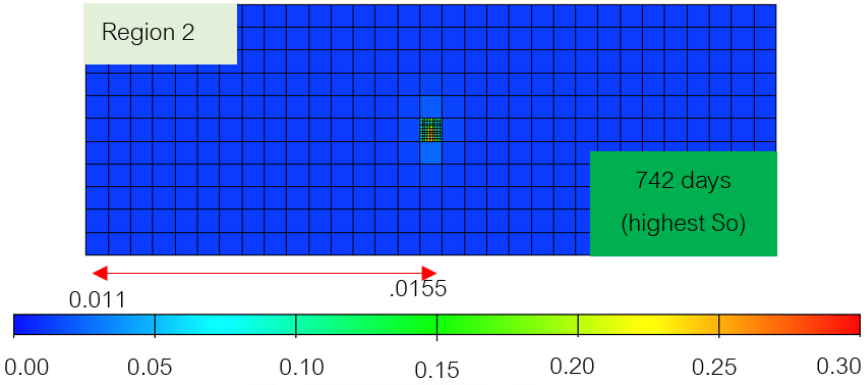

Figure 5.82 Cross-section of 6 fractures case (6FP-0.025-100D) at the highest condensate saturation in lean condensate

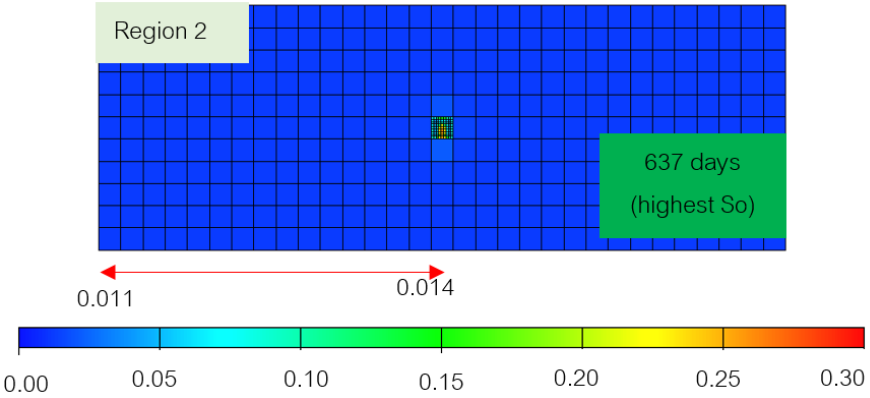

Figure 5.83 Cross-section of 9 fractures case (9FP-0.025-100D) at the highest condensate saturation in lean condensate

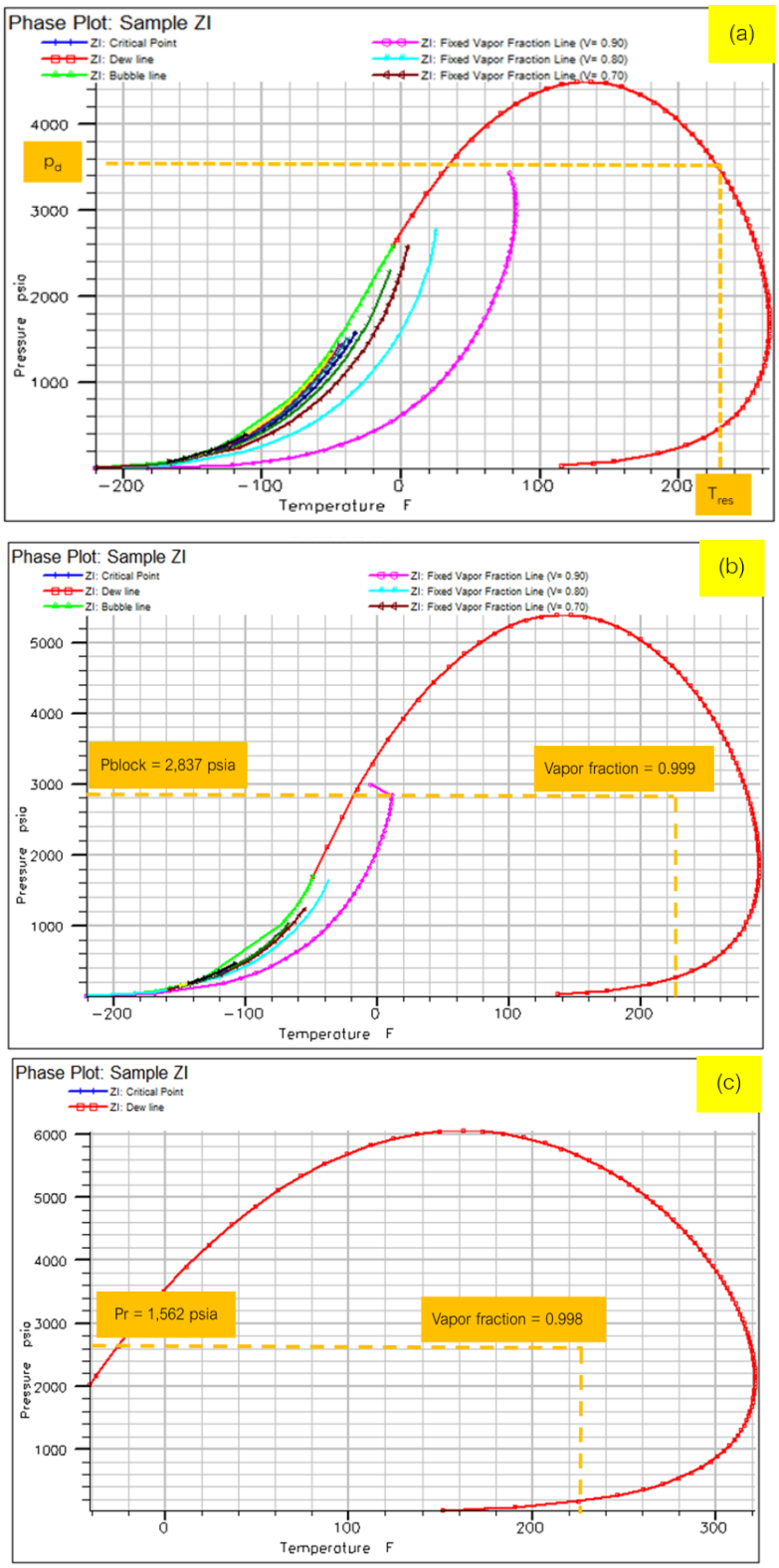

Figure 5.84 Phase behaviors of lean condensate at different time (a) at initial condition, (b) before liquid dropout is revaporized and (c) after liquid dropout is revaporized

Table 5.13 Condensate saturations and block pressures at different time for the case of 9 fractures in lean condensate

	Condensate Saturation	Block pressure (psia)	Dew point pressure (psia)
Initial condition	0	3,500	3,499
Before liquid dropout is revaporized	0.00097	2,837	4,543
After liquid dropout is revaporized	0.01404	1,562	5,624

Table 5.14 Mole percent at different time for the case of 9 fractures in lean condensate

Formula	Mole Percent		
	Initial Condition	Before liquid dropout is revaporized	After liquid dropout is revaporized
CO_2	1.06	0.06	0.06
N_2	0.21	0.32	0.32
C_1	64.81	92.99	91.94
C_2	5.27	2.15	2.16
C_3	6.23	1.18	1.21
i-C_4	1.67	0.18	0.19
C_4	3.09	0.34	0.35
i-C_5	1.37	0.10	0.11
C_5	1.31	0.09	0.10
C_6	1.59	0.45	0.52
C_7	13.39	2.13	3.04

Rich Condensate

The condensate saturation reaches up to the highest point of 0.27 when it produces to almost 1.5 years and keeps decreasing to 0.21 at the end of production for the case of non-fractured.

In the study of fracture width, the larger fracture width, the lower reduction of condensate saturation could be obtained which are 0.17, 0.16 and 0.15 for fracture width of 0.0083 ft, 0.0125 ft and 0.025 ft respectively as they are shown in Figure 5.85.

In the studying of number of fractures, the condensate saturation near wellbore can be decreased to 0.18, 0.16 and 0.15 at the end of production for 3,6 and 9 fractures respectively as they are shown in Figure 5.85.

Figure 5.86 depicts results from the study of SRV, it shows that each design has the same SRV and at the end of production shows close condensate saturation of 0.16, 0.17 and 0.18 for case A, case B and case C respectively. However, the behaviors of each case act differently with time. Especially, case C that has the combination of minimum number of fracture at 3 compound with maximum fracture with at 0.025 ft. Table 5.12 shows higher condensate saturation at the early time, this is because fracture width has smaller effect than number of fractures on the production.

And lastly, Figure 5.87 exhibits results from the study of effect of fracture permeability, condensate saturations are close and they are as low as 0.17, 0.165 and 0.16 for 50,000 mD, 100,000 mD and 150,000 mD respectively.

The conclusion of using hydraulic fracturing in rich condensate has the obvious improvement that hydraulic fracturing helps decreasing condensate blockage and condensate saturation near wellbore in every case of studied parameters. The maximum case of each parameter shows a compelling result that it can decrease condensate saturation even lower than the initial condensate saturation at 0.165.

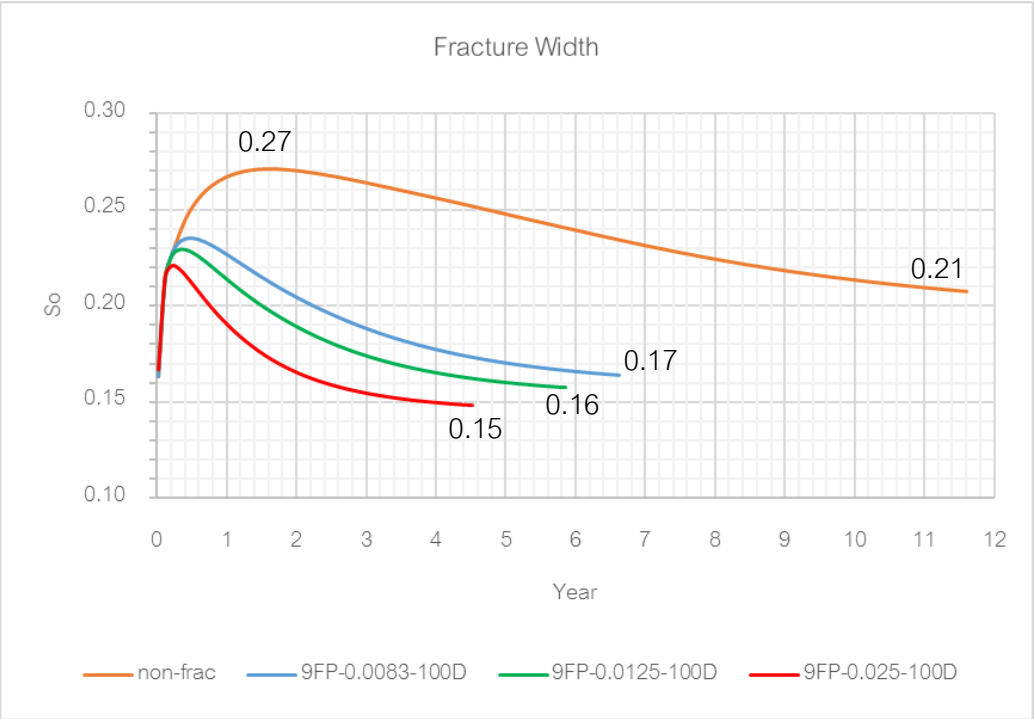

Figure 5.85: Condensate saturation near wellbore vs. time with different fracture widths in rich condensate

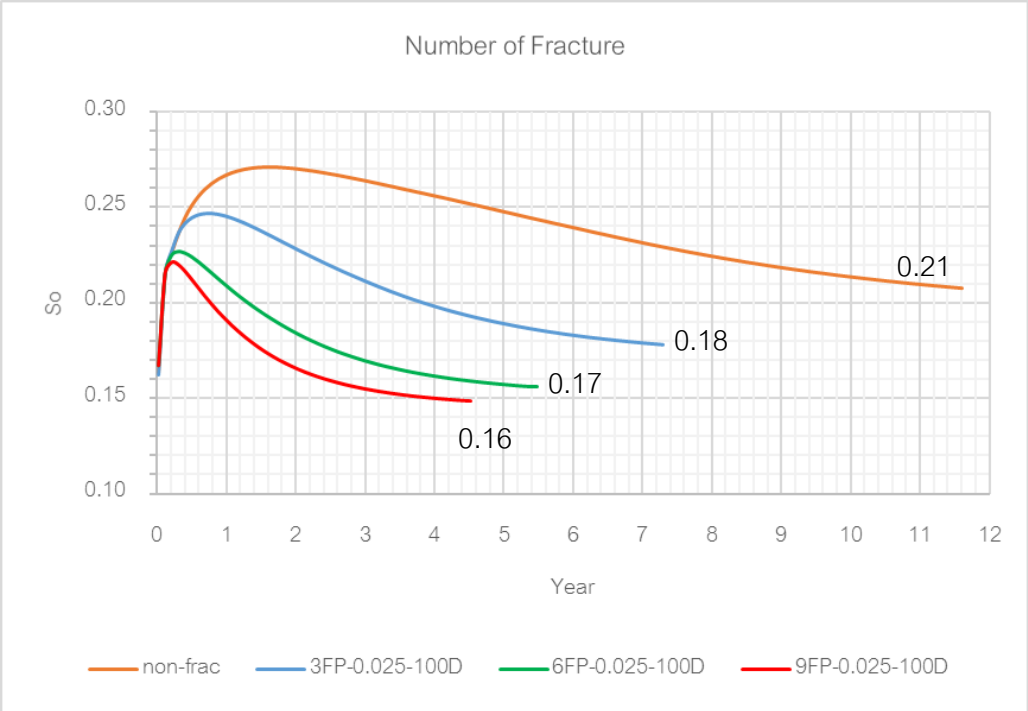

Figure 5.86: Condensate saturation near wellbore vs. time with different number of fractures in rich condensate

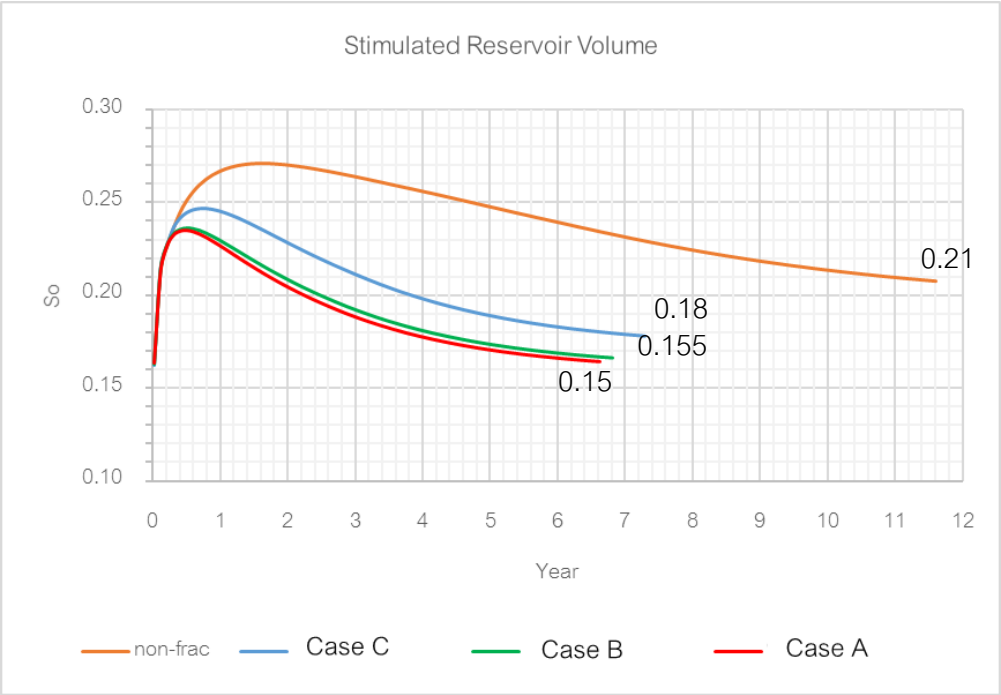

Figure 5.87: Condensate saturation near wellbore vs. time at the same stimulated reservoir volume but different design in rich condensate

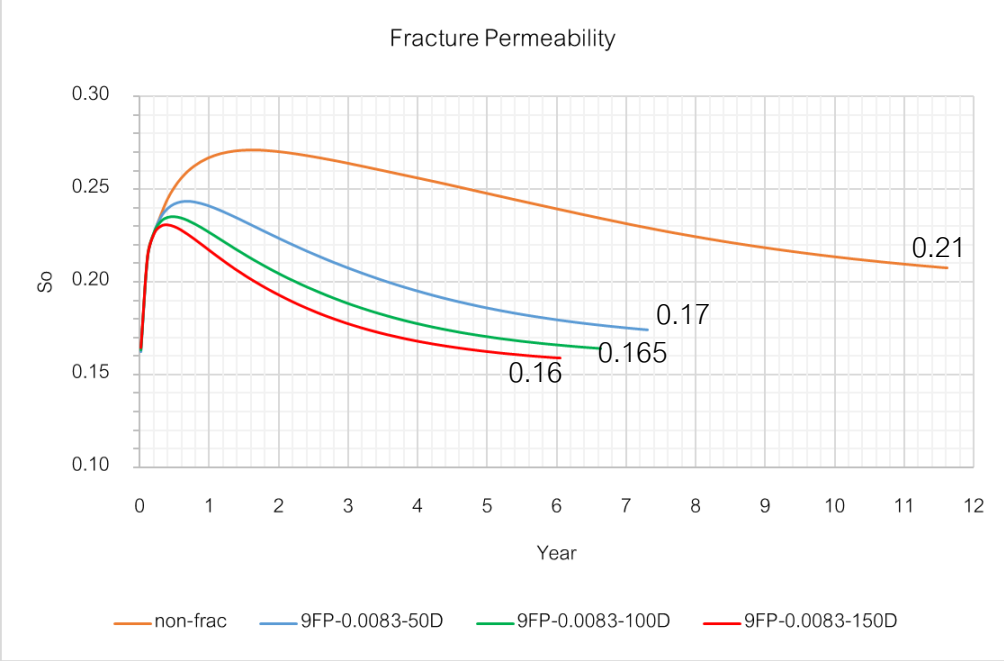

Figure 5.88: Condensate saturation near wellbore vs. time with different fracture permeability in rich condensate

The investigation of condensate region at the highest condensate saturation of non-fractured case in rich condensate is performed and shown in Figure 5.89 that initial liquid dropout in the reservoir creates condensate banking to the radius of 600 ft. from wellbore. This region is considered as region 1 according to the study of Fevang and Whitson [5] where both condensate and gas can move and cause the major loss of productivity of the well. When hydraulic fracturing was applied, it effectively decreases effect of condensate banking as they can be seen in the study of number of fracture as they are shown in Figure 5.90, Figure 5.91 and Figure 5.92

Besides the effect of hydraulic fracturing in decreasing condensate banking, the effect of revaporization of condensate should also be considered. Figure 5.93 shows the phase envelopes of rich condensate that shift to the left-hand side before revaporization, and shift to the right-hand side after revaporization occurred. Table 5.15 exhibits value of condensate saturations near wellbore that it was increased to 0.21 before dropping to 0.17 after revaporization. Because the changes of fluid compositions show higher mole percent of C_6 and C_{7+} while other components from C_1 to C_5 decrease which mean that more fluid is dropped out of gas as fluid compositions are shown in Table 5.16. Noticing that, from Figure 5.93 (c) when near wellbore block pressure decreases to 1,529 psia, it gives vapor fraction of 0.78 which means there should be liquid fraction left at 0.22 but the result in Table 5.15 shows that condensate saturation is only at 0.17. This indicates that the couple effect from both revaporization and hydraulic fracturing help decreasing condensate saturation effectively in rich condensate reservoir.

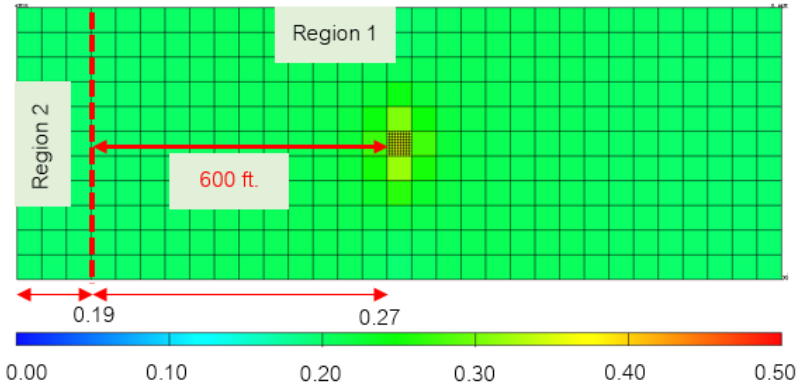

Figure 5.89 Cross-section of non-fractured case at the highest condensate saturation in rich condensate

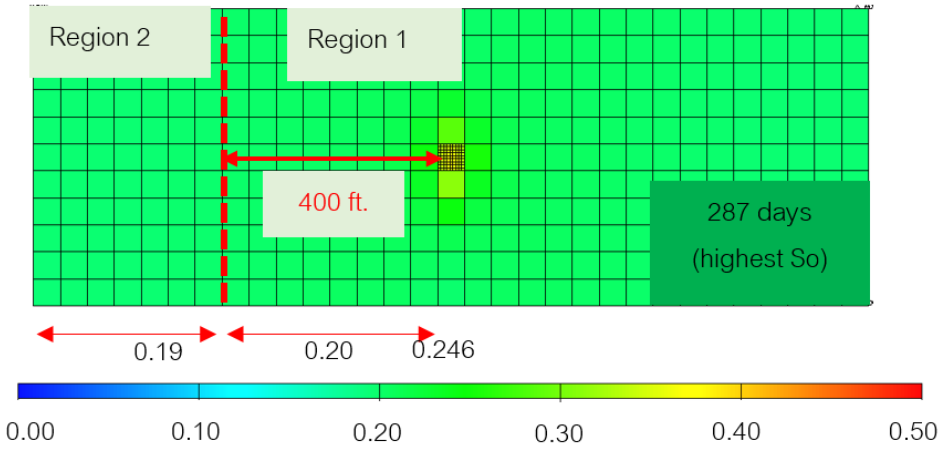

Figure 5.90 Cross-section of 3 fractures case (3FP-0.025-100D) at the highest condensate saturation in rich condensate

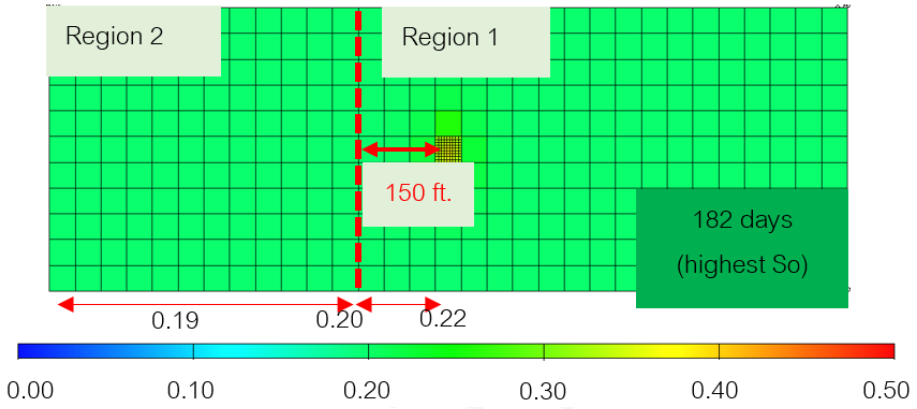

Figure 5.91 Cross-section of 6 fractures case (6FP-0.025-100D) at the highest condensate saturation in rich condensate

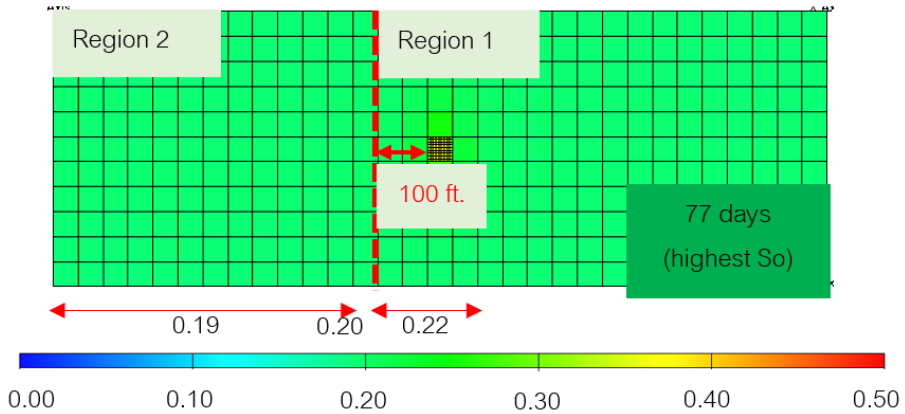

Figure 5.92 Cross-section of 9 fractures case (9FP-0.025-100D) at the highest condensate saturation in rich condensate

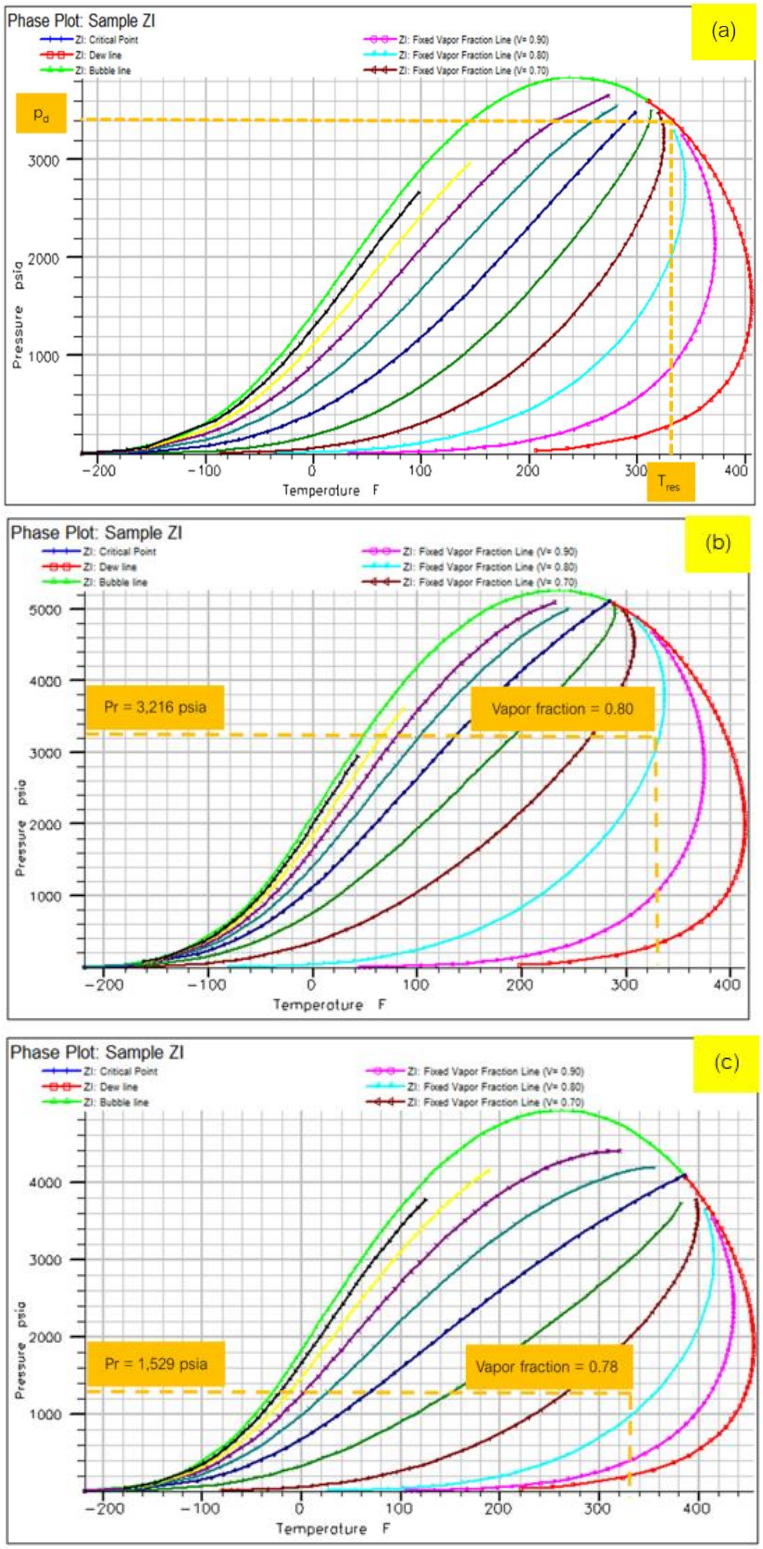

Figure 5.93 Phase behavior of rich condensate at different time a) at initial condition, (b) before liquid dropout is revaporized and (c) after liquid dropout is revaporized

Table 5.15 Condensate saturations and block pressures at different time for the case of 9 fractures in rich condensate

	Condensate Saturation	Block pressure (psia)	Dew point pressure (psia)
Initial condition	0	3,500	3,423
Before liquid dropout is revaporized	0.21	3,216	4,650
After liquid dropout is revaporized	0.17	2,005	4,745

Table 5.16 Mole percent at different time for the case of 9 fractures in rich condensate

Formula	Mole Percent		
	Initial Condition	Before liquid dropout is revaporized	After liquid dropout is revaporized
CO_2	0.17	0.09	0.09
N_2	0.19	0.13	0.13
C_1	53.39	68.46	60.60
C_2	11.14	7.68	7.51
C_3	5.97	2.82	2.96
i-C_4	2.83	1.02	1.15
C_4	2.45	0.88	1.00
i-C_5	5.63	1.63	1.84
C_5	4.88	1.42	1.72
C_6	5.66	7.79	10.14
C_{7+}	7.69	8.06	12.86

CHAPTER 6
CONCLUSIONS AND RECOMMENDATIONS

This section concludes results in this study based on dimensionless fracture conductivity and stimulated reservoir volume designs. Results in this study improve the understanding of effects on gas and condensate recovery and assists in planning and design to reach the optimum production of gas and condensate in horizontal well. The reservoir simulator was used as a tool to investigate the improvement in each case when different parameters were varied. Recommendations are provided for future study.

6.1 Conclusions

- Obvious improvement on condensate production can be observed in both lean and rich condensate compositions. Condensate production in lean condensate increased up to the range of 13.95%-18.45% and in rich condensate increased about 11.86%-12.15% compared to non-fractured case. This is because fracture width has impact on controlling inertial effect. Increasing fracture width is consequently decrease non-Darcy flow, hence, condensate relative permeability and condensate production also increased. Therefore, we can see smaller condensate production occupy in the reservoir when fracture width is increased.
- Increasing number of fractures shows good improvement in condensate recovery, in lean condensate the increment is 9.35%-18.45% and in rich condensate increased to 7.17%-11.68% compared to non-fractured case, this is because higher number of fractures allows larger contact area between fractures and reservoir. Therefore, hydrocarbon can flow from low permeability reservoir to fractures and wellbore easier. However, an interesting result can be observed in rich condensate between 6 fractures and 9 fractures only gives small increment on their condensate productions. This is because the heavy ends in rich

condensate compositions that condense and occupy in the pore space decrease the effectiveness of number of fractures.

- At the same stimulated reservoir volume or SRV, it shows slightly different results on gas and condensate production. In lean condensate, gas production increased in the range of 4.32%-4.78% while condensate production increased in the range of 9.35%-13.95%. For rich condensate, the increment of gas production is between 6.43%-7.55% and condensate production is in the range of 7.17%-11.79%. However, it can be observed that number of fractures is superior to fracture width on condensate recovery on both lean and rich condensate compositions. Especially, case A which has the design of 9 fracture planes with minimum fracture width of 0.0083 ft. Even though, fracture width can control inertial effect near fracture but number of fractures allows larger contact area for hydrocarbon to flow from the reservoir.
- The last parameter is fracture permeability which based on the best SRV design, i.e. case A. Fracture permeability shows small different of gas and condensate production between each value in both fluid compositions. Lean condensate has small benefit from increasing fracture permeability, especially in gas production that increased about 4.63%-6.50%, while condensate production increased in the range of 1.90%-2.55% compared to non-fractured case. In rich condensate, fracture permeability gives better improvement from increasing fracture permeability from 50,000 mD to 100,000 mD and 150,000 mD on both gas and condensate productions, gas production increased to the range of 6.00%-8.41% and condensate production had the increment between 10.61%-12.20% compared to non-fractured case. However, small improvement after 50,000 mD can be observed. This is because fracture permeability at 50,000 mD is already high enough and already causes a large difference between reservoir permeability and fracture permeability. Therefore, it did not show a significant

improvement even fracture permeability was increased to 100,000 mD and 150,000 mD.

- From the study of saturation profile near wellbore and the study of region of condensate banking at the highest condensate saturation indicate that, hydraulic fracturing in horizontal wells is effective in reducing condensate blockage near wellbore vicinity in every case of lean condensate. An interesting result can be observed in rich condensate where revaporization is occurred. The revaporization helps decreasing condensate saturation and with the couple effect of hydraulic fracturing, condensate saturation can be decreased lower than the effect of revaporization alone.

6.2 Recommendations

The following ideas are recommendations for future study;

- More accurate results can be achieved if geological data and Non-Darcy parameters which can be achieved from laboratory experiment.
- The complexity of fracture network, multilateral well or several wells in full field simulation should be considered to simulate, predict and understand effects of hydraulic fracturing better.
- Economic evaluation should be considered carefully and accurately to reduce risks and uncertainties and to find out the best investment opportunity.

REFERENCES

1. Fan, L., Harris, B. W., Jamaluddin, A., Kamath, J., Mott, R., Pope, G. A., Shandrygin, A. and Whitson, C. H., *Understanding Gas-Condensate Reservoirs.* Oilfield Review, 2005. **17**(4): p. 14 - 27.
2. Akpabio, J.U., Isehunwa, S. O. and Akinsete, O. O., *PVT Fluid Sampling, Characterization and Gas Condensate Reservoir Modeling.* Advances in Research, 2015.
3. Afidick, D., Kaczorowski, N. J., and Bette, S., *Production Performance of a Retrograde Gas Reservoir: A Case Study of the Arun Field.* SPE-28749-MS, 1994.
4. Barnum, R.S., Brinkman, F. P., Richardson, T. W. and Spillette, A. G. , *Gas Condensate Reservoir Behaviour: Productivity and Recovery Reduction Due to Condensation.* SPE-68173-MS, 1995.
5. Fevang, Ø.a.W., C.H., *Modeling Gas-Condensate Well Deliverability.* SPE-30714, 1995.
6. Jones, J.R.a.R., R., *Interpretation of Flowing Well Response in Gas-Condensate Wells.* SPE-14204-PA, 1985.
7. El-Banbi, A.H., McCain, W. D. and Semmelbeck, M. E., *Investigation of Well Productivity in Gas-Condensate Reservoirs.* SPE-59773-MS, 2000.
8. Carlson, M.R.M.a.M., J. W. G. J., *The Effects of Retrograde Liquid Condensation On Single Well Productivity Determined Via Direct (Compositional) Modelling Of A Hydraulic Fracture In A Low Permeability Reservoir.* SPE-29561-MS, 1995.
9. Settari, A., Bachman, R. C., Hovem, K. A., and Paulsen, S. G., *Productivity of Fractured Gas Condensate Wells - A Case Study of the Smorbukk Field.* SPE-35604-PA, 1996.
10. Al-Hashim, H.S.a.H., S. S., *Long-Term Performance of Hydraulically Fractured Layered Rich Gas Condensate Reservoir.* SPE-64774-MS, 2000.

11. Carvajal, G.A., Danesh, A., Jamiolahmady, M., and Sohrabi, M., *The impact of pertinent parameters on the design of hydraulic fracturing in gas condensate reservoirs.* SPE-94074-MS, 2005.

12. Mahdiyara, H., Jamiolahmady, M. and Sohrabib M. , *Improved Darcy and non-Darcy Flow Formulations Around Hydraulically Fractured Wells.* Journal of Petroleum Science and Engineering, 2011. **78**(1): p. 149-159.

13. Ali, J.K., McGauley, P. J., and Wilson, C. J., *The Effects of High-Velocity Flow and PVT Changes Near the Wellbore on Condensate Well Performance.* SPE-38923-MS, 1997.

14. Narayanaswamy, G., Pope, G. A., Sharma, M. M., Hwang, M. K., and Vaidya, R. N., *Predicting Gas Condensate Well Productivity Using Capillary Number and Non-Darcy Effects.* SPE-51910-MS, 1999.

15. Mott, R., *Engineering Calculations of Gas Condensate Well Productivity.* SPE-77551-MS, 2000.

16. Belhaj, H.A., Agha, K. R., Nouri, A. M., Butt, S. D., Vaziri, H. F. and Islam, M. R., *Numerical Simulation of Non-Darcy Flow Utilizing the New Forchheimer's Diffusivity Equation.* SPE-81499-MS, 2003.

17. Forchheimer, P., *Wasserbewegung durch Boden.* Z. Ver. Deutch, 1901: p. 1782-1788.

18. Chaudhry, A.U., *Gas Well Testing Handbook.* 2003, MA, USA: ELSEVIER Science.

19. Geertsma, J., *Estimating the Coefficient of Inertial Resistance in Fluid Flow Through Porous Media.* SPE-4706-PA, 1974.

20. Asar, H., and Handy, L. L., *Influence of Interfacial Tension on Gas/Oil Relative Permeability in a Gas-Condensate System.* SPE-11740-PA, 1988.

21. McDougall, S.R., Salino, P. A., and Sorbie, K. S., *The Effect of Interfacial Tension Upon Gas-Oil Relative Permeability Measurements: Interpretation Using Pore-Scale Models.* SPE-38920-MS, 1997.

22. Blom, S.M.P., and Hagoort, J., *How to Include the Capillary Number in Gas Condensate Relative Permeability Functions?* SPE-49268-MS, 1998.

23. Moradi, B., Tahami, A., Dehghani, H., Alishir, M. and Dehghan, A., *Investigation and Comparison of Production in Vertical, Horizontal, Slanted and Hydraulically Fractured Wells in a Gas Condensate Field.* Journal of Petroleum Science Research (JPSR), 2014: p. 145-152.

24. Rahim, Z., Al-Anazi, H., Al-Kanaan, A., Habbtar, A. and Al-Omair, A. *IMPROVED GAS RECOVERY—2 (Conclusion): Productivity increase using hydraulic fracturing—expectation vs. reality*. 2012; Available from: http://www.ogj.com/articles/print/vol-110/issue-5/drilling-production/improved-gas-recovery-2-conclusion-productivity-increase.html.

25. Economides, M.J., Hill, A.D., and Ehlig-Economides, C., *Petroleum Production Systems*. 1993, New Jersey: PTR Prentice Hall.

26. Agarwal R.G., C.R.D.a.P.C.B., *Evaluation and Prediction of Performance of Low Permeability Gas Wells Stimulated by Massive Hydraulic Fracturing.* SPE-6838-PA, 1979.

27. Economides, M., Oligney, R., and Valko, P., *Unified Fracture Design Bridging the Gap Between Theory and Practice*. 2002, Alvin, Texas: Orsa Press.

28. Soliman, M.Y., Hunt, J.L., and Azari, M., *Fracturing Horizontal Wells in Gas Reservoirs.* SPE-59096-PA, 1999.

29. Economides, M.J.a.N., K.G., *Reservoir Stimulation, third edition*. 2000, New York: John Wiley & Sons.

30. Butula, K.K., Yudin, A., Magdeyev, I., Chernyak, V., and Samoilov, M., *Fracturing Considerations in Mid Permeability Gas Condensate Formations.* SPE-176577-MS, 2015.

31. Barker, J.W., *Experience with Simulation of Condensate Banking Effects in Various Gas Condensate Reservoirs.* IPTC-10382-MS, 2005.

32. Hegre, T.M., *Hydraulically Fractured Horizontal Well Simulation.* SPE-35506-MS, 1996.

33. Kroemer, E., Abou-Sayed, I. S., Babu, D. K., and Cohen, M. F., *Compositional Simulation of Well Performance for Fractured and Multiple Fractured Horizontal Wells in Stratified Gas Condensate Reservoirs.* SPE-37995-MS, 1997.

34. Thitaram, P., *Effect of Reservoir Fluid Composition on Carbon Dioxide Injection in Gas Condensate Reservoirs*, in *Department of Mining and Petroleum Engineering*. 2009, Chulalongkorn University.

35. Association, G.P., *Engineering Data Book FPS Version volume I & II (Electronic)*. 1998.

36. Schlumberger, *Eclipse Technical Description 2014.1*.

APPENDICES

Appendix A

A-1) Non-fractured Cases

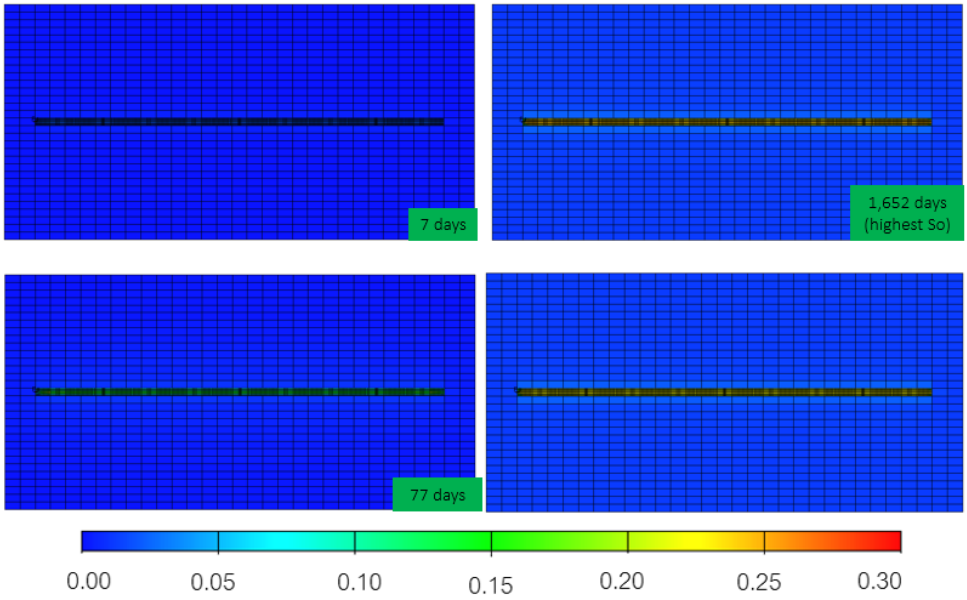

Figure A.1 Condensate saturation profile vs. time of non-fractured reservoir in lean condensate

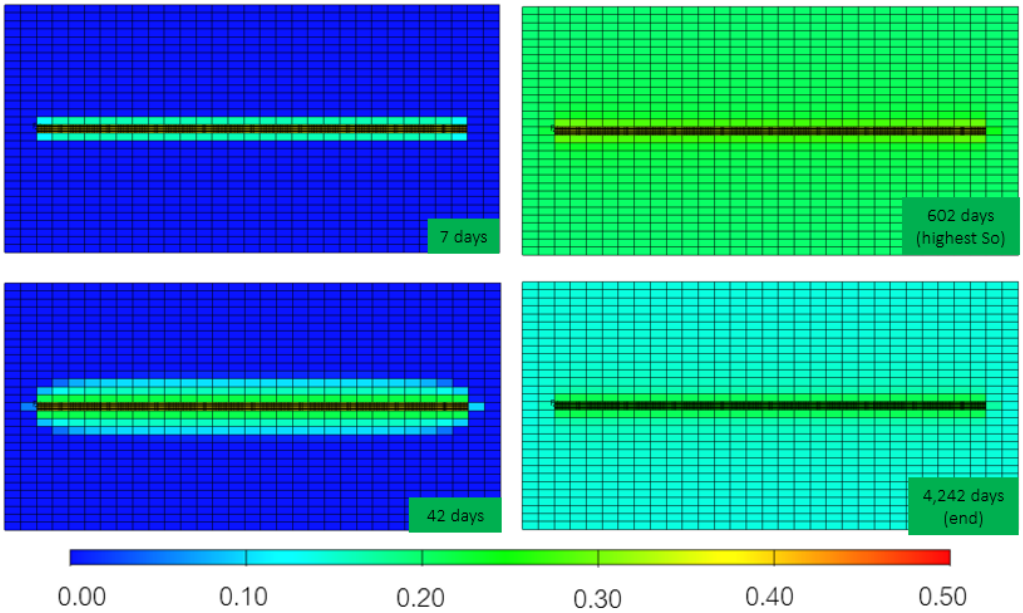

Figure A.2 Condensate saturation profile vs. time of non-fractured reservoir in rich condensate

A-2) Effect of Fracture Width

Lean Condensate

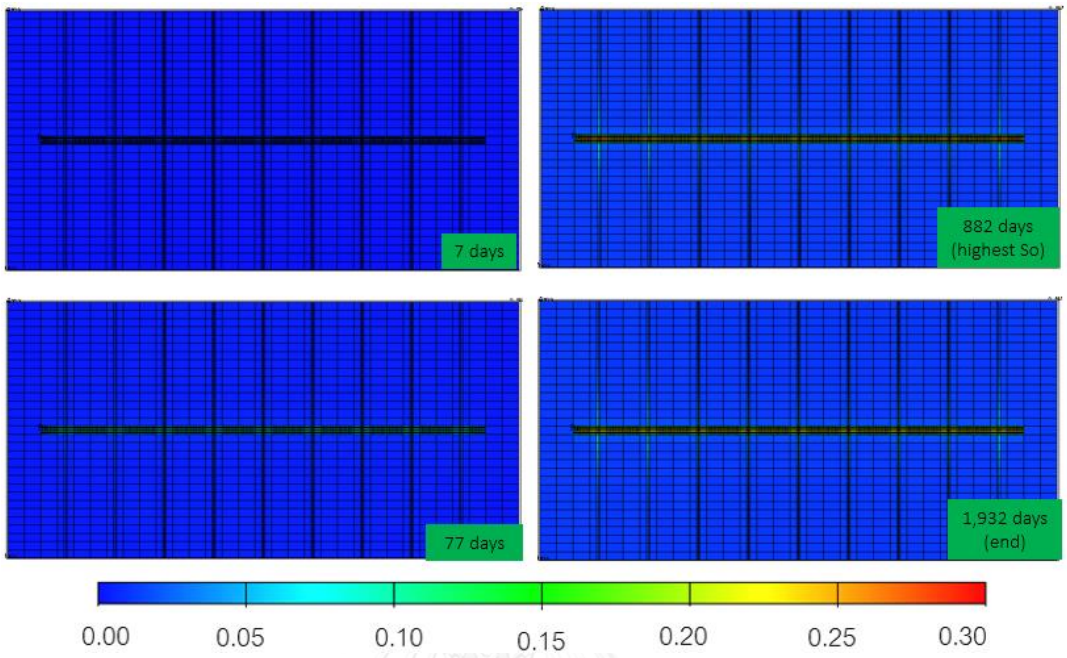

Figure A.3 Condensate saturation profile vs. time of fracture width of 0.0083 in lean condensate

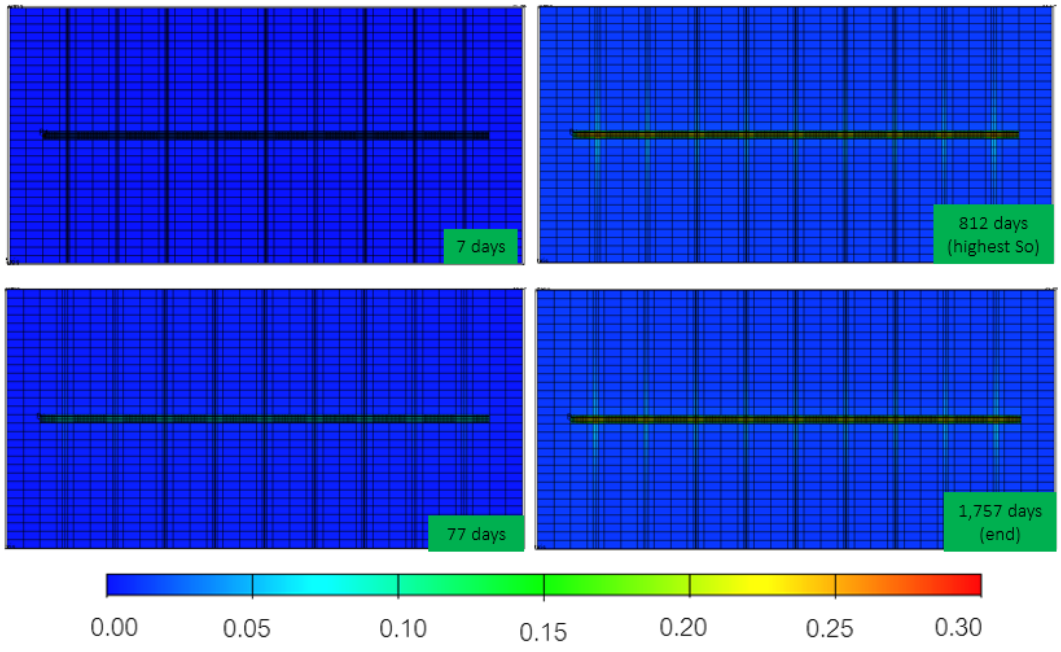

Figure A.4 Condensate saturation profile vs. time of fracture width of 0.0125 in lean condensate

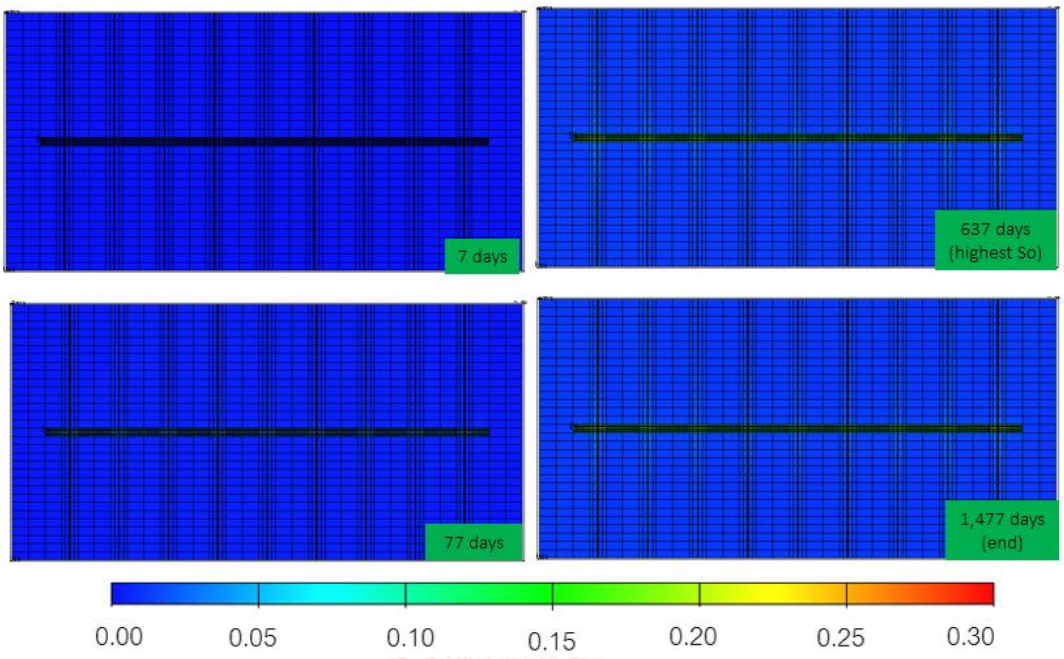

Figure A.5 Condensate saturation profile vs. time of fracture width of 0.025 in lean condensate

Rich Condensate

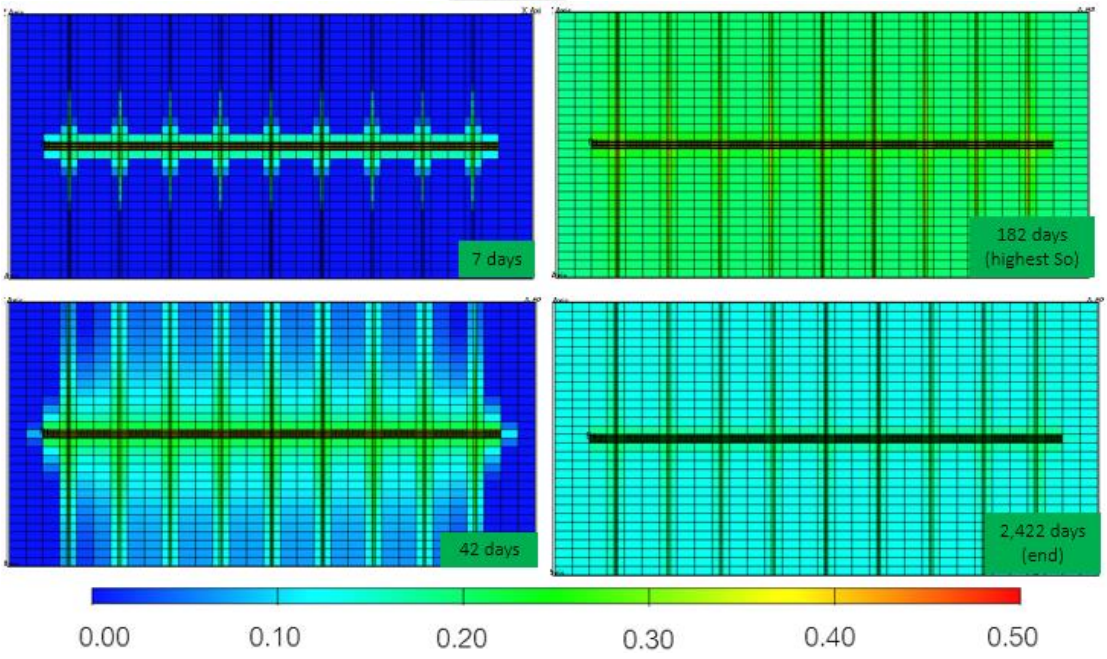

Figure A.6 Condensate saturation profile vs. time of fracture width of 0.0083 in rich condensate

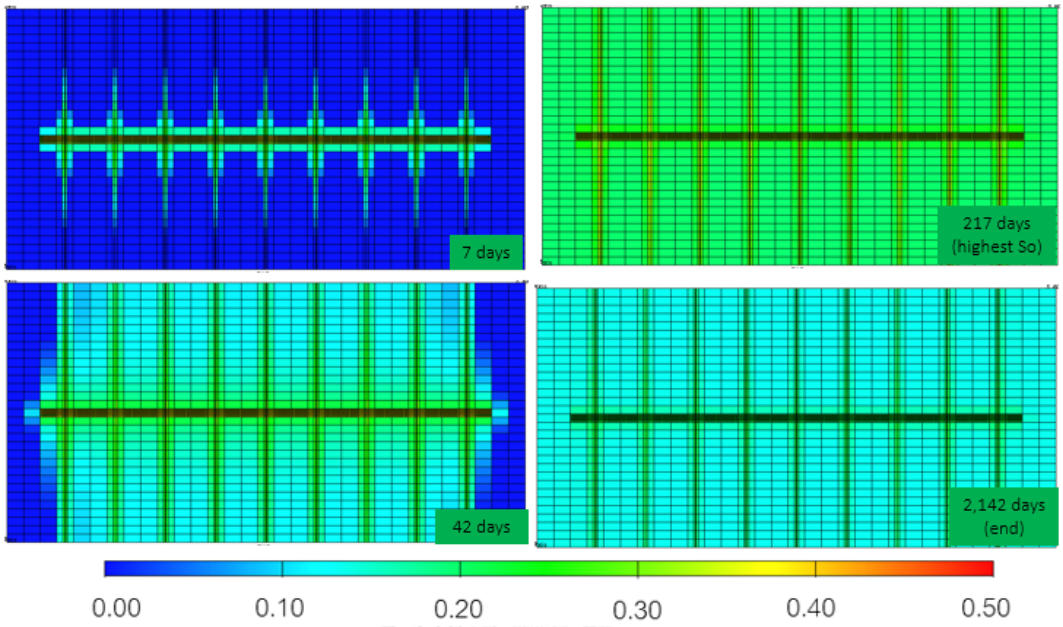

Figure A.7 Condensate saturation profile vs. time of fracture width of 0.0125 in rich condensate

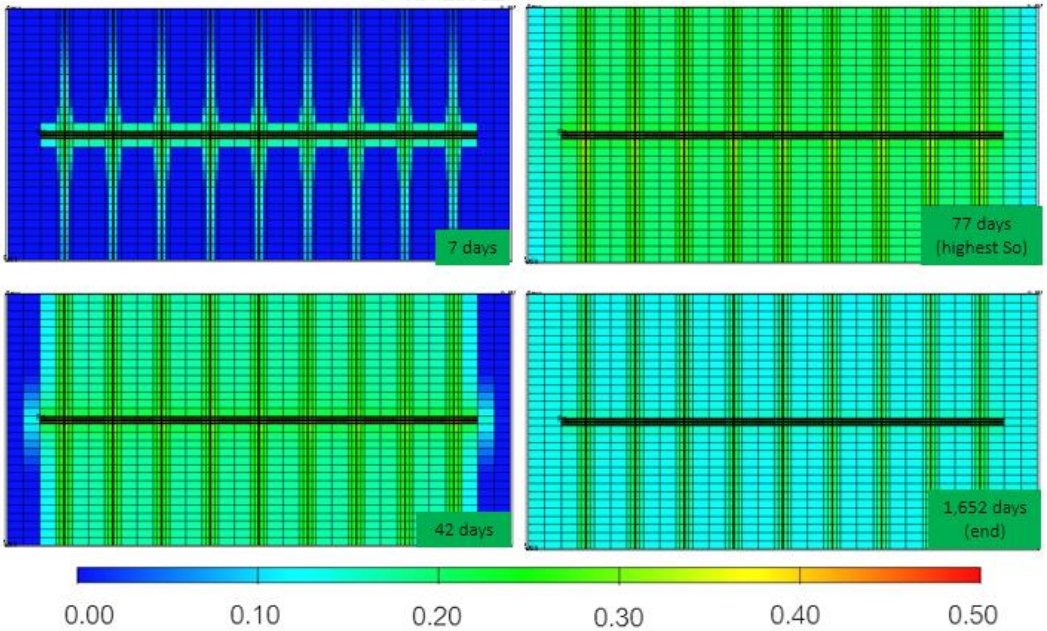

Figure A.8 Condensate saturation profile vs. time of fracture width of 0.025 in rich condensate

A-3) Effect of Number of Fracture

Lean Condensate

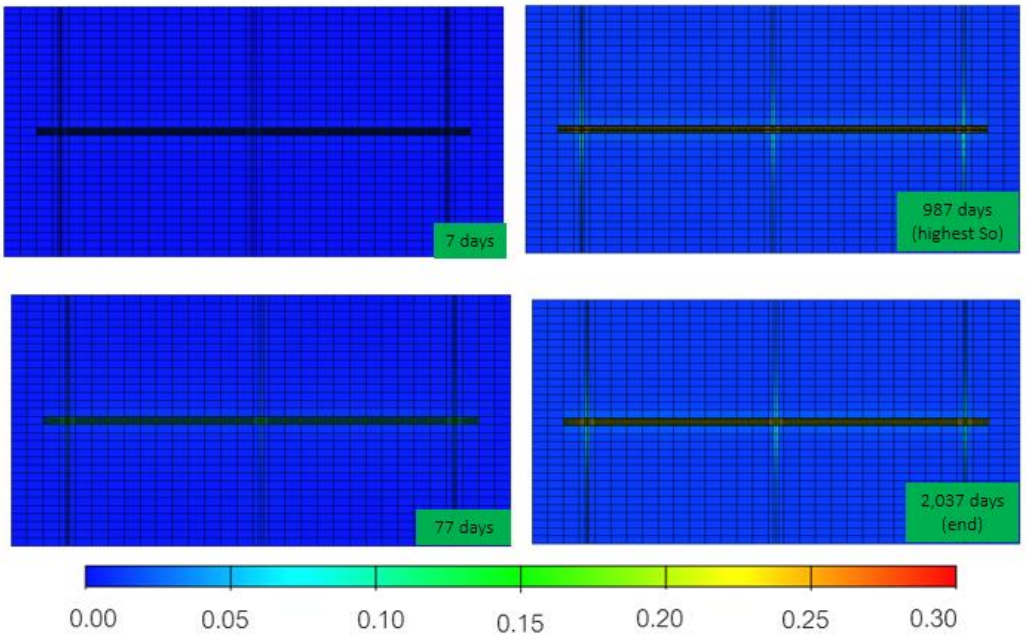

Figure A.9 Condensate saturation profile vs. time of 3 fractures in lean condensate

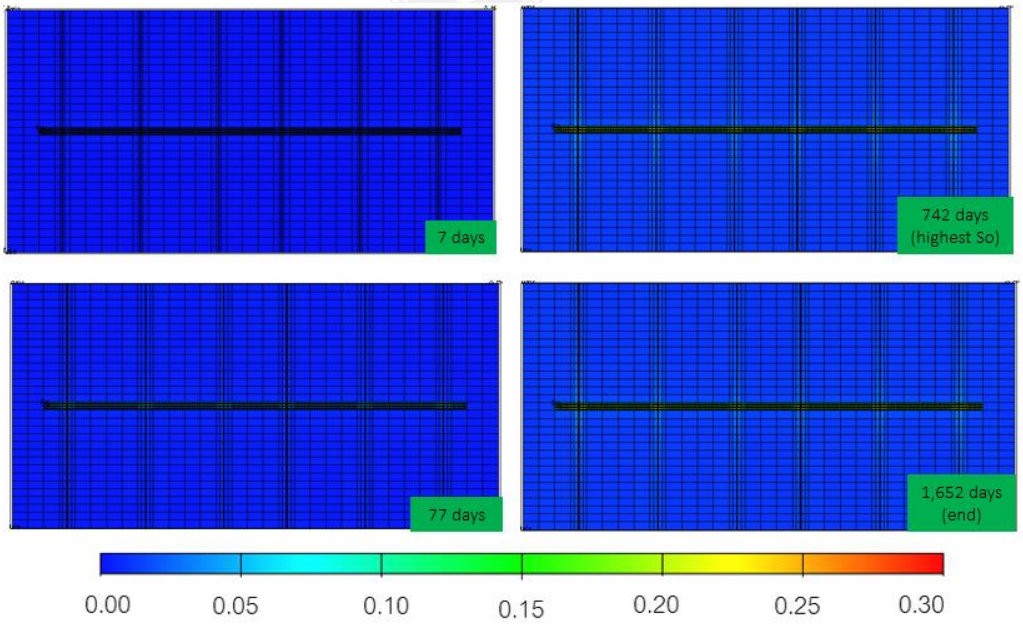

Figure A.10 Condensate saturation profile vs. time of 6 fractures in lean condensate

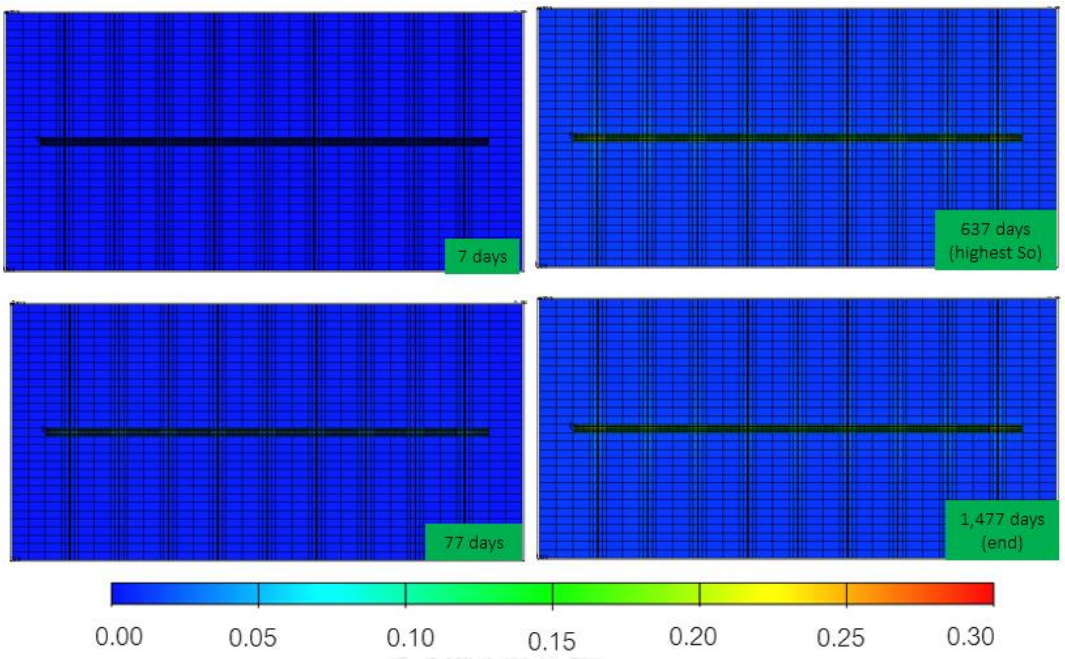

Figure A.11 Condensate saturation profile vs. time of 9 fractures in lean condensate

Rich Condensate

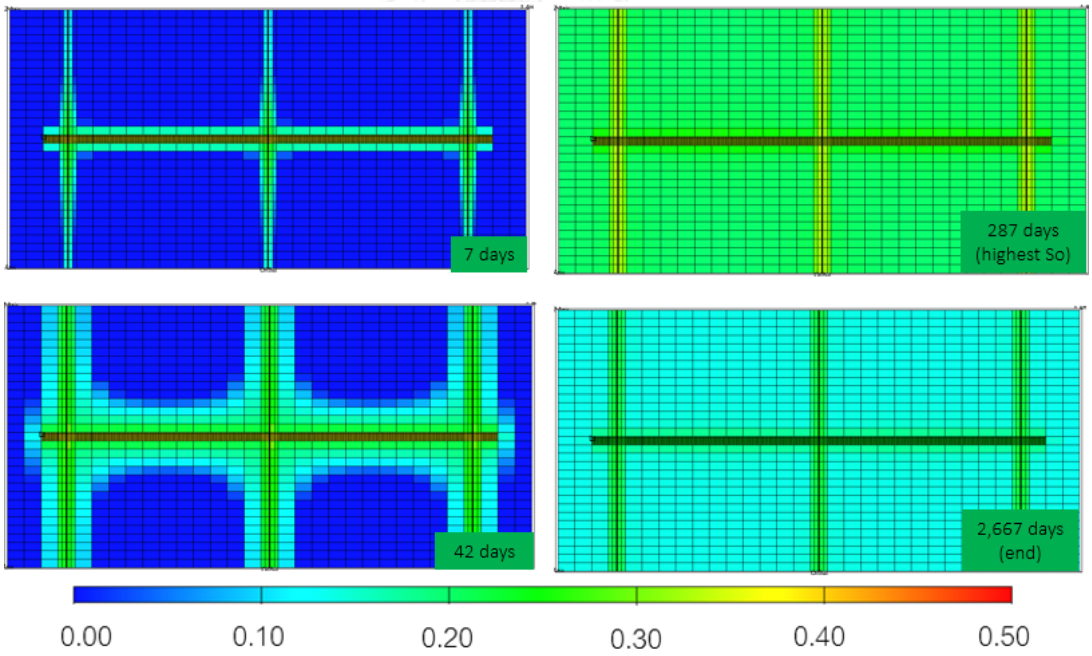

Figure A.12 Condensate saturation profile vs. time of 3 fractures in rich condensate

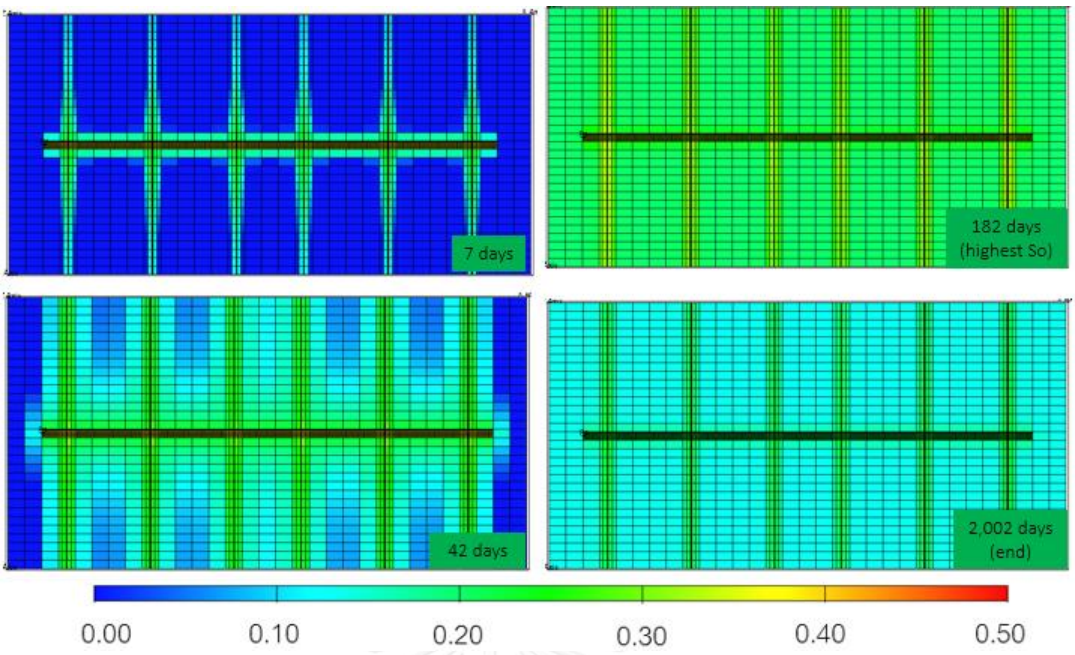

Figure A.13 Condensate saturation profile vs. time of 6 fractures in rich condensate

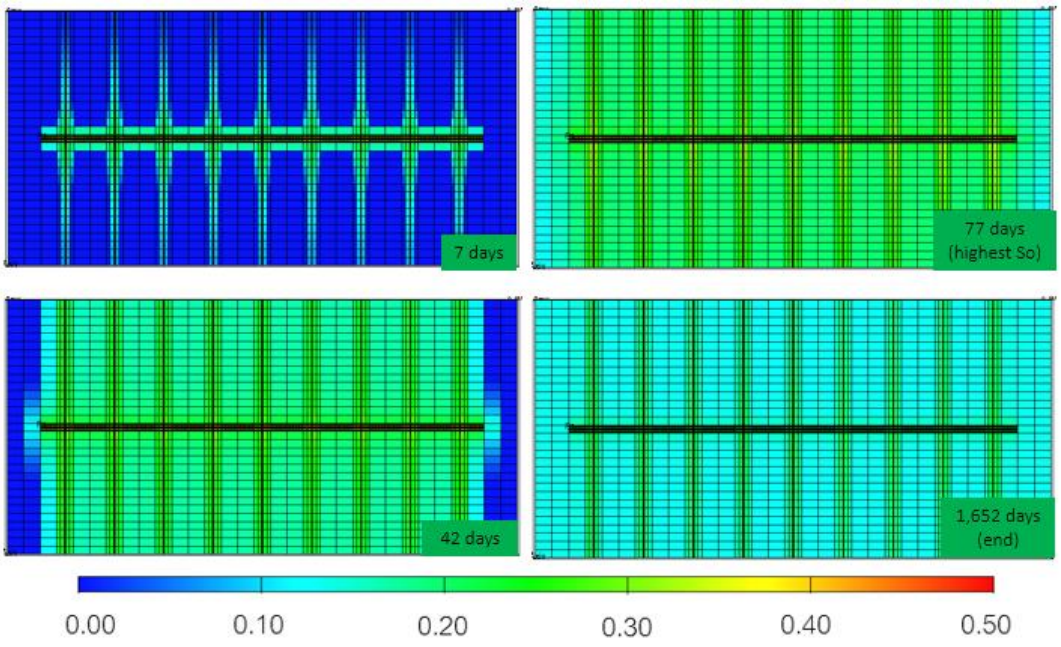

Figure A.14 Condensate saturation profile vs. time of 9 fractures in rich condensate

A-4) Effect of Stimulated Reservoir Volume (SRV)

Lean Condensate

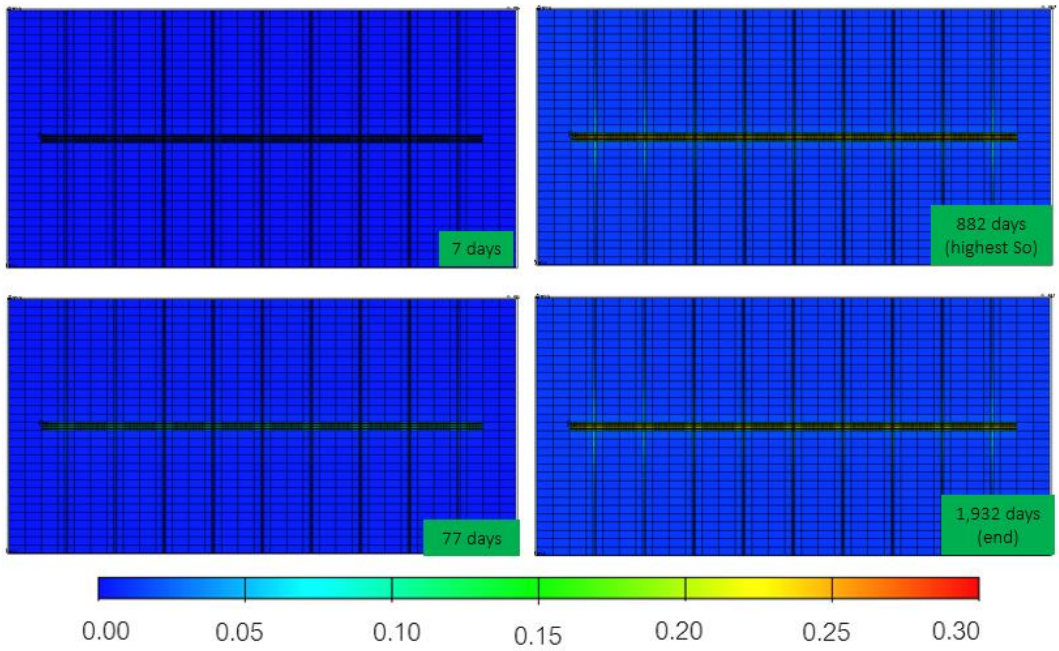

Figure A.15 Condensate saturation profile vs. time of SRV (case A) in lean condensate

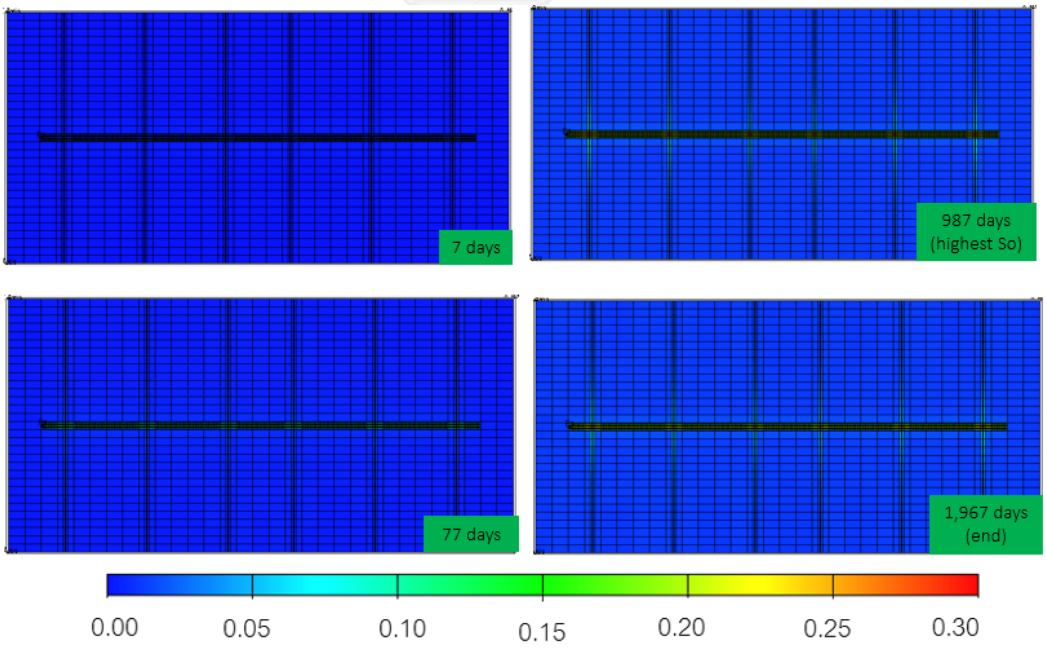

Figure A.16 Condensate saturation profile vs. time of SRV (case B) in lean condensate

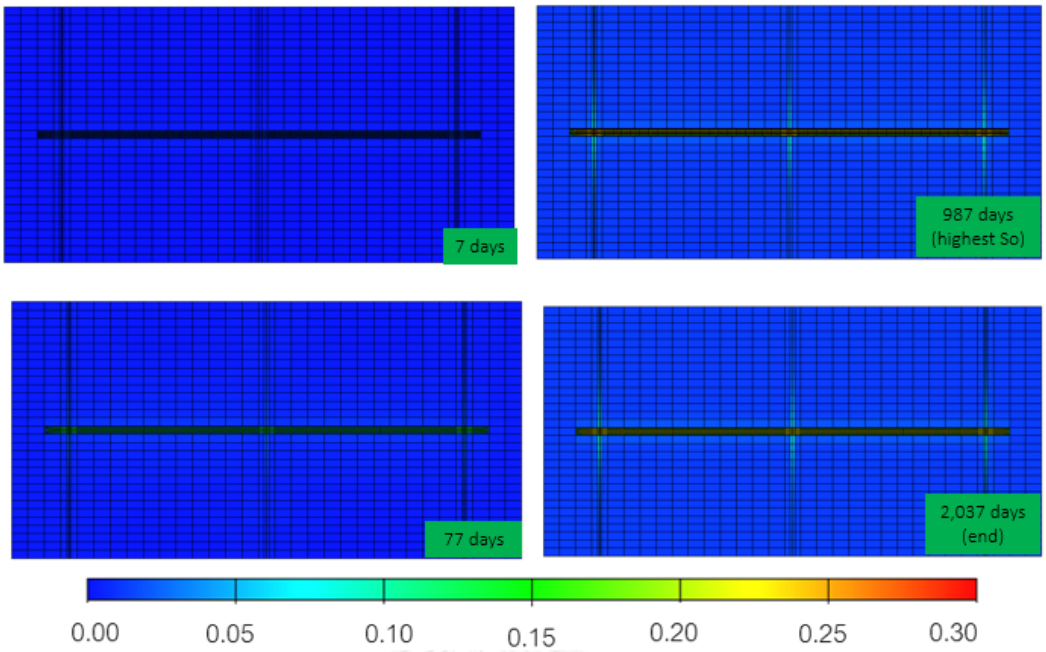

Figure A.17 Condensate saturation profile vs. time of SRV (case C) in lean condensate

Rich Condensate

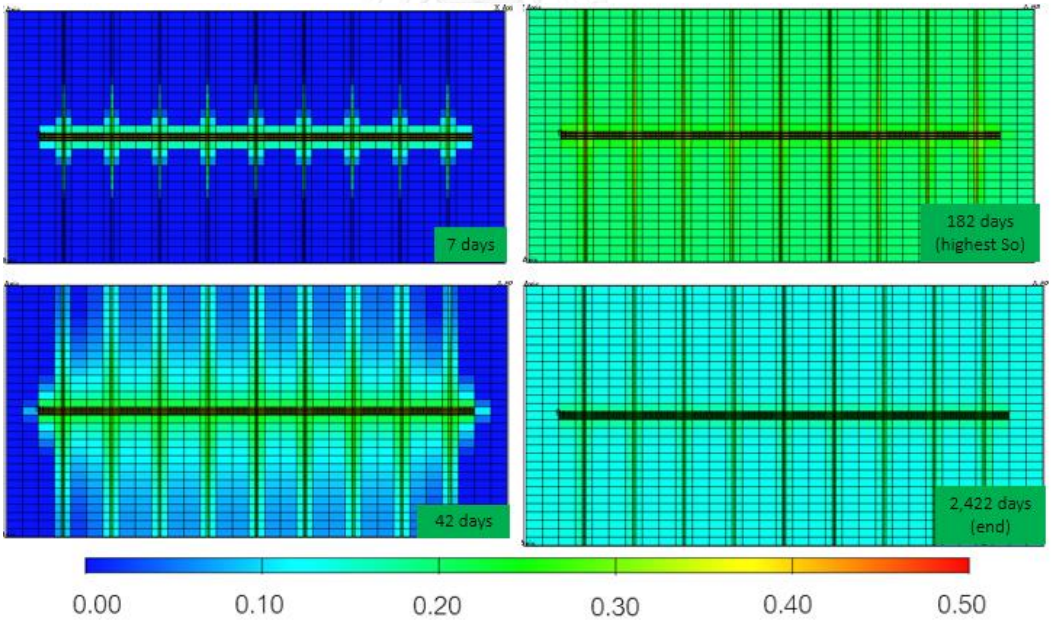

Figure A.18 Condensate saturation profile vs. time of SRV (case A) in rich condensate

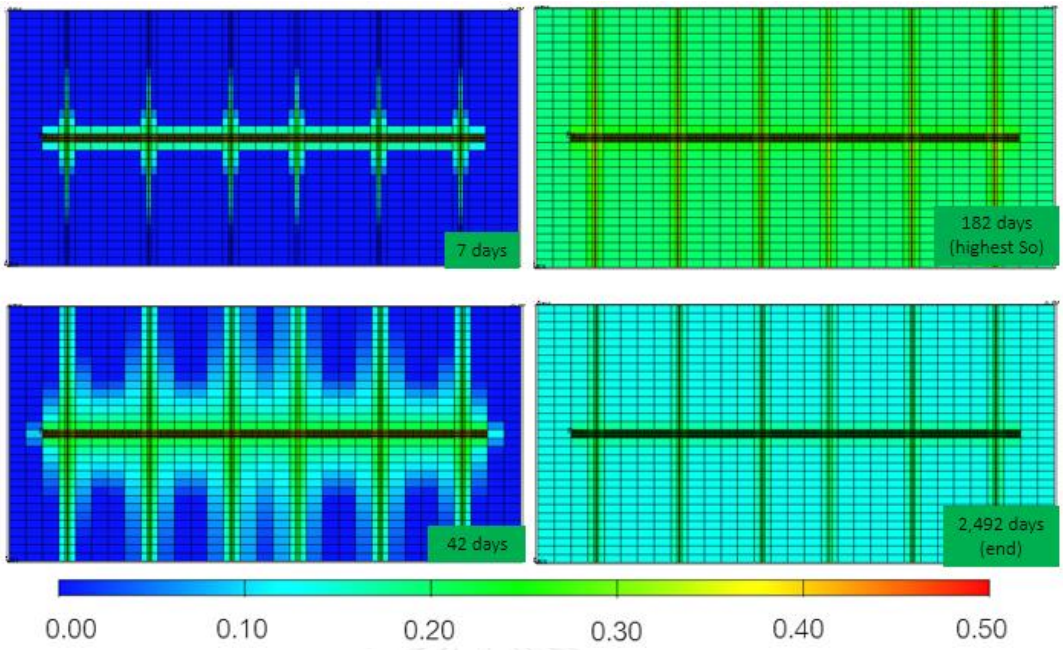

Figure A.19 Condensate saturation profile vs. time of SRV (case B) in rich condensate

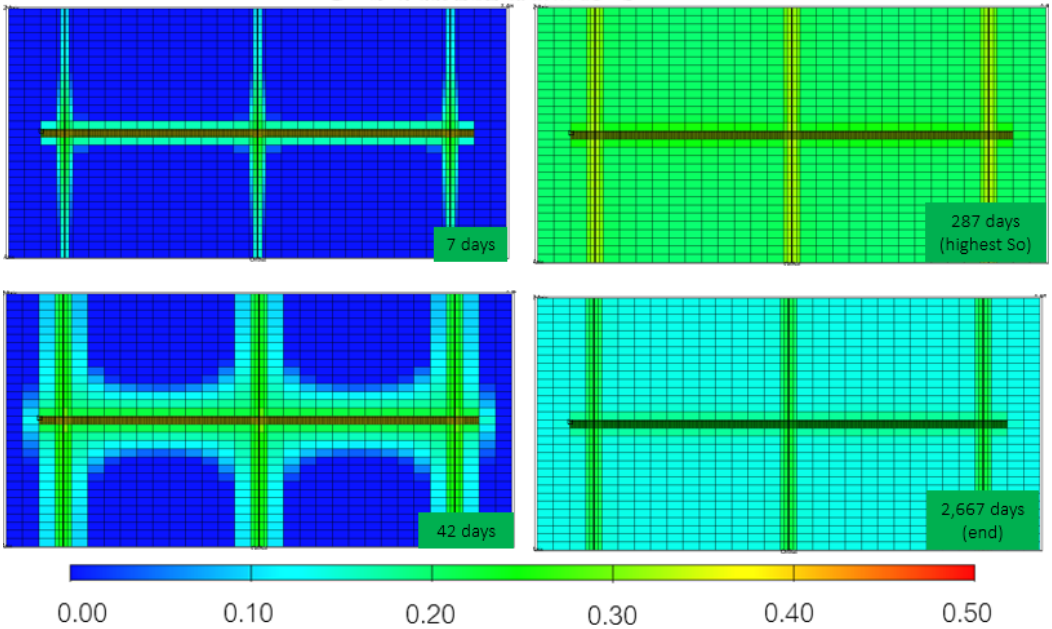

Figure A.20 Condensate saturation profile vs. time of SRV (case C) in rich condensate

A-5) Effect of Fracture Permeability

Lean Condensate

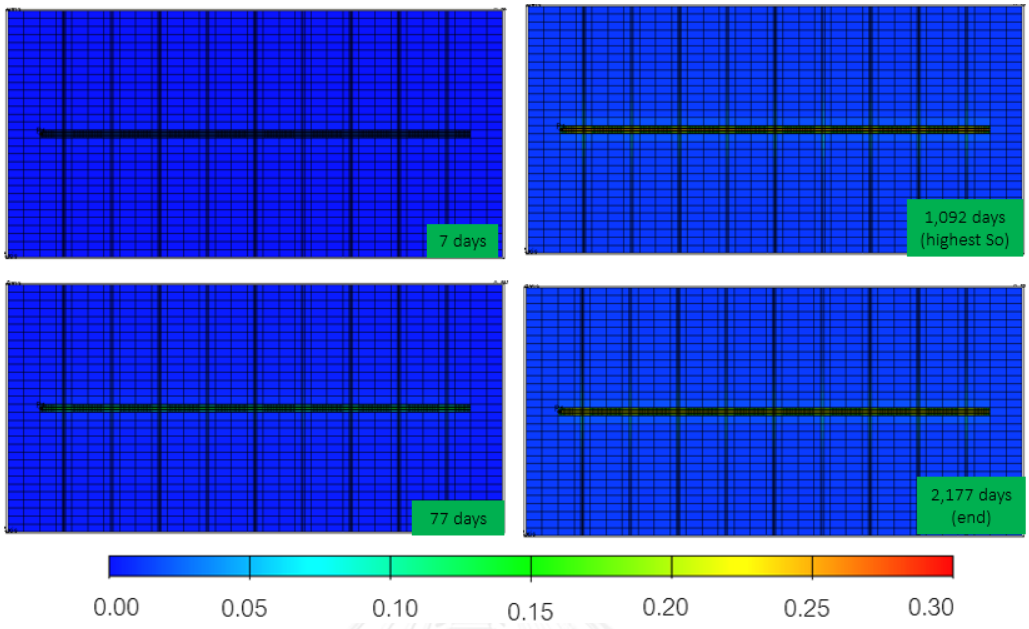

Figure A.21 Condensate saturation profile vs. time of fracture permeability at 50,000 mD in lean condensate

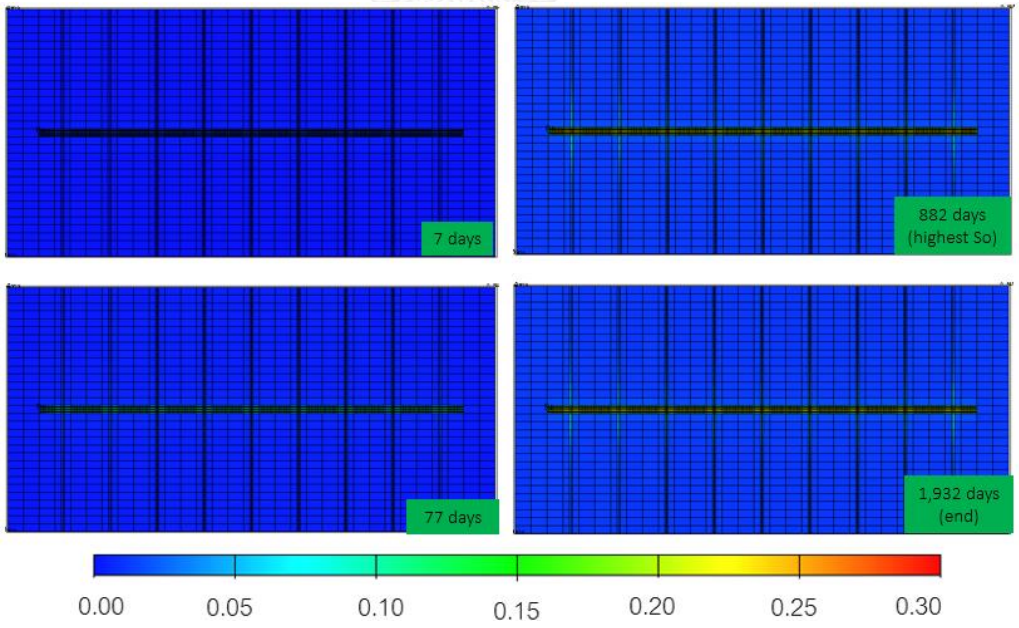

Figure A.22 Condensate saturation profile vs. time of fracture permeability at 100,000 mD in lean condensate

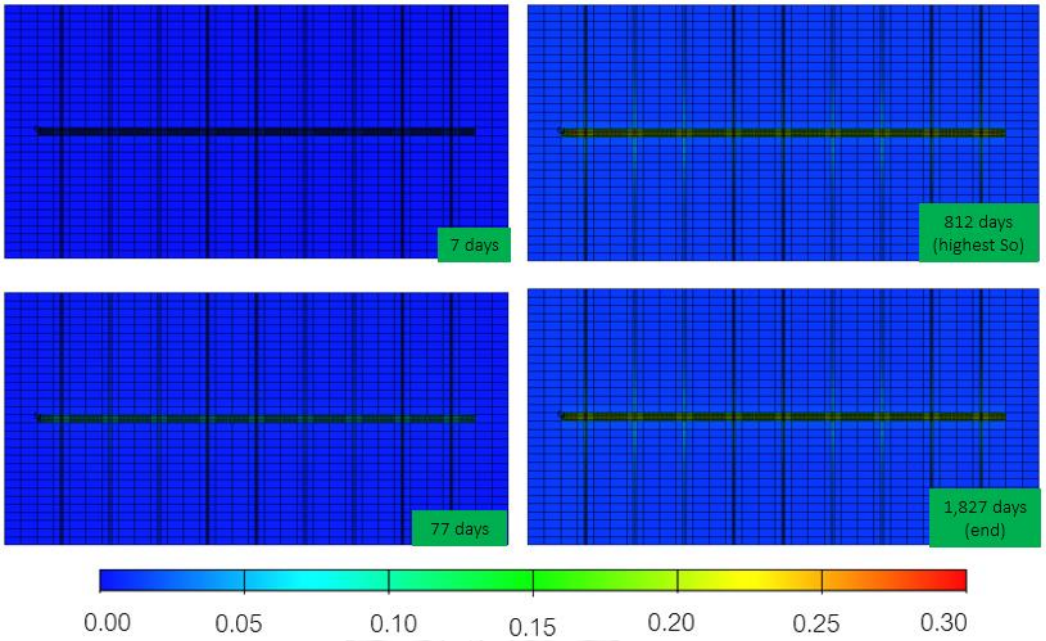

Figure A.23 Condensate saturation profile vs. time of fracture permeability at 150,000 mD in lean condensate

Rich Condensate

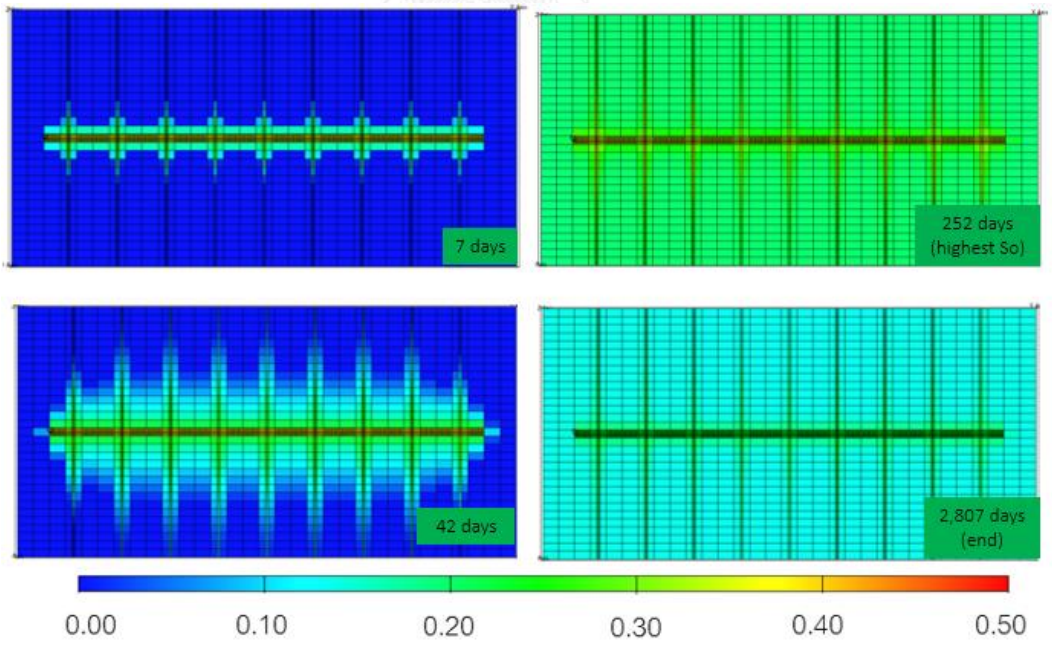

Figure A.24 Condensate saturation profile vs. time of fracture permeability at 50,000 mD in rich condensate

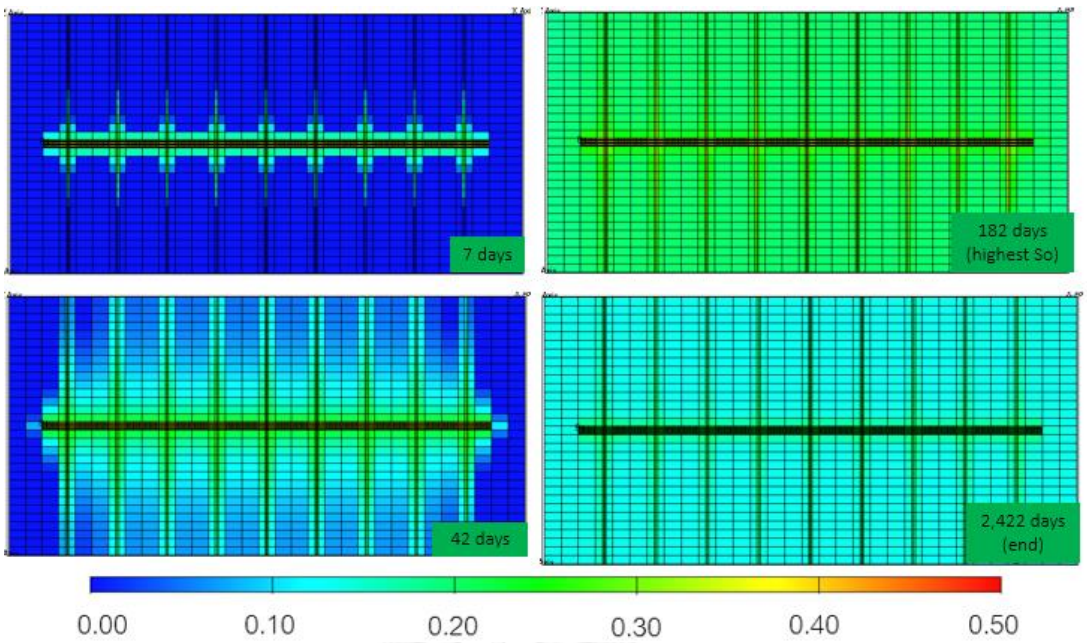

Figure A.25 Condensate saturation profile vs. time of fracture permeability at 100,000 mD in rich condensate

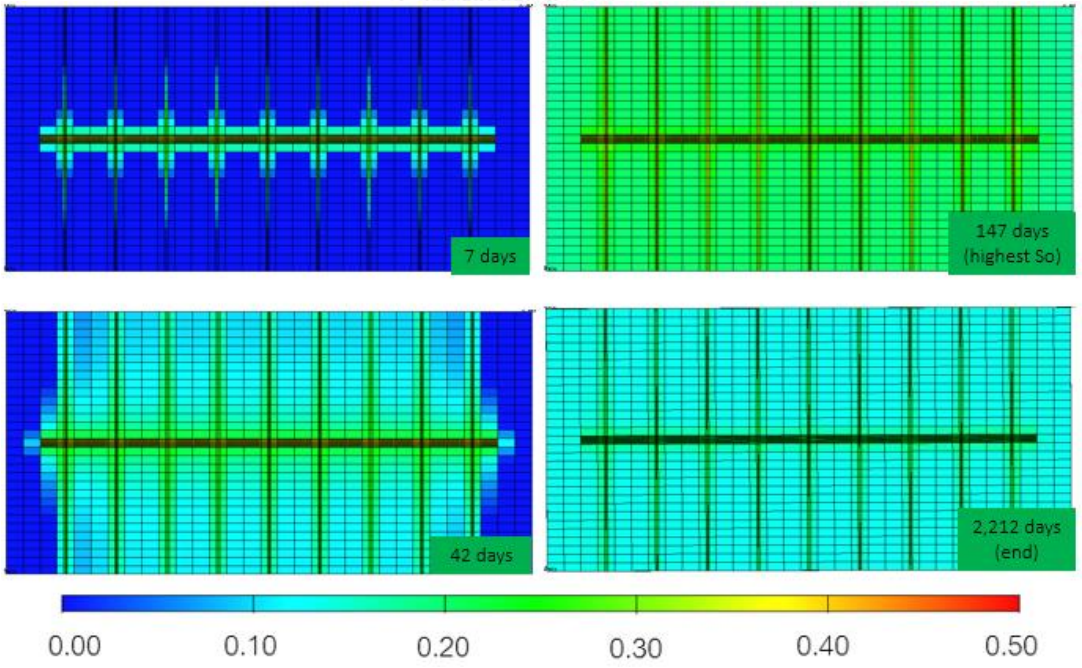

Figure A.26 Condensate saturation profile vs. time of fracture permeability at 150,000 mD in rich condensate

Appendix B

B-1) Non-fractured Cases

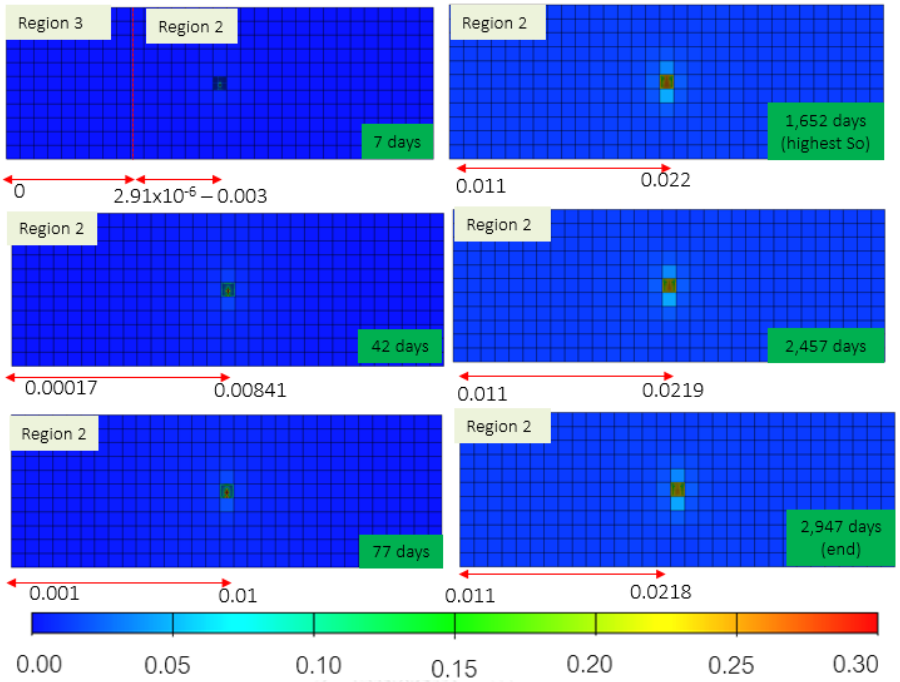

Figure B.1 Cross-section at the highest condensate saturation of non-fractured reservoir in lean condensate

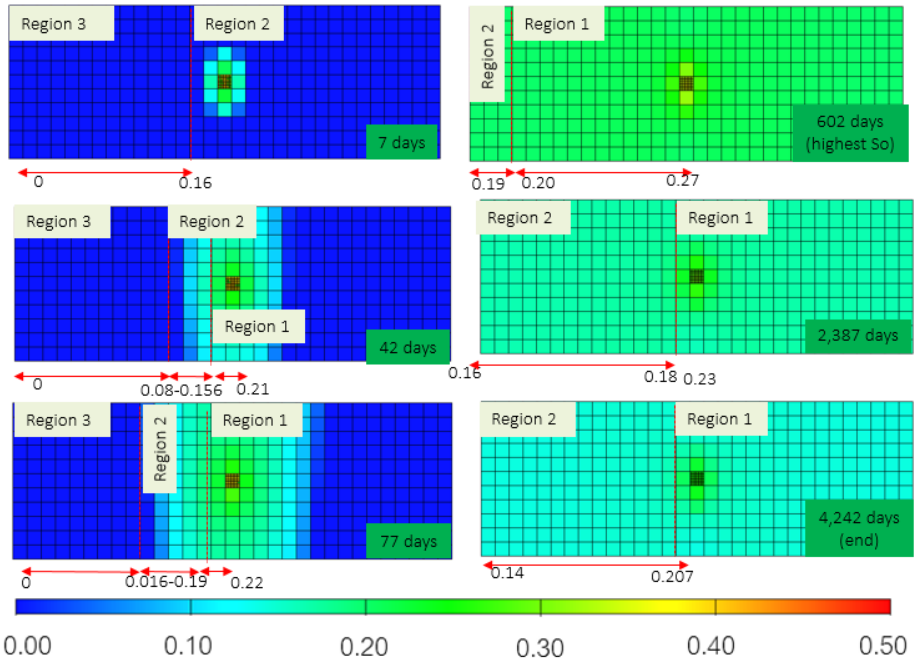

Figure B.2 Cross-section at the highest condensate saturation of non-fractured reservoir in rich condensate

B-2) Effect of Fracture Width

Lean Condensate

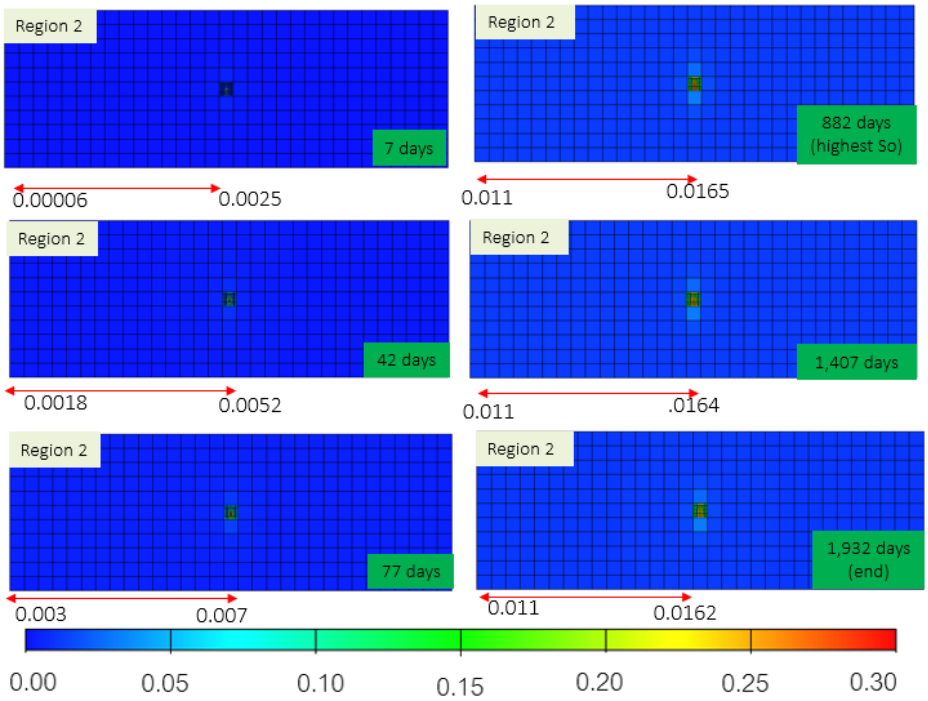

Figure B.3 Cross-section at the highest condensate saturation of fracture width of 0.0083 ft. in lean condensate

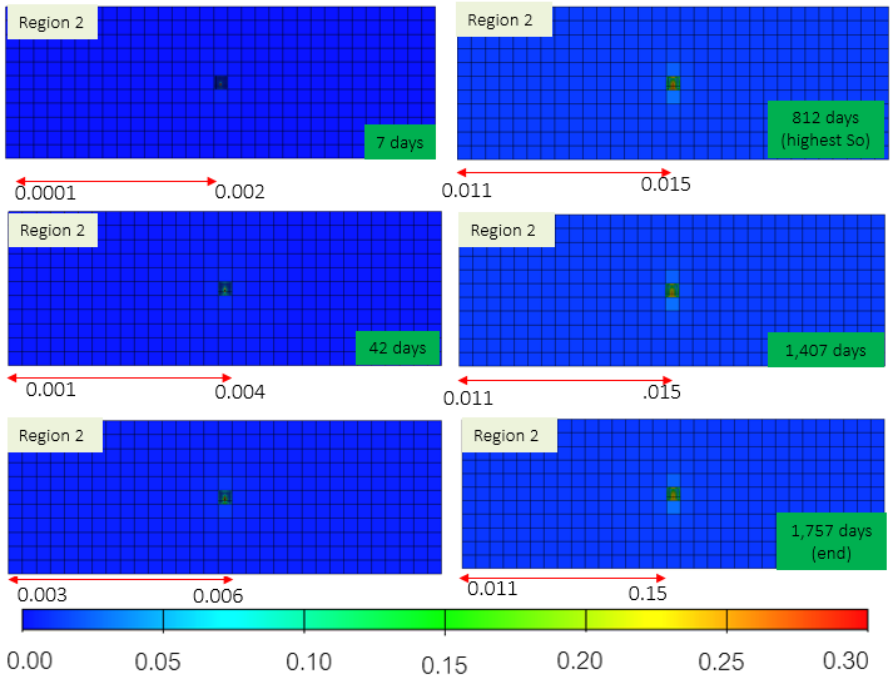

Figure B.4 Cross-section at the highest condensate saturation of fracture width of 0.0125 ft. in lean condensate

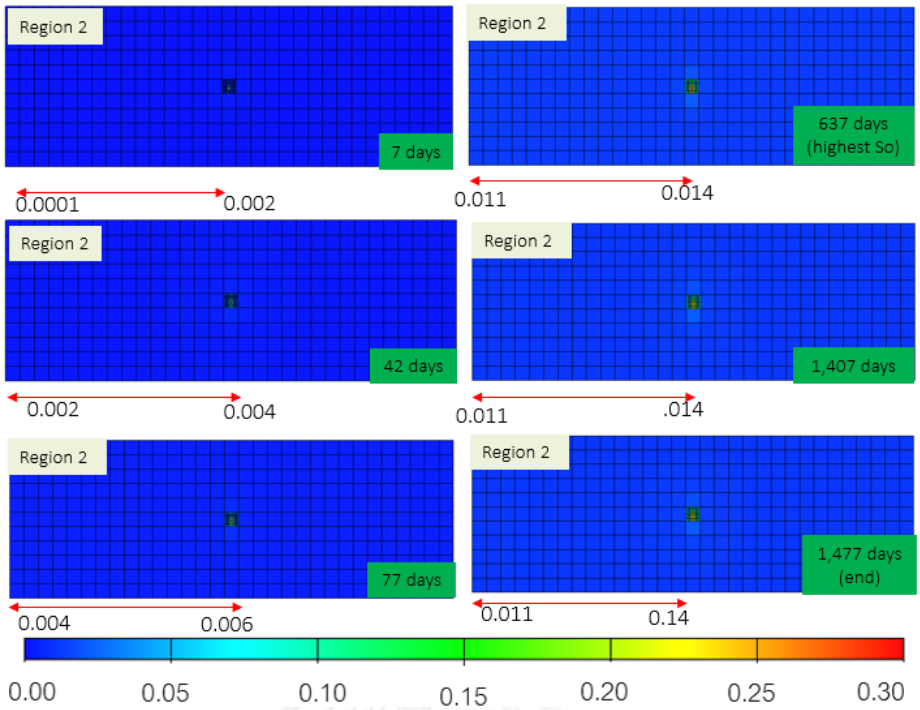

Figure B.5 Cross-section at the highest condensate saturation of fracture width of 0.025 ft. in lean condensate

Rich Condensate

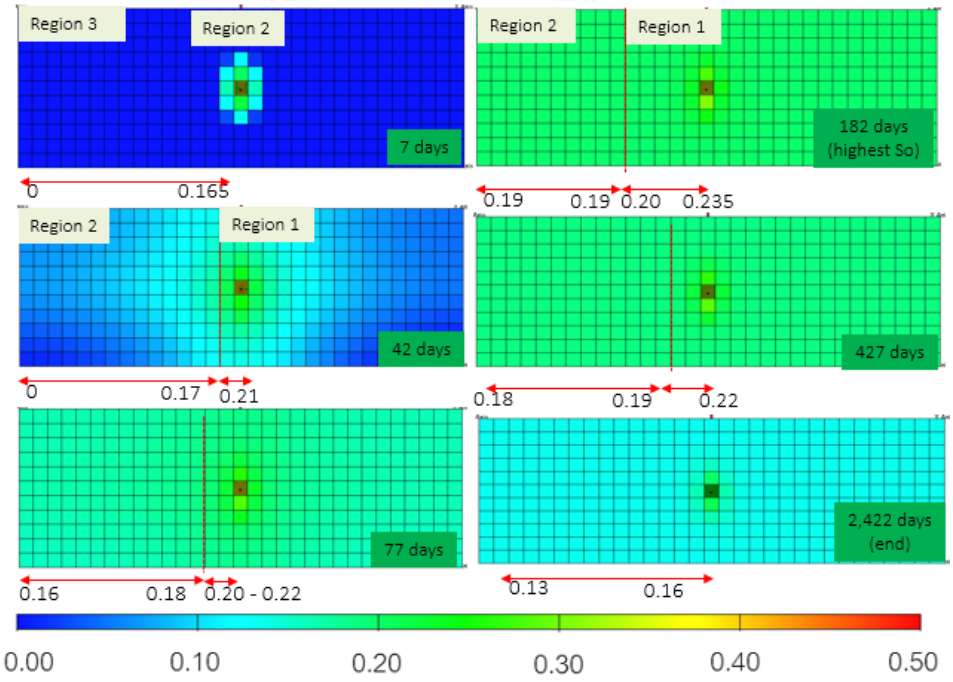

Figure B.6 Cross-section at the highest condensate saturation of fracture width of 0.0083 ft. in rich condensate

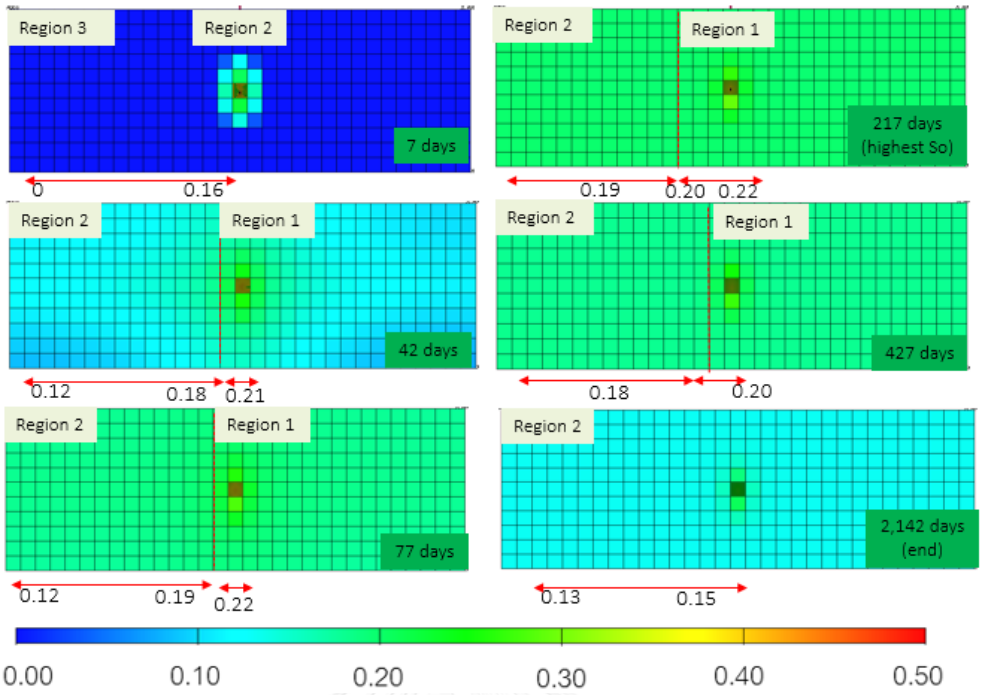

Figure B.7 Cross-section at the highest condensate saturation of fracture width of 0.0125 ft. in rich condensate

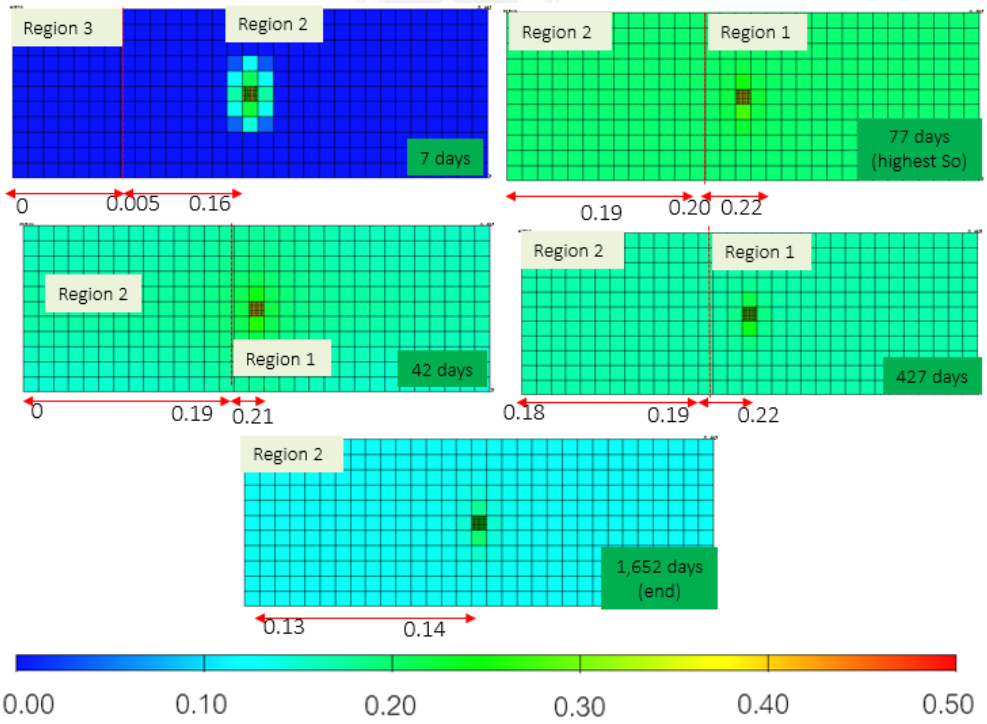

Figure B.8 Cross-section at the highest condensate saturation of fracture width of 0.025 ft. in rich condensate

B-3) Effect of Number of Fracture

Lean Condensate

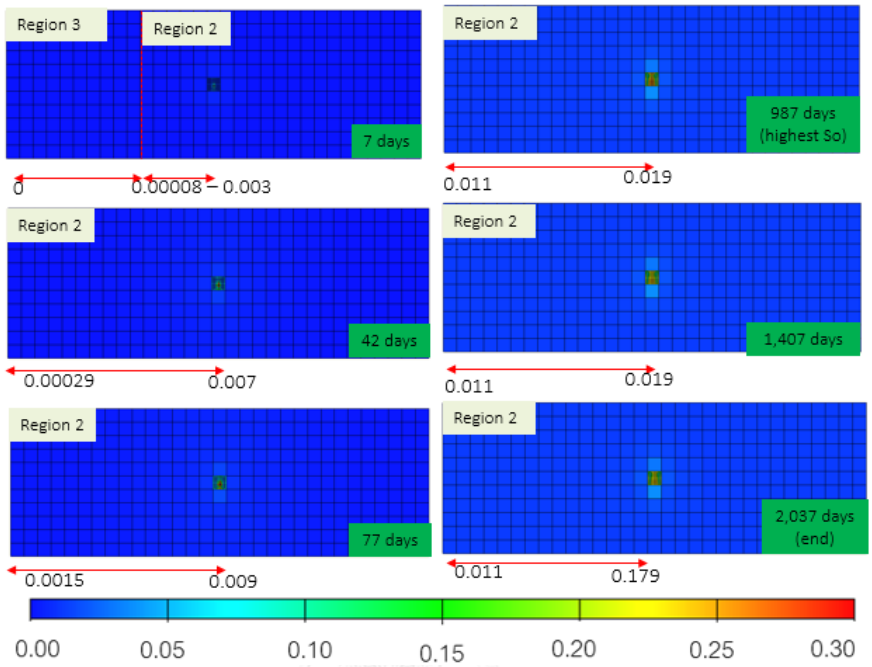

Figure B.9 Cross-section at the highest condensate saturation of 3 fractures in lean condensate

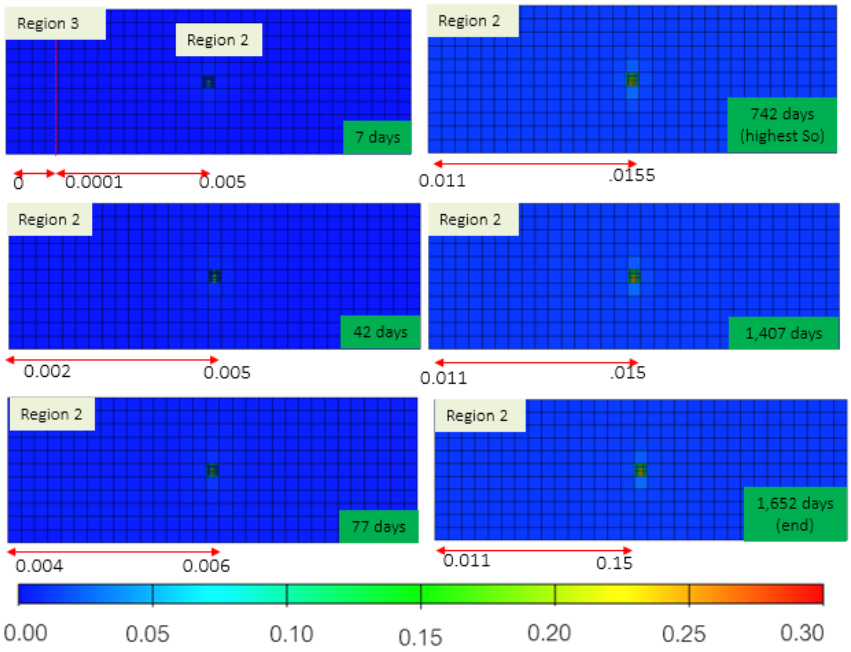

Figure B.10 Cross-section at the highest condensate saturation of 6 fractures in lean condensate

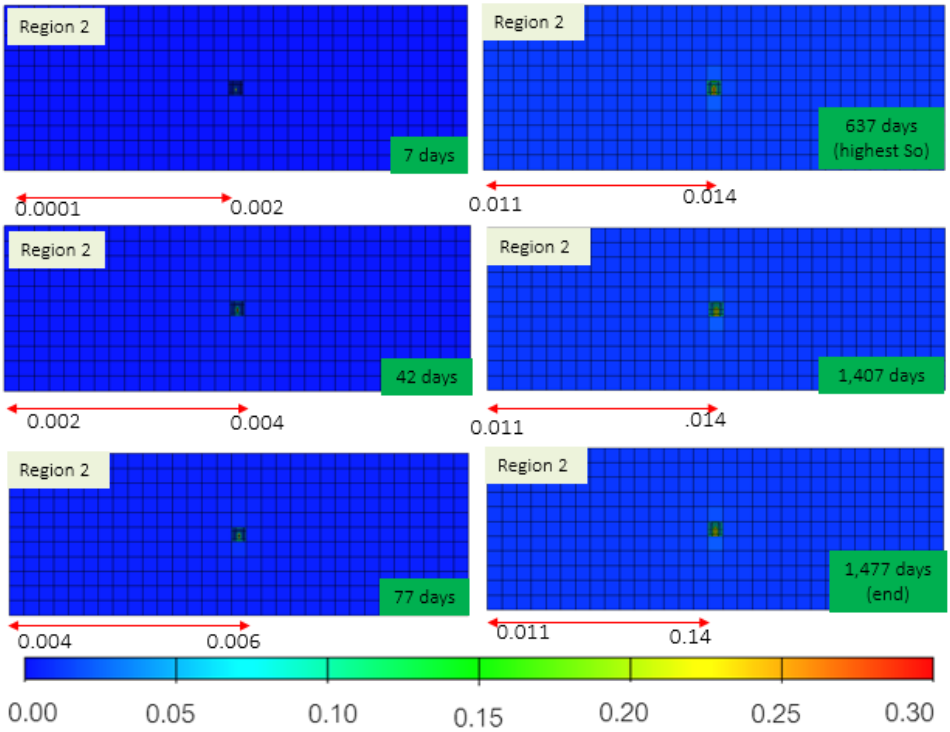

Figure B.11 Cross-section at the highest condensate saturation of 9 fractures in lean condensate

Rich Condensate

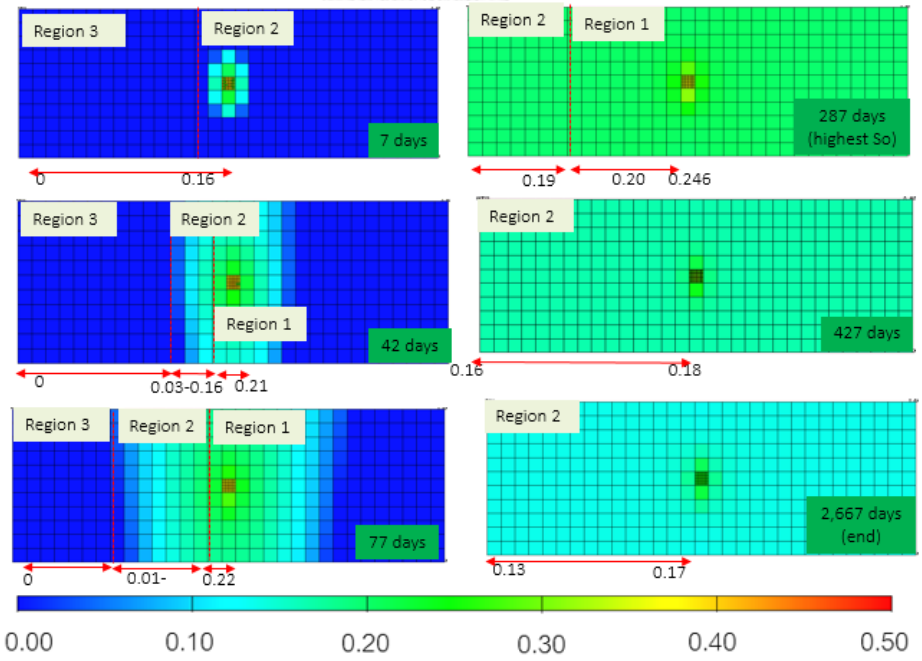

Figure B.12 Cross-section at the highest condensate saturation of 3 fractures in rich condensate

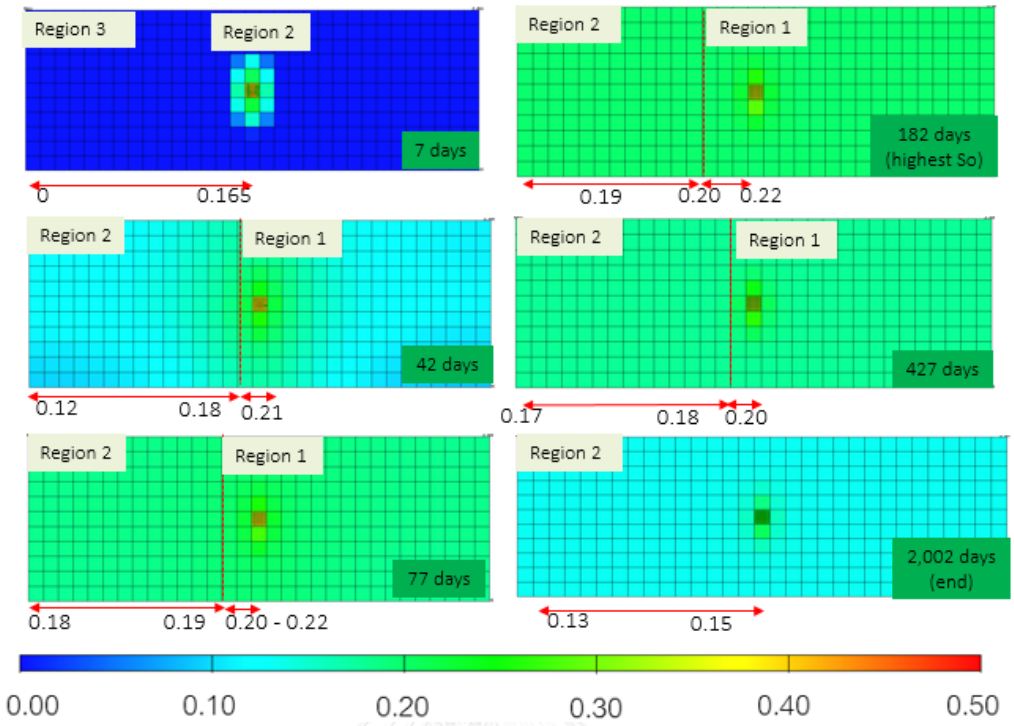

Figure B.13 Cross-section at the highest condensate saturation of 6 fractures in rich condensate

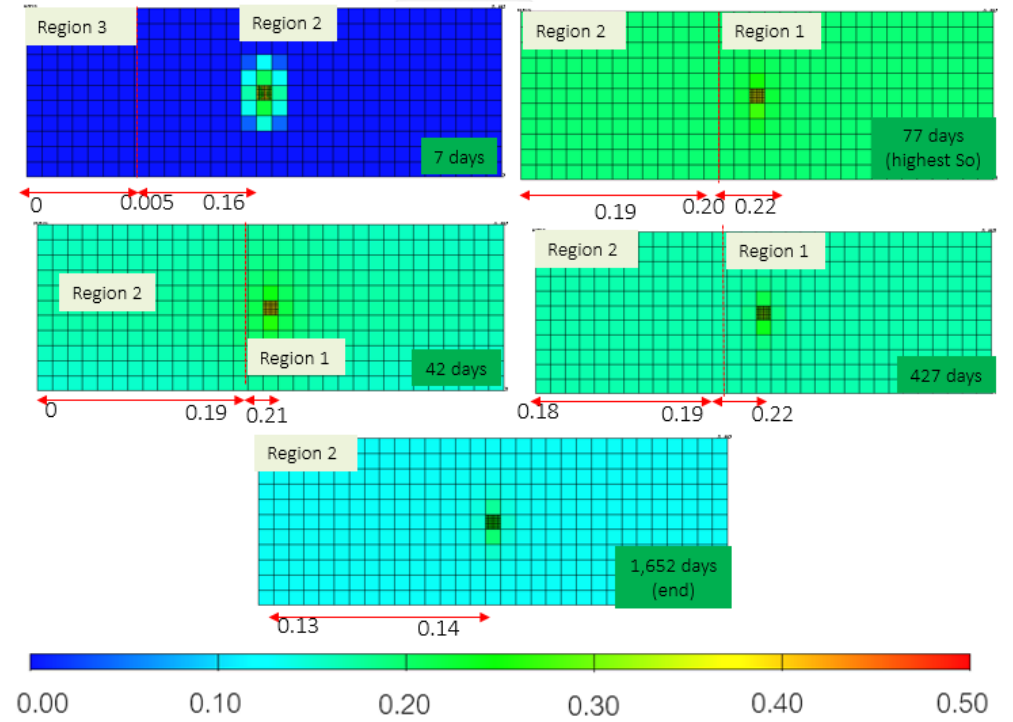

Figure B.14 Cross-section at the highest condensate saturation of 9 fractures in rich condensate

B-4) Effect of Stimulated Reservoir Volume (SRV)

Lean Condensate

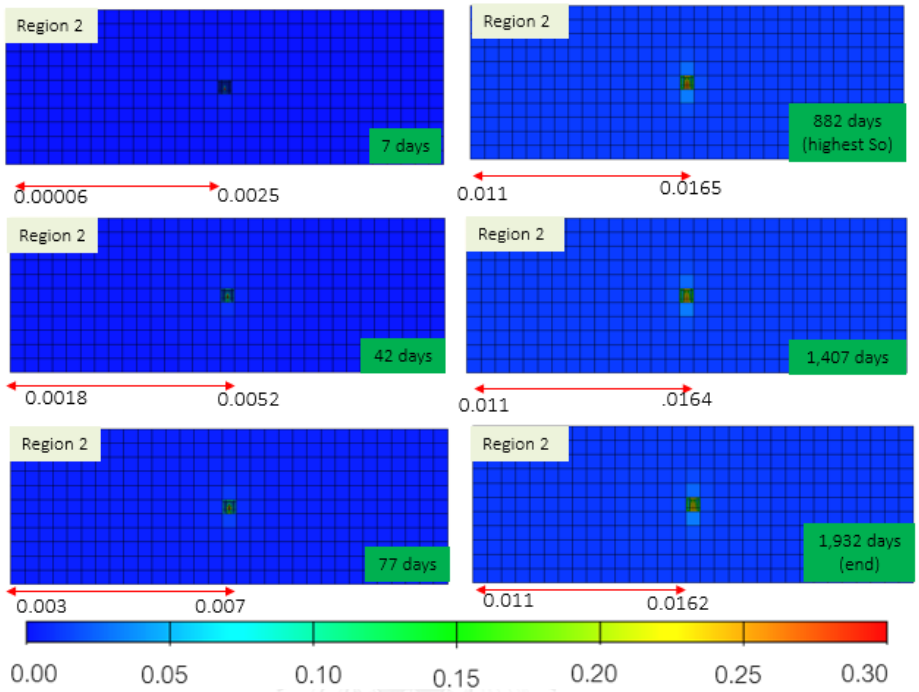

Figure B.15 Cross-section at the highest condensate saturation of SRV (case A) in lean condensate

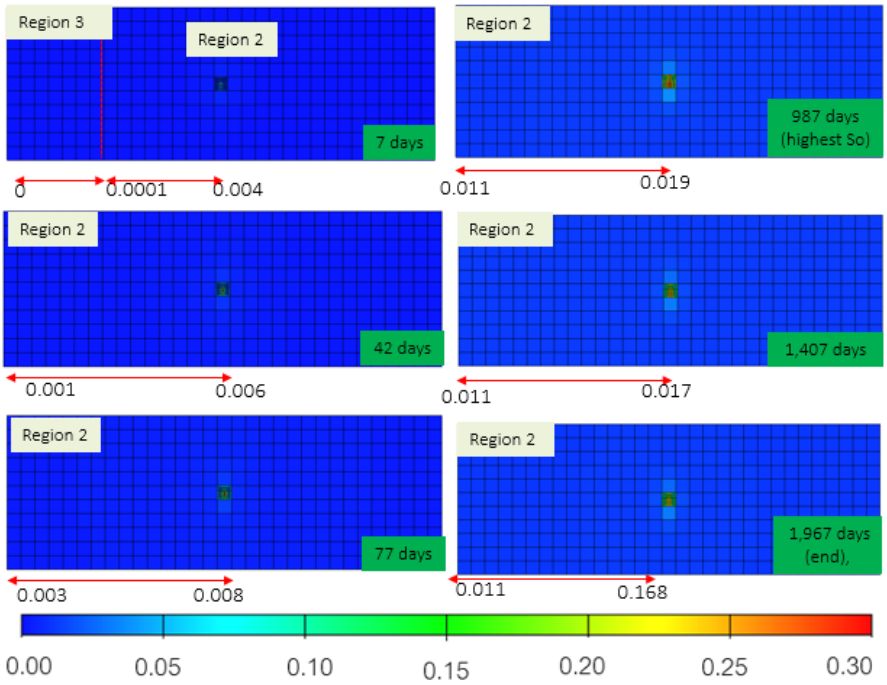

Figure B.16 Cross-section at the highest condensate saturation of SRV (case B) in lean condensate

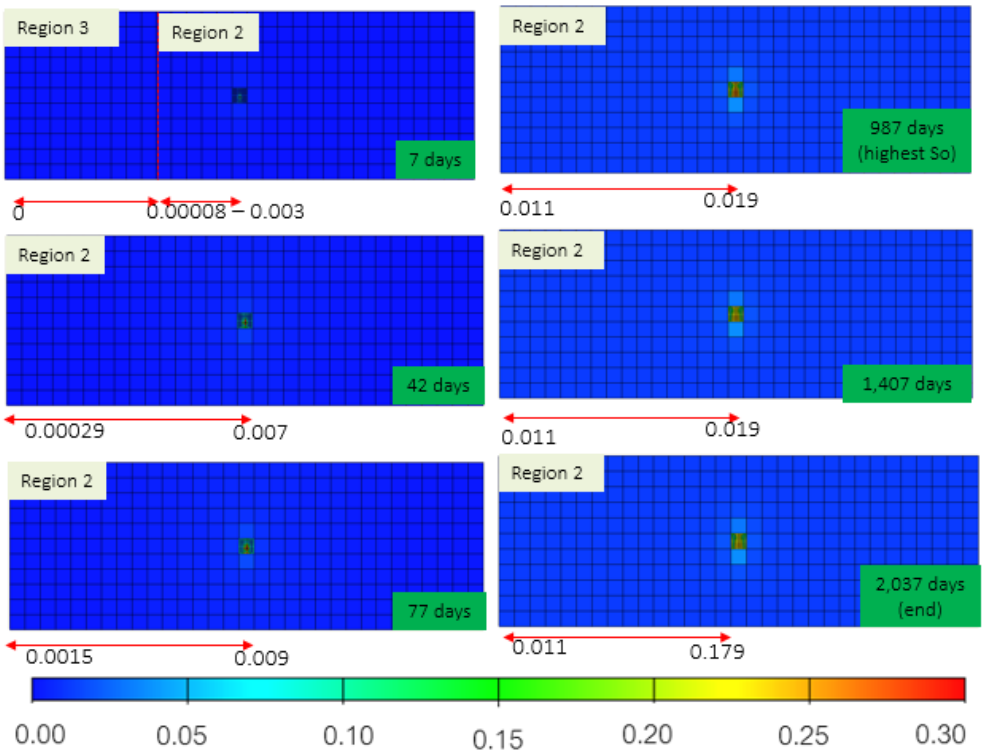

Figure B.17 Cross-section at the highest condensate saturation of SRV (case C) in lean condensate

Rich Condensate

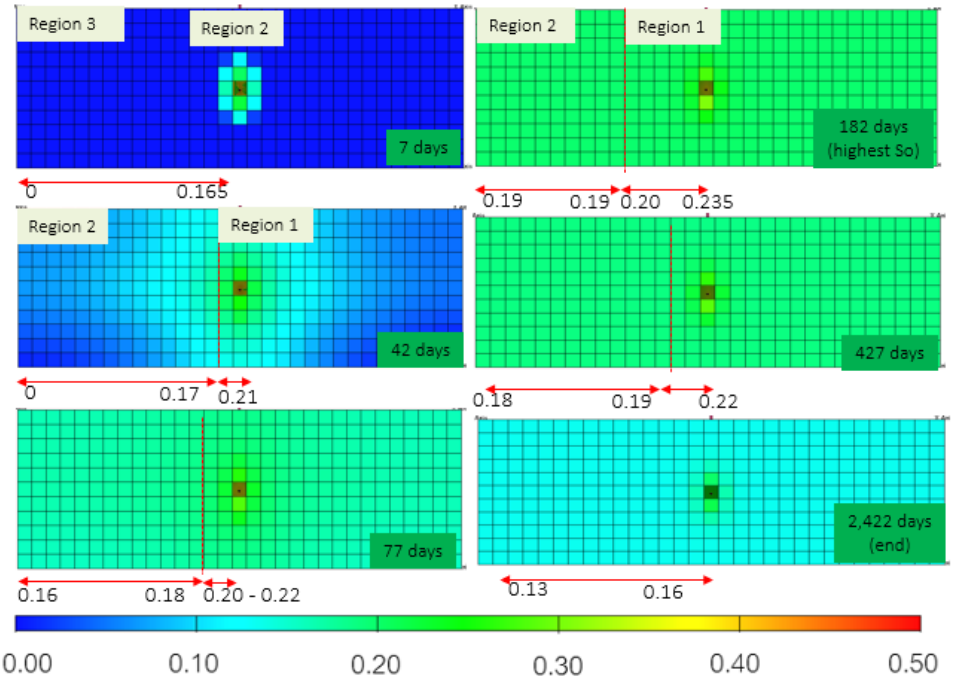

Figure B.18 Cross-section at the highest condensate saturation of SRV (case A) in rich condensate

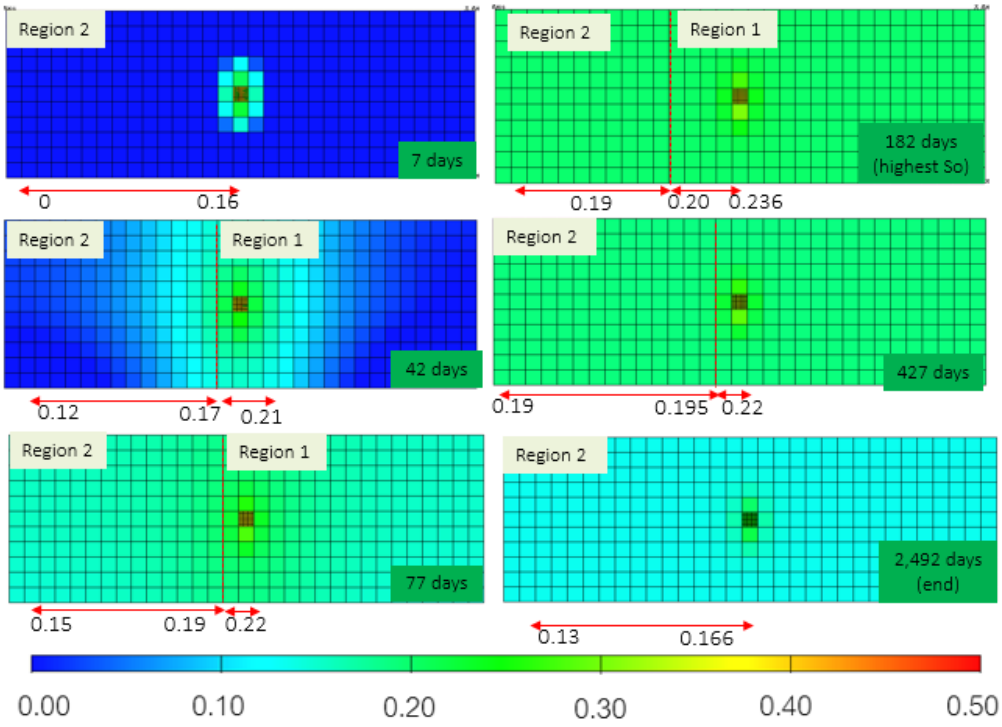

Figure B.19 Cross-section at the highest condensate saturation of SRV (case B) in rich condensate

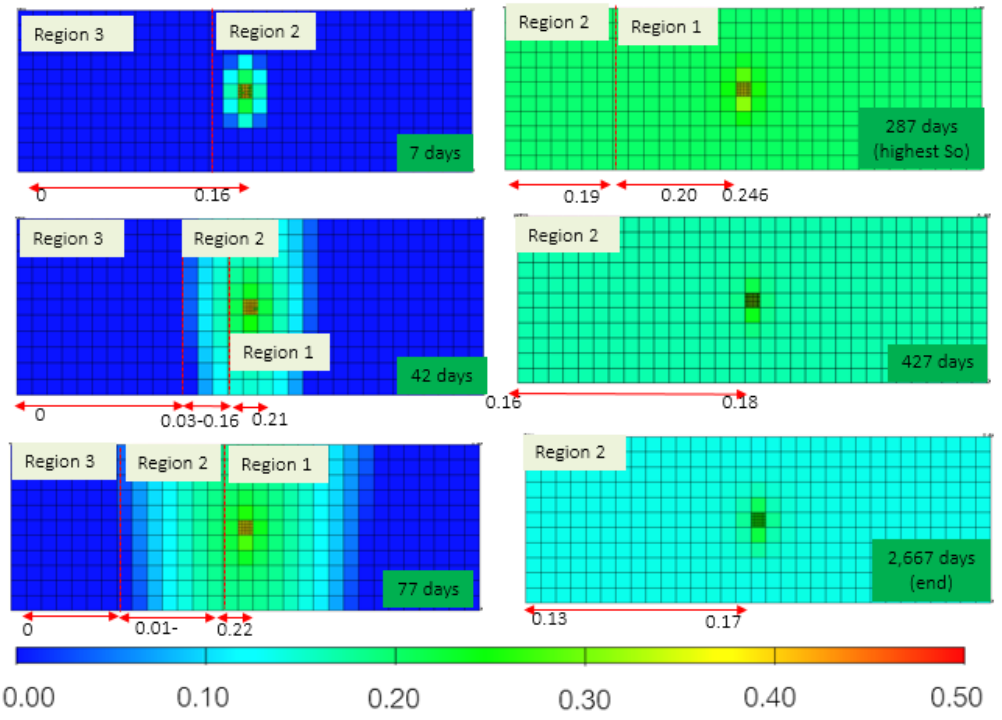

Figure B.20 Cross-section at the highest condensate saturation of SRV (case C) in rich condensate

B-5) Effect of Fracture Permeability

Lean Condensate

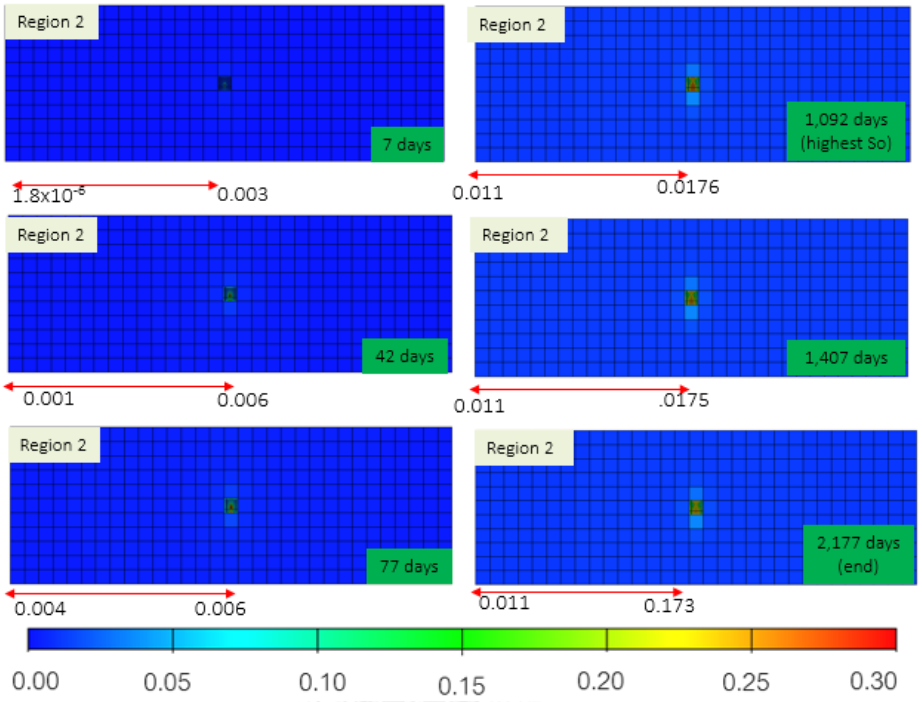

Figure B.21 Cross-section at the highest condensate saturation of fracture permeability at 50,000 mD in lean condensate

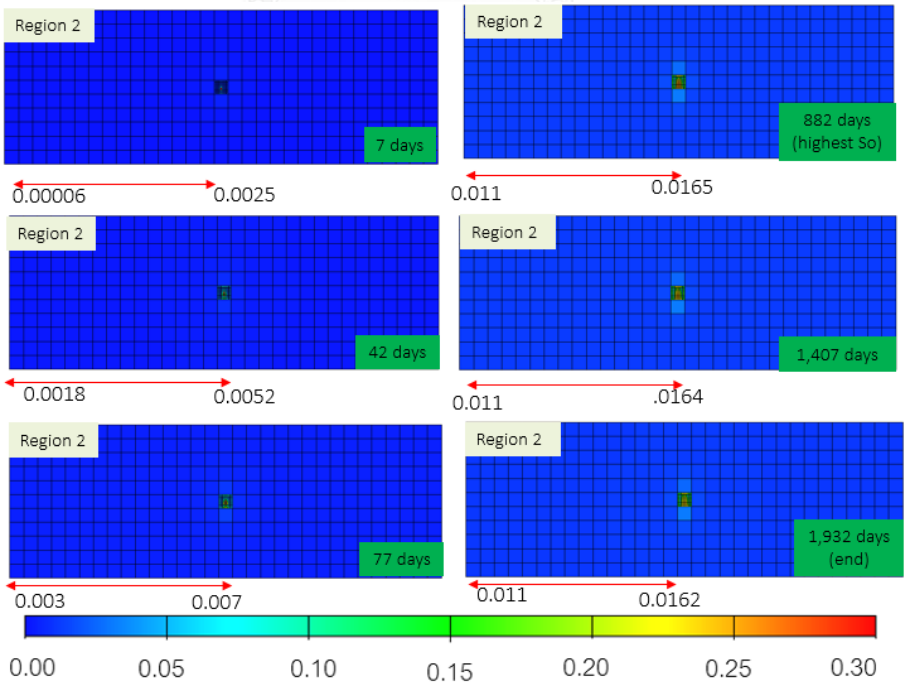

Figure B.22 Cross-section at the highest condensate saturation of fracture permeability at 100,000 mD in lean condensate

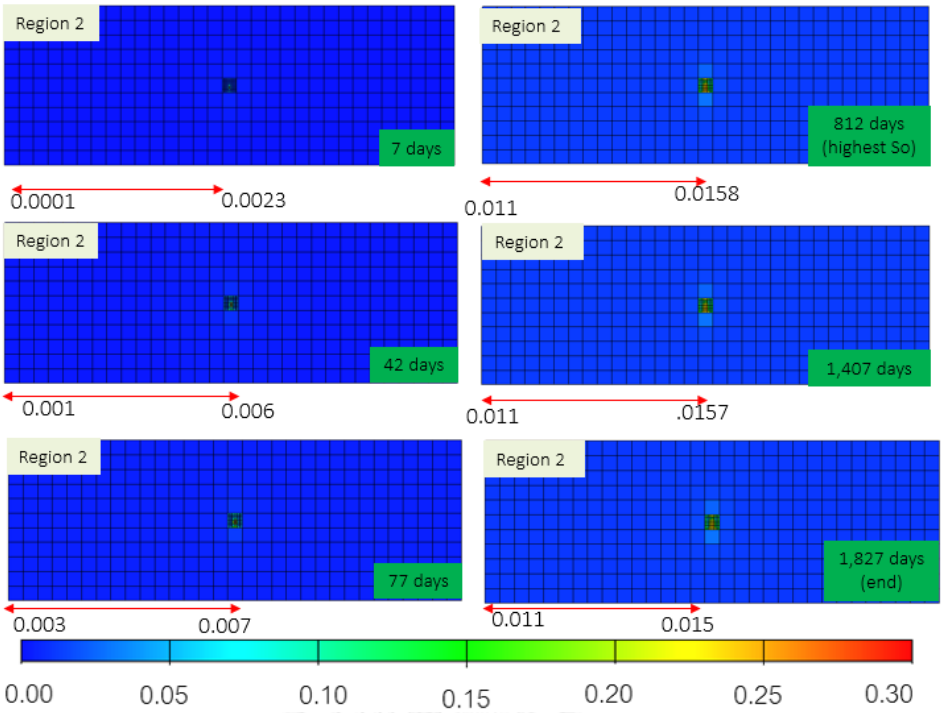

Figure B.23 Cross-section at the highest condensate saturation of fracture permeability at 150,000 mD in lean condensate

Rich Condensate

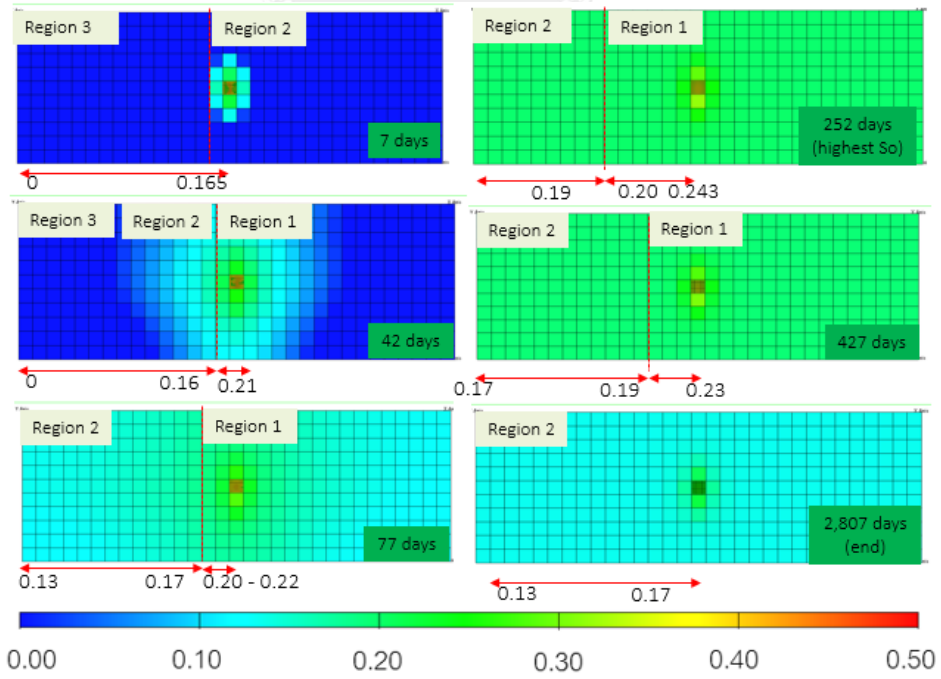

Figure B.24 Cross-section at the highest condensate saturation of fracture permeability at 50,000 mD in rich condensate

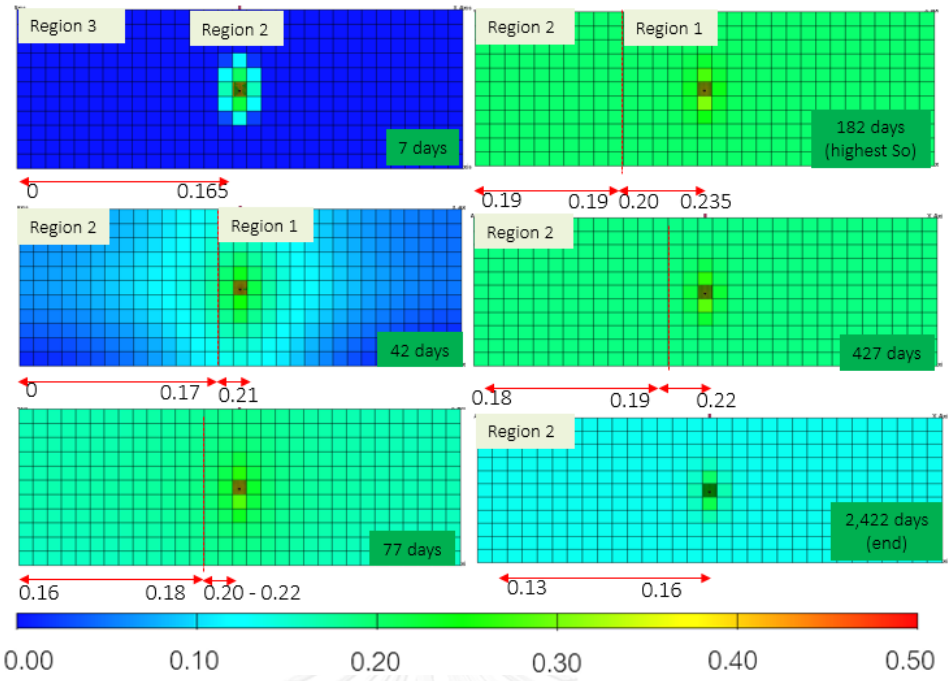

Figure B.25 Cross-section at the highest condensate saturation of fracture permeability at 100,000 mD in rich condensate

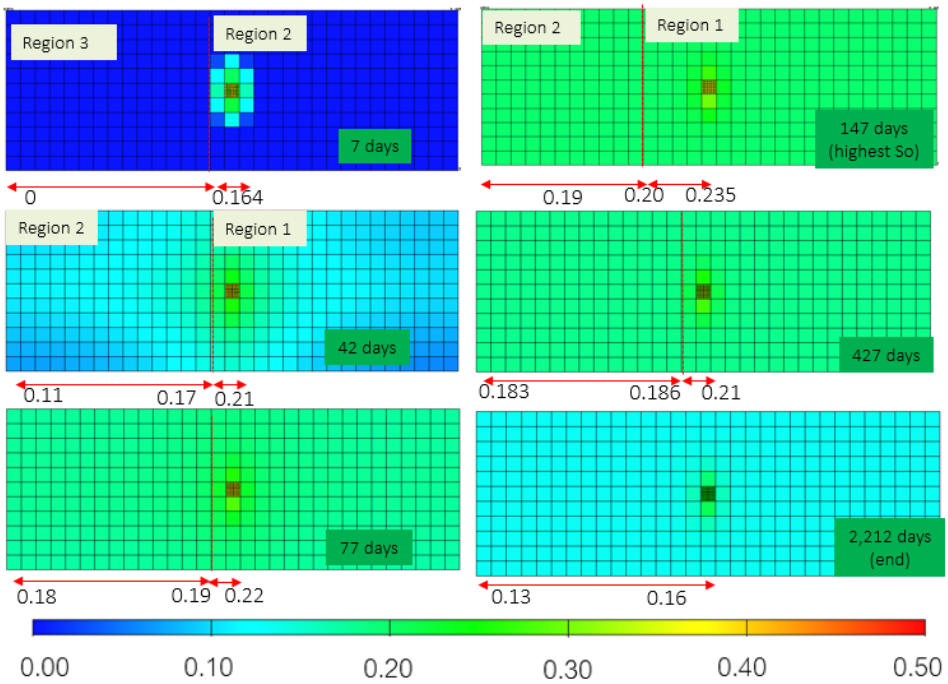

Figure B.26 Cross-section at the highest condensate saturation of fracture permeability at 150,000 mD in rich condensate

VITA

Karanthakarn Mekmok was born on August 10th, 1988 in Saraburi, Thailand. She received her Bachelor of Science in Geology from the Faculty of Science, Chulalongkorn University in 2011. After her graduation, she had got an opportunity to work in STS Engineering Consultants Co., Ltd. in the position of geophysicist for 3 months before continued her studies in Master of Petroleum Engineering program at the Department of Mining and Petroleum Engineering, Faculty of Engineering, Chulalongkorn University in August 2014.